



The
University
Of
Sheffield.

**Neuropilin-1 (NRP1) and VEGF isoforms
as major players in sarcoma response to
vascular-targeted therapies for cancer**

A thesis submitted in partial fulfilment of the requirements for the
degree of Doctor of Philosophy by

Ruth Hannah Edith Thomas

Supervised by Dr Chryso Kanthou and Professor Gillian Tozer

The University of Sheffield
Faculty of Medicine, Dentistry and Health
Department of Oncology and Metabolism

July 2020

Acknowledgements

Thank you first and foremost to the Sarcoma UK, Rosetrees Trust and The University of Sheffield, as without their funding, this body of work would not exist.

There is no doubt in my mind that this whole experience would have had a whole different outcome if it were not for the unerring support of my fantastic supervisors Dr Chryso Kanthou and Professor Gill Tozer; I am truly lucky to have had these two formidable women in my corner. Chryso, where to start? Perhaps with 'what I think we could do'? But in all seriousness, thank you from the bottom of my heart for believing in me, especially when I couldn't believe in myself. You gave me the freedom to just get on with it, yet I knew if I needed it, you were there to offer your advice and guide me. Yes, the last year has been a challenge for me personally but overall I reckon we've had more laughs than tears over the last four years. I look forward to what's to come and to working with my now dear friend. Thank you Gill for your patience and guidance when you should have been off, ukulele in hand, enjoying your retirement. I am eternally grateful.

A massive thank you to Matt Fisher, for imparting just a tiny fraction of your knowledge and expertise during the *in vivo* work and sharing some of you IHC secrets. Our comical ethical debates in the lab with Jack were a highlight and the introduction to the world of podcasts (namely Sam Harris) has changed my perspective on the world.

I am aware that I am an accumulation of every interaction I have had in my life so far, so to thank everyone would be impossible. There are a some key people that have been generous enough to share their scientific knowledge and wisdom with me that it would be remiss of me not to mention by name though; Dr Neil Burden and Dr Ruth McAdam, who schooled me in molecular biology and Dr Chris Plumpton for all things cell culture related during my stint in industry. Thank you to Bas Brinkhof, who was there for me to sound out my molecular biology ideas and to Vicky Cookson for her help on all things CRISPR. Also, thank you to Dr Nasreen Akhtar for her sound advice, to Maggie Glover for cutting all my sections and to Dr Will English.

Last but not least thank you to the friends and family that have stood on the side-lines cheering me on, not quite knowing what to do or say to this bonkers human when in full melt-down mode; just being there was more than enough and it meant the world to me. So to Bev, Adam, Grandma, Lucy,

Rick, Louise, Rob, Christine, Toby, Rebecca, and Shannice thank you for being my cheerleaders. Because I am a crazy cat lady I cannot exclude my girls, Lily and Velma, from my list of supporters, although if there are any erroneous spaces, word or letters in this thesis they are as a result of their input!

Finally, to my mum.....although you are not here to share this with me, I carry you with me at all times. You are my inspiration; your influence is strong in everything I do and I hope that, if you were still here today, you would be proud of how I evolved and what I have achieved. I love you.

Declaration

I, Ruth Thomas, confirm that Thesis is an original report of my research work under the guidance of my supervisors Dr Chryso Kanthou and Professor Gillian Tozer. The experimental work was performed by myself and any contribution by others is explicitly indicated in the corresponding methods section. References have been provided on all supporting literature and resources.

I am aware of the University's Guidance on the Use of Unfair Means (www.sheffield.ac.uk/ssid/unfair-means). This work has not been previously presented for an award at this, or any other, university.

Abstract

Vascular endothelial growth factor-A (VEGF) is a major target of anti-angiogenic cancer therapies. Alternative VEGFA gene splicing generates isoforms with different biological activities regulated by matrix binding and signalling through VEGF receptors and co-receptor neuropilin-1 (NRP1). Main human isoforms are VEGF₁₂₁, VEGF₁₆₅ and VEGF₁₈₉ (VEGF₁₂₀, VEGF₁₆₄ and VEGF₁₈₈ in mouse). Anti-VEGF therapy has made a huge clinical impact, but only in some patients, with clinical data suggesting that high circulating VEGF₁₂₁ and low NRP1 may predict response. Using mouse fibrosarcoma cells expressing individual VEGF isoforms (fs120, fs164 and fs188) and differential NRP1 levels, this study explored mechanistic links between NRP1 and VEGF isoforms and their potential as predictive anti-VEGF therapy biomarkers.

Transient and CRISPR/Cas9n NRP1 knockdown in fs188 cells (fs188-NRP1KD) reduced migration without altering proliferation compared to wild type cells (fs188wt). NRP1 overexpression in fs120 cells also retarded migration compared to fs120wt cells. However, kinases driving proliferation and migration including AKT, Src and ERK-1/2 were unaffected by NRP1 overexpression and knockdown while signalling of hepatocyte growth factor that utilises NRP1 as co-receptor was only inhibited in one fs188-NRP1KD clone.

Vascularisation of fs188-NRP1KD and fs120-NRP1OE tumours was comparable to corresponding wt tumours; however, NRP1 modification resulted in smaller tumours. Fs120-NRP1OE tumours appeared more desmoplastic than fs120wt tumours with fewer dilated vessels. Anti-VEGF antibody B20-4.1.1 treatment reduced tumour growth and vascularisation in all VEGF188 tumours regardless of NRP1 levels, although growth reduction commenced earlier in the fs188-NRP1KD's. Fs120wt tumours were unresponsive to B20-4.1.1, whilst fs120-NRP1OE growth was significantly reduced without a reduction in vascularisation.

Results of this study are consistent with the emerging idea that the prognostic and predictive value of NRP1 is context dependent. It is unlikely that VEGF isoforms and NRP1 alone are predictive of anti-VEGF therapy response; further work is required to unravel the complexities surrounding biomarker discovery.

Oral and Poster Presentations

University of Sheffield Medical School Research day (June 2019)

Poster presentation: The role of neuropilin-1 and VEGF isoforms in soft tissue sarcoma and their potential as predictive biomarkers of response to vascular-targeted therapies.

BACR Student Conference, The Crick Institute, London (Nov 2018)

Poster presentation: The role of neuropilin-1 and VEGF isoforms in soft tissue sarcoma and their potential as predictive biomarkers of response to vascular-targeted therapies.

EuSARC Residential Workshop on The Biology of Sarcoma (June 2018)

Oral presentation: The role of neuropilin-1 and VEGF isoforms in soft tissue sarcoma and their potential as predictive biomarkers of response to vascular-targeted therapies.

University of Sheffield Medical School Research day (June 2017)

Oral presentation: The role of neuropilin-1 and VEGF isoforms in soft tissue sarcoma and their potential as predictive biomarkers of response to vascular-targeted therapies.

BMS & UKCAS Joint Conference (April 2017)

Poster presentation: Interactions of neuropilin-1 and VEGF isoforms in the development of vascular-targeted treatment strategies

Sarcoma UK – Sarcoma Research Symposium, “What causes sarcoma?” (Sept 2016)

Poster presentation: Neuropilin-1 and VEGF isoforms as major players in soft tissue sarcoma response to vascular-- targeted therapies for cancer.

Contents

Acknowledgments	i
Declaration	iii
Abstract	iv
Oral and poster presentations	v
List of Figures	x
List of Tables	xii
List of Abbreviations	xiii
Chapter 1 Introduction.....	1
1.1 Developmental angiogenesis	1
1.1.1 Sprouting angiogenesis	2
1.1.2 Intussusceptive angiogenesis.....	5
1.2 Tumour vascularisation.....	5
1.2.1 Tumour angiogenesis	5
1.2.2 Vascular mimicry.....	7
1.2.3 Vessel co-option.....	7
1.2.4 Tumour vasculogenesis.....	8
1.3 Vascular endothelial growth factor (VEGF).....	8
1.3.1 An introduction to VEGF	8
1.3.2 VEGF receptors, VEGF binding and signalling	10
1.3.3 VEGF isoforms	13
1.4 The Neuropilins.....	18
1.4.1 Role of NRP1 during development.....	19
1.4.2 Tissue distribution of the neuropilins	19
1.4.3 NRP1 binds multiple ligands	20
1.4.4 NRP1 Isoforms.....	22
1.4.5 NRP1 and its interactions with VEGF isoforms	24
1.4.6 NRP1 in tumour growth and angiogenesis	26
1.4.7 VEGF ₁₆₅ mediated NRP1/VEGFR2 cross-cell complexes.....	27
1.4.8 NRP1 in desmoplasia.....	30
1.5 Vascular-targeted therapy in cancer.....	31
1.5.1 Anti-angiogenic therapy in cancer	31

1.5.2	Vascular Disrupting Agents (VDAs)	38
1.5.3	Combining VDAs with chemotherapy and radiotherapy	39
1.5.4	Combining VDAs with targeted therapy	39
1.6	Soft tissue sarcoma and anti-angiogenic therapy	42
1.6.1	Soft tissue sarcoma	42
1.6.2	Current treatment of STS	42
1.6.3	Angiogenesis in STS	43
1.7	Anti-angiogenic treatment in STS	43
1.7.1	VEGF pathway inhibitors in non-GIST STS	43
1.7.2	Bevacizumab in STS	45
1.7.3	Gastrointestinal stromal tumours	46
1.8	Biomarkers	48
1.8.1	Patient response and resistance to anti-angiogenic therapy	48
1.8.2	Assessment of clinical efficacy of vascular-targeted therapy	50
1.8.3	The importance of biomarkers in anti-angiogenic therapy	50
1.8.4	Predictive biomarkers for VEGF pathway inhibitors	51
1.8.5	VEGF as a prognostic biomarker	52
1.8.6	VEGF as a predictive biomarker	52
1.8.7	VEGF isoforms as a predictive biomarker	53
1.8.8	NRP1 as a prognostic biomarker	54
1.8.9	NRP1 as a predictive biomarker	55
1.9	Summary	56
1.10	Hypothesis	57
1.11	Aims	57
1.12	Specific Aims	59
Chapter 2 Materials and Methods		60
2.1	Cell culture	60
2.1.1	Primary and secondary cell culture	60
2.1.2	Cell subculture	60
2.1.3	Fibrosarcoma cell lines	62
2.1.4	HUVECs	62
2.2	Short interfering RNA (siRNA) lipofection of fibrosarcoma cells	64
2.2.1	siRNA	64
2.2.2	Lipid-mediated transfection	64
2.2.3	siRNA transfection of fswt and fs188 cells	64

2.3	Adhesion Assay	65
2.3.1	Coating plates with ECM proteins.....	65
2.3.2	Cell seeding and adhesion.....	66
2.3.3	Doubling times and growth curves	66
2.4	Migration Assay	67
2.4.1	Migration of cells with transient NRP1 KD.....	67
2.4.2	Migration of cells with stable NRP1 KD/overexpression	67
2.4.3	Migration assay quantification	68
2.5	Anchorage independent cell growth	68
2.5.1	Preparation of thick collagen	68
2.6	Western Blotting	69
2.6.1	Protein extraction from cells	69
2.6.2	Protein quantification	70
2.6.3	Sodium dodecylsulphate-polyacrylamide gel electrophoresis (SDS-PAGE).....	70
2.6.4	Transfer of proteins to a membrane.....	71
2.6.5	Immunological protein detection	71
2.6.6	ECL protein detection.....	72
2.6.7	Semi-quantitative analysis of western blots.....	73
2.7	Genetic modification of fs cell lines	73
2.7.1	DNA isolation and purification	73
2.7.2	Restriction enzyme digest.....	74
2.7.3	Agarose gel electrophoresis.....	75
2.7.4	Colony PCR.....	75
2.7.5	Generation of stable NPR1 knockdown fs cell lines.....	77
2.7.6	Generation of stable NRP1 overexpressing fs cells lines	83
2.8	Flow cytometry and fluorescence-activated cell sorting (FACS)	89
2.8.1	Flow cytometry to detect GFP expression	89
2.8.2	Flow cytometry for NRP1 and NRP2 expression	90
2.8.3	FACS to identify fs cell transfectants	92
2.9	Clonal isolation of GFP positive cells	92
2.10	Single VEGF isoform verification in genetically modified fs cells	93
2.10.1	RNA isolation from fs cells	93
2.10.2	First strand cDNA synthesis	93
2.11	<i>In vivo</i> models	93
2.11.1	Ethical approval and animal husbandry.....	94

2.11.2	Subcutaneous tumour implant and end-point definitions	94
2.11.3	Intraperitoneal drug injection.....	95
2.11.4	Tumour and lung excision and preparation.....	95
2.12	Haematoxylin and eosin (H & E) staining.....	95
2.12.1	H & E staining method	96
2.12.2	Imaging Sections and analysis software	96
2.12.3	Analysis of necrosis in H & E stained sections	96
2.13	Immunohistochemistry (IHC)	97
2.13.1	De-waxing, rehydration and epitope retrieval.....	97
2.14	Immunostaining of tumour sections.....	97
2.14.1	IHC with Mouse on Mouse (MOM) Immunodetection Kit.....	98
2.14.2	Tumour vascular density analysis	98
2.15	Masson's Trichrome staining.....	99
2.16	Statistical analysis.....	100
Chapter 3 Consequences of transient NRP1 knockdown on fswt/fs188		
behaviour <i>in vitro</i>		
		101
3.1	Introduction.....	101
3.2	Aim.....	102
3.3	Differential expression of NRP1 in fs cells expressing different VEGF isoforms	103
3.4	Knockdown of NRP1 in fswt and fs188 cells.....	104
3.4.1	NRP1 siRNA knockdown.....	104
3.5	Effects of NRP1 knockdown on NRP2 expression.....	107
3.6	Effect of NRP1 KD on VEGFR2, PDGFRβ, β1 integrin and fibronectin.....	108
3.7	Effect of NRP1 KD on ERK1/2 phosphorylation	110
3.8	NRP1 KD in fibrosarcoma cells does not affect adhesion to various ECM proteins.	112
3.9	Effects of NRP1 KD on migration of fibrosarcoma cells	114
3.10	Discussion.....	116
Chapter 4 Development of stable NRP1 overexpressing and knockdown		
fibrosarcoma cells.....		
		120
4.1	Introduction.....	120
4.2	Aim.....	121
4.3	CRISPR/Cas9 gene-editing system	121
4.4	TransIT-X2[®] delivers pSpCas9n(BB)-2A-GFP-sgRNA DNA to fs188 cells more effectively than Lipofectamine[®] and FuGene 6[®]	124
4.5	NRP1 protein expression is depleted in pooled CRISPR/Cas9n modified fs cells.....	126

4.6	Successful KD of NRP1 protein expression in fs188 cells using CRISPR/Cas9n	126
4.7	NRP1 overexpression in fs120 and fs164 cells	130
4.8	Successful overexpression of NRP1 in fs120 and fs164 cells.....	132
4.9	Migration of fs cells expressing single VEGF isoforms is reliant on NRP1 expression levels 134	
4.10	NRP1 expression does not alter proliferation rates in fs cells expressing single VEGF isoforms.....	138
4.11	Downstream signalling consequences of modified NRP1 expression	139
4.12	Discussion.....	144
Chapter 5 <i>In vivo</i> effects of NRP1 modification in fibrosarcoma cells expressing VEGF188 or VEGF120 on anti-VEGF therapy.....		149
5.1	Introduction.....	149
5.2	Aim.....	149
5.3	NRP1 KD in fs188 cells does not attenuate solid tumour formation	149
5.4	Effect of NRP1 on fs188 and fs120 tumour growth and response to anti-VEGF treatment 153	
5.5	Fs188 tumours were more necrotic than fs120 tumours.....	157
5.6	Tumour vascular effects of NRP1 modification and anti-VEGF treatment	159
5.7	Effect of NRP1 modification and anti-VEGF therapy on vascular morphology	161
5.8	Vascular wall maturity in fs188 and fs120 NRP1 modified tumours	164
5.9	Collagen expression in fs188 NRP1 KD and fs120 NRP1 OE tumours	167
5.10	Discussion.....	170
Chapter 6 General Discussion and Future work.....		180
6.1	Why look at VEGF isoforms and NRP1 in cancer?	180
6.2	Influence of NRP1 expression with single VEGF isoforms <i>in vitro</i>	181
6.2.1	<i>In vitro</i> Migration	182
6.2.2	<i>In vitro</i> Signalling.....	184
6.3	NRP1 modification in fs cells results in smaller tumours <i>in vivo</i>	185
6.4	Fibrosarcoma sensitivity to B20-4.1.1 following NRP1 modification	187
6.5	Conclusions.....	189
6.6	Lessons learned and future work	193
Chapter 7 Bibliography		195

List of Figures

Figure 1.1 Sprouting angiogenesis	4
Figure 1.2 VEGFR activation	12
Figure 1.3 VEGF isoforms as a result of alternative splicing	15
Figure 1.4 NRP1 ligands and co-receptors	21
Figure 1.5 Neuropilin-1 Structure	23
Figure 1.6 Proposed VEGFR2 and NRP1 interactions between endothelial and tumour cells	29
Figure 1.7 Mode of action of FDA approved anti-angiogenic drugs targeting the VEGF axis.....	37
Figure 2.1 Fibrosarcoma morphology	63
Figure 2.2 Image J wound-healing analysis.....	68
Figure 2.3 Western blotting sandwich setup	71
Figure 2.4 Chemiluminescent detection of proteins.....	72
Figure 2.5 pSpCas9n(BB)-2A-GFP plasmid map and verification	79
Figure 2.6 sgRNAs targeting NRP1	80
Figure 2.7 Construction of pCLIIP-NRP1-eGFP vector for NRP1 overexpression.....	85
Figure 2.8 FACSCaliber™ settings and gating of fs cells and GFP positive cell populations.....	91
Figure 2.9 Analysis of necrosis in H & E stained tissue sections	96
Figure 2.10 CD31 staining example.....	99
Figure 3.1 NRP1 expression in fibrosarcoma cells	103
Figure 3.2 NRP1 siRNA KD in fswt and fs188 cells	105
Figure 3.3 NRP1 KD in fs188 and fswt cells with alternative siRNA.....	106
Figure 3.4 NRP2 expression in NRP1 KD cells	107
Figure 3.5 Expression of associated receptors and fibronectin following NRP1 siRNA1 KD in fswt and fs188 cells.....	109
Figure 3.6 ERK1/2 phosphorylation in NRP1 KD cells	111
Figure 3.7 Effect of NRP1 KD on fswt and fs188 cell adhesion	113
Figure 3.8 Migration of fs188 and fswt cells following NRP1 KD.....	115
Figure 4.1 Schematic of Cas9 and Cas9n induced DSB	123
Figure 4.2 KD of NRP1 protein expression using CRISPR/Cas9n in pools of fs188 cells transfected with three sgRNA pairs targeting the NRP1 gene	126
Figure 4.3 Evaluation of NRP1 protein expression in fs188 clones transfected with CRISPR/Cas9n and sgRNA1, sgRNA2 or sgRNA3.....	127
Figure 4.4 Fs188 NRP1 KD clones taken forward for <i>in vivo</i> studies	129

Figure 4.5 The <i>piggyBac</i> transposon overexpression system	131
Figure 4.6 Fs120 and fs164 NRP1 overexpressing clones	133
Figure 4.7 Migration of fs188 NRP1 KD cells	135
Figure 4.8 Migration of fs164 NRP1 overexpressing cells.....	136
Figure 4.9 Migration of fs120 NRP1 overexpressing cells.....	137
Figure 4.10 Expression levels of cMET and downstream signalling proteins in NRP1 modified fs188 and fs120 cells.....	141
Figure 4.11 Effect of exogenous HGF on fs188 cells.....	142
Figure 4.12 Effect of exogenous HGF on fs120 cells.....	143
Figure 5.1 Fs188wt and fs188 NRP1 KD tumour growth curves.....	151
Figure 5.2 Fs188wt and fs188 NRP1 KD pilot experiment tumour vascularity.....	152
Figure 5.3 Growth of fs188 and fs120 tumours with modified NRP1 expression receiving anti-VEGF treatment.....	155
Figure 5.4 Response of fs188 and fs120 tumours with modified NRP1 expression to anti-VEGF treatment.....	156
Figure 5.5 Tumours expressing VEGF188 are more necrotic than those expressing VEGF120.....	158
Figure 5.6 Anti-VEGF treatment reduces vascular density in tumours expressing VEGF188 but not VEGF120.....	160
Figure 5.7 Vessel morphology in NRP1 modified fs188 and fs120 tumours following B20-4.1.1 treatment.....	162
Figure 5.8 Fs188 and fs120 NRP1 modified tumour vascularity following treatment with B20-4.1.1 or control IgG.....	163
Figure 5.9 Vascular wall maturity in fs188 and fs120 NRP1 modified tumours	166
Figure 5.10 Collagen expression in fs188 and fs120 NRP1 modified tumours	169
Figure S1. Effect of fibronectin concentration on adhesion of fs188 and fswt cells with and without NRP1 KD.....	222
Figure S2. Ki67 staining of untreated VEGF188 and VEGF120 expressing tumours.....	223

List of Tables

Table 1.1 FDA approved angiogenesis inhibitors targeting the VEGF axis inhibitors currently in the clinic	36
Table 1.2 Clinical trials with VDAs	41
Table 1.3 Anti-angiogenic agents with activity in STS	47
Table 2.1 Cell lines and their culture medium requirements	61
Table 2.2 NRP1 and control siRNAs	65
Table 2.3 GoTaq G2 PCR mastermix	76
Table 2.4 sgRNA ligation mastermix	81
Table 2.5 Q5 [®] High-Fidelity DNA polymerase PCR mastermix	86
Table 2.6 In-Fusion [®] Cloning Reaction	88
Table 4.1 Transfection efficiency using TransIT-X2 [®] , Lipofectamine [®] and FuGene 6 [®] in fs188 cells.	125
Table 4.2 Population doubling times of fs188wt, fs188 NRP1 KD cells, fs120wt and fs120 OE cells grown on plastic	138
Table 5.1 Vascular associated α SMA staining scoring	165
Table 5.2 Collagen scoring in untreated fs tumours	168
Table 6.1 Summary of <i>in vitro</i> results	191
Table 6.2 Summary of <i>in vivo</i> results	192

List of abbreviations

Abbreviation	Definition
α SMA	α -Smooth muscle actin
AA (aa)	Amino acid
ABC	Avidin-biotin complex
ABL	Abelson murine leukemia viral oncogene homolog
ALK	Anaplastic lymphoma kinase
Ang-1	Angiopoietin-1
Ang-2	Angiopoietin-2
ANOVA	Analysis of variance
ARHGAP17	Rho GTPase Activating Protein 17
AS	Angiosarcoma
ASPS	Alveolar soft part sarcoma
ATP	Adenosine triphosphate
BC	Breast cancer
BCR	Breakpoint cluster region
bFGF	Basic fibroblast growth factor
BLAST	The Basic Local Alignment Search Tool
BMC	Basement membrane protein complex
bp	Base pairs
BSA	Bovine serum albumin
CAF	Cancer associated fibroblast
Cas9	CRISPR-associated 9
Cas9n	CRISPR-associated 9 nickase
CD	Cluster of differentiation
Cdc42	Cell division control protein 42
CDK	Cyclin-dependent kinase
cDNA	Complimentary DNA
CEB	Cell extraction buffer
CendR	C-end rule
cMET	MNNG HOS transforming gene
Conc.	Concentration
CRISPR	Clustered regulatory interspaced short palindromic repeat
crRNA	CRISPR-derived ribonucleic acids
DABA	3,3'-diaminobenzidine
DFS	Disease free survival
DII1	Delta-like ligand 1
DII4	Delta-like ligand 4
DMEM	Dulbecco's modified eagle's medium
DNA	Deoxyribonucleic acid
dNTP	Deoxynucleoside triphosphate
DPBS	Dulbecco's phosphate buffered saline
DR	Direct repeats

Abbreviation	Definition
DSB	Double-stranded break
dsRNA	Double-stranded ribonucleic acid
DSS	Distal splice site
DTT	Dithiothreitol
<i>E. Coli</i>	<i>Escherichia coli</i>
EBM	Endothelial basal medium
EC	Endothelial cell
ECL	Enhanced chemiluminescence
ECM	Extra cellular matrix
EDTA	Ethylenediaminetetraacetic acid
EGF	Epidermal growth factor
eGFP	Enhanced green fluorescent protein
EGFR	Epidermal growth factor receptor
EHS	Engelbreth-Holm-Swarm tumor
EMA	European Medicines Agency
EMT	Endothelial to mesenchymal transition
EPCs	Endothelial progenitor cells
ERG	ETS related gene
ERK	Extracellular signal-regulated kinase
ESC	Embryonic stem cell
ETS	Erythroblast transformation specific
FACS	Fluorescence-activated cell sorting
FAK	Focal adhesion kinase
FBS	Fetal bovine serum
FCS	Fetal calf serum
FDA	Federal Drug Agency
FFPE	Formalin fixed paraffin embedded
FGF	Fibroblast growth factor
FGFR	Fibroblast growth factor receptor
FOLFIRI	Folinic acid, 5-fluorouracil and irinotecan
FOLFOX	Folinic acid, fluorouracil, and oxaliplatin
Fs	Fibrosarcoma
Fs120	Fibrosarcoma 120
Fs120wt	Fibrosarcoma wild type
Fs164	Fibrosarcoma 164
Fs188	Fibrosarcoma 188
Fs188wt	Fibrosarcoma 188 wild type
FSC	Forward scatter
Fswt	Fibrosarcoma wild type
GAC	Gastric cancer
GBM	Glioblastoma multiforme
GIPC1	G alpha interacting protein C terminus 1
GIST	Gastrointestinal stromal tumours

Abbreviation	Definition
GOI	Gene of interest
h	Hours
HBSS	Hank's Balanced Salt Solution
HCC	Hepatocellular carcinoma
HDMEC	Human dermal microvascular ECs
HDR	Homology directed repair
HER2	Human epidermal growth factor-2
HGF	Hepatocyte growth factor
HIER	Heat-Induced epitope retrieval
HIF-1	Hypoxia-inducible factor-1
HRP	Horseradish peroxidase
HSC	Hepatic stellate cells
HSPG	Heparin sulphate proteoglycan
HUAEC	Human umbilical arterial endothelial cells
HUVEC	Human umbilical vein endothelial cells
IAG	Intussusceptive arborisation
IBR	Intussusceptive branch remodelling
IF	Immunofluorescence
IL	Interleukin
IFP	Interstitial fluid pressure
IgG	Immunoglobulin
IHC	Immunohistochemistry
IMG	Intussusceptive microvascular growth
IMS	Industrial methylated spirit
IMT	Inflammatory myofibroblastic tumours
Indels	Insertion or deletion mutations
IP	Intraperitoneal injection
ITR	Inverted terminal repeats
JAG-1	Jagged-1
JAG-2	Jagged-2
KD	Knockdown
KO	Knockout
LDS	Lithium dodecylsulfate
LMS	Leiomyosarcoma
LS	Luciferase-2
mA	Milliamps
mAb	Monoclonal antibody
MAM	Meprin A5, c μ -phosphatase
MAPK	Mitogen-activated protein kinase
mBC	Metastatic breast cancer
mCRC	Metastatic colorectal cancer
MEF	Mouse embryonic fibroblasts
Min	Minute

Abbreviation	Definition
miRNA	Micro ribonucleic acid
MOM	Mouse on mouse
mRCC	metastatic renal cell carcinoma
mRNA	Messenger ribonucleic acid
NB	Neuroblastoma
NF	Nuclease free
NFDM	Non-fat dried milk
NGS	Next generation sequencing
NHEJ	Non-homologous end-joining
non-sil	Non-silencing
NRP	Neuropilin
NRP1	Neuropilin-1
NRP2	Neuropilin-2
ns siRNA	Non-silencing short interfering ribonucleic acid
NSCLC	Non-small cell lung cancer
OE	Overexpression
Oligos	Oligonucleotides
ON	Overnight
Opti-MEM	Opti-modified eagle's medium
ORR	Overall response rate
OS	Overall survival
pAb	Polyclonal antibody
PAE	Porcine aortic endothelial
PAGE	Polyacrylamide gel electrophoresis
PAM	protospacer adjacent motif
PC	Prostate carcinoma
PCR	Polymerase chain reaction
PDAC	Pancreatic ductal adenocarcinoma
PDGF	Platelet-derived growth factor
PDGFR	Platelet derived growth factor receptor
PECAM-1	Platelet endothelial cell adhesion molecule
pERK1/2	Phosphorylated extracellular signal-regulated kinase 1/2
PFS	Progression free survival
PI3K	Phosphatidylinositol 3-kinase
PLCy	Phospholipase Cy
PIGF	Placental growth factor
PIGF2	Placental growth factor-2
PMSF	Phenylmethylsulphonyl fluoride
PMTs	Photomultiplier tubes
pNET	Pancreatic neuroendocrine tumours
PNK	T4 polynucleotide kinase
Ppm	Phosphomolybdic
Ppt	Phosphotungstic

Abbreviation	Definition
pre-crRNA	precursor-ribonucleic acids
PSS	Proximal splice site
pVEGF	Phosphorylated VEGF
RCC	Renal cell carcinoma
RC $\alpha\beta$	Rhodocetin- $\alpha\beta$
RE	Restriction enzyme
RECIST	Response Evaluation Criteria In Solid Tumours
RISC	Ribonucleic acid-induced silencing complex
RNA	Ribonucleic acid
RNAse	Ribonuclease
rpm	Revolutions per minute
RT	Room temperature
RTK	Receptor tyrosine kinase
RT-PCR	Reverse transcriptase-polymerase chain reaction
RT-qPCR	Quantitative reverse transcription polymerase chain reaction
s/c	Subcutaneous
SCID	Severe combined immunodeficient
SDS	Sodium dodecyl sulphate
SEM	Standard error of the mean
Sema3A	Semaphorin-3A
Sema3E	Semaphorin-3E
Sema3F	Semaphorin-3F
SFT	Solitary fibrous tumours
sgRNA	short guide ribonucleic acid
shRNA	Short hairpin ribonucleic acid
siRNA	Short interfering ribonucleic acid
SOC	Super optimal broth with catabolite repression
SSC	Side scatter
STAT3	Signal transducer and activator of transcription 3
STS	Soft tissue sarcoma
SV40	Simian virus 40 (large T antigen)
TAE	tris acetate ethylenediaminetetraacetic acid
TBA	Tubulin binding agents
TBST	Tris buffered saline- 0.1% Tween 20
TC	Thyroid cancer
TCGA	The Cancer Genome Atlas
TE	Tris-Ethylenediaminetetraacetic acid
TGF β	Transforming growth factor- β
Tie1	Tie receptor 1
Tie2	Tie receptor 2
TKI	Tyrosine kinase inhibitor
T _m	Primer melting temperature
TME	Tumour microenvironment

Abbreviation	Definition
tracrRNA	<i>trans</i> -activating ribonucleic acids
Tyr	Tyrosine
UMTCC	Urothelial metastatic transitional cell cancer
VDA	Vascular disrupting agent
VEGF	Vascular endothelial growth factor A
VEGF-B	Vascular endothelial growth factor B
VEGF-C	Vascular endothelial growth factor C
VEGF-D	Vascular endothelial growth factor D
VEGF-E	Vascular endothelial growth factor E
VEGF-F	Vascular endothelial growth factor F
VEGFR	Vascular endothelial growth factor receptor
VEGFR1	Vascular endothelial growth factor receptor 1
VEGFR2	Vascular endothelial growth factor receptor 2
VEGFR3	Vascular endothelial growth factor receptor 3
VPF	Vascular permeability factor
WHO	The World Health Organisation
WT (wt)	Wild-type

Chapter 1

Introduction

An increasing number of anti-angiogenic cancer therapies, which aim to inhibit the vascular endothelial growth factor (VEGF) pathway, have gained FDA approval in the treatment of a variety of different cancers. Anti-angiogenic drugs have changed the landscape in targeted therapy for many patients, yet the efficacy of VEGF inhibitors between patients varies wildly; in some patients, these agents are extremely effective whereas in others there is little to no response and resistance is inevitable. Improved technologies such as whole genome sequencing have accelerated the shift towards stratified medicine in cancer treatment. Thus identification of patients that would gain clinical benefit from anti-VEGF therapeutics has brought the development of validated biomarkers to the forefront of the anti-angiogenesis field.

During retrospective biomarker analysis of clinical trials in cancers where anti-angiogenic therapies have been approved for use, neuropilin-1 (NRP1), a co-receptor for VEGF, and individual VEGF isoforms were identified as potential biomarkers in response to VEGF targeted therapy. There are therefore grounds to elucidate the, as yet unknown, mechanistic links between NRP1 and VEGF isoforms and evaluate their potential as predictive biomarkers.

To understand the complexities and challenges involved with predictive biomarker elucidation for anti-VEGF therapies this chapter will first outline both physiological and pathological angiogenesis. It will then go on to discuss the involvement of VEGF and NRP1 in these processes and the current clinical position of anti-VEGF treatment. Finally, it will summarise the role of angiogenesis in soft tissue sarcoma (STS) and the current treatments available before focussing on the challenges faced with anti-VEGF therapies in the clinic and biomarker evaluation.

1.1 Developmental angiogenesis

In the developing embryo, blood vessels are formed *de novo* by endothelial precursor cells (EPCs), also known as angioblasts, during the process of vasculogenesis. This initial network of vessels, called the primary capillary plexus, provides a scaffold for angiogenesis, which is the formation and remodelling of blood vessel networks from the pre-existing vasculature (Risau, 1997). Angiogenesis is a tightly

regulated process which, under normal physiological conditions, becomes quiescent after embryonic and perinatal development. In adulthood, angiogenesis is only reactivated transiently in response to events such as injured tissue repair and in the female reproductive system. Sustained and uncontrolled reactivation of angiogenesis is a common feature in pathological conditions such as diabetic retinopathy and cancer (Klagsbrun and D'amore, 1991). In pathological angiogenesis, tissue hypoxia and/or nutrient deprivation trigger an angiogenic response that is characterised by the lack of a resolution phase (Fagiani and Christofori, 2013). Angiogenesis is a complex process involving a number of different cell types and the extracellular matrix (ECM) working in concert with various cytokines and growth factors. Angiogenic stimuli activate endothelial cells (ECs) that line the blood vessels; these activated ECs go on to achieve the highly dynamic process of vascular network construction by exhibiting a diverse range of gene expression profiles and a plethora of functional properties (Adams and Alitalo, 2007). Penetration of avascular tissues relies on the interaction of endothelial and mural cells with the ECM and the vascular basement membrane.

Angiogenesis occurs mainly via two distinct mechanisms, sprouting angiogenesis or intussusceptive angiogenesis (Burri and Tarek, 1990). Sprouting angiogenesis relies on EC proliferation whereas intussusceptive angiogenesis is reliant on the internal division of capillaries and EC redistribution (Djonov *et al.*, 2000).

1.1.1 Sprouting angiogenesis

Initiation of vessel sprouting requires the differentiation of ECs into three subtypes; polarised and migratory 'tip cells' that lead the vessel sprout, proliferating 'stalk cells' that form the vessel lumen and quiescent 'phalanx' cells that line the new vessels. This phenotypic specialisation is both reversible and transient, and is dependent on a tightly regulated balance of proangiogenic and angiostatic factors (Gerhardt *et al.*, 2003, Zecchin *et al.*, 2017). An imbalance of these factors leads to an 'angiogenic switch' being activated and new vessel sprouts are formed through the activation of previously quiescent ECs. A key orchestrator in this process is vascular endothelial growth factor A (VEGFA, referred to from hereon in as VEGF). VEGF biology will be discussed in further detail in a subsequent section. In addition to the VEGF pathway, the fate of mature ECs is regulated by signalling through Notch pathway receptors (Notch-1, Notch-3 and Notch-4) and associated ligands, Delta-like ligand 1 (Dll1), Delta-like ligand 4 (Dll4), Jagged-1 (JAG-1) and Jagged-2 (JAG-2). Fibroblast growth factors (FGFs) and angiopoietins, secreted either by the ECs themselves or by stromal cells, also play key roles in the process (Fagiani and Christofori, 2013).

In a process that is driven by hypoxia-dependent proangiogenic signals, ECs exposed to high concentrations of VEGF at the angiogenic front differentiate into tip cells. Tip cells migrate up the VEGF gradient, developing long filopodia, recruiting mural cells, invading the ECM and sensing the surrounding environment for guidance cues. VEGF activation of its cognate receptor, VEGF receptor 2 (VEGFR2), on tip cells activates a signalling cascade that upregulates Dll4 expression which in turn acts on adjacent ECs. The role of VEGFRs will be explored in more detail in subsequent sections (See section 1.3.2). Dll4 activation of Notch downregulates VEGFR2, VEGF receptor 3 (VEGFR3) and the VEGFR2 co-receptor neuropilin-1 whilst simultaneously upregulating VEGF receptor 1 (VEGFR1) expression which acts as a VEGF trap. Subsequently, Notch signalling predominates and promotes the stalk cell phenotype. Stalk cells proliferate in response to VEGF, creating the vessel lumen, synthesising a basement membrane and incorporating pericytes and vascular smooth muscle cells that have been recruited by tip cells (Potente *et al.*, 2011, Ribatti and Crivellato, 2012, Siemerink *et al.*, 2013, Zecchin *et al.*, 2017). Stalk cells express high levels of proangiogenic JAG-1, this antagonist of Dll4 dampens Dll4-Notch signalling in neighbouring tip cells and sustains VEGF receptor expression at the vascular front (Benedito *et al.*, 2009). Vessel loops are formed by the fusion of tip cells with cells in neighbouring vessel sprouts. Vascular anastomosis is promoted at vessel branches by localisation of macrophages expressing VEGFC, which prompts VEGFR3 activation together with tip cell expression of Dll4 (Fagiani and Christofori, 2013, Zecchin *et al.*, 2017).

Tie receptors 1 and 2 (Tie1 and Tie2) are receptor tyrosine kinase (RTKs) expressed almost exclusively by ECs, and are indispensable during developmental angiogenesis and vessel maturation. Angiopoietin-1 and -2 (Ang-1 and Ang-2) are growth factors that are essential for the secondary stages of vascular network formation and are natural ligands for Tie2 (Thomas and Augustin, 2009). Activation of Tie2 by angiopoietins promotes EC sprouting, migration and survival. Conversely, Tie1 does not bind Ang-1 or -2 and is considered an orphan receptor (Mueller and Kontos, 2016). This said, Tie1 has been suggested to play a role in regulation of vascular integrity and EC survival (Kontos *et al.*, 2002) and has been shown to differentially regulate Tie2 activity in tip and stalk cells. In tip cells, EC expression of Tie1 negatively regulates Tie2 and contributes to tip cell morphology, whilst in stalk cells, Tie1 interacts with Tie2 to sustain Tie2 signalling and support stalk cell remodelling (Savant *et al.*, 2015). Ang-1 is vital to vessel maturation; it is primarily expressed by mesenchymal cells, acting in a paracrine manner, it mediates EC migration, survival and adhesion. Whereas, under physiological conditions, Ang-2 is almost solely expressed by EC cells, thus acting in autocrine manner. Upregulated by hypoxia, Ang-2 is expressed during vascular remodelling and promotes neo-vascularisation alongside VEGF (Thomas and Augustin, 2009, Fagiani and Christofori, 2013).

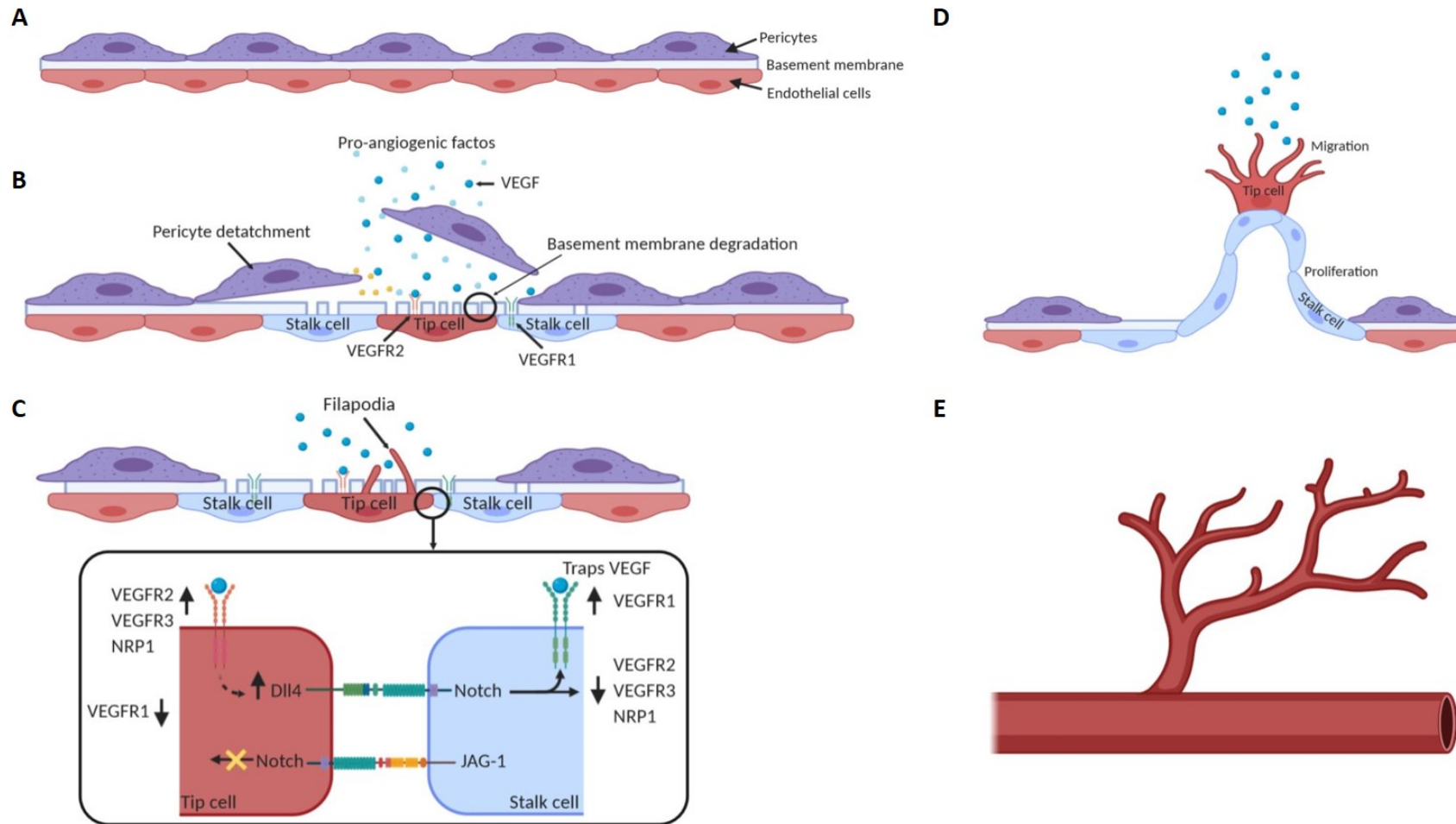


Figure 1.1 Sprouting angiogenesis

A) Quiescent blood vessel. B) Proangiogenic signals, such as VEGF, promote pericyte detachment and basement membrane degradation. C) ECs differentiate into tip and stalk cells depending on exposure to VEGF. D) Tip cells develop filapodia and migrate up the VEGF gradient. Stalk cells proliferate and synthesise basement membrane. E) Mature vessels result in a new vascular network.

1.1.2 Intussusceptive angiogenesis

Intussusceptive angiogenesis is essentially the formation of transluminal tissue pillars, the outcome of which depends on the frequency, location and timing of pillar development. It can be divided into three main phases; intussusceptive microvascular growth (Connolly *et al.*, 1989), intussusceptive arborisation (IAG) and intussusceptive branch remodelling (IBR) (Djonov *et al.*, 2002). During organ development these phases initially occur in tandem and in later development become independent of one another (Makanya *et al.*, 2009). IMG is expansion of the primary capillary plexus in both complexity and size. IAR formation of vascular trees and IBR refers to vessel remodelling and pruning at branching points of small arteries and veins (Burri *et al.*, 2004).

1.2 Tumour vascularisation

The most common way in which tumours establish their own microcirculation is through sprouting angiogenesis. However, increasing evidence supports alternative mechanisms of tumour vascularisation that are non-angiogenic. Moreover, vascularised tumours may also exhibit a mix of both angiogenic and non-angiogenic regions and metastatic lesions from primary sites may differ in their vascularisation mechanisms.

1.2.1 Tumour angiogenesis

In the late 1930s it was suggested that tumours release specific factors to stimulate blood vessel growth, and in 1941 Harry Green observed that although transplanted tumours were still viable, they failed to grow or develop blood vessels. It was not until 1963, when Folkman and Becker presented the first evidence that tumours were unable to exceed 1-2mm³ without neovascularisation, that the concept of tumours requiring their own vasculature for growth was explored (Folkman *et al.*, 1963). These findings led to the seminal article by Folkman in 1971 that hypothesised the therapeutic potential for targeting tumour angiogenesis by targeting factors produced by tumour cells (Folkman, 1971). Since publication of the landmark paper 'The Hallmarks of Cancer' in 2000 (Hanahan and Weinberg, 2000) and in the subsequently updated 'Hallmarks of Cancer: The Next Generation' (Hanahan and Weinberg, 2011), alongside other factors such as avoiding immune destruction, resistance to cell death, sustaining proliferative signalling and evasion of growth suppressors, to name but a few, sustained angiogenesis has been regarded as a prerequisite for tumour progression.

As a tumour reaches 1-2mm³ in size, its demand for oxygen, alongside nutrient and metabolite exchange, exceeds the capacity of local vessel supply (Folkman, 1971). Tumours that are located more than 100-200 µm from capillaries are often exposed to hypoxic conditions as a result of the limited diffusion distance of oxygen (Thomlinson and Gray, 1955). Under these conditions and in the absence of adequate vascular support, tumour growth is restricted. Tumours may remain dormant or become necrotic, therefore angiogenesis plays a pivotal and rate-limiting role in their progression (Naoyo *et al.*, 2006). To meet the increasing demands of the tumour, chronic and sustained angiogenesis is activated. The result is vascular remodelling and abnormal vessel growth that supports tumour growth and facilitates metastases to distal sites (Chung and Ferrara, 2011).

Normal tissue microvascular networks have evenly distributed, mature vessels that allow adequate perfusion of oxygen and metabolites. The tumour vasculature is fundamentally different from this, and is typified by a network of immature, hyperpermeable and structurally chaotic vessels. This anarchic vasculature consists of leaky vessels with inconsistent diameters and blind ends that give rise to a disrupted, erratic blood flow and altered interstitial fluid pressure (IFP). The immature nature of the tumour vessels is characterised by poor pericyte coverage, an abnormal basement membrane and a disrupted EC lining (Siemann, 2011).

Adaptive metabolic changes by tumour cells, such as elevated glycolysis, enables utilization of glucose to generate ATP even under severe hypoxia, allowing them to survive and proliferate under conditions that are ordinarily toxic to normal cells (Chiche *et al.*, 2010). The hypoxic conditions within the tumour and the tumour microenvironment as a result of increased metabolic demands and compromised blood flow increases the expression of the transcription factor hypoxia-inducible factor-1 (HIF-1). Elevated HIF-1 triggers a cascade of signalling events leading to the upregulation of proangiogenic factors, ultimately resulting in the activation of the angiogenic switch. Key players in this cascade are members of the VEGF family and other growth factors such as hepatocyte growth factor (HGF), basic fibroblast growth factor (bFGF), platelet-derived growth factor (PDGF) and epidermal growth factor (EGF) and the angiopoietins. The tortuous, heterogeneously perfused blood vessels that arise from the ensuing hypervascularisation further exacerbates the hypoxic conditions of the tumour microenvironment, thus sustaining expression of proangiogenic factors (Papetti and Herman, 2002, Bergers and Benjamin, 2003).

1.2.2 Vascular mimicry

In a process referred to as vascular mimicry, highly invasive tumour cells are capable of forming vascular channels comprising of basement membrane and devoid of ECs and fibroblasts (Maniotis *et al.*, 1999). During the early phases of tumour growth, this perfused microcirculation created by aggressive tumour cells, appears to be able to integrate with pre-existing vessels whilst maintaining their integrity and without induction of angiogenesis (Folberg *et al.*, 2000).

1.2.3 Vessel co-option

An alternative hypothesis to the accepted dogma of tumour angiogenesis is vessel co-option. Vessel co-option is a non-angiogenic method of tumour vascularisation whereby the pre-existing tissue vasculature is hijacked by tumour cells in order to support tumour growth and dissemination. A recent review by Kuczynski *et al.* (2019) has highlighted that, although evidence for vessel co-option-like processes has been presented by numerous independent investigators in various cancers since the early 1900s, the range of terminology used to describe these processes is in part responsible for the fractured body of literature. Predominantly observed in subgroups of both primary tumours and metastases within well vascularised-tissues such as the brain, lung and liver, tumour cells can hijack the pre-existing vasculature to fulfil their metabolic demands in lieu of angiogenesis. Independent studies in both human and murine models have provided evidence of the processes involved during vessel co-option and have found that it is both tissue context dependant and also cancer subtype dependant (Donnem *et al.*, 2018). A prime example of this is in non-small cell lung cancer (NSCLC), where a number of differing growth patterns of vessel co-option have been described (reviewed in depth by (Kuczynski *et al.*, 2019). These include an 'alveolar pattern', whereby tumour cells fill the alveoli and engulf the alveolar capillaries without destroying them (Pezzella *et al.*, 1997), a 'lepidic pattern' that sees cancer cells replace pneumocytes but ultimately angiogenesis occurs and 'perivascular cuffing' where vessels are co-opted through cancer cells, forming cuffs around existing vessels. In all cases, the preservation and incorporation of both tissue specific vessel morphology and characteristic tissue stromal morphology makes vessel co-option quite distinct from angiogenesis histologically. Moreover, expression markers of non-malignant tissue vessels is maintained, for example co-opted vessels in gliomas can maintain expression of blood brain barrier associated markers (Claes *et al.*, 2007) and lung co-opted vessels have been shown to stain positively for the alveolar wall vascular basement membrane marker LH39 (Passalidou *et al.*, 2002). In the liver, the vessel co-option process is similar to that seen during 'lepidic pattern' of co-option in NSCLC; in this tissue, hepatocytes are replaced by neoplastic cells and the sinusoidal vessels are co-opted (Stessels *et al.*, 2004). In gliomas however, it is the 'perivascular cuffing' pattern that predominates, other

patterns of vascularisation have been identified, whether or not these are purely non-angiogenic is based on conjecture (Carbonell *et al.*, 2009).

Current opinion appears to suggest that only a small minority of tumours are purely non-angiogenic, and that where vessel co-option does occur, to a varying degree, it is accompanied by angiogenesis (Donnem *et al.*, 2018, Kuczynski *et al.*, 2019).

1.2.4 Tumour vasculogenesis

Up until the late 1990s it had been assumed that the additional ECs required during postnatal neovascularisation arose from the division and proliferation of local ECs. However, this assumption was challenged by evidence of bone-marrow derived endothelial progenitor cells (EPCs), also referred to as hemangioblasts, that held the capacity to differentiate into ECs both *in vitro* and *in vivo* (Asahara *et al.*, 1997, Lin *et al.*, 2000). Subsequently, Lyden *et al.* (2001) presented evidence, using angiogenesis-defective mice, that EPCs could participate in tumour neovascularisation. EPCs home in on sites undergoing vascular repair/angiogenesis and integrate with damaged vessels either through activation of local ECs or by differentiation into mature ECs (Real *et al.*, 2008). Recruitment of bone-marrow derived cells is initiated via tumour-associated paracrine signalling by growth factors, cytokines and hypoxia-related pathways. VEGF recruits VEGFR2⁺ EPCs (Ribatti, 2004, Kopp *et al.*, 2006), ECs within the tumour-induced stroma overexpress CC cytokines that recruit CCR2⁺ and CCR5⁺ EPCs (Spring *et al.*, 2005) and adiponectin induces EPC migration via the PI3-kinase/Cdc42/Rac1 pathway (Nakamura *et al.*, 2009).

In addition to the classical EPCs, a number of other cell populations have been identified as contributing to vasculogenesis, inclusive of infiltrating neutrophils, CD11b⁺ myeloid cells, F4/80 CD11b⁺ tumour-associated macrophages (TAMs) and Tie2⁺ monocytes (Calzi *et al.*, 2010). To what extent each of these populations support tumour vasculogenesis, or if indeed they do at all, is still up for debate.

1.3 Vascular endothelial growth factor (VEGF)

1.3.1 An introduction to VEGF

In 1979 Dvorak *et al.* identified a molecule secreted in tumour cell supernatants that induced vascular permeability, which they (unimaginatively) named vascular permeability factor (VPF). In 1989, independently of one another, researchers at Monsanto Company, Connolly *et al.* and Napoleone

Ferrara's group published back to back articles demonstrating that VPF was a potent EC specific mitogen. Ferrara's group, cloned the gene for this factor which was named VEGF (Leung *et al.*, 1989), and it is this name that was adopted by the scientific community for what is now widely regarded as the principal regulator in both physiological and pathological angiogenesis and vascular permeability. Subsequent studies have identified VEGF as an important cytokine not only for ECs, but also for neural cells, fibroblasts and cells that participate in immune responses (Senger, 2010). Although research has mainly focussed on the function of VEGF with regard to vascular permeability, angiogenesis and lymphangiogenesis, it is now apparent that VEGF has a broader spectrum of functions within the tumour microenvironment, acting on both tumour and stromal cells (Goel and Mercurio, 2013).

VEGF-A (referred to as VEGF) is the prototypical member of a family of growth factors that consists of several related proteins: VEGF-B, VEGF-C, VEGF-D, placental growth factor (PlGF), virally encoded VEGF-E and snake-venom derived VEGF-F (Olsson *et al.*, 2006). Commonly referred to as the 'VEGF family', this collection of related growth factors exhibit differential expression patterns and receptor specificity and subsequently elicit distinct biological functions (Koch *et al.*, 2011). Three structurally related VEGF receptor tyrosine kinases, VEGFR1 (Flt-1), VEGFR2 (KDR/Flk-1), VEGFR3 (Flt-4) and two non RTKs, NRP1 and NRP2, have so far been identified as receptors for VEGF; each of which play discrete roles in VEGF signalling (Figure 1.1) (Ferrara *et al.*, 2003).

VEGF is expressed at high levels by virtually all malignant tumour cells and is released by an array of cells within the tumour microenvironment (TME), including cancer associated fibroblasts (CAFs), macrophages, pericytes, neutrophils and ECs. As a result of this, VEGF is widely accepted as being the one of most important, if not the most important factor during tumour angiogenesis (Carmeliet and Jain, 2011, Peach *et al.*, 2018). VEGF secreted by tumour cells and cells in the TME triggers EC migration and proliferation and enhances vascular permeability; the result is the surrounding blood vessels becoming leaky and inefficient, thus exacerbating and sustaining hypoxia and continued VEGF secretion, ultimately leading to tumour progression (Yancopoulos *et al.*, 2000). Positive correlation of tumour vascularity and high VEGF expression are widely documented and this upregulation is repeatedly associated with poorer patient prognoses (Goel and Mercurio, 2013).

As touched upon above, VEGF is not only released by tumour cells, but also by additional stromal cells within the TME. Distinct signals within the TME results in the polarisation of TAMs to either an M1 or M2 phenotype (Galdiero *et al.*, 2013). Within a hypoxic TME, TAMs are polarised in favour of the M2 phenotype that is characterised by upregulated expression of a number of pro-angiogenic factors and cytokines, amongst which is VEGF. Furthermore, through the release of interleukin-1 β (IL-1 β), TAMs

stimulate HIF-1 α expression in tumour cells, which in turn upregulates VEGF production by the tumour cells (Werno *et al.*, 2010). Another myeloid cell within the TME that received less attention are tumour-associated neutrophils (TANs). Like TAMs, TANs undergo polarisation that is dependent on conditions within the TME that results in an anti- (N1) or a pro- (N2) tumourigenic phenotype. In terms of their ability to sustain tumour angiogenesis, N2 TANs are another rich source of VEGF within the TME (Fridlender *et al.*, 2009, Jablonska *et al.*, 2010). Up until a study published by Maharaj *et al.* in 2006, it was thought that ECs only expressed VEGF *in vivo* under pathological conditions such as hypoxia, however Lee *et al.* (2007) went on to show that EC survival in non-pathological conditions was reliant on autocrine VEGF signalling, thus cementing ECs as being a prolific source of VEGF within the TME.

1.3.2 VEGF receptors, VEGF binding and signalling

VEGF predominantly acts on vascular ECs, however, the wide expression range of VEGFRs on other cell types such as macrophages, haemopoietic cells, pericytes and fibroblasts as well as tumour cells gives rise to further roles for VEGF outside of angiogenesis (Peach *et al.*, 2018).

VEGFR1 and VEGFR2 are regarded as the primary VEGFRs on ECs and although both are indispensable during vascular morphogenesis, they perform disparate and non-overlapping roles (Fong *et al.*, 1995, Shalaby *et al.*, 1995). VEGF affinity for VEGFR1 is 10-fold higher than for VEGFR2 yet ligand/ receptor binding between VEGF and VEGFR1 only induces weak kinase activity (Chappell *et al.*, 2013), in contrast, VEGF binding to VEGFR2 promotes receptor dimerisation, trans-autophosphorylation, internalisation and ubiquitination. The precise role of VEGFR1 in EC function is less clear, though it is known to have a role as a decoy receptor, thus preventing VEGFR2 signalling and controlling angiogenic sprout formation (Kappas *et al.*, 2008). Therefore, VEGFR2 is regarded as the predominant receptor for VEGF signal transduction on ECs (Fantin *et al.*, 2013). VEGF-C and -D associate with VEGFR3 which is primarily involved in lymphangiogenesis and proteolytic processing of VEGF-C and -D gives rise to isoforms which bind to VEGFR2 (Koch *et al.*, 2011). At present, there is little to no evidence of VEGF binding to VEGFR3 (Goel and Mercurio, 2013).

VEGFR2 signalling is enhanced and stabilised by the formation of an active signalling complex with NRP1 (Parker *et al.*, 2012b). Additionally, VEGFR2 dimerisation in the absence of ligand has been observed using fluorescence resonance energy transfer, however, the signalling induced via non-ligand induced dimerisation results in extremely low levels of receptor phosphorylation (Sarabipour *et al.*, 2016). NRP1 also supports VEGF autocrine signalling independently of VEGFR2 suggesting that

it is able to function alone or in complex with another tyrosine kinase receptors (Bachelder *et al.*, 2001). Following ligand binding, VEGFR2 becomes phosphorylated at multiple tyrosine residues, giving rise to complementary activation of differential functional pathways as summarised in Figure 1.1.

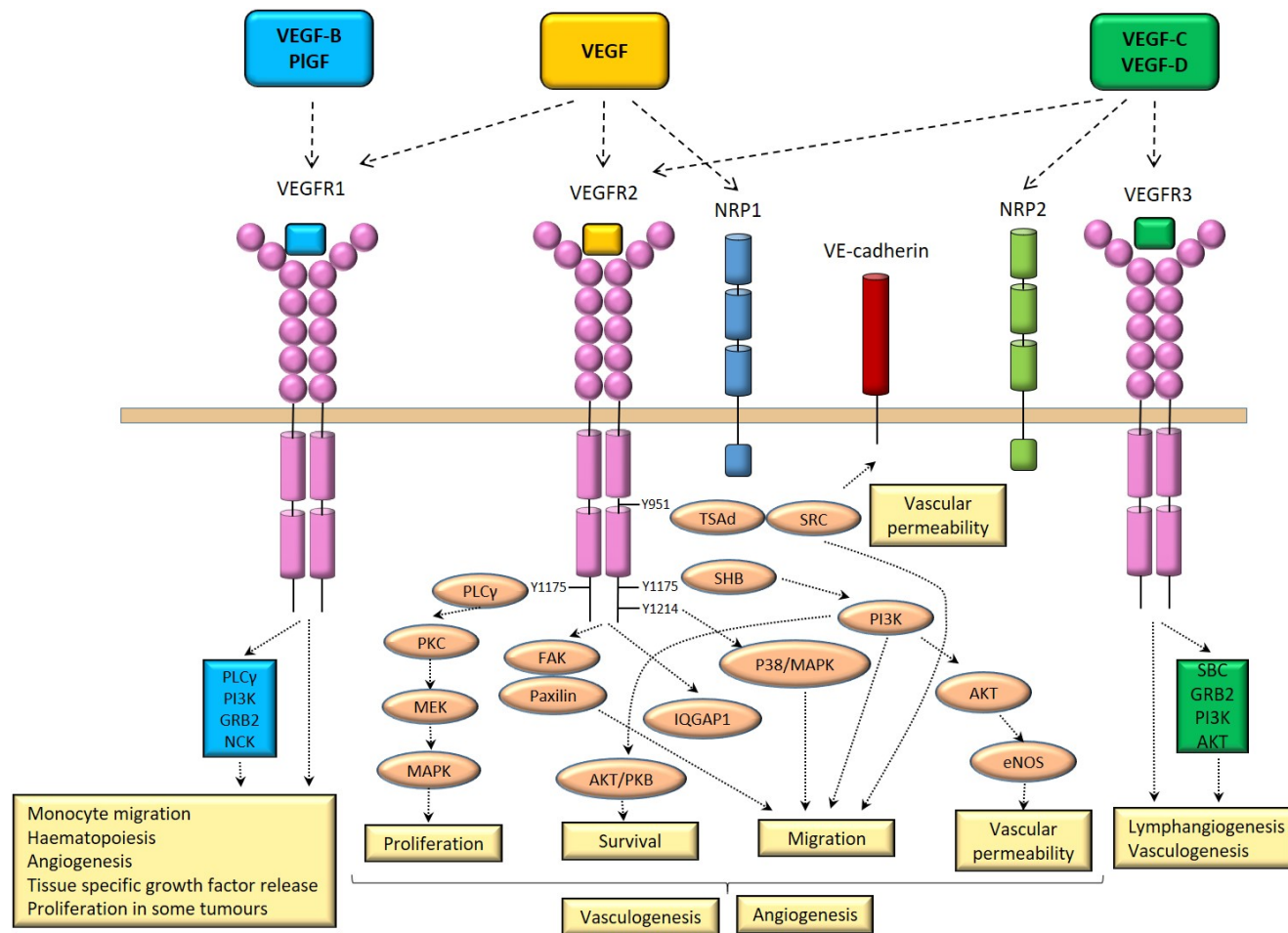


Figure 1.2 VEGFR activation

The VEGF family of growth factors have characteristic receptor binding patterns. VEGF-B & PlGF selectively bind VEGFR1. VEGF binds VEGFR1, VEGFR2 and NRP1, however VEGFR2 is the main VEGF signalling receptor, functioning either homodimerically or through heteroduplexes with NRP1. VEGF-C and -D preferentially bind VEGFR3 during lymphangiogenesis, which is further facilitated through the co-option of NRP2. Proteolytically cleaved VEGF-C and -D can bind and activate VEGFR2. Figure adapted from (Ferrara and Adamis, 2016)

1.3.3 VEGF isoforms

The diversity and complexity of cellular responses elicited by VEGF are largely due to the multitude of VEGF isoforms that arise from either proteolytic processing or alternative splicing of pre-mRNA. Alternative splicing of the 8 exon *VEGFA* gene results in numerous VEGF isoforms ranging from 111 to 206 amino acids in length (Robinson and Stringer, 2001, Mineur *et al.*, 2007, Vempati *et al.*, 2014, Smith *et al.*, 2015). Each isoform exhibits differential expression patterns in normal tissues and in tumours and has distinct properties and functions in normal physiological and tumour angiogenesis (Neufeld *et al.*, 1996, Harper and Bates, 2008, Chen *et al.*, 2010, Vempati *et al.*, 2014). The main human isoforms, and subsequently most widely studied isoforms, are VEGF₁₂₁, VEGF₁₆₅ and VEGF₁₈₉ with VEGF₁₆₅ reported being the most abundant and biologically active (Whitaker *et al.*, 2001, Jia *et al.*, 2006); corresponding murine isoforms are one amino acid shorter (i.e. VEGF₁₂₀, VEGF₁₆₄ and VEGF₁₈₈) but hold the same biological capabilities (Vempati *et al.*, 2014) (Figure 1.2). It is widely thought that VEGF₁₆₅ is the most potent and bioavailable mitogen, largely due to its ability to potentiate VEGFR2 signalling through forming complexes with co-receptor NRP1. Conversely, in the absence of any post-translational modifications, VEGF₁₈₉ exhibits weaker chemoattractant and mitogenic properties (Plouët *et al.*, 1997).

Exons 1-5 are conserved across all isoforms, and encode a cysteine knot domain which is responsible for signalling and mediating homodimerisation, interacting directly with VEGFRs (Parker *et al.*, 2012b). As a consequence of the incorporation or deletion of exons 6 and 7, the various VEGF isoforms exhibit differing affinities for the ECM via their ability to bind heparin sulphate proteoglycan (HSPG) and differential receptor selectivity (Tillo *et al.*, 2015). The omission of exons 6 and 7 in VEGF₁₂₁ results in a freely diffusible, soluble isoform whereas VEGF₁₆₅, which is only devoid of exon 6, is still capable of binding to HSPGs and is therefore partially retained in the ECM (Soker *et al.*, 1998, Gabhann and Popel, 2005).

Although some studies have previously reported the existence of anti-angiogenic VEGF isoforms (denoted VEGF_{xxx}b) in normal human tissue generated through the use of an alternative distal splice site within exon 8 of VEGF (Bates *et al.*, 2002, Nowak *et al.*, 2010, Biselli-Chicote *et al.*, 2012), more recent data provides evidence to the contrary (Harris *et al.*, 2012, Lomet *et al.*, 2018). In these studies, VEGF_{xxx}b could not be identified in mouse, human or sheep tissue. Additionally (Bridgett *et al.*, 2017) presented RNA sequencing data from multiple human tissues that suggest VEGF_{xxx}b to be either non-existent or present at extremely low levels *in vivo*. These data bring into question the existence of anti-angiogenic isoforms and suggest that VEGF_{xxx}b identified in previous studies may have been

artefactual polymerase chain reaction (PCR) products (Harris *et al.*, 2012, Bridgett *et al.*, 2017, Lomet *et al.*, 2018). Studies in support of the existence of anti-angiogenic VEGF_{xxx}b isoforms report them to be highly homologous with their pro-angiogenic counterparts, differing only in their C-terminus (Qiu *et al.*, 2009, Manetti *et al.*, 2011); it is reported that the VEGF_{xxx}b isoforms competitively bind to VEGFRs, yet they fail to activate the angiogenic pathways that pro-angiogenic isoforms facilitate (Nowak *et al.*, 2010). It is generally believed that expression of VEGF_{xxx}b is downregulated in tumour cells (Biselli-Chicote *et al.*, 2012); in renal cell carcinoma for example, downregulation of VEGF_{xxx}b isoforms led to a switch in the level of VEGFR activation and subsequently levels of angiogenic signalling increased (Bates *et al.*, 2002). These conflicting data leaves the existence or role of VEGF_{xxx}b in question, therefore the focus of the subsequent sections will be of the more widely studied and relevant pro-angiogenic VEGF isoforms.

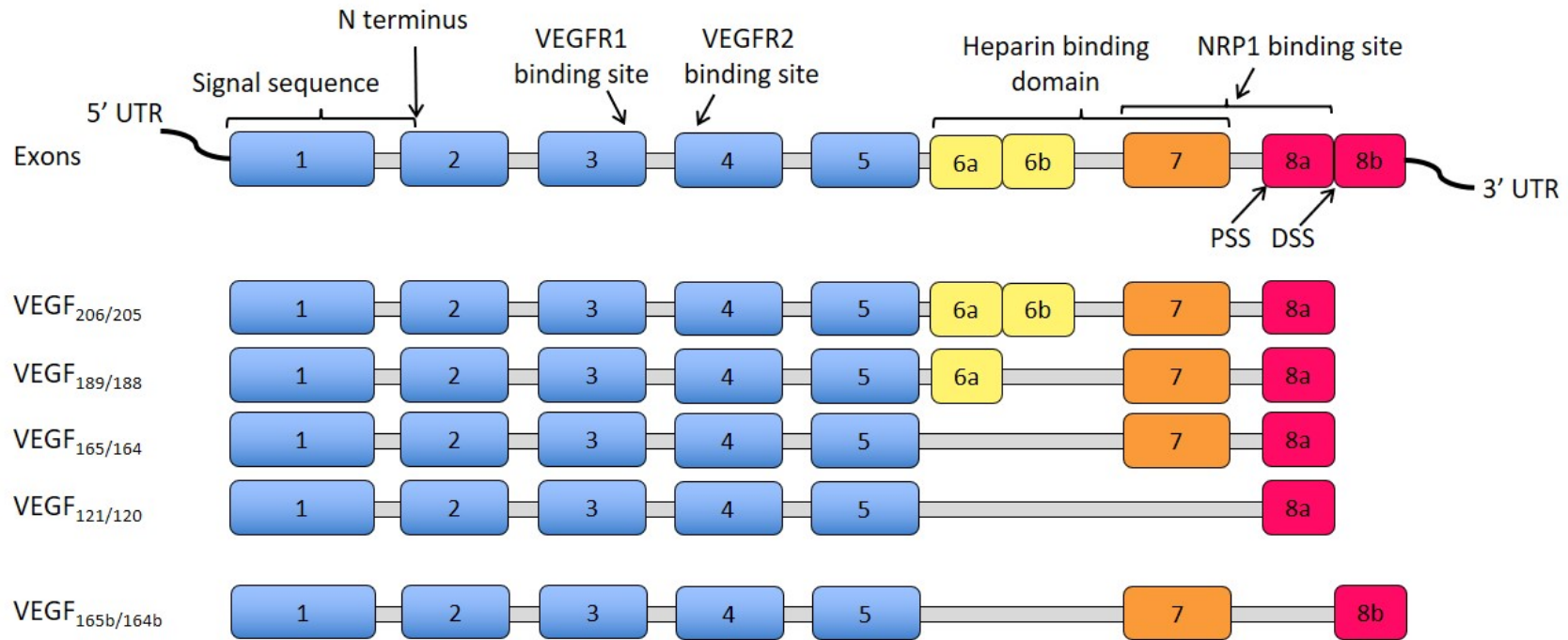


Figure 1.3 VEGF isoforms as a result of alternative splicing

VEGF₁₂₁, VEGF₁₆₅ and VEGF₁₈₉ with VEGF₁₆₅ are the predominant human VEGF isoforms resulting from alternative splicing of the VEGFA gene. Exons 1-5 are conserved across the isoforms. Exon 1 encodes the signal sequence, exon 2 the N-terminal dimerisation domain, exon 3 the VEGFR1 binding and N-glycosylation site and exon 5 the plasmin cleavage site. Exons 6 and 7 encode the heparin binding domain, the inclusion of which impacts on the biological properties of the isoform. The high-affinity NRP1 binding site is encoded by exon 7, exon 8a also participates in NRP1 binding but to a lesser extent. PSS or DSS selection results in isoforms differing in C-terminal domain sequence. Pro-angiogenic isoforms, VEGF_{xxx}, arise from PSS selection whilst anti-angiogenic isoforms, VEGF_{xxx}b, are a product of DSS selection. Proximal splice site (PSS); Distal splice site (DSS)

The mitogenic activity of VEGF relies heavily on its heparin binding, cell surface and receptor binding capabilities. Under hypoxic stress, all three major VEGF isoforms are expressed by tumour cells, however, the bioavailability of VEGF₁₆₄ and VEGF₁₈₈ depends on their release from extracellular heparin sulphate proteoglycans (HSPGs) by heparinase or by proteolytic cleavage. As such, longer ECM bound isoforms act in an autocrine manner to maintain homeostasis, whereas soluble VEGF₁₂₀ and VEGF₁₁₁ act as paracrine signals that create a VEGF gradient and recruit other cell types to promote vessel sprouting in hypoxic areas of tissue, such as in the vicinity of tumours (Guyot and Pagès, 2015, Yamamoto *et al.*, 2016). Given the diffusible nature of VEGF₁₂₀ it is most likely that this isoform functions primarily as a chemoattractant for ECs, whereas VEGF₁₈₈, which is sequestered locally on the cell surface or ECM, works to maintain and stabilise vessels (Ng *et al.*, 2001). Although the mechanisms by which VEGF isoforms elicit their distinct signalling responses in tumour cells remains elusive, studies in ECs have provided valuable insights into the biological consequences of the individual isoforms. Through the promotion of heterodimer formation between VEGFR2 and NRP1, VEGF₁₆₅ enhances vessel branching through p38/ mitogen-activated protein kinase (MAPK) activation whereas the bridging of this complex by VEGF₁₂₁ fails to upregulate the same downstream signalling cascade (Soker *et al.*, 2002, Kawamura *et al.*, 2008, Fantin *et al.*, 2013).

The ratio of VEGF isoform expression varies among adult organs, which is indicative of a role in creating tissue specific vascular networks. In organs that are initially vascularised by vasculogenesis such as the heart, liver and lungs, VEGF₁₈₈ is more abundant, whereas VEGF₁₆₄ and VEGF₁₂₀ predominate in organs vascularised by angiogenesis. Through the deletion of VEGF exons 6 and 7 in embryonic stem cells (ESCs), Carmeliet *et al.* (1999) developed transgenic mice expressing only VEGF₁₂₀ (VEGF^{120/120}). Around half of the VEGF^{120/120} neonates died within a few hours of birth, and those that survived failed to thrive, dying before P14 from myocardial ischemia as a result of incomplete myocardial vessel remodelling and vascular defects. Expression of NRP1 and EC markers Tie2 and VE-cadherin were also significantly reduced in VEGF^{120/120} mice. In addition, through the development of mouse ECs expressing single VEGF isoforms it has been shown that the expression of VEGF₁₂₀ alone is insufficient in driving VEGFR2 activation and accumulation; the result being non-viable homozygous VEGF₁₂₀ embryos and suppressed proliferation in culture (Yamamoto *et al.*, 2016). Vascularisation of major organs in VEGF^{120/120} mice was found to be retarded, again indicating that although VEGF₁₂₀ may support initial vascularisation, it is insufficient to support vessel growth, maturation and remodelling (Ng *et al.*, 2001). Thus, in order for normal angiogenesis to occur, both VEGF₁₆₄ and VEGF₁₈₈ are indispensable. During embryo development, expression of the longer heparin-binding isoforms produced a more stable network of vessels with a narrow branching

morphology, whereas vessels arising from expression of VEGF₁₂₀ alone along were tortuous and leaky, with poor perfusion (Ng *et al.*, 2001). Although VEGF_{120/121} expression alone is insufficient for normal embryo development, mRNA- reverse transcriptase PCR (RT-PCR) data indicates an increase in the relative expression of this isoform in cancers such as breast, colon, lung, ovarian and melanoma (Vempati *et al.*, 2014).

Further to these studies, Tozer *et al.* (2008a) have shown that the tumours arising from fibrosarcoma (fs) cells expressing single VEGF isoforms influence their surrounding vascular architecture. Fs cells exclusively expressing VEGF₁₂₀ develop unstable, immature vessels with poor pericyte coverage whereas fs cells exclusively expressing VEGF₁₈₈ develop a much more structured, less permeable vascular network.

There are 19 phosphorylation sites on the C-terminal tail of VEGFR2. Although the mechanisms are largely still unclear, preferential activation and subsequent downstream signalling events at these sites appear to be largely regulated by specific VEGF isoforms (Chen *et al.*, 2010, Fearnley *et al.*, 2016). Using an *in vitro* EC model Fearnley *et al.* (2016) have shown that binding of VEGF₁₂₀, VEGF₁₄₅ or VEGF₁₆₅ results in isoform-dependent endocytosis, ubiquitination and proteolysis of VEGFR2. Although all three isoforms bind to VEGFR2 with similar affinities, the result is differential programming of the cytoplasmic domain and subsequent post-translational modifications that modify patterns of VEGFR2 trafficking and proteolysis.

1.4 The Neuropilins

The neuropilins are multifaceted, highly conserved, vertebrate-specific, type 1 single-pass transmembrane glycoproteins. Neuropilin (NRP), initially named A5 antigen, was first identified as a neuron-specific receptor in the nervous system of *Xenopus* tadpoles by Takagi *et al.* (1991). Further studies went on to identify NRP as high affinity receptor for the class 3 semaphorins (Sema3). He and Tessier-Lavigne (1997) provided the first evidence of NRP as a component of the receptor complex required to mediate the chemo-repulsive effects of secreted Sema3 (now referred to as Sema3A) in neurons during neural development and axonal guidance. In a concurrent study, a NRP-like protein was identified as a high affinity receptor for semaphorin-E (SemaE) and semaphorin-IV (Sema-IV) (now referred to as Sema3E and Sema3F) but not Sema3A (Chen *et al.*, 1997), thus the original NRP was renamed NRP1 and the newly discovered NRP as NRP2. Since these initial findings, it has been established that the seven members of the secreted Sema3 family (Sema3A-G) signal through receptor complexes comprised of NRP1 or -2 and type A or D plexin respectively (Raimondi and Ruhrberg, 2013). *In vivo* work with neuronal specific Sema3A negative mice has demonstrated a critical role for Sema3A-NRP1 interactions during neuronal development, an interaction that is dispensable in vascular development (Gu and Giraudo, 2013).

In 1998, NRP1 was identified in both tumour and endothelial cells as a co-receptor for members of the VEGF superfamily. Soker *et al.* (1998) identified a central role for NRP1 in the promotion of vessel growth in which it mediated the interactions of VEGF-A, VEGF-B, VEGF-E and PlGF2 and their associated receptors VEGFR1, VEGFR2 and VEGFR3. Subsequently, NRP1 was identified as a major non-tyrosine kinase receptor for VEGF during angiogenesis, acting both independently and as a co-receptor with VEGFR2 (Miao *et al.*, 2000, Murga *et al.*, 2005, Vander Kooi *et al.*, 2007). The significance of VEGF isoforms and NRP1 mediated signalling will be discussed in more depth in subsequent sections. NRP1 was also subsequently shown to be a co-receptor for several other ligands involved in tumour growth in addition to VEGF family members. In this context, NRP1 expressed on tumour cells regulates their growth, survival and migration in an angiogenesis-independent manner. These functions of NRP1 will also be discussed in more detail in section 1.4.6.

Human NRP1 and NRP2 have been mapped to chromosomes 10p12 and 2q34 respectively (Rossignol *et al.*, 1999); both genes contain 16 introns and 17 exons (Figure 1.3). Sharing 44% primary sequence homology, NRP1 and NRP2 are closely structurally related; both are composed of five extracellular domains, a transmembrane domain and a short cytoplasmic tail (Figure 1.3) (Appleton *et al.*, 2007). NRP1 is primarily thought to associate as a homodimer, however, it also forms heterodimers/

oligomers with NRP2 and has the capacity to arrange itself into larger oligomeric structures through interactions mediated by the *c/ meprin A5*, *c μ-phosphatase (MAM)* and transmembrane domains (Cai and Reed, 1999, West *et al.*, 2005, Vander Kooi *et al.*, 2007). The C-terminal SEA motif binds G alpha interacting protein C terminus 1 (GIPC1) and synectin and links NRP1 to the cytoskeleton via myosin IV during receptor internalisation (Valdembri *et al.*, 2009, Yaqoob *et al.*, 2012). The absence of an intracellular kinase domain would suggest that NRPs lack the ability to initiate intracellular signalling cascades independently and thus require recruitment of other RTKs.

1.4.1 Role of NRP1 during development

Through potentiating VEGFR2 signalling, NRP1 drives *in vivo* vessel development by increasing EC motility and vascular permeability, without impacting on cellular proliferation (Peach *et al.*, 2018). NRP1 is vital for normal vascular development and the development of neural patterning (Gu *et al.*, 2003, Herzog *et al.*, 2011). Depletion of NRP1 results in embryonic lethality due to underdeveloped and non-branching blood vessels in the systemic, cardiac and neuronal vasculature, whilst overexpression culminates in excessive blood vessel production and cardiovascular malformation (Gu *et al.*, 2002). More recently, through the generation of a mouse line harbouring a point mutation in the VEGF binding region of the NRP1 locus, that causes disruption of VEGF binding to NRP1 failed to replicate the catastrophic vascular abnormalities seen in EC specific NRP1 knock out models during embryonic development (Gelfand *et al.*, 2014). These data suggest an alternative hypothesis to the currently accepted view of embryonic angiogenesis being dependent on VEGF-NRP1 binding (Pan *et al.*, 2007a) and present the possibility of either an unidentified ligand binding to NRP1 or that VEGF mediated developmental angiogenesis is dependent on the role of NRP1 as a co-receptor with VEGFR2 (Fantin *et al.*, 2014, Gelfand *et al.*, 2014). Gelfand *et al.* (2014) presented *in vivo* evidence indicating that NRP1 regulates VEGF/ VEGFR2 signalling during embryonic angiogenesis via modulating EC surface VEGFR2 presentation, recycling and degradation, which is consistent with previous *in vitro* data. Furthermore, they observed that NRP1 was able to regulate VEGFR2 in the absence of VEGF binding, suggesting the ability of these two receptors to form complexes independently of VEGF-NRP1 binding.

1.4.2 Tissue distribution of the neuropilins

NRP1 and NRP2 are widely expressed in both embryonic and adult tissues, yet they exhibit distinct roles in vascular, lymphatic and neuronal development (Liu *et al.*, 2015). During early embryonic development, NRP1 is expressed on arteries and is associated with angiogenesis whilst NRP2 expression predominates on veins and mediates lymphangiogenesis (Bielenberg *et al.*, 2006, Parker

et al., 2012b). High NRP1 expression is associated with vascular tissues such as the heart and placenta; lung, kidney, and pancreas exhibit moderate expression and relatively low levels are found in the adult brain. Contrastingly, NRP2 expression in adult vasculature is limited to veins and lymphatic cells and is associated with neural-crest derived cells. In terms of pathological conditions, NRP1 expression has been described on a broad range of cells inclusive of multiple tumour cell types, vascular smooth muscle cells, tissue macrophages and a range of neural cells (Jia *et al.*, 2006, Fantin *et al.*, 2013, Jia *et al.*, 2014, Niland and Eble, 2019). In addition to a central role in angiogenesis and tumour growth and invasion, the characterisation of NRP1 expression in subsets of T cells, dendritic cells and B cells has identified a diverse role for this co-receptor in both physiological and pathological immune responses (Roy *et al.*, 2017).

1.4.3 NRP1 binds multiple ligands

NRP1 is an extremely versatile receptor that provides non-overlapping binding sites for numerous ligands, thus ligand binding is not necessarily competitive. In addition to the aforementioned VEGF and Sema3 family, NRP1 interacts with multiple heparin-binding proteins along with other ligands to form ternary complexes with their cognate receptors (Figure 1.3). Currently, PlGF, HGF, EGF, platelet derived growth factor (PDGF)-C and -D, bFGF, transforming growth factor- β (TGF β) have all been identified as growth factors that utilise NRP1 in the formation of co-receptor complexes with their associated receptors. The formation of these supramolecular protein structures modifies downstream signalling cascades and results in alternative biological consequences to canonical receptor activation (Migdal *et al.*, 1998, West *et al.*, 2005, Sulpice *et al.*, 2008, Rizzolio *et al.*, 2012, Guo and Vander Kooi, 2015, Li *et al.*, 2016a). Consequentially, whether NRP1 mediated signalling results in stimulatory or inhibitory signals is reliant on the ligand and recruited RTK, or in the case of TGF β 1, receptor serine kinase.

To further add to the diversification of NRP1 binding ligands, rhodocetin- $\alpha\beta$ (RC $\alpha\beta$), a soluble toxin found in snake venom, has recently been identified as a protein which forms a ternary complex between NRP1 and cMet which is the receptor for HGF that subsequently disrupts cell-matrix interactions in endothelial and tumour cell membranes (Niland *et al.*, 2013, Niland *et al.*, 2018).

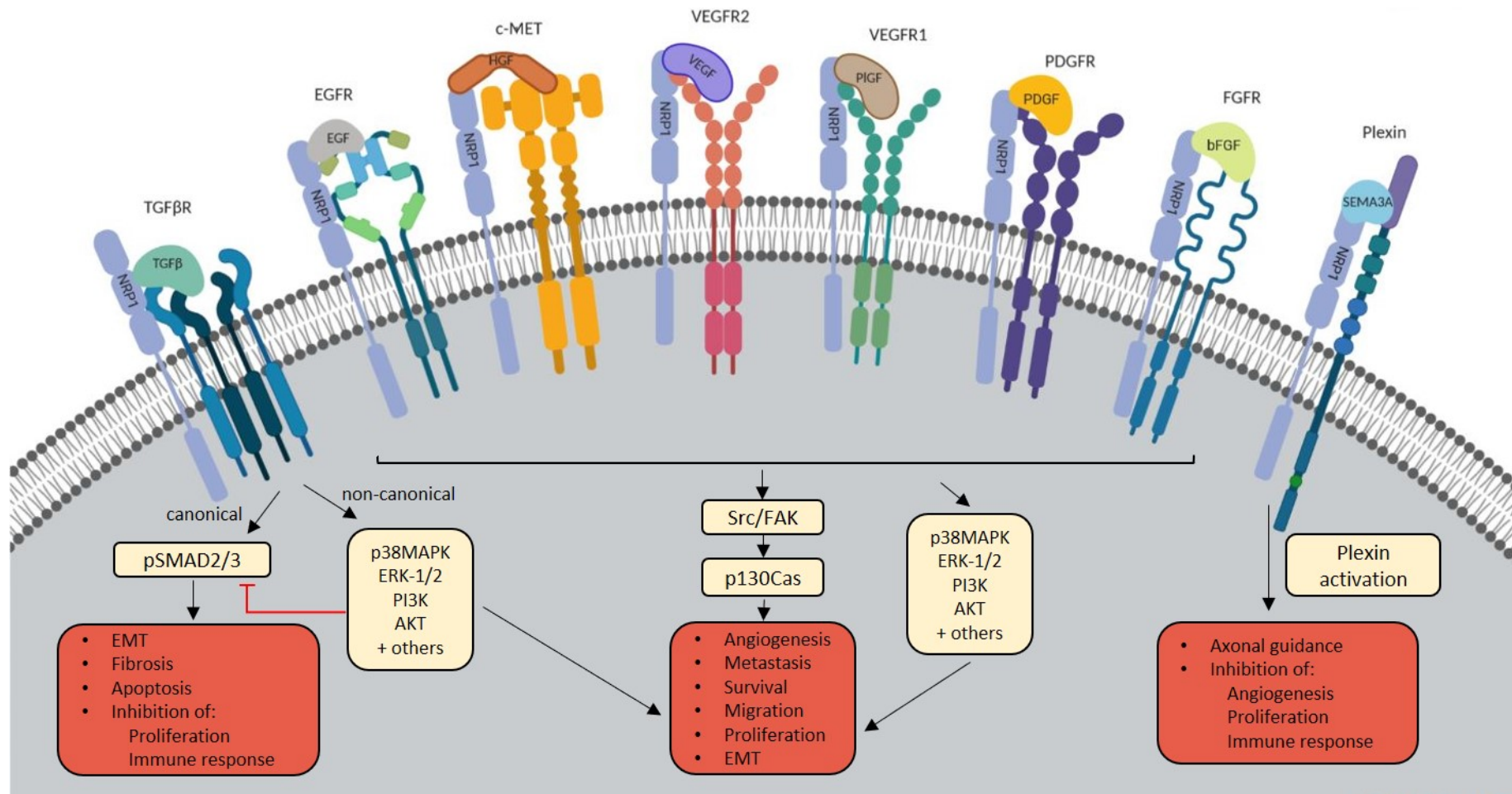


Figure 1.4 NRP1 ligands and co-receptors

NRP1 acts as a co-receptor for a large range of ligands to form heterodimers with their cognate receptors.

1.4.4 NRP1 Isoforms

In addition to the 923 amino acid (aa) full-length NRP1 protein, several isoforms resulting from alternative splicing have been described (Figure 1.4). Ranging in size from 551 to 916 aa, four of these isoforms are soluble variants lacking the c domain, the transmembrane domain and cytoplasmic tail (Cackowski *et al.*, 2004). Containing only the first 11 and 12 exons (out of a total of 17 exons) s_{11} NRP1 and s_{12} NRP1 respectively, have been identified in human prostate PC3 carcinoma cells, heart, brain, kidney, liver, lung, trachea and placenta. *In vivo* studies suggest that s_{12} NRP1 may be anti-tumourigenic through the sequestration of VEGF₁₆₅ but not VEGF₁₂₁ (Gagnon *et al.*, 2000). This is unsurprising as VEGF₁₂₁ lacks the high affinity NRP1 binding site. It has been suggested that sNRP1 may also sequester HGF as it has been shown compete the binding of HGF to NRP1 *in vitro* (Panigrahy *et al.*, 2014). Two further soluble isoforms, s_{III} NRP1 and s_{IV} NRP1, were identified by Cackowski *et al.* (2004). These isoforms show an affinity for VEGF₁₆₅ binding comparable to s_{12} NRP1 and, like s_{12} NRP1, competitively bind VEGF receptors and sequester VEGF₁₆₅. A fifth variant which is functionally comparable to full-length NRP1, NRP1 Δ E16, is thought to exist as a result from the skipping of exon 16, however, this has only been observed in a very select number of cell lines *in vitro* (Fuh *et al.*, 2000) and was found to be barely detectable in a further cell model (Hendricks *et al.*, 2016). Most recently, differential expression of a further isoform, NRP1- Δ 7, has been detected in various normal and cancerous human and mouse cell lines and tissues. This isoform differs to full-length NRP1 by the loss of 7 amino acids just 2 amino acids downstream from an O-glycosylation site. Defective glycosylation gives rise to a functionally different NRP1 splice variant isoform and subsequently phenotypically different cancer cells. In a pancreatic tumour xenograft model, it was demonstrated that NRP1- Δ 7 inhibits tumour growth and angiogenesis (Hendricks *et al.*, 2016). Given that sNRP1 appears to sequester angiogenic ligands thus acting as an endogenous angiogenic inhibitor during development (Panigrahy *et al.*, 2014), it may seem reasonable to hypothesise that, if expressed by tumours, sNRP1 may also elicit anti-angiogenic effects.

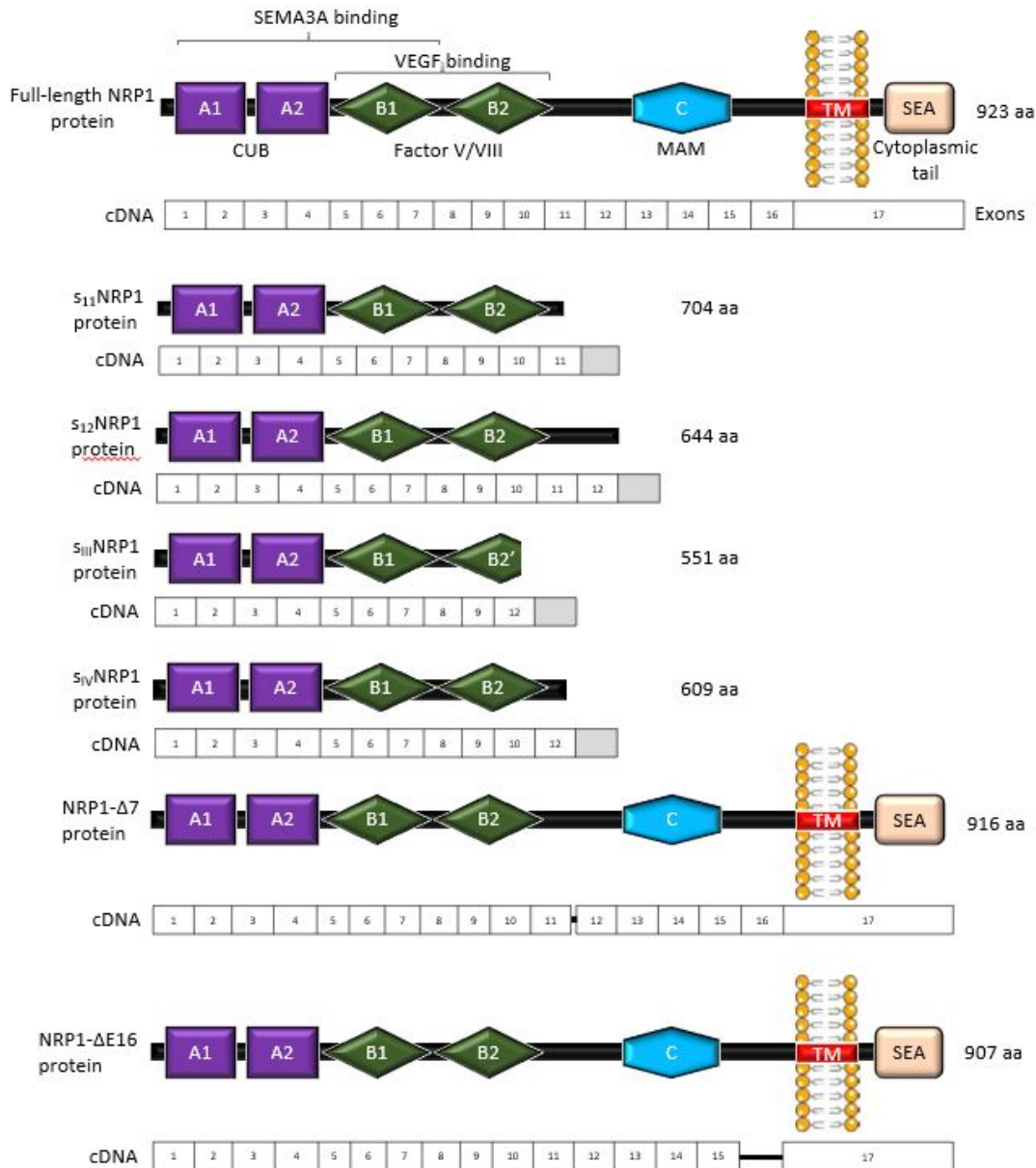


Figure 1.5 Neuropilin-1 Structure

NRP1 contains 5 extracellular domains; a1 and a2 are CUB domains, which are homologous with proteases responsible for C1 complex activation in the classical complement pathway, C1r and C1s. B1 and b2, also referred to as the coagulation factor V and VIII domains and the meprin A5, c μ -phosphatase (MAM) c domains. The intracellular cytoplasmic domain appears to have no independent signalling function. The C-terminal SEA motif, a PDZ binding domain, binds G alpha interacting protein C (GIPC)/synectin. The 'a' and 'b' domains are implicated in ligand binding; a1/a2 together with b1 are required for SEMA3A binding and VEGF binding is mediated by b1/b2. The 'c' domain appears to be functionally essential and facilitates hetero- and homodimerisation. The cytoplasmic SEA domain is critical for NRP1 internalisation. The four sNRP1 isoforms are C-terminally truncated of the b2-domain. Functionally comparable NRP1 Δ E16 results from the skipping of exon 16 and NRP1- Δ 7 arises from the loss of 7 aas directly upstream of an O-glycosylation site, leading to a functionally distinct NRP1 variant. TM (transmembrane)

1.4.5 NRP1 and its interactions with VEGF isoforms

The binding of VEGF₁₆₅ to both NRP1 and NRP2 is well established. Furthermore, the presence of a conserved covalent glycosaminoglycan site at Serine 612 of NRP1 (not present in NRP2) enhances VEGFR2 signalling in ECs through enhancing VEGF₁₆₅ binding and delaying VEGFR2 degradation (Shintani *et al.*, 2006). VEGF₁₆₅, PlGF-2 and VEGF-B bind the b1 and, to a lesser extent, the b2 domain of NRP1 via their heparin binding domains encoded in exons 6 and 7 (Mamluk *et al.*, 2002). Thus, NRP1 is often referred to as an isoform-specific VEGF receptor, as the high affinity NRP1 binding site in exon 7 is absent from the shorter VEGF variants VEGF_{109/110}, VEGF_{120/121} and VEGF₁₄₅ (Appleton *et al.*, 2007, Niland and Eble, 2019). There is however conflicting data regarding this; *in vitro* studies of VEGF/ NRP1 interactions suggest that VEGF isoforms lacking exon 7 are unable to bind to NRP1 (Soker *et al.*, 1998, Hervé *et al.*, 2008), whereas others have demonstrated that VEGF₁₂₁ directly interacts with NRP1 at a lower affinity than VEGF₁₆₅ (Parker *et al.*, 2012b), but is unable to form the same functional signalling complex with VEGFR2 which VEGF₁₆₅ facilitates (Whitaker *et al.*, 2001, Pan *et al.*, 2007a). Additionally, two kinds of VEGF₁₆₅ binding to NRP1 have been identified; a low affinity interaction termed 'fast-on-fast-off' in which the half-life of VEGF binding is 10 min and a high-affinity interaction which has a longer half-life of 15 h (Koch *et al.*, 2014). The ternary complexes formed between NRP1, VEGF and VEGFR2 result in VEGFR2 internalisation and intracellular trafficking which is mediated by the NRP1-PDZ domain binding to GIPC1/ synectin (Salikhova *et al.*, 2008). Structural *in vitro* studies suggest that, although exon 7 contains the NRP1 binding site, it is a C terminal arginine within exon 8a of VEGF, an exon conserved in all isoforms, which is crucial for binding to NRP1 (Parker *et al.*, 2012b). This follows the C-end rule (CendR) proposed by Teesalu *et al.* (2009) which states the essentiality of a C-terminal arginine in peptides binding to the b1 domain of NRP1 and triggering receptor/receptor-complex activity. Other NRP1 ligands besides VEGF, such as semaphorins and TGFβ, share this interaction topology adding strength to the structural and computational models proposed (Zanuy *et al.*, 2013). This hypothesis is further corroborated by Koch *et al.* (2014), who showed that T241 fibrosarcoma cells expressing C-terminal truncated NRP1 displayed a preference for low-affinity VEGF₁₆₅ binding in comparison to T241 cells expressing full length NRP1, where high and low affinity binding of VEGF₁₆₅ was equal (Koch *et al.*, 2014). Earlier experiments used a cross-linking approach to fix VEGF₁₆₅ or VEGF₁₂₁ to HUVECs (endogenously expressing VEGFR1, VEGFR2, NRP1 and NRP2) (Gitay-Goren *et al.*, 1996, Soker *et al.*, 1996), MDA-MB-231 (expressing NRP1 and not VEGFR2) and porcine aortic endothelial (PAE) (Pàez-Ribes *et al.*) cells (modified to express either NRP1 or VEGFR2 or both NRP1 and VEGFR2) (Soker *et al.*, 1998). They report undetectable VEGF₁₂₁ binding to NRP1 in human umbilical vein endothelial cells (HUVECs), MDA-MB-231 cells and PAE cells expressing NRP1 alone. Subsequent studies that have presented opposing data suggest the competition binding assays used by Gitay-

Goren *et al.* (1996) and Soker *et al.* (1996) were not sufficiently sensitive enough to detect low affinity binding of VEGF₁₂₁. Additionally, it has been suggested that the cross-linker used by Soker *et al.* (1998) may not have been suitable for the *in vitro* cell system developed (Sarabipour and Mac Gabhann, 2018).

To date, there have been no *in vivo* studies examining whether NRP1 is VEGF isoform-specific, which raises the question as to whether findings from these *in vitro* studies are relevant in a physiological context. Heparin has been shown to enhance interactions between VEGF₁₆₅ and NRP1, however it is currently unknown whether NRP1/ VEGF/ VEGFR2 interactions are directly or indirectly mediated or regulated by external factors such as HSPGs (Mamluk *et al.*, 2002, Simons *et al.*, 2016), therefore further work in this area is required to fully elucidate the relevance of individual VEGF isoforms in this context.

Studies investigating VEGF/ NRP1 interactions have largely focused on VEGF₁₂₁ and VEGF₁₆₅ with investigation into whether VEGF₁₈₉ is an activating NRP1 ligand on non-neuronal cells receiving little attention (Tillo *et al.*, 2015). *In vitro*, VEGF₁₈₉ reportedly binds to NRP1 with a higher affinity than VEGF₁₆₅ (Vintonenko *et al.*, 2011) and has been implicated in vascular branching during the early stages of angiogenic invasion. Experimental data also suggests that VEGF₁₆₅ and VEGF₁₈₉ may differentially influence the metastatic potential of locally aggressive tumours (Di Benedetto *et al.*, 2015). In VEGF isoform-specific expressing BC cells VEGF₁₈₉ binding to NRP1 resulted in tumour cells with a lower invasive capacity (Hervé *et al.*, 2008); additionally, NRP1 knockdown in VEGF₁₈₉ expressing cells resulted in reduced cell apoptosis, whereas NRP1 knockdown in VEGFR₁₆₅ expressing cells had no effect (Vintonenko *et al.*, 2011). In agreement with these data, mouse fibrosarcoma cells expressing only the VEGF₁₈₈ isoform and expressing elevated NRP1 levels also exhibit pro-apoptotic tendencies (Kanthou *et al.*, 2014).

VEGF knockout (KO) in MDA-MB-231 cells (231^{VEGFKO}) resulted in smaller, more rounded cells that migrated more slowly. These phenotypic changes were mirrored when NRP1 was knocked down and sNRP1 introduced (231^{NRPKD} and 231^{sNRP1} respectively) suggesting that direct VEGF-NRP1 interactions in the absence of VEGFR1/2 may contribute to the morphological and migration changes observed (Kiso *et al.*, 2018). The model they present suggests interaction of VEGF₁₆₅, but not VEGF₁₂₁, with NRP1 leading to a downregulation of Rho GTPase Activating Protein 17 (ARHGAP17); this downregulation activates cell division control protein 42 (Cdc42), which in turn increases filopodia formation and subsequent enhanced motility.

In light of evidence suggesting that some tumour cells respond to both autocrine and paracrine VEGF signals in the absence of VEGFRs, it is postulated that other receptors are contributing to and/ or mediating VEGF signalling. The receptor that has gained the most attention with regard to this is NRP1, however the mechanisms through which this might occur have still to be identified.

1.4.6 NRP1 in tumour growth and angiogenesis

A large body of evidence indicates an integral functional role for NRP1 in tumour biology and pathological angiogenesis (Pan *et al.*, 2007a, Staton *et al.*, 2013, Fantin *et al.*, 2014), but the underlying mechanisms involved have yet to be fully elucidated. The ability of NRP1 to associate with other membrane receptors, such as cMet, epidermal growth factor receptor (EGFR) and platelet derived growth factor (PDGFR), has implicated this promiscuous co-receptor in a range of cellular processes that are inclusive of migration, adhesion and cell survival (summarised in Figure 1.3). The relevance of non-endothelial NRP1 expression as well as tumour cell derived NRP1 in tumour growth and tumour angiogenesis remains unclear. Several studies provide conflicting reports on the consequences of tumour derived NRP1 overexpression; data has been presented demonstrating both promotion and inhibition of tumour growth and vascularisation (Koch *et al.*, 2014). NRP1 expression varies considerably between tumour types, and has been shown to be different in primary and metastatic tumours in cancers of the same origin (Jubb *et al.*, 2012). In the vast majority of cancers, high expression of NRP1 correlates with a more aggressive phenotype, increased metastasis, advanced disease and poor patient prognosis.

Although the majority of studies focus on NRP1 as a co-receptor with VEGFR2, in tumour cells lacking VEGFR2, VEGF signalling mediated by NRP1 is still observed. This indicates that NRP1 transduces signals independently, potentially via the intracellular domain (Ruffini *et al.*, 2013), or with another co-receptor (Xu and Xia, 2013). NRP1 expressed on tumour cells was shown to mediate VEGF-induced tumorigenesis by sustaining autocrine Ras activation; as NRP1 lacks kinase activity, the assumption was made that another as yet unknown co-receptor may be required for signal transduction.

Some studies show that tumour cells co-expressing NRP1 and VEGFR2 secrete higher levels of VEGF and present a more invasive phenotype in comparison to cells expressing the receptors individually (Ruffini *et al.*, 2013); this suggests that co-expression enhances VEGF/ VEGFR2 autocrine signalling which in turn promotes angiogenesis and tumour progression. In addition, an increasing amount of data provides evidence of NRP1 overexpression positively correlating to an increase in aggressiveness

and invasiveness of tumour cells. When NRP1 was overexpressed in tumour cells, tumours appeared larger and more vascular and a reduction in tumour cell apoptosis was accompanied by an increase in tumour EC proliferation (Miao *et al.*, 2000, Appleton *et al.*, 2007, Ruffini *et al.*, 2013). Conversely, depletion of NRP1 expression in murine melanomas led to smaller tumours and >90% NRP1 inhibition resulted in their near complete absence (Fantin *et al.*, 2014). Additionally, NRP1 silencing in hepatocellular carcinoma xenograft tumours led to a decrease in angiogenesis which subsequently reduced tumour progression (Xu and Xia, 2013).

1.4.7 VEGF₁₆₅ mediated NRP1/VEGFR2 cross-cell complexes

Pro-angiogenic ligands such as VEGF are secreted by tumour cells and, depending on the isoform, may diffuse distally or be sequestered locally. As already discussed, NRP1 and VEGFR2 are expressed on a number of differing cell types within the TME; therefore, some VEGF isoforms cannot only form NRP1/VEGF/VEGFR2 complexes in the same cells but also between neighbouring cells. Simultaneous binding of NRP1 and VEGFR2 by VEGF on the same endothelial or tumour cell results in a homotypic (*cis*) complex, on neighbouring ECs a heterotypic (*trans*) complex, or between endothelial and tumour cells in a juxtacrine (*trans*) configuration (Figure 1.5) (Fantin *et al.*, 2013, Koch *et al.*, 2014). Early studies indicated that *trans* interactions, originally termed juxtacrine interactions, mediated by VEGF may in part be responsible for an increase in tumour angiogenesis and therefore enhanced tumour growth (Miao *et al.*, 2000, Soker *et al.*, 2002). However, more recently Koch *et al.* (2014) developed an *in vivo* mouse model using T241 fibrosarcoma cells (no endogenous NRP1 expression) and B16F10 melanoma cells (endogenous NRP1 expression), neither of which express VEGFR2, to investigate both *cis* and *trans* NRP1/VEGF/VEGFR2 signalling. Briefly, T241 cells were modified to overexpress NRP1 and NRP1 was knocked down in B16F10, the modified T241 or B16F10 cells were then implanted into either WT mice or inducible EC-specific NRP1 KO mice. In this model, NRP1 expression on tumour cells suppressed angiogenesis and tumour growth; however, once tumours eventually established they were well vascularised suggesting that angiogenesis was rescued by NRP1-independent mechanisms. Their initial *in vitro* experiments using PAE cells modified to express NRP1 or VEGFR2 individually or together, identified novel differences in VEGF₁₆₅ mediated NRP1/VEGFR2 complex formation and receptor internalisation kinetics. In the *cis* arrangement NRP1/VEGFR2 complexes formed quickly and transiently whereas in the *trans* conformation complexes did form, but with delayed kinetics. Furthermore, when stimulated with VEGF₁₆₅, the presence of both VEGFR2 and NRP1 on the same cell enhanced receptor internalisation and downstream phospholipase C γ (PLC γ) and extracellular signal-regulated kinase (ERK)-1/2 phosphorylation occurred quickly and transiently. Conversely, in the *trans*

NRP1/VEGF₁₆₅/VEGFR2 conformation, receptor internalisation was arrested and PLC γ and ERK-2 phosphorylation was sustained whilst ERK-1 phosphorylation was markedly decreased in comparison. However, despite effects on downstream signalling, phosphorylation of VEGFR2 occurred at with similar kinetics in both *cis* and *trans* complexes, thus indicating that VEGF induced VEGFR2 activation is not dependent on NRP1 (Koch *et al.*, 2014). Taken as a whole, this would suggest that the suppression of angiogenesis was due, at least in part, to the arrest of receptor internalisation, leading to reduced downstream angiogenic signalling and an imbalance of ERK-1/2 signalling. NRP1 expression was not detected on any other cell types within the tumour, which also suggests that the initial NRP1-dependent tumour suppression was unlikely to be related to immunity or inflammation.

To further support the data from the mouse models, Morin *et al.* (2018) went on to study VEGFR2 and NRP1 expression and complex formation in several different human cancers alongside the fibrosarcoma mouse model used by Koch *et al.* (2014). Once again, they found *trans* complexes correlated with a decrease in vessel formation and branching along with a reduction in tumour proliferation. What is intriguing in this study is that, as a whole both pancreatic ductal adenocarcinoma (PDAC) and gastric cancer (GAC) expressed relatively high levels of NRP1, yet the distribution throughout the tumours were different. In PDAC ratio of tumour to vascular NRP1 was higher than in GAC. Furthermore, the high density of NRP1/VEGFR2 *trans* complexes in PDAC samples correlated with improved patient survival, whereas the low density of *trans* complexes detected in GAC samples was associated with a poorer prognosis. These data indicate that expression levels of NRP1 on tumour cells relative to ECs dictates whether *cis* or *trans* NRP1/VEGF/VEGFR2 complexes dominate and thus influence the angiogenic outcome.

In contrast however, the previously detailed study by Koch *et al.* (2014) showed that vessel sprouting occurred in areas where ECs that expressed NRP1 were in close proximity to cells that were lacking NRP1.

These studies illustrate the complexities of NRP1 and VEGF signalling in the vasculature. They also suggest that a finite balance of NRP1 expression level and distribution between various cell types may alter tumour growth and angiogenesis if disrupted. To further add to the complexity of these interactions, considerations need to be made with regard to the spatial arrangement of tissue within the tumour. Tumours are notoriously heterogenous and it is highly likely that there may be areas that are *trans* or *cis* complex dominant or an equal mix of both. More detailed mechanistic and computational modelling is required to gain further understanding of these interactions.

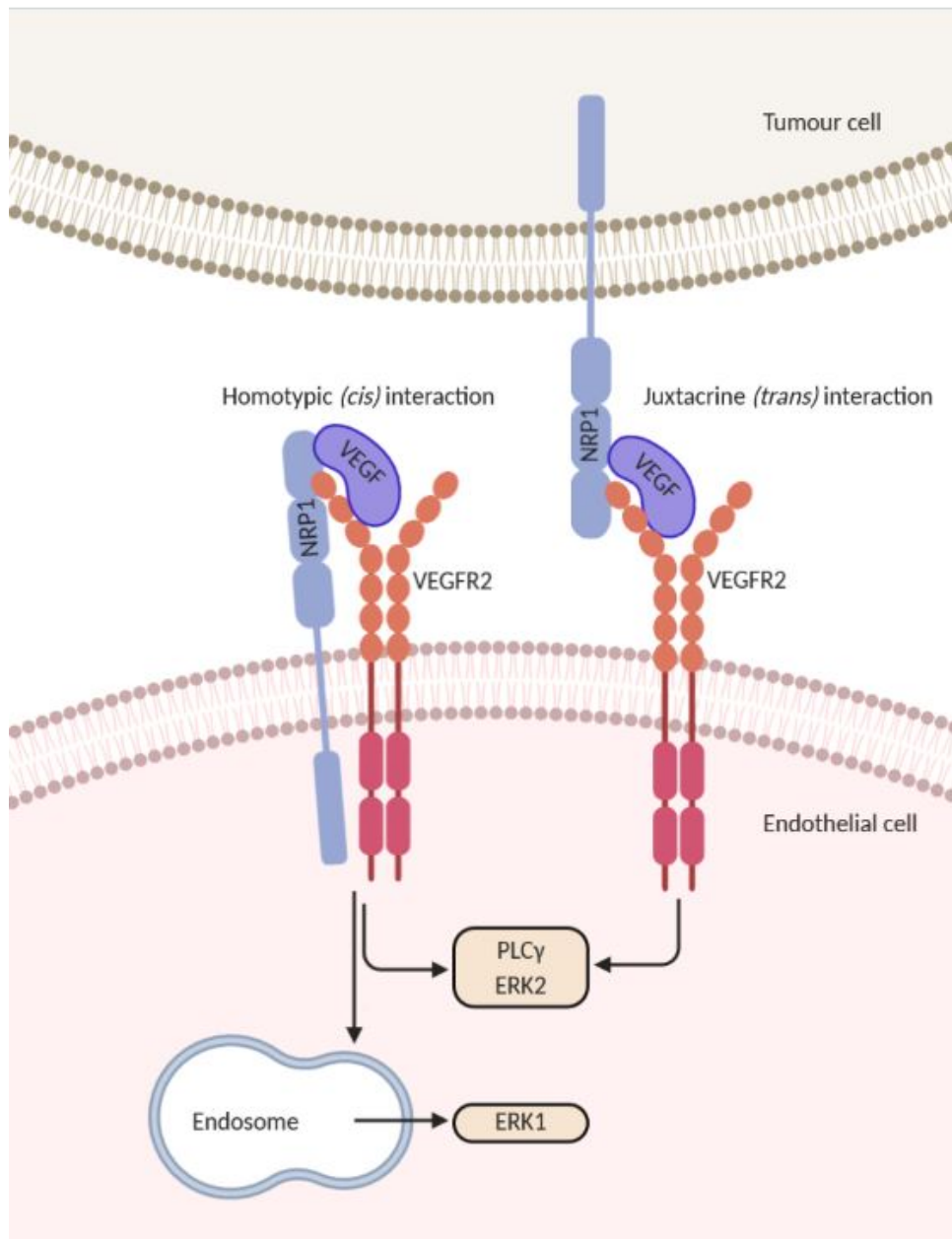


Figure 1.6 Proposed VEGFR2 and NRP1 interactions between endothelial and tumour cells

Homotypic (*cis*) NRP1/VEGFR2/VEGF complexes result in receptor internalization and activation of ERK1/2 and PLC γ . Juxtacrine (*trans*) NRP1/ VEGFR2/VEGF complexes result in a lack of receptor internalization and suppresses ERK1 activation, however ERK2 and PLC γ are still activated. Figure adapted from (Koch *et al.*, 2014)

1.4.8 NRP1 in desmoplasia

An increase in ECM deposition and fibrosis or desmoplasia within the tumour stroma, is associated with a more aggressive tumour phenotype (Paszek *et al.*, 2005, Schedin and Keely, 2011). A key molecular component within the tumour stroma is fibronectin; upon interaction with endothelial $\alpha 5\beta 1$ integrin, soluble fibronectin dimers assemble into insoluble fibronectin fibrils (fibrillogenesis) that associate with collagen to form a rigid, fibrillar network (Valdembri *et al.*, 2009, Yaqoob *et al.*, 2012). The result is tumour matrix remodelling, increased tumour rigidity and stromal activation that in turn promotes tumour progression (Levental *et al.*, 2009). Fibrillogenesis is a critical step in stromal activation; NRP1 has been shown to promote $\alpha 5\beta 1$ integrin mediated fibronectin adhesion to ECs and subsequent fibronectin matrix assembly (Valdembri *et al.*, 2009). TGF β -activated fibroblasts within the tumour microenvironment, myofibroblasts, play a pivotal role in fibronectin fibrillogenesis and regulation of desmoplasia (Schedin and Keely, 2011). *In vitro* work indicates that NRP1 promotes tumour matrix stiffening, leading to increased tumour cell proliferation through amplification of myofibroblast engagement with fibronectin and fibril assembly (Yaqoob *et al.*, 2012). It is unclear as to whether NRP1 forms complexes with integrins in the same way that it does with RTKs. However, what is apparent is that NRP1 holds the capacity to modulate expression of certain integrins in ECs and upregulate Tenascin-C/integrin- $\beta 3$ signalling when overexpressed in breast cancer (BC) cells (Naik *et al.*, 2018).

Abnormal endothelial to mesenchymal transition (EMT) has been linked to the development of cancer associated fibroblasts and fibrosis in cancer. Dense desmoplasia is a characteristic of PDAC and is a malignancy where NRP1 is frequently overexpressed. Acting this time as a receptor for TGF β , NRP1 appears to play a regulatory role in TGF β -induced EMT and associated fibrosis. Furthermore, NRP1 expression has been shown to upregulate pro-fibrotic gene expression and tumour fibrosis in PDAC (Matkar *et al.*, 2016) and promote a myofibroblast phenotype (Niland and Eble, 2019).

1.5 Vascular-targeted therapy in cancer

Therapeutic interventions that target the tumour vasculature can be broadly split into two groups; therapies that inhibit or interfere with tumour angiogenesis through target specific inhibition (anti-angiogenic therapy), or agents that disrupt and destroy the immature tumour vasculature, referred to as vascular-disrupting agents (VDA)s.

1.5.1 Anti-angiogenic therapy in cancer

Since the idea of targeting tumour angiogenesis was presented by Judah Folkman (Folkman, 1971) and the subsequent establishment of VEGF as the key mediator in pathological angiogenesis, the focus of anti-angiogenic medicine has largely centred around disrupting neovascular signalling. In particular, disruption of the VEGF/VEGFR axis has been targeted and the development of target-specific antibodies, protein fragments and small molecule receptor tyrosine kinase inhibitors (TKIs) have gained the most attention (Jászai and Schmidt, 2019). There are now 11 FDA approved anti-angiogenic drugs that disrupt the VEGF signalling pathway licensed for use as both mono and combination therapies in a range of cancers (Table 1.1).

Of the VEGFRs, VEGFR2 is considered the most important in the angiogenic signalling cascade and targeting its function in the development of anti-angiogenic cancer drugs has proved popular. In general, blockade of the VEGF axis is achieved via two main approaches: 1) restriction of ligand-mediated receptor activation through either ligand sequestration or competitive inhibition or 2) by blocking kinase activation thus inhibiting the subsequent downstream signalling cascade that would ordinarily result in angiogenesis (Figure 1.6).

The first anti-angiogenic drug to gain FDA approval in 2004 was the recombinant anti-VEGF monoclonal antibody (mAb) bevacizumab (Avastin®). Based on the premise that bevacizumab not only elicited direct antiangiogenic effects, but also might improve the delivery of chemotherapy, a pivotal phase III clinical trial demonstrated that the addition of bevacizumab to folinic acid, 5-fluorouracil and irinotecan (FOLFIRI) improved progression free survival (PFS), overall survival (OS) and overall response rate (ORR) of previously untreated metastatic colorectal cancer (mCRC) patients (Hurwitz *et al.*, 2004). Following the approval of this target-specific therapy, which sequesters circulating VEGF, research into agents that could disrupt the VEGF pathway gained momentum. Although a further VEGFR2 targeting mAb, ramucirumab, and a VEGF trap synthesised as recombinant fusion protein, ziv-aflibercept, have since been approved for clinical use, the lions' share of FDA approved anti-angiogenic drugs that disrupt the VEGF axis are small molecule TKIs. These molecules were primarily designed to

down-regulate VEGF/VEGFR signalling by competitively or allosterically inhibiting the tyrosine kinase domains of specific receptors, however, they in fact exhibit affinities to multiple receptor tyrosine kinases, inclusive of PDGFRs, fibroblast growth factor receptor 1 (FGFR1), EGFR and c-KIT.

Folkman's original hypothesis was that anti-angiogenic therapy would prevent the development of new vessels thus starving the tumour and limiting its growth (Folkman, 1971). This was further supported by preclinical data from human xenograft models, where treatment with an anti-VEGF mAb led to regression in primary tumours, marked reductions in vascular density and reductions in metastases (Kim *et al.*, 1993, Warren *et al.*, 1995). Despite promising preclinical results, the clinical benefit of the more targeted macro-molecular anti-VEGF drugs (bevacizumab, ramucirumab and aflibercept) as a monotherapy in solid tumours is generally limited. However, some benefit has been found for its monotherapy in recurrent glioblastoma multiforme (GBM) and ovarian cancer (Friedman *et al.*, 2009, Zhang *et al.*, 2017b). Disease progression in ovarian cancer is associated with dysfunctional tumour associated lymphatic vessels that is analogous to the leaky, tortuous tumour vasculature. The increased permeability and impaired lymphatic drainage subsequently leads to the recurrent build-up of malignant ascites fluid; it is suggested that VEGF blockade aids in the reduction of ascites build-up (Goel *et al.*, 2011). A recent *in vitro* study using human GBM cells (U87-MG) found that bevacizumab directly suppressed cell proliferation in a dose dependent manner and promoted apoptosis (Huang *et al.*, 2018a). The mechanism of action of bevacizumab is still not completely clear; however, it appears from these studies that there may be more to its clinical repertoire than just anti-angiogenesis. Seemingly, the most promising avenues of enquiry with these macromolecular biologicals is in combination therapy; both clinical and preclinical studies have reported that when combined with chemotherapy, photodynamic therapy, immunotherapy, microRNA (miRNA) therapy or radiotherapy, the treatment efficacy of these drugs can be improved (Hamming *et al.*, 2017).

The anti-VEGF pathway TKIs have proved more successful as single agents than the more targeted biologicals described above and are used as both first and second line treatment in numerous malignancies (Table 1.1). The reasons behind this are still largely unclear, except for in the case of metastatic renal cell carcinoma (mRCC). The treatment of mRCC with TKIs (primarily sorafenib and sunitinib) as monotherapies has proven to be clinically beneficial in terms of PFS. The particular sensitivity of this class of tumours to TKIs arises from an underlying loss of von Hippel Lindau activity leading to a reliance on VEGF for progression (Escudier *et al.*, 2012). Efforts to expand the repertoire of malignancies that can be treated with TKIs and to prolong their efficacy through combining them with chemotherapy have thus far been disappointing in terms of OS (Vasudev and Reynolds, 2014).

In a process referred to as “vascular normalisation”, VEGF blockade can result in the pruning of immature vessels to leave a more stable and functional vascular network (Jain, 2001). This alteration of the tumour vasculature subsequently results in transient reduction of blood vessel density, vascular permeability and interstitial fluid pressure thus reducing the leakiness of tumour vessels (Raut *et al.*, 2012). By destroying the tortuous, highly immature vasculature and remodelling the remaining vessels into more mature vessels that also tend to have a better coverage of pericytes, anti-VEGF agents modify the tumour microenvironment and potentially allow synergy with other treatment modalities (Jain, 2001, Jain, 2005, Bertolini *et al.*, 2011). There appears to be a narrow window in which anti-angiogenic therapy results in phenotypically ‘normal’ tumour vasculature with improved perfusion, which in turn allows for improved delivery of chemo-, radio- or immunotherapy. A small imaging study in paediatric OS recently demonstrated that, 24 h following bevacizumab treatment, the average tumour permeability and tumour vessel density significantly decreased below initial baseline measurements, before rapidly returning to baseline levels after 72 h. This initial decrease in vessel permeability was suggested to be indicative of transient vessel normalisation (Guo *et al.*, 2015). In NSCLC, prolonged treatment with anti-angiogenic agents re-increases tumour hypoxia, resulting in the exacerbation of a pro-tumourigenic TME which reduces delivery of chemotherapy to the tumour (Van der veldt *et al.*, 2012). Clinical and preclinical studies both suggest that a well-considered strategy is required in order to improve the delivery of systemic therapy in combination with anti-VEGF therapies (Li *et al.*, 2018).

When administered as a monotherapy anti-angiogenic therapies blocking just one angiogenic pathway are unlikely to be curative, however, if combined with more conventional therapies such as radio- or chemotherapy their clinical efficacy can be increased. While as described above a temporary reduction in tumour hypoxia and subsequent transient window of vascular normalisation often happens during the first days of anti-angiogenic treatment (Jain, 2001), prolonged treatment with anti-angiogenic agents may result in an increase in tumour hypoxia, resulting in the exacerbation of a pro-tumourigenic TME and which reduces delivery of chemotherapy to the tumour (Van der veldt *et al.*, 2012).

When administered as a monotherapy, the anti-tumour activity of specific anti-VEGF therapy falls short of the initial preclinical results, yet when combined with chemotherapy their clinical efficacy can be increased. In contrast, the broader range TKIs are primarily approved for administration as a monotherapy (Table 1.1). Moreover, their combination with cytotoxic therapy does not appear to improve PFS and evidence suggests that combining TKIs with chemotherapy may lead to toxicity (Jain

et al., 2006, Jayson *et al.*, 2016, Comunanza and Bussolino, 2017). Achieving improved anti-VEGF drug efficacy through combination with chemotherapy is reliant on cancer type and dosing schedule. In breast, melanoma and ovarian cancer, anti-VEGF treatment is reported to increase perfusion of cytotoxic drugs whereas in CRC and head and neck cancer the reverse appears to be true (Lai and Friedman, 2019). Given that vascular normalisation is perhaps the most accepted mechanism by which anti-VEGF and chemotherapy together have a more potent anti-tumour effect, these differing effects on tumour perfusion are vitally important in choosing the optimal dosing schedule. There is some controversy surrounding anti-angiogenic therapy with TKIs (Singh *et al.*, 2012), and some preclinical studies have suggested that, when used in a neoadjuvant setting, they might actually increase tumour invasiveness and refractoriness (Ebos *et al.*, 2009, Pàez-Ribes *et al.*, 2009). Further to this, in an experimental model of Lewis Lung Carcinoma, it was demonstrated that combining neoadjuvant sunitinib treatment with gemcitabine or topotecan counteracted the metastatic dissemination observed in earlier preclinical studies (Rovida *et al.*, 2013). To date, no clinical trials have been published that support these preclinical findings, which is likely due to the fact that TKIs administered in an adjuvant setting in the clinic.

In comparison to combining anti-angiogenic therapies with chemotherapy, there are less clinical studies that focus on their combination with radiotherapy. Unlike chemotherapy, the combination of radiotherapy with anti-angiogenic agents is not clinically approved. A number of phase I and II studies combining bevacizumab with radiotherapy showed an increased benefit when therapies were combined in comparison to either treatment alone. Hypoxia significantly reduces the efficacy of radiotherapy. Hence, if the transient drop in tumour hypoxia following anti-angiogenic induced vessel normalisation could be accurately determined, it seems logical that this would be the optimal time for tumour irradiation (Winkler *et al.*, 2004). Several preclinical studies support this theory and have shown that administration of radiotherapy during the short window of vessel normalisation is the most effective scheduling of the two treatment modalities (Winkler *et al.*, 2004, Dings *et al.*, 2007). The vessel normalisation hypothesis however does not account for the enhanced growth delay of tumours when VEGF was inhibited either during or before radiotherapy. Furthermore, even under conditions where anti-VEGF induced hypoxia occurred in the tumour, the addition of radiotherapy still enhanced tumour responses. VEGF plays a role in protecting ECs against radiation, and in the absence of tumour vessel normalisation, VEGF sequestration may help sensitise ECs to irradiation (Gorski *et al.*, 1999, Williams *et al.*, 2007). Thus, in these studies, the reported improvements in response from concomitant administration of radiotherapy and anti-VEGF treatment might be attributed to the enhancement of EC radiosensitivity (Kanthou and Tozer, 2019). Preclinical and clinical studies have

both investigated the importance of the sequence of treatment modalities, and although the lack of standardised drug doses makes it hard to draw any hard and fast conclusions, most have demonstrated that adjuvant radiotherapy is more efficacious than neoadjuvant or concurrent administration.

In light of recent advances in the field of immunotherapy, combinations of anti-angiogenic therapy with immune checkpoint inhibitors are currently under investigation (Lai and Friedman, 2019). The rationale behind combining these two treatment modalities is that pro-angiogenic molecules promote an immunosuppressive TME (Fukumura *et al.*, 2018). Thus, blocking immunosuppressive molecules, such as VEGF, with anti-angiogenic drugs whilst encouraging an immune response with checkpoint inhibitors should theoretically result in a more immune-supportive TME. Promising data from preclinical studies has led to numerous clinical trials in a range of cancer types combining not only checkpoint inhibitors and anti-angiogenic therapy, but also standard chemotherapy. Whether this multimodal approach is the future of cancer treatment awaits the results of larger phase III trials and more work needs to be done in terms of understanding the synergy between these treatments (Ciciola *et al.*, 2020).

Drug	FDA approval	Approved Disease	Clinical Use
Biologicals			
Bevacizumab <i>Anti-VEGF mAb</i>	2004 2006	mCRC	With chemotherapy
	2009	mRCC	With interferon-alfa
	2014	r ovarian, fallopian or primary peritoneal cancer	With chemotherapy, followed by as a single agent
	2006	m/r NSCLC	With chemotherapy
	2009	r glioblastoma	Single agent
	2014	m/r cervical cancer	With chemotherapy
Ramucirumab <i>Anti-VEGFR2 mAb</i>	2014	a/m gastric or gastroesophageal junction adenocarcinoma	Single agent or with paclitaxel in advanced disease
	2014	mNSCLC	With docedaxel
	2015	a/m CRC	With FOLFIRI
	2019	HCC	Single agent
Ziv-Aflibercept <i>VEGF-trap Recombinant fusion protein</i>	2012	mCRC	With FOLFIRI
Small molecule receptor tyrosine kinase inhibitors (RTKi)			
Sunitinib	2006 2017	a/r RCC	Single agent and as adjuvant therapy
	2006	GIST	Single agent
	2011	a/r, progressive or unresectable pNET	Single agent
Sorafenib	2005	a RCC	Single agent
	2007	Unresectable HCC	Single agent
	2013	m/r iodine-refractory TC	Single agent
Axitinib	2012	a RCC	Single agent
Pazopanib	2009	a RCC	Single agent
	2012	a STS (non-adipocytic or GIST)	Single agent
Vandetanib	2011	m or unresectable medullary TC	Single agent
Regorafenib	2012	Refractory and mCRC	Single agent
	2013	a/m unresectable or refractory GIST	Single agent
	2017	Refractory HCC	Single agent
Lenvatinib	2015	Differentiated or iodine-refractory TC	Single agent
	2016	a RCC	With evrolimus
	2018	Unresectable HCC	Single agent
	2019	a endometrial carcinoma	With pembrolizumab
Cabozantinib	2012	Medullary TC	Single agent
	2016 2017	a/previously untreated RCC	Single agent
	2019	HCC	Single agent

Table 1.1 FDA approved angiogenesis inhibitors targeting the VEGF axis inhibitors currently in the clinic

a, advanced; m, metastatic; r, recurrent; mAb, monoclonal antibody; CRC, colorectal cancer; RCC renal cell carcinoma; NSCLC, non-small cell lung cancer; GIST, gastrointestinal stromal tumours; HCC, hepatocellular carcinoma; FOLFIRI, folinic acid, 5-fluorouracil and irinotecan; pNET, pancreatic neuroendocrine tumours; TC, thyroid cancer; STS, soft tissue sarcoma.

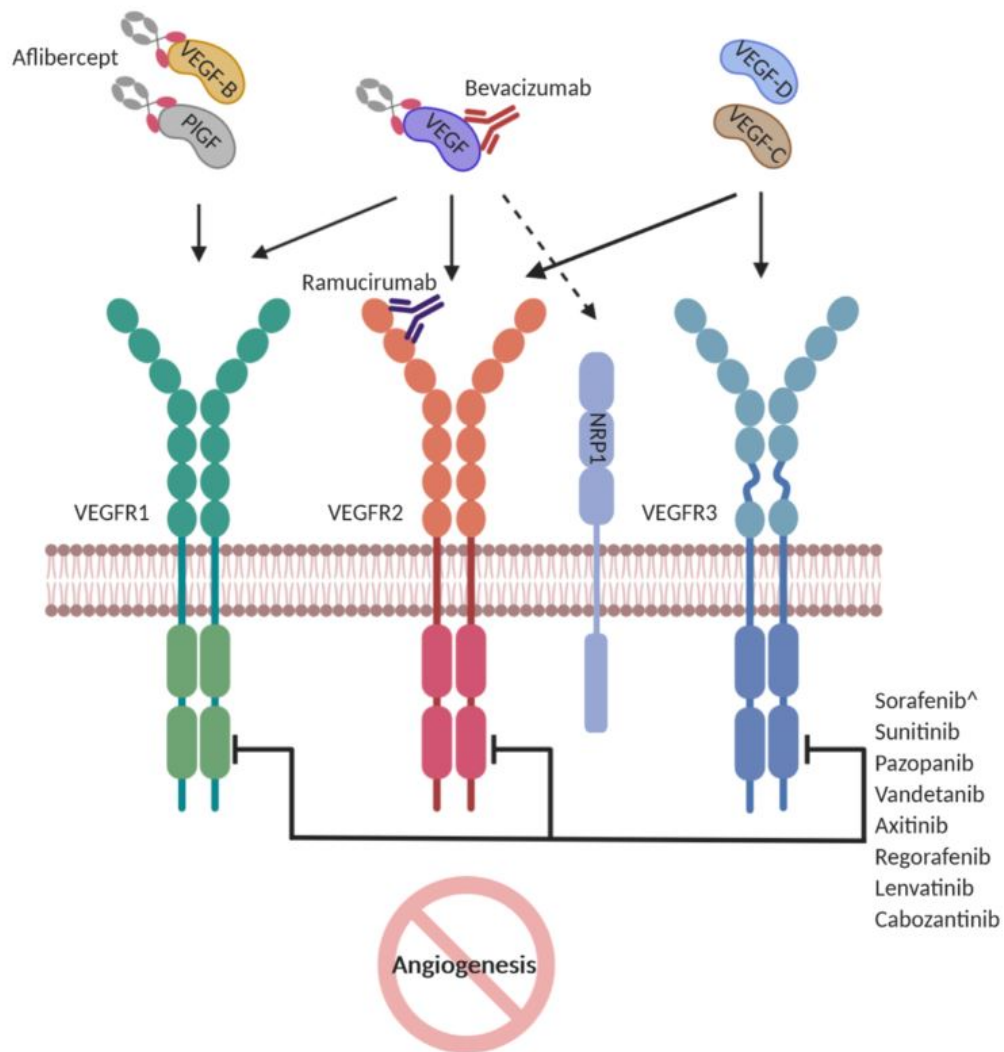


Figure 1.7 Mode of action of FDA approved anti-angiogenic drugs targeting the VEGF axis

Bevacizumab and aflibercept restrict ligand-mediated receptor activation through ligand sequestration or competitive inhibition. Sorafenib, sunitinib, pazopanib, vandetanib, axitinib, regorafenib, lenvatinib and cabozantinib inhibit kinase activation thus inhibiting the subsequent downstream signalling cascade that would ordinarily result in angiogenesis

[^]Sorafenib only inhibits VEGFR2 & 3 kinase activity

1.5.2 Vascular Disrupting Agents (VDAs)

In contrast to anti-angiogenic approaches that inhibit tumour angiogenesis through interrupting specific angiogenic signalling cascades, VDAs shut down the already established tumour vasculature and to starve the tumour, resulting in secondary tumour-cell death whilst leaving normal tissue vessel intact (Siemann *et al.*, 2005, Tozer *et al.*, 2005, Siemann *et al.*, 2017). There are two major groups of VDA, the microtubule binding agents and the flavonoids; both have distinct modes of action but share the same main target of ECs lining the tumour blood vessels. The main flavonoid developed as a VDA and tested in clinical trials was 5,6-dimethylxanthenone-4-acetic acid (DMXAA). The molecular actions of DMXAA are still largely unclear, but it is thought to induce toxic cytokine production. Induction of interferon-inducible protein, serotonin, nitric oxide and tumour necrosis factor (TNF α) have all been implicated in the antitumor effects of DMXAA (Lippert, 2007, Roberts *et al.*, 2007). Tubulin-binding agents (TBAs) cause microtubule depolymerisation through binding to either the colchicine or vinca sites of tubulin. Numerous drugs in the TBA class of VDAs have been developed and entered clinical trials, amongst these are combretastatin A-4 3-O-phosphate (CA4P; fosbretabulin), Ombrabulin and BNC105 / BNC105P (Dumontet and Jordan, 2010, Gill *et al.*, 2019).

Targeting the rapidly growing, immature, chaotic tumour vessels has proved an effective therapeutic strategy that has led to both preclinical and clinical trials of VDAs that target the colchicine-binding domain of β -tubulin (microtubule binding VDAs). Although the precise mechanisms by which these compounds result in the collapse of the tumour rather than normal vasculature has yet to be fully elucidated, preclinical studies have suggested that EC rigidity in mature established vessels is dependent on the actin cytoskeleton rather than the intracellular tubulin cytoskeleton upon which immature ECs are reliant on (Tozer *et al.*, 2008a, Siemann *et al.*, 2017). Disruption of tumour blood flow following the VDA treatment occurs within 1 - 6 hours and if sustained can lead to necrosis of the tumour (Sheng *et al.*, 2004, Tozer *et al.*, 2008b). VDA-induced vascular shutdown is effective in causing central tumour necrosis but in doing so induces tumour hypoxia which, alongside a residual viable tumour rim which is more resistant to this type of agent, invariably contributes to the problematic issue of tumour resistance to VDAs (El-Emir *et al.*, 2005, Tozer *et al.*, 2008b). Resistance to VDAs is thought to be due to membrane ATP binding cassette (ABC) efflux pumps, poor induction of apoptosis and ineffective interaction with their target (Dumontet and Jordan, 2010). Generally, tumour shrinkage is modest and transient in single-agent VDA approaches (Clémenson *et al.*, 2013). VDAs are characterised by extensive necrosis of the tumour core; the resulting pro-angiogenic hypoxic conditions result in the rapid revascularisation at the viable tumour rim, thus sustaining tumour regrowth and treatment resistance (Tozer *et al.*, 2008b). As a result, the clinical benefit of VDAs has

been evaluated predominantly in combination with other agents, although none have ever reached the clinic (summarised in Table 1.2).

1.5.3 Combining VDAs with chemotherapy and radiotherapy

The synergistic effects of VDAs with other therapies is reliant on the scheduling of administration. In general, pre-clinical studies conclude that the hypoxic TME that immediately follows VDA treatment renders tumours radioresistant and hampers the delivery of systemic chemotherapy (Tozer *et al.*, 2008b, Liang *et al.*, 2016). In theory, the administration of chemotherapy before a VDA would allow for delivery of the cytotoxic agent before trapping it in the tumour via vascular shutdown. In agreement with this hypothesis, Siemann *et al.* (2002) found the delivery of cisplatin 1 - 4 h prior to treatment with VDAs resulted in maximal anti-tumour effect with the converse being true when VDAs were administered 1 - 2h prior to chemotherapy. In contrast, one study has reported VDA administration 1 hr after cisplatin in rodent tumours and human tumour xerograph models enhanced tumour sensitivity to chemotherapy (Martinelli *et al.*, 2007). Very few clinical trials have evaluated VDAs in combination with radiotherapy, however pre-clinical studies have demonstrated there is potential benefit in combining these two treatment modalities. Given that VDAs would create an environment that is detrimental to radiation-induced DNA damage, administering radiotherapy prior to VDAs may seem the most obvious scheduling regimen. There are studies that align with this theory, however, there are also studies that suggest radiation following VDA treatment to have a superior additive effect. One explanation for this may be that the remaining tumour rim is thought to comprise of well oxygenated, highly proliferative cells that are theoretically more sensitive to irradiation (Siemann and Rojiani, 2002, Tozer *et al.*, 2008b, Clémenson *et al.*, 2013, Liang *et al.*, 2016).

1.5.4 Combining VDAs with targeted therapy

The combination of VDA-induced vascular shutdown and inhibition of vessel regrowth using targeted anti-angiogenic agents theoretically serves as a two-pronged attack on tumour vasculature. Pre-clinical studies have supported the hypothesis that co-administration of VDAs and anti-angiogenic agents improves the efficacy of both treatment modalities in comparison to their use as monotherapies (Siemann *et al.*, 2017). Although the majority of these studies have focussed on bevacizumab, combination of sunitinib (Nguyen *et al.*, 2016) and pazopanib with VDAs have also improved efficacy in CRC liver metastases and ovarian cancer respectively. The latter combination of pazopanib with CA4P progressed into early clinical trials, however acute hypertension led to premature discontinuation of the trial (Morgan *et al.*, 2018). Further studies are required to fully understand the mechanisms that led to this toxicity.

In recent years the focus on immunotherapy and the use of checkpoint inhibitors has led to it becoming one of main treatment modalities for cancer. As with other targeted therapies, there are tumours that do not respond to this form of treatment which are referred to as 'immunologically cold'. In a pre-clinical mammary carcinoma model, pre-treatment with CA4P or OXi4503 improved the sensitivity of these immunologically cold tumours to checkpoint inhibitors (Horsman *et al.*, 2020). These recent results further highlight the potential for VDAs in combination with other therapeutic options in overcoming treatment resistant tumours.

VDA	Development phase and indication	Combination therapy
BNC105 / BNC105P	Phase I (Multiple cancer types) Phase I (CLL) Phase II (mRCC and CRC) Phase II (Mesothelioma as monotherapy)	Carboplatin & gemcitabine (Ovarian cancer) Ibrutinib (CLL) Everolimus (mRCC) Nivolumab (CRC)
CKD-516 (NOV120401)	Phase I (Solid tumours as monotherapy) Phase I/IIa (CRC)	Irinotecan (CRC)
Crolibulin (EPC2407)	Phase II (Thyroid cancer)	Cisplatin
Denibulin (MN-029)	Phase I (Multiple cancer types)	None
Fosbretabulin (CA4P)	Phase I (Multiple cancer types) Phase II (GB) Phase II (Thyroid cancer) Phase II (GI-NETs/pNETs) Phase II (Melanoma) Phase III (Ovarian cancer)	Carboplatin, paclitaxel & bevacizumab (NSCLC) Carboplatin & paclitaxel (Thyroid cancer) Everolimus (pNETS) Nivolumab (Melanoma) Carboplatin & paclitaxel (Ovarian cancer) Bevacizumab (Ovarian cancer) Pazopanib (Ovarian cancer)
Lexibulin (CYT997)	Phase I (Multiple cancer types) Phase Ib (GB) Phase II (MM)	Carboplatin (GB)
Oxi4503 (CA41P)	Phase I (Multiple cancer types) Phase II (Hepatic tumours) Phase II (AML)	Cytarabine (AML)
Plinabulin (NPI-2358)	Phase I/II (Multiple cancer types) Phase II (NSCLC) Phase II (SCLC)	Nivolumab (Melanoma) Docetaxel (NSCLC) Nivolumab & ipilimumab (SCLC)
Soblidotin (TZT-1027)	Phase I (Multiple cancer types) Phase II (Sarcoma) Phase II (NSCLC)	Carboplatin (Multiple solid cancers)
Verubulin (MPC-6827)	Phase I (Multiple cancer types) Phase I/II (GB)	Carboplatin (GB) Temozolamide (GB)

Table 1.2 Clinical trials with VDAs

VDAs that have undergone evaluation in clinical trials in combination with standard therapy.

m, metastatic; AML, acute myeloid leukaemia; CRC, colorectal cancer; GB, glioblastoma; MM, multiple myeloma; RCC, renal cell carcinoma; NSCLC, non-small cell lung cancer; GI, gastrointestinal; pNET, pancreatic neuroendocrine tumours; SCLC, small cell lung cancer. Table adapted from Gill *et al.* (2019).

1.6 Soft tissue sarcoma and anti-angiogenic therapy

1.6.1 Soft tissue sarcoma

Soft tissue sarcomas (STS) are a heterogeneous group of malignancies with a low rate of incidence across all populations that arise from mesenchymal cell precursors. Located in the non-epithelial extraskelatal tissue, there are in excess of 80 histological subtypes which are classified according to the adult tissue which they most resemble i.e. angiosarcomas recapitulate vascular endothelium (Goldblum *et al.*, 2014, Casali *et al.*, 2018). As a result of the numerous subtypes and their occurrence in virtually any anatomical site, there are a huge number of possible histological combinations that all have different therapeutic implications and clinical outcomes (Stiller *et al.*, 2013). The World Health Organisation (WHO) classifies STS under the following 12 headings; adipocytic, fibroblastic/myofibroblastic, so-called fibrohistocytic, smooth muscle, pericytic (perivascular), skeletal muscle, vascular, chondro-osseous, gastrointestinal stromal tumours (GIST), nerve sheath, tumours of uncertain differentiation and finally undifferentiated/unclassified sarcomas (Jo and Fletcher, 2014). In more challenging sarcoma subtypes, molecular features and genetic alterations may be considered; these sarcomas can be broadly classified as having either simple karyotypes or complex aneuploidy karyotypes (Bleloch *et al.*, 2017). STS (with the exclusion of GIST) are a principle group of rare cancers in Europe, accounting for approximately 1% of all cancers in adults and ~7% of childhood cancers. In adults, with the exclusion of GIST, the most commonly represented histological subtypes are liposarcoma and leiomyosarcoma. In paediatric STS, rhabdomyosarcoma is the dominating subtype, affecting half the population of children with STS (Casali *et al.*, 2018, Skapek *et al.*, 2019). In the U.S. it is predicted that, in 2019, approximately 12,750 new STS cases will be diagnosed and STS will result in around 5,270 deaths (Siegel *et al.*, 2019).

As a consequence of the genetic complexities and heterogeneity in the wide spectrum of STS subtypes, pathogenesis, clinical outcome and treatment regimens vary and these tumours are therefore regarded as difficult to treat (Pasquali *et al.*, 2019).

1.6.2 Current treatment of STS

Despite the heterogeneity of STS, and with the exception of GIST, which is primarily treated with the TKI imatinib, the histology-driven treatment strategies remain relatively similar across the board (Pasquali and Gronchi, 2017). In most localised STS, treatment is multimodal and the standard primary treatment is wide surgical resection, either alone or in combination with chemo- or radiation therapy. Despite the aggressive nature of this treatment, nearly half of STS patients go on to develop ultimately

fatal advanced/metastatic disease (Sharma *et al.*, 2013). Furthermore, only 8% of STS patients with metastatic disease reach long-term survival and OS generally fails to exceed 15-30 months (Saponara *et al.*, 2017). In advanced STS, treatment varies, however chemotherapy is typically used as first-line treatment and overall response rates are ~25%. The use of adjuvant or neoadjuvant chemotherapy being of benefit still remains unresolved and it is suggested that there are chemoresistant and chemosensitive STS subtypes. Meta- and pooled analyses, as well as individual studies into the efficacy of systemic chemotherapy have presented conflicting evidence regarding local remission, distal metastases and overall recurrence across the STS subtypes following treatment (Linch *et al.*, 2014, Saponara *et al.*, 2017). The same holds true with radiotherapy; although radiation may improve local control of sarcoma of the extremities, there are conflicting data surrounding whether it is of benefit in other STS subtypes (Bleloch *et al.*, 2017). The only single-agent chemotherapeutic drugs that achieve a response rate of over 20% in advanced/metastatic STS are doxorubicin, epirubicin or ifosfamide, and once again the efficacy of these drugs varies wildly between histological subtypes (Lehnhardt *et al.*, 2005). Gemcitabine, trabectin and eribulin are further chemotherapeutics that have also shown some activity as single-agents in leiomyosarcoma and liposarcoma. Combination chemotherapy is the most widely accepted and extensively explored treatment approach in metastatic STS, however comparison studies between single-agent and combination therapy regimens have thus far failed to identify which option is more beneficial to OS of STS patients (Bleloch *et al.*, 2017). Once again this is most likely due to the mixed cohorts within these studies together with variable response of the histological subtypes to these treatments.

1.6.3 Angiogenesis in STS

As with all tumours, STS rely on angiogenesis for progression and dissemination and angiogenesis and high vascularisation are common characteristics of STS. Currently there are limited effective systemic therapies available; given the importance of angiogenesis in STS, an attractive option is targeted interruption of angiogenic signalling cascades.

1.7 Anti-angiogenic treatment in STS

1.7.1 VEGF pathway inhibitors in non-GIST STS

As discussed above, targeting tumour angiogenesis is already a widely accepted treatment option in more prevalent malignancies. The anti-tumour effects of anti-angiogenic treatment in animal models of human sarcoma and the success of VEGF targeted therapies in other cancers, such as RCC, has led to a sharp increase in trials evaluating their effectiveness in non-GIST STS (Sleijfer *et al.*, 2008, Vo *et*

al., 2016). Unfortunately, trial validation is severely hampered by the heterogeneity and rarity of this cohort and so far much of this research has failed to translate into the clinic. Given the relative rarity of STS, recruitment for sufficiently powered phase III trials has led to treatment efficacy being evaluated in unselected patient populations that include a jumble of subtypes and various levels of pre-treatment (Choe and Riedel, 2018). Between January 2000 and June 2018, only two phase I and II clinical trials in STS that included anti-angiogenic agents progressed to phase III trials, and only one of these resulted in FDA-approval of the drug in question (Lee *et al.*, 2019). The phase III PALETTE trial (Van Der Graaf *et al.*, 2012) resulted in pazopanib becoming the first FDA and (European Medicines Agency) EMA approved therapy targeting angiogenesis in advanced and non-adipocytic STS and is currently the only approved angiogenesis targeted treatment following disease progression after chemotherapy (Table 1.3). When administered as a monotherapy, anti-angiogenic agents appear to provide modest survival benefits in some STS subtypes, yet are of no significant benefit in others. Therefore focus has shifted to combining anti-angiogenic treatments with other systemic treatments (Vo *et al.*, 2016).

Based on promising Phase I trial data, demonstrating the combination of TRC105 (carotuximab), a chimeric monoclonal antibody to endoglin, with bevacizumab in solid tumours potentiated bevacizumab a further phase Ib/IIa trial combining TRC105 and pazopanib was undertaken in non-adipocytic advanced STS (Gordon *et al.*, 2014). Following a positive response from angiosarcoma (AS) patients enrolled in this trial, including durable complete response in 2 of the patients (Attia *et al.*, 2016), a phase III trial of TRC105 and pazopanib versus pazopanib alone in patients with advanced angiosarcoma (TAPPAS [NCT2979899]) is currently ongoing (Young and Woll, 2017, Mehta *et al.*, 2019).

In a retrospective analysis, sorafenib was the first anti-angiogenic TKI that showed promise in treating desmoid tumours/deep fibromatoses (Gounder *et al.*, 2011). These findings prompted a phase III trial, the results of which provided evidence for the anti-tumour activity of sorafenib in treating desmoid tumours in both a first and second line setting (Gounder *et al.*, 2018). In the sorafenib treated arm, 33% of patients achieved a partial response compared with 20% of patients in the placebo arm. Furthermore, 1-year PFS for the patients in the sorafenib treated group was 89% versus 46% for patients receiving placebo.

Another TKI that has shown to be of benefit in the palliative-care of non-liposomal doxorubicin-refractory STS patients is regorafenib. Results of the phase II trial, REGOSARC, assessed the impact of

regorafenib versus placebo in 4 cohorts of patients: liposarcoma, leiomyosarcoma, synovial sarcoma and other non-adipocytic sarcomas. Overall, in the combined non-adipocytic patient cohorts there was a 3 month improvement in PFS and despite a high number of crossover patients from the placebo arm there was a trend toward improved OS of ~4 months (Berry *et al.*, 2017).

In summary, TKIs show varying levels of activity across the STS subtypes. AS and solitary fibrous tumours (SFT) appear to be sensitive to sorafenib. The anti-tumour activity of sunitinib has been reported in alveolar soft part sarcomas, SFT, clear cell and extraskeletal myxoid chondrosarcoma and responses to both sorafenib and sunitinib have been reported in advanced dermatofibrosarcoma protuberans. Encouraging results in the treatment of alveolar soft part sarcoma with cediranib and the activity of tivozanib, an as yet unlicensed TKI, in heavily pre-treated STS have also been reported (Frezza *et al.*, 2017). The introduction of TKIs in the management of STS has produced encouraging results, however, with the exception of pazopanib, no other anti-angiogenic agents have received FDA-approval in STS (Table 1.3) but based on clinical trial data are administered 'off-label' on a case-by-case basis (Eberst *et al.*, 2014).

1.7.2 Bevacizumab in STS

A search of the Clinical Trials database (Clinicaltrials.Gov, 2019) with the terms 'bevacizumab' and 'sarcoma, soft tissue' delivers a list of 34 trials dating from 2005 to the present. The majority of which are evaluating the benefit of combining bevacizumab with other treatments such as radiotherapy, chemotherapy or immunotherapy. Published results from the completed trials present contradictory evidence for the efficacy of bevacizumab in STS, which highlights the need to stratify patient populations most likely gain benefit from this line of treatment.

ASs overexpress VEGF and preclinical studies highlight angiogenesis as a key component of AS progression, therefore the assessment of anti-angiogenic agents in this rare and aggressive STS subtype seems a rational line of enquiry. The first single-arm phase II trial in AS and epithelioid hemangioendothelioma using bevacizumab as a monotherapy provided encouraging results, with 50% of the cohort showing stable disease with a mean time until disease progression of 24 weeks (Agulnik *et al.*, 2012). Two phase II clinical trials assessing the activity bevacizumab in combination with paclitaxel in AS have subsequently been completed. The first of which, comparing combination treatment to paclitaxel alone, reported disappointing results. Response rates in the combination arm were lower (29% vs. 46%) and the six month PFS rate was identical in both treatment arms. Furthermore, the addition of bevacizumab resulted in a higher rate of serious adverse effects (Ray-

Coquard *et al.*, 2015). The most recent study was a small (n=16) single arm study which reported similar PFS rates as Ray-Coquard *et al.* (2015) and 3 serious adverse events (Bui *et al.*, 2018).

A single-arm phase II study suggested inclusion of bevacizumab (15 mg/kg on day 1 of a 21 day cycle for 6 cycles) to the standard gemcitabine and docetaxel regimen of treatment in a mixed cohort of 35 STS patients may be of benefit to PFS. The Response Evaluation Criteria In Solid Tumours (RECIST) response rate of 49% and 3-month PFS survival of 76% reported in this study seems favourable; however, it is hard to draw any definitive conclusions from these data, as although patient withdrawal was not directly as a result of disease progression, the study failed to meet its primary endpoint. Interestingly, 4 of the 5 AS patients enrolled had demonstrable tumour shrinkage (Dickson *et al.*, 2015). In contrast, a recent phase II trial showed no significant improvement in event free survival when adding bevacizumab to standard chemotherapy in both childhood and adolescent patients with metastatic STS (Chisholm *et al.*, 2017). In short, no real progress has been made in terms of robust clinical trial data. This is largely due to the multitude of study designs and the heterogeneity of patient cohorts which in turn results in a disconnect when trying to look at the data as a whole.

Anti-angiogenic therapy, either as a single-line treatment or in combination with chemotherapy may prove beneficial in a subset of STS patients due to the highly vascular nature of these tumours. As the evaluation of predictive biomarkers in anti-VEGF therapy in STS is currently lacking, it is of interest to determine whether the results from biomarker studies in clinical trials detailed below can translate to STS.

1.7.3 Gastrointestinal stromal tumours

The most successful advance in STS treatment with VEGF pathway inhibitors in recent years is in GIST. Pazopanib and sunitinib are used upon disease progression following imatinib therapy. Although not designed as an anti-angiogenic drug, through inhibition of BCR-ABL, c-KIT, PDGFR α and β signalling cascades, imatinib causes a reduction in VEGF expression which subsequently leads to a reduction in tumour angiogenesis. (Debiec-Rychter *et al.*, 2006).

Drug name	Brand name	STS subtypes with anti-VEGF therapy activity
Afilbercept	Zaltrap	Metastatic gynecologic soft-tissue
Bevacizumab	Avastin	Angiosarcoma, solitary fibrous tumour/hemangiopericytoma
Cediranib		IMT with ALK translocation, ASPS
Pazopanib	Votrient	Non-adipocytic STS ^d , GIST ^a
Regorafenib	Stivarga	GIST, doxorubicin-pretreated advanced, non-adipocytic STS.
Sorafenib	Nexavar	GIST ^a , desmoid tumours, angiosarcoma, solitary fibrous tumour/hemangiopericytoma
Sunitinib	Sutent	GIST, angiosarcoma, ASPS, solitary fibrous tumour/hemangiopericytoma
Tivozanib		In phase III trials ^c

Table 1.3 Anti-angiogenic agents with activity in STS

VEGF pathway inhibiting agents that are either FDA approved for the treatment of STS or can be used off-label (Casali *et al.*, 2018, Von Mehren *et al.*, 2018)

^a FDA approved for disease progression following treatment with imatinib, sunitinib and regorafenib, ^c Currently not FDA-Approved, ^d Recommended only for palliative therapy

GIST, gastrointestinal stromal tumours; ASPS, alveolar soft part sarcoma; IMT, inflammatory myofibroblastic tumour; ALK, anaplastic lymphoma kinase; NSCLC, non-small cell lung cancer; RCC, renal cell carcinoma; UMTCC, urothelial metastatic transitional cell cancer; CRC, colorectal cancer; IgG, immunoglobulin

1.8 Biomarkers

Biomarkers are specific tissue, cellular or functional characteristics that can be evaluated to determine the outcome of physiological processes, pathophysiological processes or assess the likely response to therapeutic intervention. Prognostic biomarkers are used to estimate disease progression in the absence of therapy, whereas predictive biomarkers are used to gauge the likely response of a patient receiving therapy. Additionally, biomarkers that change after or during treatment, referred to as pharmacodynamic biomarkers, can be used to ascertain how a patient is responding to therapy and whether or not modifications need to be made (Jain *et al.*, 2009).

1.8.1 Patient response and resistance to anti-angiogenic therapy

The use of anti-angiogenic drugs targeting VEGF signalling has improved therapeutic options in several cancers, yet patient response to these agents remains unpredictable and in many cases unsustainable. Clinical trials have shown that improved PFS observed in indications such as GBM, breast and ovarian cancer does not translate to clinically meaningful rates of OS (Hegde *et al.*, 2018). Resistance to anti-angiogenic agents is a major challenge in this emerging class of targeted therapy and the underlying mechanisms are still largely unclear. In the majority of patients that are initially responsive to treatment, tumours ultimately acquire resistance, hence low OS rates and poor durability of stable disease, whilst others appear to be intrinsically resistant. In some malignancies, such as RCC, patients experience stabilised disease for a prolonged period, whereas in other cancers, such as pancreatic and prostate cancer, progression rapidly follows an initial response and at worst, treatment is not efficacious at all (Lambrechts *et al.*, 2012). Originally, it was thought that by targeting the more genetically stable ECs surrounding tumours with angiogenesis inhibitors would be less susceptible to induction of resistance (Van Beijnum *et al.*, 2015). Unfortunately, this is not the case. Resistance to anti-angiogenic drugs does occur and is a significant barrier in their efficacy; some tumours are intrinsically resistant, whilst others acquire resistance over the course of treatment as a result of tumour adaptations. The multifaceted evolution of tumours in response to anti-angiogenic drugs is extremely complex. The numerous adaptations and escape mechanisms employed by tumours that are either intrinsically resistant or acquire resistance to anti-angiogenic drugs are both tumour and drug dependent. Broadly speaking, the principle mechanisms involved in the refractory to anti-VEGF therapy can be categorised

thus: hypoxia induced, inflammatory/immune cell mediated, alternative vascularisation associated or as a result of blood vessel normalisation (Ribatti, 2016).

Anti-VEGF therapy is somewhat paradoxical; a treatment that cuts off the tumour's oxygen supply can result in some cells surviving treatment in a hypoxic environment and, as discussed in a previous section, hypoxia is the primary trigger of pro-angiogenic growth factor release. The hypoxic tumour microenvironment created through successful blockade of the VEGF axis not only increases the release of pro-angiogenic growth factors and cytokines, it also results in metabolic reprogramming of tumour cells. Clinical and preclinical data have provided evidence that inhibition of a single growth factor can induce the expression of others. One of the primary adaptations is the activation of alternative pro-angiogenic pathways whilst the original drug target remains inhibited (Jiménez-Valerio and Casanovas, 2017). As touched upon earlier, the VEGF/VEGFR axis is not the only pathway associated with angiogenesis and EC activation (Figure 1.1 and Figure 1.3) and it has been suggested that the inhibition of VEGF and its receptors may cause tumours to switch from VEGF-dependent angiogenic processes to a VEGF-independent state (Jászai and Schmidt, 2019). Ang-1 and -2, Dll4, FGF1 and 2, PDGF-C, HGF, TGF β , Ephrins, interleukins and their cognate receptors are just some of the alternative angiogenic pathways that can be exploited by the tumour to circumvent reliance on the VEGF axis for vascularisation (Van Beijnum *et al.*, 2015, Khan and Bicknell, 2016). Additionally, other members of the VEGF family, namely VEGFC and PlGF, are strongly linked to resistance in VEGF monotherapy. The NRPs have been implicated in these mechanisms, as both NPR1 and NPR2 bind PlGF; moreover, NPR2 also binds with VEGFC and interacts with VEGFR2 (Gacche, 2015). Elevation of hypoxia related growth factors also leads to the recruitment of bone-marrow derived myeloid cells, tumour associated macrophages and CAFs, all of which are associated with alternative angiogenic mechanisms and promotion of vascularisation (Ribatti, 2016).

In the context of the vessel normalisation hypothesis, VEGFR2 signalling inhibition in particular is implicated in more stabilised vessels through upregulated Ang-1/Tie2 signalling and increased pericyte coverage of tumour blood vessels. Not only can pericytes activate compensatory pro-angiogenic PDGFR-mediated signalling in adjacent CAFs, they are also reported to render vessels impermeable to anti-VEGF agents (Gacche, 2015, Jászai and Schmidt, 2019).

1.8.2 Assessment of clinical efficacy of vascular-targeted therapy

The accurate assessment of therapeutic response is essential. In the majority of clinical trials the RECIST criteria is used to assess tumour shrinkage or disease progression in response to targeted therapies. This radiographic method of assessing tumour burden typically uses X-ray computed tomography (CT), positron emission tomography (PET) and magnetic resonance imaging (MRI) to assess tumour size. A reduction of $\geq 30\%$ from baseline measurements is deemed an objective response and an increase of $\geq 20\%$ in relation to the lowest tumour size through the study is regarded as disease progression (Eisenhauer *et al.*, 2009). However, vascular-targeted therapies may result in different anti-tumour effects, such as tumour density alterations rather than overall tumour shrinkage (Pasquali and Gronchi, 2017). What has become more apparent is that, especially in the case of STS, RECIST may not be the most effective measure of tumour response.

An emerging field in tumour imaging is radiomics. Advanced imaging analysis combines both conventional and novel imaging techniques to provide additional information that is currently not being used to predict or monitor treatment response (Lambin *et al.*, 2012, Aerts *et al.*, 2014). In a small proof of concept study, Yin *et al.* (2017) combined radiomic analysis with PET/MRI scans to quantify microvascular density (MVD) and assess angiogenesis in primary clear-cell RCCs. Although small, this study highlighted the potential for mining conventional scanning techniques for structural and functional information that may be more indicative of the effects of anti-vascular treatments.

1.8.3 The importance of biomarkers in anti-angiogenic therapy

Unlike some other targeted therapies, which are administered to patients who exhibit specific biomarkers, there are no defined selection criteria for anti-angiogenic agents, and therefore they are generally administered based on indication. Clinical trials of bevacizumab and other VEGF pathways inhibitors in both single-line and combination therapy have reported a marked variation in patient response (Van Cutsem *et al.*, 2012); a number of trials evaluating VEGF inhibitor efficacy in an adjuvant setting have produced negative results, thus highlighting the fact that this particular line of therapy does not benefit all patients. Of particular note was the withdrawal of FDA approval for the use of bevacizumab in metastatic BC (mBC); phase III clinical trials demonstrated an improvement in PFS when combined with chemotherapy, however it failed to improve OS (Miller *et al.*, 2007, Miles *et al.*, 2010, Robert *et al.*, 2011). On the face of it these results seem discouraging, however, they don't really tell the whole story,

as there are subsets of patients for which anti-VEGF therapy is enormously beneficial in terms of OS. These underwhelming clinical results could be improved upon through biomarker discovery. If the risk of administering anti-VEGF treatment to patients who are either intrinsically resistant or more likely to acquire resistance was mitigated, then clinical trials in select patient populations may provide a clearer picture of their efficacy. Additionally, predictive biomarkers could aid in the optimisation of dosing, scheduling or co-administration of anti-angiogenic agents in order to improve their efficacy. It is therefore an urgent requirement to elucidate robust predictive biomarkers to identify patients that would benefit from treatment with VEGF pathway inhibitors.

1.8.4 Predictive biomarkers for VEGF pathway inhibitors

Up until fairly recently, analyses of biomarker candidates that predict response to anti-VEGF therapy have largely focussed on molecules or characteristics associated with angiogenesis. To this end, both tissue and circulating expression levels of total VEGF, VEGF isoforms and VEGF receptors have been broadly evaluated pre-clinically and clinically for their suitability as predictive biomarkers (Lambrechts *et al.*, 2013). An untargeted approach to biomarker identification, such as genomic and proteomic profiling of the entire tumour genome/proteome, has the potential to uncover less obvious biomarkers that are not directly linked to angiogenesis. A recent example of this is in sorafenib resistant HCC. Proteomic analysis of the sorafenib resistant Huh7 cell line, identified the overexpression of the 78 kDa glucose regulatory protein (GRP78) which was subsequently found to be associated with shorter PFS in sorafenib treated HCC patients (Feng *et al.*, 2019). A hugely powerful tool that allows quantification of gene expression levels across the whole genome is next generation sequencing (NGS), which is likely to prove invaluable in future biomarker studies. Furthermore, analyses of open access global databases such as the Cancer Genome Atlas (TCGA) are also giving rise to new information with regard to tumour biology that could prove invaluable in the search for biomarkers.

Preclinical animal studies and clinical trials have identified a number of tumour, circulating, genetic, physiologic and imaging biomarkers of anti-angiogenic therapies that warrant further investigation. Inconsistencies in the data however have proved a challenge, therefore these investigations have yielded very little in terms of successfully identifying a single biomarker that can reliably predict patient outcomes in response to anti-VEGF therapy (Jahangiri and Aghi, 2012, Lambrechts *et al.*, 2013). One confounding factor is likely due to the extensive

overlap and cross talk between angiogenic signalling cascades. Efforts are further hampered by the co-administration of other therapies either prior to or alongside anti-VEGF agents.

1.8.5 VEGF as a prognostic biomarker

In terms of prognostic value, high circulating baseline levels of VEGF are consistently attributed to a poorer prognosis in numerous cancers (Hegde *et al.*, 2018). In STS, RNA, protein and serum VEGF overexpression has been reported, yet there is very little information in terms of its reliability as a prognostic biomarker. A handful of studies report a correlation between high serum or tumour VEGF with higher tumour grade and stage (Graeven *et al.*, 1999, Chao *et al.*, 2001, Yudoh *et al.*, 2001, Yoon *et al.*, 2006). More recently, high tumour VEGF was identified as a negative prognosticator of recurrence-free, metastases-free and disease-specific survival in STS arising from the extremities and trunk. In contrast, it was not prognostic in STS arising from visceral and retroperitoneal locations (Kilvaer *et al.*, 2014).

1.8.6 VEGF as a predictive biomarker

In contrast to the strong prognostic value of VEGF, its potential as a pre-treatment predictive biomarker is less clear. On the premise that the clinical outcome of targeted therapy may be influenced by initial expression of the therapeutic target/s, a number of trials have carried out analyses of baseline VEGF, VEGF isoforms and VEGF receptor expression levels. Tumour VEGF levels did not appear to be a predictor of survival benefit for bevacizumab treatment efficacy in mCRC or mBC, yet the predictive value of circulating VEGF levels is up for debate (Jubb *et al.*, 2006, Jubb *et al.*, 2011). One explanation for this is the observation that, in metastatic disease at least, circulating VEGF levels do not directly correlate with VEGF expression in the primary tumour (Hegde *et al.*, 2013). In a prospective NSCLC clinical study, high pre-treatment levels of phosphorylated VEGF (pVEGF) were predictive of a better response in patients receiving bevacizumab plus chemotherapy compared to chemotherapy only, although it did not predict OS (Dowlati *et al.*, 2008). The same has been reported in single-arm studies in breast, endometrial and ovarian cancer, but these results were not substantiated by others (Lambrechts *et al.*, 2013). Furthermore, retrospective analyses of pVEGF levels from five randomised trials of bevacizumab in mCRC, NSCLC and mCC, four of which were major phase III studies, confirmed the strong prognostic value of pVEGF but failed to identify any correlation between baseline pVEGF and improvements in PFS and/or OS (Hegde *et al.*, 2013).

In agreement with Hegde *et al.* (2013), biomarker evaluation of the retrospective phase III clinical trial AVAGAST (advanced gastric cancer) showed that high baseline pVEGF was again prognostic but not predictive in mCRC, NSCLC and mRCC (Van Cutsem *et al.*, 2012). Conversely, Van Cutsem *et al.* (2012) identified high baseline pVEGF correlated with improved PFS and OS in the bevacizumab treated advanced gastric cancer patients. These results echoed findings from the same laboratory group that reported high baseline pVEGF as a predictor of improved response to bevacizumab during predictive biomarker analysis of the phase III AVADO trial in human epidermal growth factor-2 HER2-negative metastatic breast and the phase III AViTA trial in pancreatic cancer (Van Cutsem *et al.*, 2012). A meta-analysis of three phase III breast cancer trials, BEATRICE (triple negative BC), AVEREL (Her2-positive locally recurrent mBC) and AVADO (Her2-negative mBC) also reported that patients with above median levels of baseline pVEGF had an improvement in disease control with the addition of bevacizumab to chemotherapy, whilst patients below median pVEGF levels showed no gain by the addition of bevacizumab to their treatment regimen (Dos Santos *et al.*, 2015). Through genotype-by-treatment interaction testing, a meta-analysis performed using individual patient data from six randomised phase III clinical trials in gastric (AVAGAST), colorectal, breast (AVADO), lung (AVAiL) and pancreatic (AViTA) cancer identified a genetic variant of the VEGFA gene that showed a weak genotype-by-treatment interaction (De Haas *et al.*, 2014). The VEGFA variant was deemed as potentially predictive of bevacizumab treatment outcome as it significantly affected VEGF expression levels, yet failed to reach significance after the interaction analysis. On the other hand, recent results published from the MERiDiAN trial, the first phase III study that prospectively evaluated pVEGF as a predictive biomarker for bevacizumab efficacy in mBC, have brought into question the previously suggested predictive value of pVEGF. Although addition of bevacizumab to paclitaxel correlated to improved PFS, there was no correlation between baseline pVEGF and treatment benefit (Miles *et al.*, 2017). To add a further layer of complexity to these discordant results, a meta-analysis of 11 mCRC studies, Zhao *et al.* (2016) concluded both high pVEGF and intratumoral VEGF were predictive of poor PFS and OS in patients receiving bevacizumab.

1.8.7 VEGF isoforms as a predictive biomarker

To date, antibodies that can specifically detect individual VEGF isoforms do not exist. The multiplexed enzyme-linked immunosorbent assay (ELISA) used in three of the studies mentioned above; the AVADO (Miles *et al.*, 2010), the AVAGAST (Van Cutsem *et al.*, 2012) and the AViTA trial (Lambrechts *et al.*, 2012), were reported to have a preference for the shorter,

soluble VEGF isoforms VEGF₁₁₀ and VEGF₁₂₁. This led to the hypothesis that the expression pattern of VEGF isoforms may serve as a more promising predictive marker of response to anti-VEGF therapy than total circulating VEGF levels. In the first small single-arm study of two separate studies in recurrent GBM carried out by the same research group, low levels of intratumoral VEGF₁₂₁ mRNA correlated with improved clinical responses to bevacizumab (D'alessandris *et al.*, 2015). The second study, which although still small, included a control arm and found low baseline plasma levels of VEGF₁₂₁ was associated with improved PFS and OS in response to bevacizumab treatment (Martini *et al.*, 2018). A small study on metastatic renal carcinoma has also shown high tumour levels of VEGF₁₂₁ to be predictive of benefit to sunitinib treatment (Paule *et al.*, 2010). Though definitive conclusions cannot be drawn from these small studies, their results warrant further investigations in larger cohorts, provided sensitive techniques that can distinguish between different isoforms can be developed. Interestingly, pre-clinical data from English *et al.* (2017) is in concordance with the clinical findings. Murine fs cells expressing the single VEGF₁₂₀ isoform metastasised more readily to the lung and showed increased sensitivity to the anti-VEGF antibody B20-4.1.1.

1.8.8 NRP1 as a prognostic biomarker

Tumour progression is a multifaceted process that is driven and supported by multiple cell types both within the tumour and in the tumour microenvironment. NRP1 is expressed by such a wide range of cells associated with the processes of tumour progression it is of no surprise that expression levels are of prognostic relevance. NRP1 has been shown to play a key role in promoting metastases, cancer stem cell-ness, dedifferentiation of cells, desmoplasia, immunoinhibitory signalling and EMT through various discrete pathways (Niland *et al.*, 2018). NRP1 expression levels predominantly correlate with tumour growth, increased tumour cell survival, greater metastatic potential and increased VEGF-dependent angiogenesis (Parikh *et al.*, 2004, Appleton *et al.*, 2007, Liu *et al.*, 2015). Upregulated NRP1 expression in numerous malignancies inclusive of breast, lung, prostate and CRC, HCC, neuroblastoma, astrocytoma and osteosarcoma is generally associated with poorer clinical outcome (Niland and Eble, 2019). A handful of studies have published data to the contrary. Experimental *in vivo* and *in vitro* data using human pancreatic carcinoma cells (FG and Panc-1 cells) showed NRP1 overexpression correlated with reduced tumour incidence and volume, enhanced chemoresistance and inhibition to anoikis (Gray *et al.*, 2005, Wey *et al.*, 2005). In colon cancer, a single study supports the notion that preserved NRP1 expression may provide patients with a better prognoses (Kamiya *et al.*, 2006). In clinically localised prostatic cancer,

one study has reported that, together with high Sema3A levels, high NRP1 expression may be prognostic of a more favourable patient outcome. Interestingly in the same study, high NRP1 was also detected in advanced hormone-refractory prostatic cancer (HRPC), however Sema3A expression was lower. They suggest that, in the case of prostatic cancer, whether NRP1 is pro- or antitumorigenic is dependent on the predominant ligand, as the VEGF/Sema3A ratio was higher in hormone refractory prostate cancer (Yacoub *et al.*, 2009). Most recently, NRP1 knockdown in neuroblastoma enhanced invasiveness *in vitro* and, through the analysis of public datasets, correlated with shorter patient survival (Ishizuka *et al.*, 2018). Nonetheless, even though these few studies do raise the possibility of NRP1 as a tumour-suppressor, both clinical and experimental data predominantly associates NRP1 with poor prognosis.

As is the recurring theme, there is distinct lack of data with regard to NRP1 expression in STS; however, retrospective analysis of 50 resected primary uterine leiomyosarcoma LMS tumours found high NRP1 expression was linked to more advanced clinical grade and worse prognosis, consequently researchers have proposed NRP1 may be of use as a predictor of postoperative survival in uterine LMS (Bobinski *et al.*, 2018). In osteosarcoma, the same pattern is evident. Osteosarcoma tissue from 166 primary tumours showed significantly elevated mRNA and protein levels of NRP1 in comparison to matched non-cancerous bone tissue. Furthermore, advanced clinical grade osteosarcomas exhibited higher NRP1 protein expression, an increase in distal metastases and poorer response to chemotherapy. In comparison to osteosarcomas with low NRP1 expression, patients with high NRP1 expressing tumours had large high grade tumours, distal metastases, poor response to chemotherapy and had significantly shorter OS and disease free survival (DFS) times (Zhu *et al.*, 2014).

Within a small cohort of NSCLC lesions, a statistically significant increase in NRP1 expression in the cytoplasmic region of tumour cells and in ECs was identified in comparison with benign tumours. Additionally, a positive correlation was observed in the OS of patients identified as having low NRP1 expression. OS in patients with high NRP1 expression was 10 months in comparison to 14.5 months in patients with low NRP1 expression (Ding *et al.*, 2014).

1.8.9 NRP1 as a predictive biomarker

Retrospective analysis of primary tumour tissue from a phase III trial in heavily pre-treated mBC patients (AVF2119g) concluded that patient subgroups with low expression of endothelial NRP1 showed a trend toward benefit from the addition of bevacizumab to

capecitabine (Jubb *et al.*, 2011). Similarly in CRC, low baseline NRP1 correlated with increased benefit from bevacizumab with chemotherapy (Lambrechts *et al.*, 2013). To add strength to the potentially predictive value of NRP1 expression, tissue biomarker studies from the AVAGAST trial in gastric cancer revealed that patients with low baseline tumour expression levels of NRP1 gained greater benefit from bevacizumab treatment in terms of both PFS and OS than those with high expression levels (Van Cutsem *et al.*, 2012). Retrospective analysis of a 31 tissue samples from a phase II clinical trial in which irinotecan-refractory mCRC patients were treated with either bevacizumab and cetuximab, or bevacizumab and cetuximab plus irinotecan, found that high intratumoural mRNA levels of NRP1 were associated with longer OS in both arms of the study (Zhang *et al.*, 2010). In the absence of a control arm, it is impossible to determine whether expression levels in this particular study were prognostic or predictive.

Recently a phase II trial in patients with previously untreated mCRC compared the efficacy of the VEGFR TKI tivozanib combined with modified folinic acid, fluorouracil, and oxaliplatin (mFOLFOX) against bevacizumab/mFOLOX. *Post hoc* evaluation of serum biomarkers found there was an increase in PFS in patients with low baseline serum NRP1 in both arms, which was consistent with previous reports for the prognostic value of NRP1. More importantly, patients with low NRP1 gained increased benefit from tivozanib/mFOLFOX in comparison to those with high baseline NRP1 (Benson *et al.*, 2016).

In contrast, a small trial in astrocytoma and GBM found no correlation between NRP1 expression and patient response to bevacizumab (Miles *et al.*, 2013, Baumgarten *et al.*, 2015). Nonetheless, authors identified a variance in NRP1 expression not only across the tumour grades but also between white and grey matter. It is therefore unsurprising that, in a small cohort of 18 patients with differing tumour grades, no statistically significant evidence was presented in terms of a predictive biomarker in response to bevacizumab treatment.

1.9 Summary

Over the last fifteen years a number of VEGF pathway inhibitors have entered the clinic and have led to substantial clinical improvements in various malignancies. Nevertheless, the magnitude of their positive impact has been overshadowed by disappointing clinical results as a result of variability in patient response. Positive PFS with the incorporation of anti-VEGF agents to treatment regimens has been widely reported, yet in a number of cases it did not

translate to OS. STS are a diverse and aggressive class of rare tumours of mesenchymal origin that rely heavily on angiogenesis for progression and dissemination. The positive correlation between VEGF expression, higher malignancy grade and poorer prognosis in STS has been well-documented and as such, targeting VEGF is considered a promising approach for improving patient survival. Since FDA approval of the RTKI pazopanib in 2012 for treatment of non-liposomal STS there has been little progress made in expanding the range of licensed agents targeting VEGF. One of the principle reasons behind this is the lack of robust biomarkers for selecting patients that are more likely to respond to this type of therapy. To date, no biomarkers for anti-VEGF patient stratification have been successfully validated in any malignancy. The complexities of tumour vascularisation make it unlikely that a lone biomarker can be predictive of the success of anti-VEGF therapies. Therefore approaches that incorporate one or more molecular signatures or characteristics may prove more successful.

VEGF isoforms are differentially expressed between tissues and elicit distinct biological consequences via their main signalling receptor, VEGFR2, and through the formation of VEGFR2/VEGF/NRP1 complexes. Promising data from large clinical trials has identified the individual potential of VEGF isoforms and NRP1 as predictive biomarkers of response to anti-VEGF therapy. The mechanisms between VEGF isoforms and NRP1 during tumour formation and vascularisation have not been widely explored and are therefore poorly understood. Given the divergent nature of the individual VEGF isoforms and their differential downstream signalling consequences when mediating VEGFR2/NRP1 complexes, the disruption of these interactions with anti-VEGF agents is of interest. Elucidating the underlying molecular mechanism of their predictive potential is essential if these findings are to translate back to the clinic and will determine whether they have predictive potential either individually or together.

1.10 Hypothesis

NRP1 and VEGF isoforms, either individually or in combination, are suitable pre-treatment biomarkers of tumour response to anti-VEGF therapy.

1.11 Aims

Tumours developed from mouse fs cells expressing single VEGF isoforms (fs120, fs164 and fs188) and wild-type controls (fswt) expressing all three isoforms establish distinct vascular motifs (Tozer *et al.*, 2008a). Furthermore, preclinical studies have provided evidence of differential responses to anti-VEGF therapy (English *et al.*, 2017). Fs120 cells metastasise more

readily to the lung and are more sensitive to anti-VEGF treatment in comparison to fs188 cells, thus paralleling the clinical data. *In vitro* studies have also identified differences in characteristics that are associated with cancer growth and metastases. Additionally, NRP1 expression between these cell lines also differs; fs120 and fs164 express significantly lower levels than fs188 and fswt (Kanthou *et al.*, 2014). Interestingly, in agreement with Koch *et al.* (2014), fs188 cells expressing high levels of NRP1 result in slower *in vivo* tumour establishment (Tozer *et al.*, 2008a, Kanthou *et al.*, 2014). These data suggest that there are distinct differences in tumour behaviour that may be reliant on the interplay of individual VEGF isoforms and NRP1 that warrant further investigation.

The principle aims of this study were to investigate the mechanistic links between NRP1 and VEGF isoforms and to establish the potential predictive value of NRP1 and VEGF isoforms for anti-VEGF therapy in STS.

1.12 Specific Aims

- Investigate *in vitro* effects of silencing NRP1 expression in fs188 and fswt cells (Chapter 3)
- Stable knockdown and overexpression of NRP1 in fs cell lines (Chapter 4)
- Evaluate the effect of NRP1 modification in fs cell lines *in vitro* in terms of proliferative and migratory characteristics (Chapter 4)
- Evaluate the effect of NRP1 knockdown in fs188 cells and overexpression in fs120 cells *in vivo* in terms of tumours growth, vascularisation and fibrosis (Chapter 5)
- Examine the influence of NRP1 expression on anti-VEGF therapy in fs188 and fs120 tumours, focusing on tumour growth and vascular characteristics (Chapter 5)

Chapter 2

Materials and Methods

For a full list of reagents and suppliers please refer to Appendix 1

2.1 Cell culture

2.1.1 Primary and secondary cell culture

Mammalian cells cultured *in vitro* are useful and powerful tools that are widely utilised to create model systems for investigation of cellular responses to particular conditions. Broadly speaking, mammalian cells can be categorised as primary or secondary cultures. Primary cultures are cells isolated directly from living tissue, and when they have exhausted nutrients and substrates in their media or surpass the capacity of the culture vessel they are subcultured (passaged); from this point on they are referred to as secondary cell lines/cultures or cell lines. In addition, cell lines may be either finite or continuous; finite cells have limited replicative capacity whereas continuous cell lines have undergone *in vitro* transformation to result in an immortalised cell line.

2.1.2 Cell subculture

Cell lines used during this study and the composition of the media required for standard subculture are detailed in Table 2.1.

In order to prevent cell death and promote proliferation, cells were routinely subcultured upon reaching ~80% confluence using pre-warmed reagents. Spent media was aspirated and cells were washed with Dulbecco's phosphate buffered saline (DPBS) without Ca^{2+} and Mg^{2+} before incubation for 5 min at 37°C with enough trypsin ethylenediaminetetraacetic acid (EDTA) to cover the base of the flask. Trypsin is a serine protease frequently used to dissociate adherent cells through cleavage of the peptide bonds responsible for cell-cell and cell-matrix interactions; exposure to trypsin was kept to a minimum to prevent damage to the cell membranes and subsequent cell death. The addition of the chelating agent, EDTA, neutralises Ca^{2+} and Mg^{2+} that inhibit trypsin activity. Once the cells were dissociated, serum containing media was added to neutralise the trypsin. The cell suspension was centrifuged at 1000 rpm

for 5 min and the cell pellet was resuspended in complete media and syringed gently with a 21G x 1½” microlance needle to give a single cell suspension.

Cell type	Source	Culture media
Mouse fibrosarcoma (Complete/full media)	Developed in-house (Tozer <i>et al.</i> , 2008a)	500 mL DMEM Ultraglutamine 10% (v/v) FBS 2 mM L-Glutamine 600 µg/mL Geneticin G418 sulfate 2 µg/mL Puromycin
Mouse fibrosarcoma (Antibiotic-free media)	Developed in-house (Tozer <i>et al.</i> , 2008a)	500 mL DMEM Ultraglutamine 10% (v/v) FBS 2 mM L-Glutamine
Primary human umbilical vein endothelial cells (HUVECs)	PromoCell	500 mL EBM Growth Supplement Mix <ul style="list-style-type: none"> – 1 ng/mL endothelial growth supplement – 1 ng/mL epidermal growth factor – 1 ng/mL fibroblast growth factor – 90 µg/mL heparin – 1 µg/mL hydrocortisone 10% heat inactivated FCS
H5V (immortalised murine heart endothelial cell line)	A gift from Dr A Vecchi (Garlanda <i>et al.</i> , 1994)	500 mL DMEM Ultraglutamine 10% (v/v) FBS 100 IU/ml Penicillin and 100 µg/ml streptomycin

Table 2.1 Cell lines and their culture medium requirements

Complete media requirements for the cell lines used in this study. FBS, fetal bovine serum FBS; DMEM, Dulbecco’s modified eagle's medium; EBM, endothelial basal medium

2.1.3 Fibrosarcoma cell lines

Fibrosarcoma cell lines expressing VEGF₁₂₀ (fs120), VEGF₁₆₄ (fs164), VEGF₁₈₈ (fs188) or all three isoforms (fswt) had previously been developed in our lab (Tozer *et al.*, 2008a). Briefly, primary mouse embryonic fibroblasts expressing the individual VEGF isoforms or all isoforms were isolated from heterozygous breeding pairs of single VEGF-isoform expressing mice (Vieira *et al.*, 2007). Following this, fibroblasts were immortalised and oncogenically transformed by retroviral transduction with the large T antigen of simian virus 40 (SV40) and H-RAS (Tozer *et al.*, 2008a). Frozen stock vials of fibrosarcoma cells created at early passage were rapidly thawed from liquid nitrogen stores. These cell lines were maintained in complete fibrosarcoma media (Table 2.1) and cultured in either 25 cm² or 75 cm² filter-cap flasks in a humidified incubator at 37°C, 5% CO₂. Although short tandem repeat (STR) profiling could not be used to authenticate the fs cell lines, their distinct morphological characteristics (Kanthou *et al.*, 2014), made the individual cell lines visually identifiable (Figure 2.1), therefore should any cross-contamination have occurred it would have been identified during routine passaging of the cells. Single VEGF isoform expression in the cells was confirmed using PCR and the characteristic difference of NRP1 expression was maintained. Departmental mycoplasma testing was carried out monthly and cells were used from P2 to P12.

2.1.4 HUVECs

Primary HUVECs are isolated from umbilical cord veins and are a cell type frequently used during *in vitro* angiogenesis studies. Primary HUVECs from pooled donors (PromoCell) were rapidly thawed from liquid nitrogen and maintained in complete endothelial cell media (Table 2.1) and cultured in 25 cm² filter-cap flasks in a humidified incubator at 37°C, 5% CO₂.

Culture-ware used for routine subculture and bioassays using HUVECs were coated with enough 2% gelatin, type B solution diluted 1:10 in DPBS to cover the bottom of the flask/plate for a minimum of 30 min at room temperature (RT). The 0.2% gelatin was removed immediately prior to cell seeding. HUVECs were not used past passage 4.

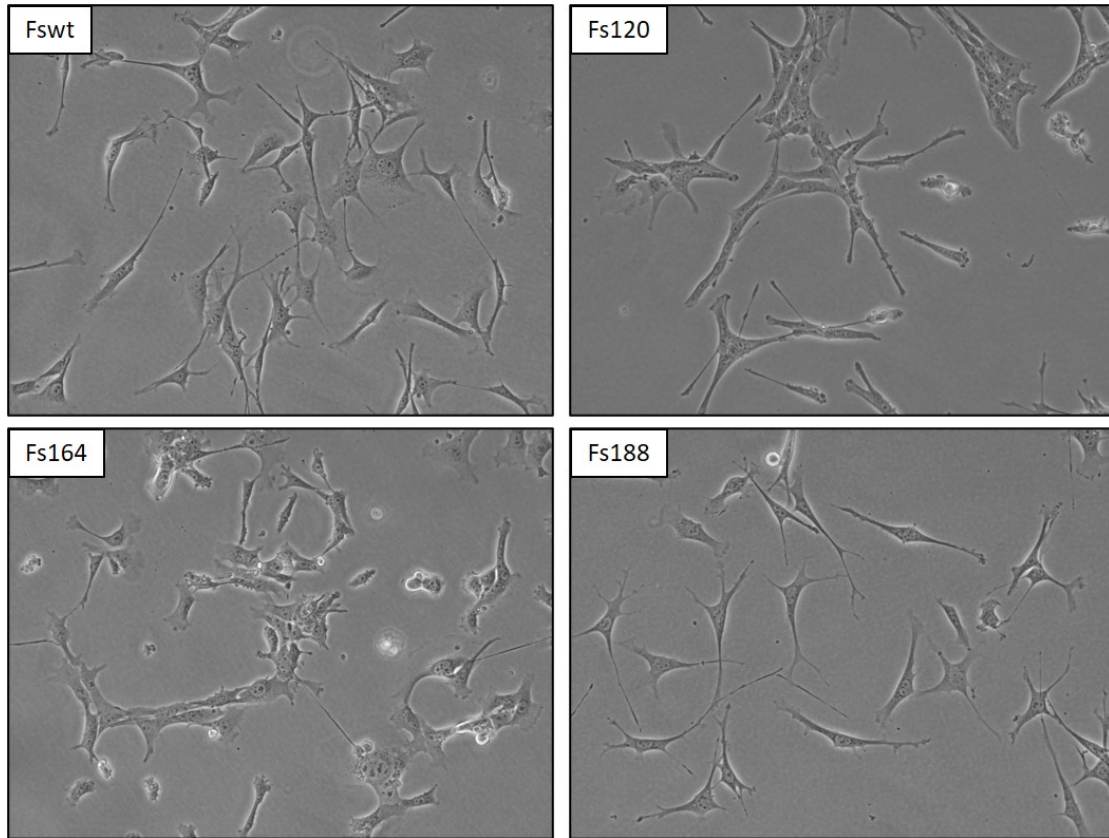


Figure 2.1 Fibrosarcoma morphology

Phase contrast images of fibrosarcoma cells grown on uncoated cell culture plastic. Images taken at 40x magnification courtesy of Dr Chryso Kanthou.

2.2 Short interfering RNA (siRNA) lipofection of fibrosarcoma cells

2.2.1 siRNA

Commercially available, synthetic siRNAs are short fragments of double-stranded RNA (dsRNA) of around 19-21 nucleotides in length that can selectively switch off expression of target genes. NRP1 targeted siRNA transfection was carried out in fswt and fs188 cells to facilitate further biological and functional assays aiming to elucidate its role in tumour cells.

2.2.2 Lipid-mediated transfection

Lipid-mediated transfection, also known as lipofection, facilitates the delivery of foreign genetic material into cells. siRNA transfection was carried out using the cationic lipid PromoFectin-siRNA Transfection Reagent. The positively charged liposomes of the PromoFectin-siRNA Transfection Reagent form a complex with the siRNA. The resulting siRNA-liposome complex fuses with the negatively charged cell membrane and enters the cell cytoplasm via endocytosis where it travels to the nucleus. The siRNA is not incorporated into the cells genome; therefore expression is transient and typically lasts 24 to 92 hours.

2.2.3 siRNA transfection of fswt and fs188 cells

Fswt and fs188 cells were seeded in 1 mL of complete media at a density of 2×10^4 cells/well in 12-well plates coated with 10 $\mu\text{g}/\text{mL}$ fibronectin and incubated 37°C , 5% CO_2 overnight.

The following day, media was aspirated and replaced with 500 μl of antibiotic-free fibrosarcoma media (Table 2.1), cells were returned to the incubator for 2 hours to recover. 4 μl PromoFectin-siRNA was combined with 30 μl of Opti-MEM reduced serum medium for each well. Individual siRNAs (Table 2.2) were combined with 10 μl siRNA diluent and 15 μl Opti-MEM to give a final concentration of 100 nM per well, i.e. 2.5 μl of 20 μM siRNA per well. The diluted PromoFectin-siRNA was then combined with the siRNA mixture and incubated at RT for a maximum of 30 min before being added to the cells. Plates were rocked gently to mix and returned to the incubator for 24 hours. Cells were trypsinised and returned to the wells and allowed to recover for 2 hours before the transfection process was repeated. Typically cells were lysed 24 hours after the second transfection with supplemented cell extraction buffer (CEB) (Section 2.6.1).

siRNA	Supplier	Target sequence
ON-TARGETplus SMARTPool mouse NRP1	Dharmacon (L-040787-00)	GAAUUGCUGUGGAUGAUAU AGUAAGUGGUGUCAUCAAU CCACAAGGUUCAUCAGGAU GGAAUGUUCUGUCGCUAUG
ON-TARGETplus Mouse NRP1 set of 4 siRNA 1 siRNA 2 siRNA 3 siRNA 4	Dharmacon (J-040787) J-040787-05 J-040787-06 J-040787-07 J-040787-08	GAAUUGCUGUGGAUGAUAU AGUAAGUGGUGUCAUCAAU CCACAAGGUUCAUCAGGAU GGAAUGUUCUGUCGCUAUG
GeneSolution siRNA Mm_NRP1_5 Mm_NRP1_4 Mm_NRP1_3 Mm_NRP1_1	Qiagen (1027416) SI05170837 SI01331288 SI01331281 SI01331267	CAGGGCCGATTCAGGACCATA TGGCTGCAAGATAACAGATTA CTGCATCTTCACAGTATGGTA CCGAATGTTCTCAGAACTATA
siGLO green transfection indicator	Dharmacon (D-001630-01-05)	N/a
Control (non-sil.) siRNA	Qiagen (1022076)	AATTCTCCGAACGTGTACGT

Table 2.2 NRP1 and control siRNAs

Dharmacon siRNAs and the control siRNA were diluted to 20 μ M and Qiagen siRNAs were diluted to 10 μ M in RNase free water as per manufacturer's instructions.

2.3 Adhesion Assay

To determine whether NRP1 knockdown affected fibrosarcoma adhesion to ECM proteins, adhesion of control versus NRP1 siRNA transfected cells was studied on plates coated with fibronectin, laminin, collagen or uncoated plastic.

2.3.1 Coating plates with ECM proteins

A 96-well plate was coated with 5 μ g/mL Engelbreth-Holm-Swarm tumor (EHS)-laminin, 5 μ g/mL bovine plasma fibronectin and 5 μ g/cm² rat tail collagen I or left uncoated. Laminin and fibronectin were both diluted in PBS and plates were coated overnight at 4°C. Collagen was prepared in 0.02N acetic acid glacial and plates were coated for 2 hours at RT. ECM protein concentrations used were based on previous work by Kanthou *et al.* (2014). Wells were set up in triplicate for each condition.

2.3.2 Cell seeding and adhesion

Matrix protein solutions were aspirated and wells were washed 3 times with DPBS before blocking of non-specific binding sites with DMEM/ 0.1% bovine serum albumin (BSA) at 37°C, 5% CO₂ for 60 min.

Cells were harvested in complete media, syringed and centrifuged at 1000 rpm for 5 min. Cells were washed twice in DMEM/0.1% BSA before final resuspension in DMEM/0.1% BSA and syringed again to ensure a single cell suspension. Cells were resuspended at 3 x 10⁵ cells/mL in DMEM/0.1% BSA, the blocking solution was aspirated and 100 µl of cell suspension was added to each well, and cells were left to adhere for 45 min at 37°C, 5% CO₂. The timepoint of 45 min was selected to maintain consistency with previous work carried out by Kanthou *et al.* (2014) to allow for comparisons to be made. Control wells containing each of the ECM proteins were left in blocking media without cells to allow for a background absorbance reading to be calculated.

Media were aspirated and wells were washed with warm Hank's Balanced Salt Solution (HBSS) containing Ca²⁺ and Mg²⁺ to remove non-adherent cells before the adhered cells were fixed with 3.7% formalin in PBS for 20 min RT. The formalin was removed and cells were washed 4 times with PBS before they were stained with 0.25% crystal violet in 40% methanol (MeOH) for 20 min RT. Plates were rinsed extensively with water and allowed to dry overnight before the stain was released from the cells with 2% sodium dodecylsulphate (SDS)/PBS and the absorbance measured at 570 nm using a BMF FLUORStar Galaxy microtitre plate reader.

The mean absorbance of the 3 wells for each condition and cell type was taken and the mean background absorbance for each condition was deducted; GraphPad Prism 8.3.0 was used to analyse the data.

2.3.3 Doubling times and growth curves

Fs188 and fs120 cells were seeded in 6-well plates at a density of 1 x 10⁵ and 5 x 10⁴ cells/well respectively and incubated at 37°C, 5% CO₂. At 24, 48, 72 and 96 hours after plating, cells from three wells per cell line were trypsinised, centrifuged at 1000 rpm for 5 min and the cell pellet resuspended in complete media by gentle syringing with a 21G x 1½" microlance needle. Viable cells were counted using the TC20 Automated Cell Counter.

Doubling times were calculated by plotting the log 2 of initial average end-point cell number/initial cell number (N/N₀) and calculating the inverse slope at the linear part of the curve. GraphPad prism 8.3.0 was used to analyse the data.

2.4 Migration Assay

Cell motility can be an important predictor of metastatic potential in cancer cells. To study the effect of NRP1 knockdown (KD) on spontaneous cell migration, wound healing assays were carried out using Ibidi cell culture inserts to create the wound.

2.4.1 Migration of cells with transient NRP1 KD

Two-well silicone cell culture inserts were placed centrally in the wells of a 24-well cell culture dish (1 insert per well, 2 wells per cell line). The chambers of each insert were coated with 5 µg/mL fibronectin for 1 hour at RT which was removed immediately prior to cell seeding. Fs cells were initially seeded in 6-well plates and transfected with siRNA1 as detailed in section 2.2.3. On the day following the first transfection, cells were trypsinised, resuspended in antibiotic-free medium (Table 2.1) and 3.5×10^4 cells in 70 µl were plated per insert well. Cells were allowed to recover at 37°C, 5% CO₂ for 1 hour before transfecting them a second time (as detailed in 2.2.3) with reagents scaled to the volume of media used in the inserts. Cells were incubated for a further 24 hours before the cell culture inserts were removed to leave a gap/wound of 500 µm for cells to migrate across. Two images of each well were taken immediately after creating the wound and then again at intervals from 6 to 24 hours. Timepoints were selected based on initial pilot experiments and previously published findings (Kanthou *et al.*, 2014). Images were taken with a 10X objective, using a Nikon Eclipse TS100 phase contrast microscope equipped with a Jenoptik ProgRes® CapturePro camera and software.

2.4.2 Migration of cells with stable NRP1 KD/overexpression

24-well cell culture plates were set up as described above (Section 2.4.1). Fs188 and fs120 cells were trypsinised and resuspended at 3.5×10^4 cells/insert well and 4×10^4 cells/insert well respectively in complete fs media (Table 2.1). Cells were incubated for 24 hours before the cell culture inserts were removed. Images were taken with a 10X objective, using a Nikon Eclipse TS100 phase contrast microscope equipped with a Jenoptik ProgRes® CapturePro camera and Jenoptik ProgRes® CapturePro software.

2.4.3 Migration assay quantification

Images were analysed in Image J using the Wound Healing plug-in. This plug-in detected the remaining wound area to give measurement in pixels (Figure 2.1). The average area of the two images taken from the same wound was calculated and presented as $A/A_0 \times 100$ (A = wound area at timepoint, A_0 = initial wound area). This gave a percentage of the wound remaining. Use of this macro circumvented the issue of user variability when determining the edge of the wound. Statistical analysis was carried out using a 2-way ANOVA with Bonferroni post-test.

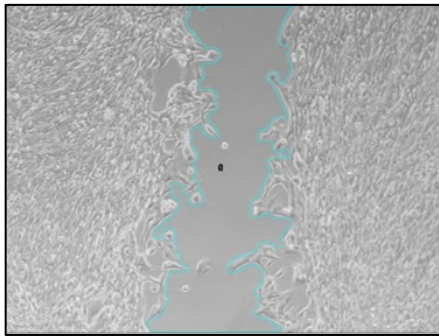


Figure 2.2 Image J wound-healing analysis

Example detection of the remaining area into which cells had not migrated.

2.5 Anchorage independent cell growth

To assess anchorage-independent cell growth and to make a visual assessment of the tumour forming potential of modified fs cell lines, cells were suspended in a thick collagen matrix.

2.5.1 Preparation of thick collagen

The method used was adapted from Artym and Matsumoto (2010) and all reagents, tubes and plates were pre-chilled on ice. A solution of 3 mg/mL collagen in growth medium was prepared on ice. The volume of collagen I required was calculated using the following formula:

Collagen I stock conc. x volume of collagen required = final collagen conc. x collagen solution required.

The required volume of stock collagen was added to a pre-chilled 7 mL bijou tube followed by 10X DMEM-low glucose and 10X reconstitution buffer (1.11 g sodium bicarbonate, 10mL 1M HEPES [0.2M final conc.], made up to 50 mL with sterile dH₂O and passed through a 0.2 µm syringe filter unit). The solution was mixed by slow and gentle pipetting without introducing air bubbles and to avoid precipitation and clump formation. 20 µl 1M sodium hydroxide

(NaOH) was added to the solution and mixed well; the pH was measured and adjusted to pH 7.0 – 7.4 by the addition of either 1N hydrochloric acid (HCl) or 1M NaOH. Cold PBS was added to bring the solution to the final volume required. 300 µl collagen was added to cover the wells of the pre-chilled 24-well plate and incubated at 37°C for ~1 hour until set. Once completely set, 1 mL of 3×10^4 cells/mL in complete fs media were added by pipetting the cell solution onto the side of the well; plates were incubated at 37°C, 5% CO₂ and images were captured using a Nikon Eclipse TS100 phase contrast microscope equipped with a Jenoptik ProgRes® CapturePro camera and Jenoptik ProgRes® CapturePro software.

2.6 Western Blotting

Western blotting is a technique used to separate and identify specific proteins within a mixture based on their molecular weight. In a three-stage process, denatured proteins are separated by gel electrophoresis, transferred (blotted) onto a membrane which is immunoprobed with specific antibodies against the protein of interest (Mahmood and Yang, 2012); the bound antibody can then be detected by either fluorescence or chemiluminescence. A band at the expected molecular weight for the specific protein should be visible; the strength of the band correlates to the amount of protein present therefore band density can be measured and used for quantification.

2.6.1 Protein extraction from cells

Cells were lysed and harvested in one of three different extraction buffers, depending on the specific experiment and whether protein quantification was required or not.

1. Cell extraction buffer was supplemented with 1 mM phenylmethylsulfonyl fluoride (PMSF) and cOmplete™ mini protease inhibitor cocktail (1 tablet dissolved in 200 µl PBS then diluted 1:5 in extraction buffer) or alternatively Halt™ protease and phosphatase inhibitor cocktails were used.
2. NuPAGE LDS sample buffer with 0.1M dithiothreitol (DTT). Proteins extracted in this buffer were analysed without quantification.
3. 63mM Tris-HCl pH6.8/2% SDS.

Cell lysates were heated at 70°C for 10 min before being syringed with a 27G x 3/4" microlance needle and stored at -20°C.

2.6.2 Protein quantification

To ensure equal loading of proteins onto the gels, colorimetric detection and quantification of proteins was carried out using the Micro BCA™ Protein Assay Kit.

In an alkaline environment Cu^{2+} is reduced by protein to Cu^{+1} ; bicinchoninic acid (BCA) is a reagent that, upon chelation with Cu^{+1} , results in a purple-coloured reaction product that emits a strong absorbance signal at ~ 562 nm. The relationship between protein concentration and absorbance is linear therefore, by creating a standard curve, the protein concentration of an unknown sample can be estimated by rearranging the equation of a straight line ($y=mx+c$).

2.6.3 Sodium dodecylsulphate-polyacrylamide gel electrophoresis (SDS-PAGE)

SDS-PAGE was used to separate proteins within whole cell lysates; this allowed for subsequent detection of specific proteins and quantification of their expression.

2.6.3.1 Gel preparation

Tris-glycine polyacrylamide gels were prepared using a percentage of acrylamide and bis-acrylamide suitable for the desired pore size. A higher percentage of acrylamide and bis-acrylamide results in a smaller pore size, therefore higher percentage gels were used for the detection of lower molecular proteins and *vice versa*.

2.6.3.2 Sample preparation and loading

Samples extracted in supplemented CEB, 63mM Tris/2% SDS were thawed on ice to prevent protein degradation; the calculated amount of sample was then diluted in NuPAGE Lithium dodecyl sulfate (LDS) sample buffer/0.1M DTT and heated at 70°C for 10 min before equal volumes of sample were loaded onto the gel. Samples extracted in NuPAGE LDS sample buffer/0.1M DTT were heated briefly at 70°C before equal volumes were loaded onto the gel. A prestained protein ladder was run alongside the samples to confirm that bands visualised were at the expected molecular weight.

Electrophoresis was carried out at a constant voltage of 150V in tris glycine SDS-PAGE buffer until the dye front reached the bottom of the gel.

2.6.4 Transfer of proteins to a membrane

Prior to protein transfer, transfer stacks/ blot filter paper and membranes were saturated in cold tris glycine electroblotting buffer/ 20% MeOH. Depending on the protein of interest, either 0.2 μm nitrocellulose or 0.2 μm polyvinylidene fluoride (PVDF) membranes were used; the PVDF membrane was activated for 5 min in 100% MeOH prior to equilibration in electroblotting buffer. Semi-dry transfer of separated proteins was carried out using either the Trans-Blot® Turbo™ Blotting system or the Novex™ Semi-Dry Blotter. The western blot sandwich was assembled (Figure 2.3) and transfer was carried out for 30 min at 25 V (up to 1A) in the Trans-Blot® Turbo™ or 20 min/membrane at 400mA in the Novex™ Semi-Dry Blotter.

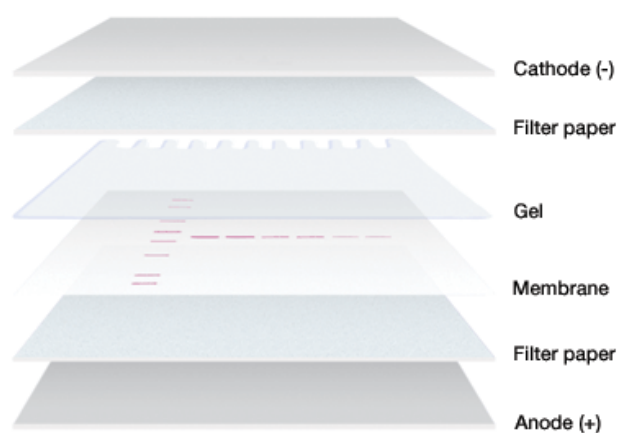


Figure 2.3 Western blotting sandwich setup

The gel was placed in direct contact with membrane, upon application of an electrical current the negatively charged proteins migrated from the gel towards the positive anode and were transferred onto the membrane. Image taken from (Bio-Rad, 2016).

2.6.5 Immunological protein detection

In order to prevent non-specific antibody binding, membranes were incubated with gentle shaking for 1 hour RT in a blocking solution of either 2% BSA/tris buffered saline 0.1% tween-20 (TBST) or 5% non-fat dried milk (NFDM)/TBST depending on the solution in which primary antibodies (Appendix 2) were diluted. The blocking solution was removed and membranes were incubated with the primary antibody overnight at 4°C with gentle shaking. The primary antibody was removed and membranes were washed in TBST for 10 min 3 times to remove any unbound antibody. Secondary antibody incubations were carried out at RT for 1 hour using a horseradish peroxidase (HRP) conjugated antibody (Appendix 2) against the species in

which the primary antibody was raised. Membranes were washed for 10 min 3 times before detection by enhanced chemiluminescence (ECL).

2.6.6 ECL protein detection

ECL detection (Figure 2.4) was performed either in a darkroom onto X-ray film or digitally with the ChemiDoc™ MP System. EZ-ECL chemiluminescence detection kit for HRP or Clarity™ Western ECL reagent were used for both methods; equal parts of luminol and enhancer reagents were mixed to give a sufficient volume of solution to cover the membrane and left to equilibrate for 5 min. Membranes were drained of excess TBST and covered with the detection solution for 3-5 min at RT. Following the incubation, excess detection solution was drained and the membrane placed between two copier transparencies or plastic food wrap.

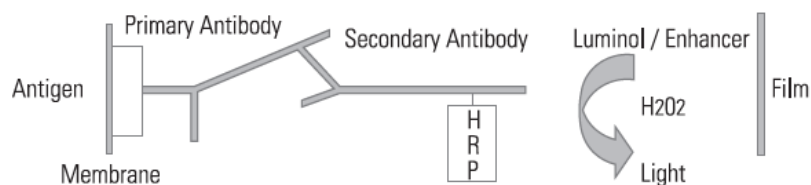


Figure 2.4 Chemilumincent detection of proteins

HRP catalyses the oxidation of luminol in the presence of hydrogen peroxidase, the result is the emission of light that corresponds to where the HRP-linked secondary antibody has bound to the specific primary antibody. The emission of light can be captured on X-ray film or digitally using a charge-coupled device (CCD) camera.

2.6.6.1 ECL detection on film

For exposure onto film, membranes were placed protein side up in a Hypercassette™ Autoradiography Cassette and a piece of film was placed onto the membrane for 30 sec to 30 min depending on the antibody used and the abundance of the protein of interest. The exposed film was immersed in Kodak GBX Developer and Replenisher for 2-3 min and rinsed in water before being transferred to Kodak GBX Fixer and Replenisher for 2-3 min. After fixation the film was rinsed in water and left to dry completely.

2.6.6.2 Digital ECL detection

For digital ECL detection, membranes were placed protein side up in the ChemiDoc™ MP Imager and visualised using the Image Lab™ software (Bio-Rad). As with signal detection using X-ray film, the antibody and protein abundance dictated the exposure time.

2.6.7 Semi-quantitative analysis of western blots

Western blots exposed onto X-ray film were scanned into Image Lab™ using the 'silver stain' protocol and white light converter screen with the ChemiDoc™ MP Imager. Densitometric analysis of the protein bands was carried out on both digital and film developed blots using the 'Lane and Bands' analysis tool within Image Lab™.

2.7 Genetic modification of fs cell lines

In order to study the role of tumour derived NRP1 *in vivo*, specifically, its influence on tumour vascularisation and tumour sensitivity to anti-VEGF therapeutics, stable NRP1 KD in fs188 cells and overexpression in fs120 and fs164 cells was carried out.

The following sections will first summarise the fundamental techniques used during both overexpression (OE) and KD of NRP1 before going on to describe the individual approaches in more depth. All work was carried out following approval from the University of Sheffield Biosafety Committee in accordance with The Genetically Modified Organisms (Contained Use) Regulations 2014 (Hse, 2014).

2.7.1 DNA isolation and purification

2.7.1.1 Bacterial cell transformation

Bacterial transformation is a technique used to replicate plasmids via the introduction of foreign DNA into a bacterial cell. Bacterial cells are artificially given the ability to uptake exogenous DNA, made competent, through chemical methods or by administering electric pulses. Chemically competent DH5α *Escherichia coli* (*E. Coli*) was used throughout.

DH5α cells were thawed completely on ice. ~100 ng of plasmid DNA was added to 50 µl DH5α cells and mixed by flicking the tube to avoid any shearing of the DNA, the mixture was incubated on ice for 30 min. DH5α/DNA were heat-shocked at 42°C in a water bath for 45 sec before being returned to ice for 2 min. 450 µl super optimal broth with catabolite repression

(SOC) media was added to the DH5 α /DNA which were then incubated for 1 hour at 37°C with shaking. 50 μ l of the DH5 α /DNA/SOC mixture was spread evenly onto LB agar plates containing the appropriate antibiotic for selection (See Appendix 1 for plate preparation). Inoculated plates were left at RT until the DH5 α /DNA/SOC mixture had soaked into the agar before being incubated lid-side down overnight in at 37°C. The following day plates were inspected for colonies. Both maxipreparation and minipreparation of plasmid DNA was carried out depending on the plasmid DNA yield required.

2.7.1.2 DNA maxipreparation

Single colonies were picked into 5 mL LB broth + antibiotic (See Appendix 1 for LB broth preparation) and incubated at 37°C for ~6 hours with shaking to provide a starter culture which was transferred to a 100 mL LB broth + antibiotic in a 500 mL conical flask; this was covered and incubated at 37°C with shaking at 225 rpm overnight. Cultures were centrifuged at 3500 rpm for 15 min at 4°C before DNA was isolated from the bacterial pellets using either the QIAfilter plasmid Maxi kit or the ZymoPURE™ II Plasmid Maxiprep kit following the manufacturer's protocol. The purified DNA pellet was dissolved in Tris-EDTA (TE) buffer pH 8.0. DNA yield and purity was measured using the Nanodrop ND-1000 before storage at -20°C. Diagnostic restriction enzyme (RE) digest was used verify plasmid identity (Section 2.7.2).

2.7.1.3 DNA minipreparation

Single colonies were picked into 5 mL LB broth + antibiotic (Appendix 1) and incubated at 37°C overnight with shaking (220 rpm). DNA from the bacterial cultures was isolated using the Monarch® plasmid mini-prep kit following the manufacturers' protocol. DNA yield and purity was measured using the Nanodrop ND-1000 before storage at -20°C.

2.7.2 Restriction enzyme digest

RE cleave DS DNA at specific short palindromic sequences of 4-6 base pairs (bp) in length referred to as restriction sites. Although some enzymes share the same recognition sequence, they cleave the DNA at different points. DNA cleavage by RE results in linear DNA fragments which, dependent on the cut site, have blunt ends, 5' or 3' overhangs. RE digest is a routinely used molecular biology technique that facilitates cloning of DNA fragments into a recipient vector. Additionally, if a plasmid sequence is known, REs can be used to digest the plasmid and analyse the resulting fragments sizes, thus allowing quick verification of plasmid identity.

All REs used during this study were from NE Biolabs; using their universal CutSmart™ buffer, DNA digestion was carried out at 37°C in all cases, the only variable was the digestion time which ranged from 30 min to 6 hrs depending on the amount of DNA to be digested. Standard reaction volumes were 1 µg of DNA digested with 1 µl of RE in 5 µl 10X CutSmart™ buffer made up to a total volume of 50 µl with nuclease free (NF) H₂O in a 0.2 µl thin walled PCR tubes. When carrying out RE digest for diagnostic purposes the reaction was quenched with the addition of a gel loading dye. For plasmid linearisation, REs were deactivated with a final incubation of 20 min 65°C or 85°C depending on the RE being used. RE digestion was carried out in a thermocycler with a heated lid.

2.7.3 Agarose gel electrophoresis

To visualise DNA fragments, agarose gel electrophoresis was used. Negatively charged DNA migrates through an agarose gel matrix towards a positive electrode and is separated based on its size; by running samples alongside a DNA ladder the approximate length of the DNA fragment can be determined. The concentration of the agarose gel is determined by the size of the bands needing to be separated; higher percentage gels of 2% are used to resolve smaller bands and lower percentage 0.8% - 1% gels are used to resolve larger bands.

The appropriate weighed volume (w/v) of agarose powder was mixed with tris acetate EDTA (TAE) buffer, this was microwaved for ~2 min until completely dissolved. The agarose was left to cool slightly before adding Midori green direct DNA stain (4 µl/ 100 mL agarose), molten gel was poured into the gel tray and a comb inserted to form the wells, this was left to set at RT until completely cool. Once cooled the gel was placed in the gel running tank, the comb removed and enough 1 x TAE buffer was poured into the tank to cover the gel and enter the wells. Samples were added alongside either a 100 bp or 1 Kb DNA ladder and run for 35-40 min at a constant current of 150V. Gels were visualised and imaged using the BioDoc-it imaging system.

2.7.4 Colony PCR

Colony PCR is a fast and effective method used to screen for plasmids contain a desired insert directly from potentially transformed bacterial colonies. By using carefully designed primers, which will only result in product amplification if the insert is present, the presence or absence of the insert can be detected.

Single colonies were picked from agar plates inoculated with potentially transformed bacteria into 40 μ l NF H₂O and mixed; 5 μ l of this mixture was added to a mastermix (Table 2.3) which was prepared in a 0.2 μ l thin-walled PCR tube on ice:

Reagent	Volume (μ l)	Final Conc.
5X Colourless/green GoTaq [®] reaction buffer	10.00	1X
GeneAmp [®] dNTP blend (2.5 mM each)	1.00	200 nM
Forward primer (100 μ M stock)	0.25	500 nM
Reverse primer (100 μ M stock)	0.25	500 nM
GoTaq [®] G2 DNA polymerase – add last	0.25	1.25 units
Template DNA	X	100 ng - 1 μ g
NF H ₂ O	X	To 50 μ l
Total volume	50.00	

Table 2.3 GoTaq G2 PCR mastermix

Mastermix for 1 standard PCR reaction. Volumes were scaled to the number of reactions per experiment + 1 to allow for any pipetting inaccuracies.

35 cycles of PCR were carried out in a thermocycler with a heated lid, using the following general parameters:

- Denaturation – 2 min at 95°C then 15 sec/cycle
- Annealing – 3°C – 5°C below primer T_m, 45 sec/cycle
- Extension – 72°C for 1 min/cycle per 1 kb DNA
- Final extension – 72°C for 5 min

The reaction was quenched by the addition of gel loading dye and 20 μ l was run on a 2% agarose gel (Section 2.7.3)

If PCR of the sample resulted in a product, the remaining 35 μ l was used to inoculate 5 mL LB broth containing the appropriate selecting antibiotic and DNA miniprep was carried out (Section 2.7.1.3).

2.7.5 Generation of stable NPR1 knockdown fs cell lines

Stable NRP1 KD in fs188 cells was carried out using clustered regulatory interspaced short palindromic repeat/CRISPR-associated 9 (CRISPR/Cas9) genome editing technology. Specifically, a Cas9 nickase mutant (Cas9n) was combined with two offset short guide RNAs (sgRNAs) targeting opposing strands of the target loci within the NRP1 gene. Pairs of sgRNAs were designed and cloned into a Cas9n (D10A nickase mutant) plasmid backbone with a 2A-eGFP tag. Pairs of sgRNA-Cas9n expression vectors were then transfected in fs188 cells. The CRISPR/Cas9 gene-editing system used during this study is described in further detail in Chapter 4.

2.7.5.1 CRISPR/Cas9n plasmid

The Cas9n (D10A nickase mutant) plasmid backbone with a 2A-eGFP tag, pSpCas9n(BB)-2A-GFP (PX461), was a gift from Feng Zhang (Addgene plasmid #48140)(Ran *et al.*, 2013b) (Figure 2.4A). The pSpCas9n(BB)-2A-GFP plasmid was supplied as a bacterial stab; an LB/ampicillin plate (See Appendix 1 for plate preparation) was streaked with bacteria and incubated at 37°C overnight. One colony was picked and maxipreparation of plasmid DNA was carried out (Section 2.7.1.2). RE digest with EcoRV-HF and XbaI for 30 min confirmed plasmid DNA identity (Figure 2.4B).

2.7.5.2 sgRNA design and construction

Suitable sgRNA pairs targeting the NRP1 gene were identified using online resources at <https://www.atum.bio/eCommerce/cas9/input> (Atum, 2019) and <http://www.e-crisp.org/E-CRISP/> (Heigwer *et al.*, 2014). The top two results from ATUM and the top result from E-CRISP were selected on the basis of their target specificity (Figure 2.6A). sgRNA sequences were aligned to the validated NCBI mouse NRP1 reference sequence NM_008727.2 to confirm sequence complementarity and to ascertain which exons and domains were being targeted. Nucleotide Blast (<https://blast.ncbi.nlm.nih.gov>) was used to further check for any potential off-target sites that may have been recognised by the sgRNA pairs.

sgRNA expression in the pSpCas9n(BB)-2A-GFP plasmid is under the control of the U6 RNA polymerase III promoter which prefers a guanine (G) nucleotide at the first base of its transcript, therefore, where the sgRNA sequence did not begin with a guanine, an extra G base

was added. In addition, 5' overhangs were created to facilitate ligation of the sgRNA into pSpCas9n(BB)-2A-GFP between the BbsI restriction sites.

Top and bottom single strand oligonucleotides (oligos) for each sgRNA (Figure 2.6B) were phosphorylated and annealed using T4 polynucleotide kinase (PNK). 10 μ M (final conc.) of each of the top and bottom strand oligos were combined with 1 μ l of T4 PNK, 1 μ l T4 DNA ligase buffer and 6 μ l NF H₂O in 0.2 μ l thin walled PCR tubes. Tubes were immediately transferred to a thermocycler set to the following parameters; 37 °C for 30 min; 95°C for 5 min; ramp down to 25°C at 5 °C min⁻¹ (0.083 °C sec⁻¹). sgRNAs were stored at -20°C until required.

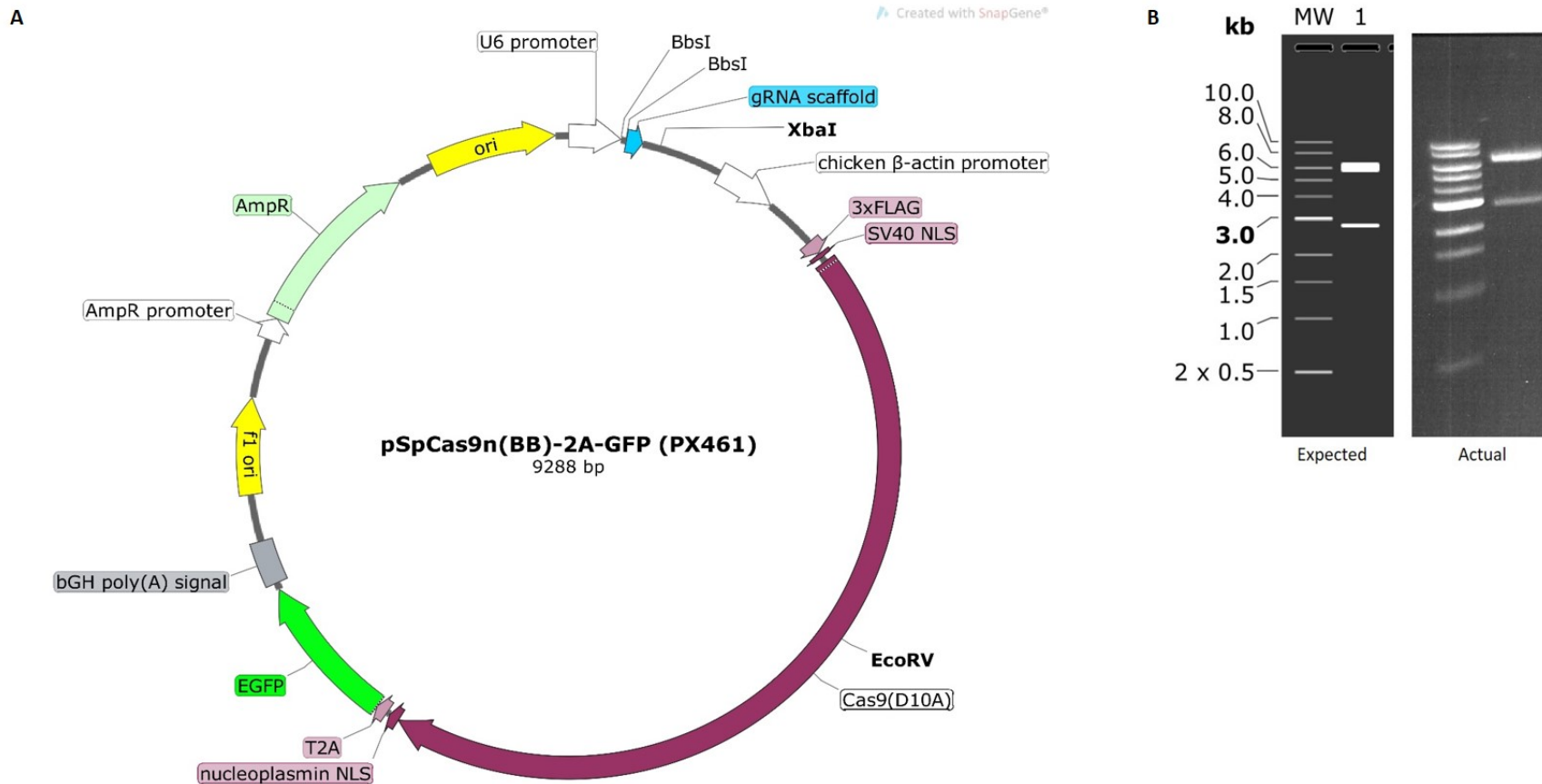


Figure 2.5 pSpCas9n(BB)-2A-GFP plasmid map and verification

A) pSpCas9n(BB)-2A-GFP plasmid map, annotated to show the BbsI restriction sites used to clone in the individual sgRNAs. B) 0.8% agarose gel showing expected DNA fragments (left) of 6496 bp and 2792 bp and actual results (right) following restriction enzyme digest of 1 μ g pSpCas9n(BB)-2A-GFP DNA with 1 μ l each of EcoRV-HF and XbaI for 30 min at 37°C

A

Position	gRNA	Distance between gRNA	Score
128,434,371	CTACCCCTGAAAATGGGTGGACTCCAGGAGAAGACTCCTACAAGGAGTGGATCCAGGTAG	7	100
128,434,330	GATGGGACTTTTACCCACCTGAGGTCCTCTTCTGAGGATGTTCTCTCACCTAGGTCCATC		
128,425,953	AATCCTCCCGGAGGAATGTTCTGTGCGTATGACCCGGCTGGAGATCTGGGATGGATT	4	93.83
128,425,915	TTAGGAGGGCCCTCTTACAAGACAGCGATACTGGCCGACCTCTAGACCCTACCTAA		

S: Specificity score A: Annotation score E: Efficiency score
for more information please see the [Help](#) pages

Name	Nucleotide sequence	SAE-Score	Target	Matchstring	Number of Hits
Nrp1_0_103173	GCCATTCATTGGTGTA TGGG NGG_GGAGATGAGAA GATAGTAAG NGG		ENSMUSG0000002581 0::Nrp1	Matchstring Info	1

B

sgRNA ID	Sequence (5' → 3')	Target Exon	NRP1 protein coding region
sgRNA1 bottom fwd	CACCGCTGGAGTCCACCCATTTTCA	6	B1
sgRNA1 bottom rev	AAACTGAAAATGGGTGGACTCCAGC		
sgRNA1 top fwd	CACCGCTCCTACAAGGAGTGGATCC		
sgRNA1 top rev	AAACGGATCCAATCCTTGTAGGAGC		
sgRNA2 bottom fwd	CACCGCGACAGAACATTCTCCGGG	4	A2
sgRNA2 bottom rev	AAACCCCGGAGGAATGTTCTGTGCGC		
sgRNA2 top fwd	CACCGACCGGCTGGAGATCTGGGA		
sgRNA2 top rev	AAACTCCAGATCTCCAGCCGGTC		
sgRNA3 bottom fwd	CACCGCCATTCATTGGTGTATGGG	9	B2
sgRNA3 bottom rev	AAACCCATACACCAATGAATGGC		
sgRNA3 top fwd	CACCGGAGATGAGAAGATAGTAAG		
sgRNA3 top rev	AAACCTTACTATCTTCTCATCTCCC		

Figure 2.6 sgRNAs targeting NRP1

A) Top hits for sgRNA pairs targeting the NRP1 gene identified using ATUM 2.0 and E-CRISP. B) Single strand oligonucleotide sequences for construction of individual sgRNAs.

2.7.5.3 Construction of Cas9n-sgRNA expression vector

pSpCas9n(BB)-2A-GFP was linearised by RE digest with BbsI-HF for 1 hour (Section 2.7.2). GeneJet Gel extraction and DNA cleanup micro kit was used to remove residual enzymes and salts from the digested DNA mixture which may affect downstream reactions. To ligate the annealed sgRNA oligo duplexes into pSpCas9n(BB)-2A-GFP a ligation mastermix was prepared on ice for each reaction (Table 2.4)

Reagent	Volume (μ l)
Linear pSpCas9n(BB)-2A-GFP (~100ng)	1
2X T7 Ligase reaction buffer	10
T7 Ligase (NE Biolabs, M0318)	1
NF H ₂ O	6
Total	18

Table 2.4 sgRNA ligation mastermix

Mastermix for ligation of annealed sgRNA oligos into linearised pSpCas9n(BB)-2A-GFP

In a 0.2 μ l thin walled PCR tube, 2 μ l annealed sgRNA oligos diluted 1:200 NF H₂O in were mixed with 18 μ l ligation mastermix (Table 2.4) and incubated for 30 min at 25°C in a thermocycler. 20 μ l DH5 α cells were transformed with 2 μ l of pSpCas9n(BB)-2A-GFP-sgRNA (Section 2.7.1.1). To determine whether the sgRNA duplexes had been successfully incorporated into pSpCas9n(BB)-2A-GFP, colony PCR was carried out on 3 colonies from each plate (Section 2.7.4) using the U6 forward primer (Appendix 4) and the specific reverse sgRNA oligo used to create the insert (Figure 2.7). If PCR resulted in the amplification of an expected product of 274 bp, pSpCas9n(BB)-2A-GFP-sgRNA DNA was submitted to the University of Sheffield Genomic Core Facility along with the U6 fwd primer (Appendix 4) for Sanger sequencing using the Applied Biosystems 3730 DNA Analyser. Returned sequences were aligned with the corresponding pSpCas9n(BB)-2A-GFP-sgRNA sequence using SnapGene® version 4.3.2 (GSL Biotech LLC) for further verification.

2.7.5.4 Optimisation of CRISPR/Cas9n transfection

There are several variables that need to be taken into consideration when carrying out transfection of mammalian cells with exogenous DNA. DNA vector size in particular is a limiting factor, as nuclear delivery of large plasmids may be hindered by their rate of intracellular transport. To determine optimal transfection conditions Lipofectamine®, FuGene® 6 and *TransIT-X2*® transfection reagents were all tested with various cell seeding densities, DNA concentrations and transfection reagent: DNA ratios. Lipofectamine® is a liposomal transfection reagent that delivers exogenous DNA into cells via the formation of cationic liposomes which fuse with the cell membrane. FuGene® 6 is a non-liposomal cationic lipid reagent, however the information surrounding its mode of action is proprietary. Finally,

TransIT-X2[®] is non-liposomal polymeric transfection reagent; cationic polymers condense exogenous DNA and form a complex which is taken up by cells via endocytosis. A generic GFP plasmid, pcDNA-GFP (C. Kanthou) was used as a positive control during the optimisation experiments alongside the original pSpCas9n(BB)-2A-GFP and modified pSpCas9n(BB)-2A-GFP-sgRNA plasmids. At 48 h post transfection with each of the transfection reagents a visual check for GFP expression was carried out using a Nikon Eclipse TS100 inverted microscope before cells were harvested for flow cytometric analysis and transfection efficiency evaluation (Section 2.8.1)

2.7.5.5 Optimised fs188 cell transfection with Lipofectamine[®]

12-well cell culture plates were coated with 5 µg/ml fibronectin for 30 – 60 min at RT prior to seeding fs188 cells in 1 mL antibiotic free media at 2×10^4 cells/well and incubated overnight at 37°C, 5% CO₂. The following day, 3 µl Lipofectamine[®] was mixed with 34.5 µl Opti-MEM[™] for each reaction and 1 µg DNA (0.5 µg each of the sense and anti-sense target sgRNA) was diluted with Opti-MEM[™] to a total volume of 37.5 µl; diluted Lipofectamine[®] and DNA were combined, mixed and incubated for 30 min RT to allow lipoplexes to form. The full 75 µl Lipofectamine[®]/DNA was added to each well, plates were rocked gently to mix before incubation at 37°C, 5% CO₂ for 48 hours.

2.7.5.6 Optimised fs188 cell transfection with FuGene[®] 6

Fs188 cells were seeded as described above (Section 2.7.5.5). The following day, 3 µl FuGene[®] 6 was mixed with enough Opti-MEM[™] to give a final volume of 100 µl after the addition of DNA and incubated at RT for 5 min; 1 µg DNA (0.5 µg each of the sense and anti-sense target sgRNA) was then added and the mixture was incubated for 30 min at RT. The full 100 µl FuGene[®] 6/DNA was added to each well, plates were rocked gently to mix before incubation at 37°C, 5% CO₂ for 48 hours.

2.7.5.7 Optimised fs188 cell transfection with *TransIT-X2*[®]

Fs188 cells were seeded as described above (Section 2.7.5.5). The following day, *TransIT-X2*[®] transfection reagent was brought to RT; 3 µl *TransIT-X2*[®] was mixed with 100 µl Opti-MEM[™] and 1 µg DNA (0.5 µg each of the sense and antisense target sgRNA), the mixture was incubated for 30 min at RT before being added to wells in a drop wise fashion and plates were rocked gently to mix before being incubated at 37°C, 5% CO₂ for 48 hours.

2.7.6 Generation of stable NRP1 overexpressing fs cells lines

Previously the *piggyBac* transposon system was used to express luciferase in the fibrosarcoma cells (English *et al.*, 2017). The fs cells are already resistant to two antibiotics and therefore a normal over-expression approach that utilises antibiotic selection to generate stable cell lines was not appropriate. Therefore the *piggyBac* transposon system was used to overexpress NRP1 in the fs120 and fs164 cells. DNA transposons mobilise around host genomes via a cut and paste mechanism; the *piggyBac* transposon system exploits this mechanism to mediate gene transfer from a donor plasmid into the host cell genome (Wu *et al.*, 2006). This approach is described in full in Chapter 4 (Section 4.6). Fs120 and fs164 cells were co-transfected with a transposase expressing plasmid and a donor plasmid containing GFP tagged NRP1.

2.7.6.1 Plasmids

The backbone of the *piggyBac* transposon vector was pCLIIP-C-LS (pCyl50, Linker, Insulator, Insulator, Puro-CAGGS promoter-Luciferase2-E2A-mStrawberry) (English *et al.*, 2017) and the transposase expression vector used was pmPB (originally provided by Allan Bradley, Sanger Institute, UK). pCMV3-mNRP1 (Sino Biological MG50509-UT) and pSpCas9n(BB)-2A-GFP (Addgene, PX461, #48140) were used to create the mNRP1-T2A-eGFP-pA donor sequence in the final pCLIIP-NRP1-GFP plasmid.

The pCMV3-mNRP1 plasmid was supplied as a bacterial stab; an LB/kanamycin plate (See Appendix 1 for plate preparation) was streaked with bacteria and incubated at 37°C overnight. One colony was picked and maxipreparation of plasmid DNA was carried out (Section 2.7.1.2). RE digest (Section 2.7.2) with HindIII-HF and XbaI for 30 min resulted in fragments of 2778 bp and 6096 bp thus confirming plasmid DNA identity. pCLIIP-C-LS and pmPB were supplied as purified DNA which was used for maxipreparation of plasmid DNA (Section 2.7.1.2).

2.7.6.2 Design of pCLIIP-NRP1-eGFP vector

The selectable markers in pCLIIP-C-LS are puromycin and mStrawberry; as a result of the fs cells already being puromycin resistant and the Luciferase2 and E2A-mStrawberry segment being a complete expression cassette, another selection method was required to select for successfully transfected clones. pCLIIP-C-LS has no unique restriction sites between the Luciferase2 and E2A-mStrawberry segment, therefore an approach whereby the Luciferase2-

E2A-mStrawberry (LS) portion was swapped for a NRP1-T2A-eGFP fragment was undertaken. Initially, several attempts were made to construct NRP1-T2A-eGFP-pA as a complete fragment, however this was unsuccessful. Therefore, a two-step strategy whereby LS was first replaced by T2A-eGFP-pA before the insertion of a mNRP1 fragment was used (Figure 2.7). Although GoTaq® G2 DNA polymerase is a form of *Taq* polymerase that exhibits 5' → 3' exonuclease activity, Q5® High-Fidelity DNA polymerase is reportedly less error prone than *Taq* polymerase, therefore this was used for all PCR amplifications during pCLIIP-mNRP1-eGFP construction to reduce the likelihood of introducing base-pair errors.

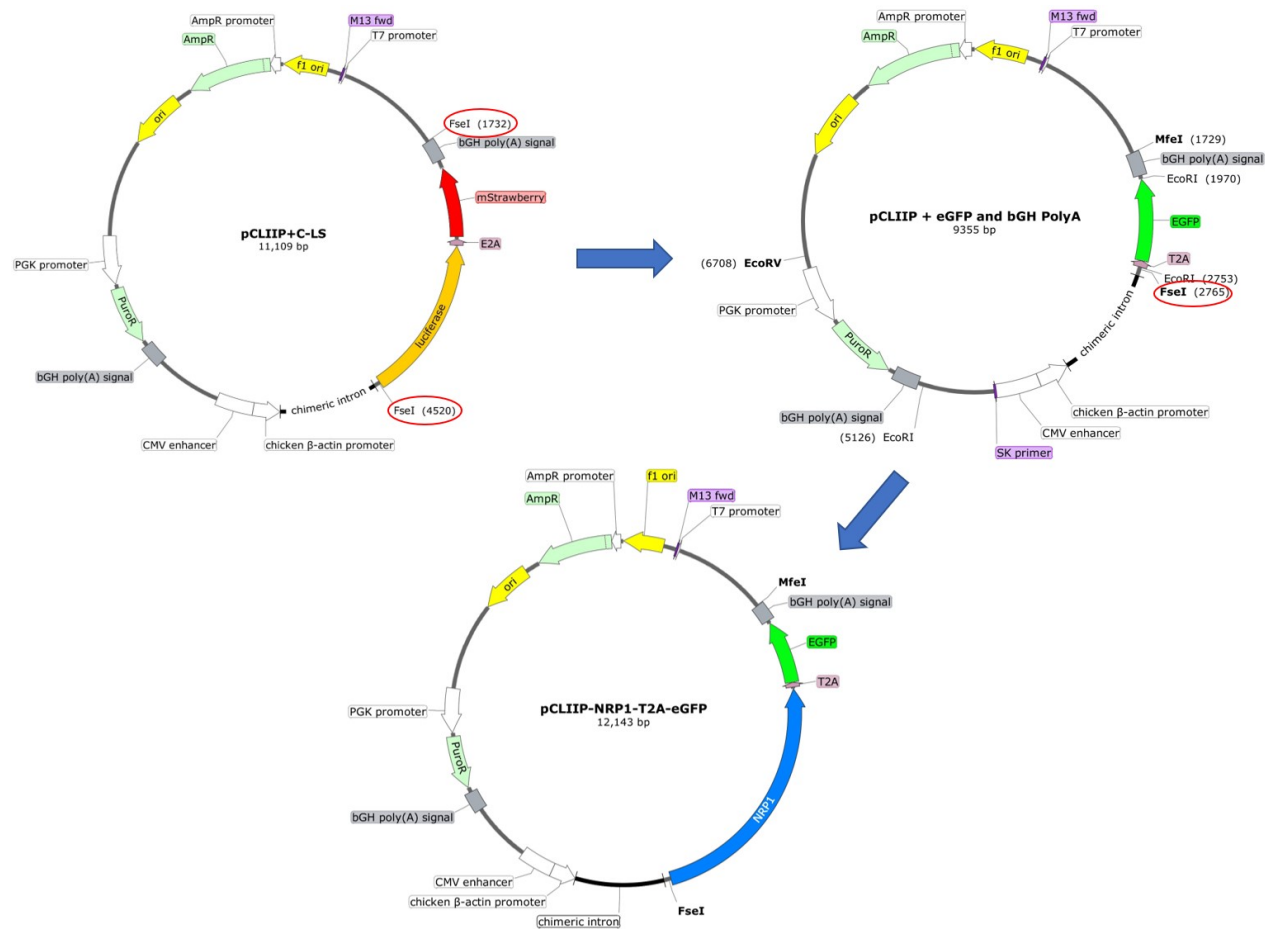


Figure 2.7 Construction of pCLIIP-NRP1-eGFP vector for NRP1 overexpression

pCLIIP-C-LS was digested with FseI to linearise the vector and remove the luciferase-E2A-mStrawberry cassette, which was then replaced with T2A-eGFP-pA amplified from pSpCas9n(BB)-2A-GFP. pCLIIP+eGFP-pA was then digested with FseI to allow insertion of mNRP1 amplified from pCMV3-mNRP1. Ligation of purified PCR fragments in to the linearised vectors was carried out using the In-Fusion® HD Cloning Kit. All steps were verified by RE digest and sequencing

2.7.6.3 Q5® High-fidelity PCR

A Q5® High-fidelity mastermix was prepared on ice as detailed in Table 2.5.

	Vol (µl)	Final Conc.
Plasmid DNA	X	500 ng
Q5® High-fidelity reaction buffer	5.00	1X
Fwd primer (10µM)	1.25	500 nM
Rev primer (10µM)	1.25	500 nM
GeneAmp dNTP blend (10mM – 2.5mM each)	2.00	200 µM each
Q5® High-fidelity DNA polymerase	0.25	0.02 U/µl
Q5® High-fidelity GC enhancer*	5.00	1X
Nuclease free water	X	to 25 µl
TOTAL	25.00	

Table 2.5 Q5® High-Fidelity DNA polymerase PCR mastermix

The table represents the volumes for one PCR reaction, volumes were scaled up for the total number of reactions in a run to minimize on pipetting errors.

*Q5® High-fidelity GC enhancer was only used with primers that had moderate-high risk of secondary structure formation.

When carrying out standard PCR with Q5® High-fidelity DNA polymerase, reactions were assembled on ice in 0.2 µl thin-walled PCR tubes and 35 cycles of PCR were carried out in a thermocycler with a heated lid, using the following general parameters:

- Denaturation – 1 min at 98°C then 10 sec/cycle
- Annealing – 50°C – 72°C (primer T_m dependent) for 30 sec/cycle
- Extension – 72°C for 30 sec/cycle per 1 kb DNA
- Final extension – 72°C for 2 min

A modified two-stage reaction protocol was used during PCR amplification of the T2A-eGFP-pA and mNRP1 fragments (Section 2.7.6.4). In the first two cycles only the 3' homologous bases (highlighted red in Appendix 4) annealed, after this the whole primer was incorporated into the template being amplified thus increasing the T_m of the primer. Therefore, the annealing step was carried out at 63°C for two cycles before being increased to 72°C for the

remaining 33 cycles. The length of the cycles was calculated as per the standard PCR template above.

2.7.6.4 Generation of individual fragments for pCLIIP-NRP1-GFP

Firstly, T2A-eGFP was PCR amplified (Section 2.7.6.3) from pSpCas9n(BB)-2A-GFP using primers designed to allow cloning between the two FseI sites flanking the LS segment of pCLIIP-C-LS (GFP to pCLIIP fwd & GFP to pCLIIP rev, Appendix 4). In addition, primers included a 5' FseI site to allow insertion of mNRP1 and a 3' MfeI site, to allow complete excision of the NRP1-T2A-eGFP-pA fragment if required at a later date. 5 µl of the PCR reaction was run on a 1.5 % agarose gel (Section 2.7.3) to verify that a product of 1025 bp had been amplified. The remainder of the reaction was purified using the GeneJET Gel extraction and DNA cleanup microkit following the manufacturers PCR cleanup, dimers removal protocol. DNA was quantified using the Nanodrop ND-1000 and stored at -20°C.

Next, mNRP1 was PCR amplified from pCMV3-mNRP1 (Section 2.7.6.3) using primers designed not only to allow cloning into the FseI site upstream of T2-eGFP-pA but to also maintain the FseI site (NRP1 to pCLIIP fwd & NRP1 to pCLIIP rev, Appendix 4). 5 µl of the PCR reaction was run on a 1.5 % agarose gel to verify that a product of 2822 bp had been amplified and the remainder of the reaction was purified and stored as described above.

pCLIIP-C-LS was linearised by RE digest with FseI (Section 2.7.2) and the reaction was run on a 0.8% agarose gel (Section 2.7.3) to verify successful digestion. The band of ~8600 bp was excised and purified with the GeneJET Gel extraction and DNA cleanup microkit following the manufacturers DNA extraction from gel protocol and quantified using the Nanodrop ND-1000 before being stored at -20°C.

2.7.6.5 Construction of vector pCLIIP-NRP1-GFP using In-Fusion® cloning

To ligate the amplified T2A-eGFP and mNRP1 fragments into pCLIIP-C-LS and pCLIIP-GFP respectively, the In-Fusion® HD Cloning kit was used. The proprietary In-Fusion® Enzyme fuses DNA fragments through the recognition of 15-bp overlaps at their ends. Therefore, primers used to amplify the T2A-eGFP and mNRP1 (Section 2.7.6.4) had been specifically designed to be complimentary to the ends of the linearised pCLIIP-C-LS and pCLIIP-eGFP left by FseI digestion. The In-Fusion® molar ratio calculator (<https://www.takarabio.com>) was used to calculate optimal amounts of vector and insert for the In-Fusion® cloning reactions. Reactions

(Table 2.6) were prepared on ice in 0.2 mL thin walled PCR tubes and incubated for 15 min at 50°C in a thermocycler with heated lid. Both a positive control reaction using a control vector and insert supplied with the cloning kit and a negative control which omitted the PCR insert were included.

Reagent	Volume
In-Fusion® HD Enzyme premix (5x)	2.0 µl
Linearised vector	50 – 200ng
Purified PCR fragment	10 – 200 ng
NF H ₂ O	to 10 µl
TOTAL	10.0 µl

Table 2.6 In-Fusion® Cloning Reaction

The detailed volumes are for one reaction and were scaled up accordingly to reduce pipetting errors.

2 µl of the In-Fusion® reaction was added to 25 µl DH5α cells for bacterial cell transformation (Section 2.7.1.1). Colony PCR (Section 2.7.4) was carried out to determine whether ligation of the PCR fragment into the vector had been successful; GFP_pCLIIP fwd and 3' FseI_seq (Appendix 4) were used to verify insertion of the T2A-eGFP-pA fragment into pCLIIP-C-LS and eGFP seq fwd and NRP1 b2 fwd (Appendix 4) were used to verify insertion of mNRP1 into pCLIIP-GFP. Minipreparation of plasmid DNA (Section 2.7.1.3) from 4 clones identified as potentially containing pCLIIP-NRP1-GFP was carried out; diagnostic RE digest with Eco-RV-HF (Section 2.7.2) resulted in two fragments of 6357 and 5790 bp as expected. Finally, DNA was submitted to the University of Sheffield Genomic Core Facility for Sanger sequencing using the Applied Biosystems 3730 DNA Analyser. Returned sequences were aligned with the corresponding sequence using SnapGene® version 4.3.2 (GSL Biotech LLC) for verification. Following sequence verification, maxipreparation of pCLIIP-NRP1-GFP plasmid DNA (Section 2.7.1.2) was carried out for use during transfection of fs120 and fs164 cells.

2.7.6.6 Fs120 and fs164 cell transfection with *TransIT-X2*® and pCLIIP-NRP1-GFP and pmPB

12-well cell culture plates were coated with 5 µg/ml fibronectin for 30 – 60 min at RT prior to seeding fs120 and fs164 cells in 1 mL antibiotic free media at 3 x 10⁴ cells/well and incubated overnight at 37°C, 5% CO₂. The following day, *TransIT-X2*® transfection reagent was brought

to RT; 3 μ l *TransIT-X2*[®] was mixed with 100 μ l Opti-MEM[™] and 1 μ g DNA (0.5 μ g each of pCLIIP-NRP1-GFP and pmPB), the mixture was incubated for 30 min at RT before being added to wells in a drop wise fashion and plates were rocked gently to mix before being incubated at 37°C, 5% CO₂ for 48 hours.

2.8 Flow cytometry and fluorescence-activated cell sorting (FACS)

Flow cytometry is a technique used to distinguish between populations of cells in a heterogenous sample based on their size, complexity or fluorescence. As single cells within a suspension are passed through a laser beam in a sensing system their relative light-scattering or fluorescence is measured. Light scattering provides information regarding cellular structure and morphology and fluorescence emission is directly proportional to the level of a bound fluorescent probe or fluorescent protein expression. As fluorescently labelled cells or cells engineered to express a fluorescent protein pass through the laser beam, fluorescence is excited and emitted photons are collected by optical detectors. Photons are converted to an electrical impulse by photomultiplier tubes (PMTs), which is then processed to give a numerical signal. FACS is the sorting and collection of fluorescing cells from a heterogenous population by flow cytometry. FACS was used to assess efficacy of transfections with GFP expressing plasmids, to sort cells based on GFP expression for clonal isolation and to analyse NRP1 and NRP2 expression.

2.8.1 Flow cytometry to detect GFP expression

Media was aspirated from the wells and transfected cells were trypsinised and spun at 1200 rpm for 5 min. The supernatant was carefully discarded and the cell pellet was washed in FACS buffer (HBSS without Ca²⁺, Mg²⁺ or phenol red + 1 % FBS) once before being resuspended in 500 μ l cold FACS buffer. Cells were syringed with a 21G needle to ensure a single cell suspension and transferred to 5 mL round-bottomed polystyrene tubes. Flow cytometry was carried out using a FACSCaliber[™] with CellQuest[®] Pro Version 6.0 software. Forward scatter (FSC) is an indicator of cell size and side scatter (SSC) measures cell complexity. Mock transfected fs cells were used to adjust the voltage and amp gain and ensure that the cell population was visible on the SSC/FSC plot (Figure 2.8). A gate (G1) was drawn round the main cell population of the SSC/FSC plot to eliminate unwanted debris from being analysed (Figure 2.6B). The voltage on the fluorescence channel of interest, FL1 for GFP, was adjusted so that autofluorescence of the cells was in the first log decade of the FL1 plot, and a gate was drawn

up to the edge of the GFP negative cell population (G2) (Figure 2.6C). Data collection stopped when 10,000 positive events had been counted within G1 and the % gated number of G2 gave an indication of fluorescence in the fs cell populations. The raw data files were imported into the FlowJo V10 software (FlowJo LLC) for a more accurate analysis of GFP and thus transfection efficiency.

2.8.2 Flow cytometry for NRP1 and NRP2 expression

Media was aspirated and cells were detached from T25 flasks using a non-enzymatic cell dissociation buffer. Cells were centrifuged at 1200 rpm for 5 min RT and resuspended in cold DPBS twice before finally being resuspended at 1×10^6 cells/mL in cold 10% normal donkey serum/ DPBS plus primary antibodies (Appendix 2). An unstained control sample without the addition of a primary antibody was also included. Cells were incubated with the primary antibody (or remained in the blocking solution) for 45 min at RT before being washed 3 times in 10% FCS/DPBS. The final cell pellet was resuspended in 100 μ l of donkey anti-goat Alexa fluor-488 diluted to 1:1000 in 10% FCS/DPBS and incubated for 30 min RT in the dark. Cells were washed twice in 10% FCS/DPBS before resuspension in 300 μ l 10% FCS/DPBS. Cells were syringed with a 21G needle to ensure a single cell suspension and transferred to 5 mL round-bottomed polystyrene tubes. Flow cytometry and analysis was carried out as described above (Section 2.8.1).

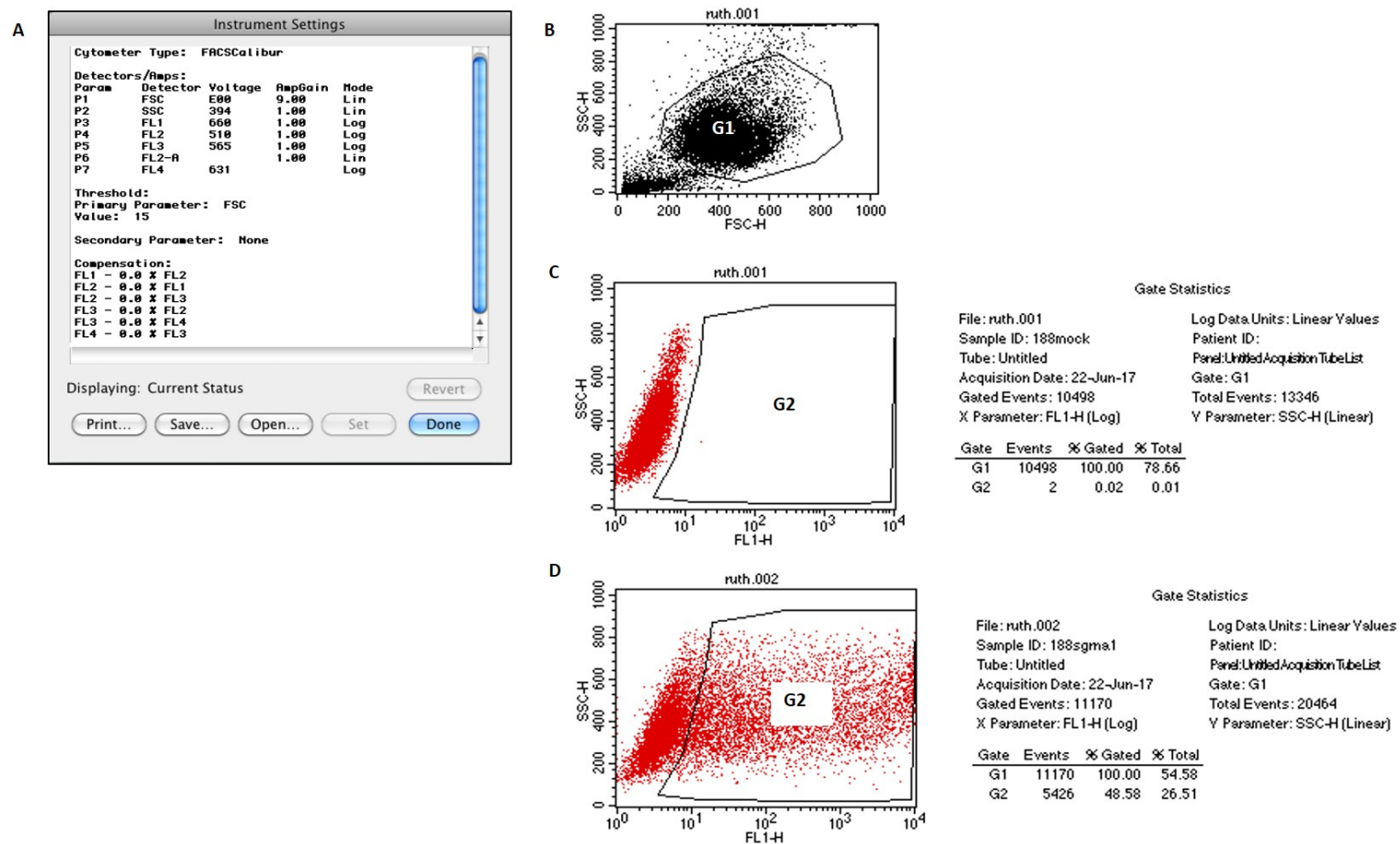


Figure 2.8 FACSCaliber™ settings and gating of fs cells and GFP positive cell populations

A) Voltage and amp gain settings were adjusted to ensure that fs cells were visible in the FSC/SSC plot, these settings were used throughout the study. B) A gate (G1) was drawn round the main fs cell population to exclude any debris within the sample. C & D) A second gate was drawn (G2) to capture the number of GFP positive cells above baseline fluorescence. The G2 % Gated number indicated the percentage of GFP positive cells within the G1 population

2.8.3 FACS to identify fs cell transfectants

Media was aspirated from the wells and cells were trypsinised and centrifuged at 1200 rpm for 5 min. The supernatant was carefully discarded and the cell pellet was resuspended in 500 µl full fs media (Table 2.1). Cells were syringed with a 21G needle to ensure a single cell suspension and kept on ice until being passed to the University of Sheffield Flow Cytometry Core Service for FACS with the BD FACSAria IIu. Mock transfected cells were used to set instrument parameters and GFP positive cell were sorted into 500 µl full fs media.

2.9 Clonal isolation of GFP positive cells

Clonal isolation of the heterogenous GFP positive cell populations was performed by resuspending the FACS sorted cells (Section 2.8.3) at very low cell densities (one cell/ well or less) and seeding them in the 96-well plates. The aim was to dispense single cells into a proportion of the wells to isolate clonal populations.

Initially, sorted cells were serially diluted to a final density of 0.5 cells/ 100 µl in full fs media (Table 2.1); 100 µl of diluted suspension was then added to each well of a 96-well plate. The remaining cells were transferred to individual T25 flasks for each sgRNA pair and the pooled cell populations were expanded and cryopreserved. After one week, no visible colonies had formed, therefore the reserved pools of cells were trypsinised and resuspended at 1 cell/ 100 µl before 100 µl of diluted cells was added to each well of three 96-well plates (referred to as A, B or C) per sgRNA pair. Again, the remaining pooled cells were transferred to a T25 flask for expansion and cryopreservation. Two cell pellets of 1×10^6 cells from each pool of CRISPR/Cas9n modified cell lines were collected for protein and gDNA extraction and stored at either -20°C or -80°C respectively. The remaining cells were cryopreserved.

After approximately one week, clonal cell populations were visible in the 96-well plates seeded at 1 cell/ well. Once wells were confluent, they were expanded into in T25 flasks. Clones were annotated to reflect the sgRNA pair they had been transfected with and the 96-well plate location they had been picked from. For example, a colony picked from well A6 in plate B transfected with sgRNA pair 3, was given the identity of 3BA6. On their first passage, each clone was cryopreserved and total cell lysates were prepared for WB analysis (Section 2.6) of NRP1 expression.

2.10 Single VEGF isoform verification in genetically modified fs cells

To verify that single VEGF isoforms were being transcribed in the genetically modified fs cells, total RNA was extracted from cell pellets.

2.10.1 RNA isolation from fs cells

RNA was isolated from cell pellets of 2×10^6 cells using the Monarch® RNA mini-prep kit following the manufacturer's protocol. The kit included a gDNA removal step that ensured only total RNA was isolated thus ensuring gene expression was being accurately assessed. RNA was eluted in 75 μ l NF H₂O, the concentration and purity was measured on the Nanodrop ND-1000 before storage at -80°C.

2.10.2 First strand cDNA synthesis

Reverse transcriptase is an RNA-dependent DNA polymerase that catalyses the conversion of fully transcribed mRNA templates to complementary DNA (cDNA). The most commonly used method for generating cDNA from mRNA requires oligo dT priming of the mRNA template. The presence of 3' poly(A) sequence (poly-A tail) distinguishes mRNA from transfer or ribosomal RNA and it is this feature that is taken advantage of by oligo(dT) priming. Oligo(dT)s are a short sequence of deoxythymidine nucleotides (normally 10-23 nucleotides) that anneal to the poly-A tail by complementary base pairing. In the presence of dNTPs, the reverse transcriptase copies the mRNA template into the cDNA sequence by extending from the annealed oligo(dT). The mRNA strand is removed and the single-stranded (ss) cDNA is converted to double-stranded (ds) DNA in the presence of an equimolar mix of dNTPs (Nam *et al.*, 2002).

Total RNA extracted from fs cells was converted to cDNA using the ProtoScript® II First Strand cDNA Synthesis Kit following the manufacturer's standard protocol with oligo d(T)₂₃ VN primers. The concentration and purity of the cDNA was measured on the Nanodrop ND-1000 before storage at -20°C.

2.11 *In vivo* models

In vivo experiments were carried out to study whether NRP1 expression modulated growth, stromal composition and metastases of fs120 and fs188 tumours treated with either the anti-mouse/human VEGF blocking antibody B20-4.1.1 or a non-immune IgG control (GP120:9674) (kindly provided by Genentech). RHET1 was a pilot study with five fs188 NRP1 KD clones plus fs188wt cells which determined whether CRISPR/Cas9n modified cell lines were capable of forming tumours *in vivo*. As a

result of this pilot experiment, a study of 100 mice split over 10 treatment groups that was divided into two experiments (RHET2 and RHET3), was carried out using two fs188 KD clones and one fs120 NRP1 OE clone plus their wt counterparts with the addition of the aforementioned treatments.

2.11.1 Ethical approval and animal husbandry

All experiments were conducted in accordance with the United Kingdom Home Office Animals (Scientific Procedures Act) 1986, with local ethical approval and recently published guidelines (Workman *et al.*, 2010) under the Personal Project Licence number PDA78C678 (Dr. Will English). Young (6-7 weeks) female CB17-SCID (CB17/*Icr-Prkdc^{scid}/IcrIcoCrl*) mice obtained from Charles River UK were used for all *in vivo* experiments. Mice were housed in 'The Barrier' side of the Biological Services Unit at no more than 5 animals per cage. Ventilated cages were kept in a temperature (22°C ± °C) and humidity (55% ± 10%) controlled environment with a 12 hrs light/ dark cycle. Pelleted mouse food and water were provided *ad libitum*. Animal treatment groups were distributed between cages in such a way that no more than two animals from the same group were in the same cage.

2.11.2 Subcutaneous tumour implant and end-point definitions

Fs cells at a low passage number (< P4) were cultured under standard conditions (Section 2.1) in multiple T175 flasks in order to achieve the number of cells required for tumour implants. On the day of implantation, cells were trypsinised and resuspended at 10⁶ cells/ 50 µl in serum free DMEM and kept on ice until the time of injection. Mice were anaesthetised using 2-3% isoflurane in O₂, fur in the region of the tumour implant was shaved and the exposed skin swabbed with 70% EtOH. Subcutaneous tumours were established by injecting 10⁶ cells into the rear dorsum of mice using a 30G needle. Once tumours had established, tumour volume was measured using callipers and weight was recorded daily. During the first small pilot experiment (RHET1) mice were culled when tumours reached a volume no larger than 520mm³. Subcutaneous tumours were measured using callipers and tumour volume (*V*) was calculated from $V = 0.52 \times d1 \times d2 \times d3$, where *d1*, *d2*, and *d3* are the three orthogonal tumour diameters. In subsequent *in vivo* experiments (RHET2 and RHET3) tumours were allowed to reach a maximum volume of 1200 mm³. During the first half of *in vivo* experiments including treatment (RHET2) a number of mice were lost before tumours reached the maximal end-point size of 1200 mm³, therefore during the second half of the study (RHET3) an experimental end-point of 48 h following the fourth treatment with either B20-4.1.1 or control IgG was used.

2.11.3 Intraperitoneal drug injection

Upon reaching a volume of 100 mm³, tumours in the RHET2 and RHET3 experiments were treated every three days with 5 mg/kg of either control IgG2a (GP120:9674) or B20-4.1.1 in saline solution (NaCl 0.9%) by intraperitoneal injection (IP) with a 30G insulin needle. For determining treatment efficacy, tumour diameters were measured throughout the growth period and tumour volumes calculated, as described above. Control IgG2a or B20-4.1.1 was diluted to 0.5 mg/mL in 0.9% w/v sodium chloride (saline solution). The volume administered was dictated by animal weight, for example, a 20 g mouse received 200 µl of the 0.5 mg/mL solution.

2.11.4 Tumour and lung excision and preparation

When animals reached the humane end-point of the experiment they were culled using the Schedule 1 method of cervical dislocation followed by exsanguination through the severing of the carotid artery to ensure complete euthanasia. Tumours were excised and weighed before being cut in half; one half was fixed in formalin and the other was cryopreserved. Lungs were snap frozen in 1.8 mL cryovials using liquid nitrogen and stored at -80°C for RNA extraction at a later date.

2.11.4.1 Formalin fixation of tumour tissue

Half of the excised tumour was immersed in 10% formalin. After 24 hours the formalin was discarded and replaced with 70% EtOH. Once all the tumours from the experiment had been collected they were placed cut-side down in tissue processing/embedding cassettes and returned to 70% EtOH. Tumours were then processed, embedded and sectioned by Mrs Maggie Glover (histology core facility).

2.11.4.2 Tissue sections

Formalin fixed paraffin embedded (FFPE) subcutaneous tumour sections were cut at a thickness of 5 µM and mounted on Superfrost® Plus microscope slides by Mrs Maggie Glover. Between 5 and 10 sections were cut per tumour for subsequent haematoxylin and eosin staining, Masson's trichrome staining and IHC for CD31, αSMA and Ki67 (see below for complete methodology).

2.12 Haematoxylin and eosin (H & E) staining

H & E staining was used to examine gross tumour morphology and analyse necrotic regions within tumour sections following treatment with either B20-4.1.1 or control IgG.

2.12.1 H & E staining method

Sections were de-waxed in Xylene twice for 5-10 min before being rehydrated in graded industrial methylated spirit (IMS) (100%, 100%, 95%, 90%, 70%) for 3 min each. Sections were rinsed in dH₂O for 1 min before immersion in Gill's haematoxylin for 2 min. Sections were washed in running tap water until the water ran clear before transferred to 70% IMS then 90% IMS for 3 min each. Sections were immersed in 1% eosin in 95% IMS for 30 sec - 1 min before being dehydrated further in 100% IMS for 3 x 30 sec. Sections were cleared in Xylene twice for 5 min each before mounting with DPX mounting media and glass coverslips.

2.12.2 Imaging Sections and analysis software

Whole slide scanning was performed using the Pannasonic 250 Digital Slide Scanner and sections were subsequently analysed using QuPath (Version 0.1.2) (Bankhead *et al.*, 2017).

2.12.3 Analysis of necrosis in H & E stained sections

Using QuPath (Version 0.1.2) (Bankhead *et al.*, 2017), the whole section area was measured by drawing around the perimeter of the tumour section, necrotic regions were then identified and drawn around (Figure 2.9). To estimate the level of tumour necrosis, the necrotic area was taken as a percentage of the whole section area.

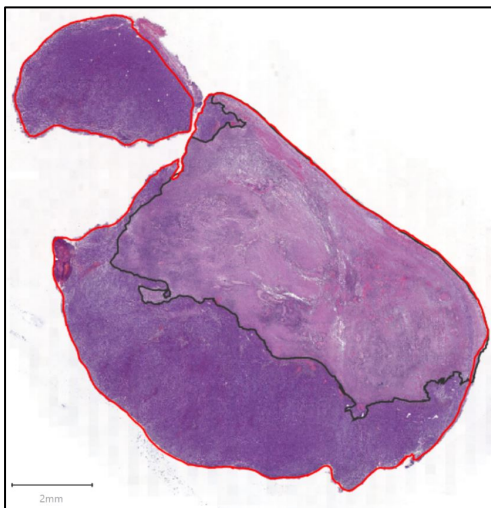


Figure 2.9 Analysis of necrosis in H & E stained tissue sections

Following whole slide scanning, tumour sections were analysed using QuPath (Version 0.1.2). Whole sections were drawn around (red outline) to calculate total tumour section area, necrotic areas were then identified (black outline).

2.13 Immunohistochemistry (IHC)

IHC enables visualisation of specific antigens in tissue sections. Through the use of antibodies specific to an antigen of interest, distribution and localisation of the antigen in a biological context can be evaluated.

2.13.1 De-waxing, rehydration and epitope retrieval

Sections were de-waxed in Histo-Clear II or Xylene twice for 10 min before being rehydrated in graded industrial methylated spirit (IMS) (100%, 100%, 95%, 70%) for 3-5 min each. Sections were placed in dH₂O for 1 min and rinsed in PBS before heat-induced epitope retrieval (HIER) was carried out.

Fixation of sections preserves tissue structure within the section, however, crosslinking fixatives such as formalin can prevent antibody binding to the target antigen. HIER aims to reverse this crosslinking and restore secondary or tertiary epitope structure to allow antibody binding. Sections were submerged in Target Retrieval Solution, a modified citrate buffer pH 6.1, and placed in a HIER pressure cooker on a 2 hour programme which heated to 121 °C for 20 minutes before cooling for the remainder of the programme. Following this, sections were rinsed in PBS twice.

2.14 Immunostaining of tumour sections

To block endogenous peroxidase activity, sections were incubated with 3% hydrogen peroxide (H₂O₂) /PBS for 20 min RT, they were then washed for 5 min in PBS before incubation with the appropriate blocking solution (Appendix 3) for 1 hour at RT to prevent non-specific antibody binding. Excess blocking solution was removed and sections were incubated overnight at 4 °C with the primary antibody (Appendix 3). Negative controls were left in blocking solution. All sections were washed 3 times in PBS for 5 min before addition of the secondary antibody (Appendix 3) at 1:200 for 1 hour RT. Following 3 x 5 min washes, horseradish peroxidase-conjugated avidin-biotin complex (ABC-HRP) reagent was prepared as per the manufacturer's protocol and applied to the sections for 30 min RT. A further 3 x 5 min PBS washes were carried out before the application of 3,3'-diaminobenzidine (DAB) peroxidase reagent, prepared following the manufacturer's protocol. DAB signal was left to develop for up to 10 min before the reaction was quenched by rinsing in tap water. Sections were counterstained with Gill's Haematoxylin for 60 sec, washed twice in PBS for 30 sec and rinsed in tap water for 5 min. Sections were allowed to air-dry overnight before mounting with DPX mounting media and glass coverslips.

2.14.1 IHC with Mouse on Mouse (MOM) Immunodetection Kit

The primary antibody for α SMA was raised in mouse, therefore a slightly modified methodology using a commercial MOM immunodetection kit was used. To block endogenous peroxidase activity, sections were incubated with 3% hydrogen peroxide (H_2O_2) /PBS for 20 min RT, they were then washed for 5 min in PBS before incubation with a working solution of MOM mouse IgG blocking solution for 1 hour at RT. Sections were washed twice in PBS before incubation for 5 min RT with a working solution of MOM diluent; excess diluent was tapped from the slides and sections were then incubated for 30 min RT with the primary antibody (Appendix 3) and negative controls were left in blocking solution. All sections were washed 3 times in PBS for 5 min before the addition of a working solution of MOM biotinylated anti-mouse IgG reagent for 10 min RT. Following 3 washes in PBS, the same protocol for avidin-biotin detection and subsequent mounting as Section 2.14 was used.

2.14.2 Tumour vascular density analysis

To assess the vascularity of tumours, CD31 (platelet endothelial cell adhesion molecule-1, PECAM-1) was used as an EC marker. CD31 is generally accepted as a reliable marker of EC differentiation; however, it is also expressed by other cells such as macrophages (Mckenney *et al.*, 2001). Visual assessment of CD31 staining identified that, in a small number of tumours, there were areas of punctate cellular staining at the periphery of the tumour that were deemed to potentially be infiltrating macrophages (Figure 2.10A). When assessing the tumour vascular density, these areas were avoided as much as possible; furthermore, the effect of these positively stained macrophages in the fields of view analysed had minimal impact on the percentage of DAB positivity as a whole. QuPath (Version 10.1.2) (Bankhead *et al.*, 2017) was used to quantify the vascular density of the tumour sections. In areas of viable tumour tissue, 10 squares measuring 750 x 750 microns were randomly drawn. The 'positive pixel count' command was then run to give the percentage of DAB positive staining per square, from which the mean percentage was calculated. In the same 10 squares, the number of vessels were categorised as either 'intact' or 'large open' and counted (Figure 2.10B). Both the mean number of total vessels per view and the mean number of the individually categorised vessels were calculated.

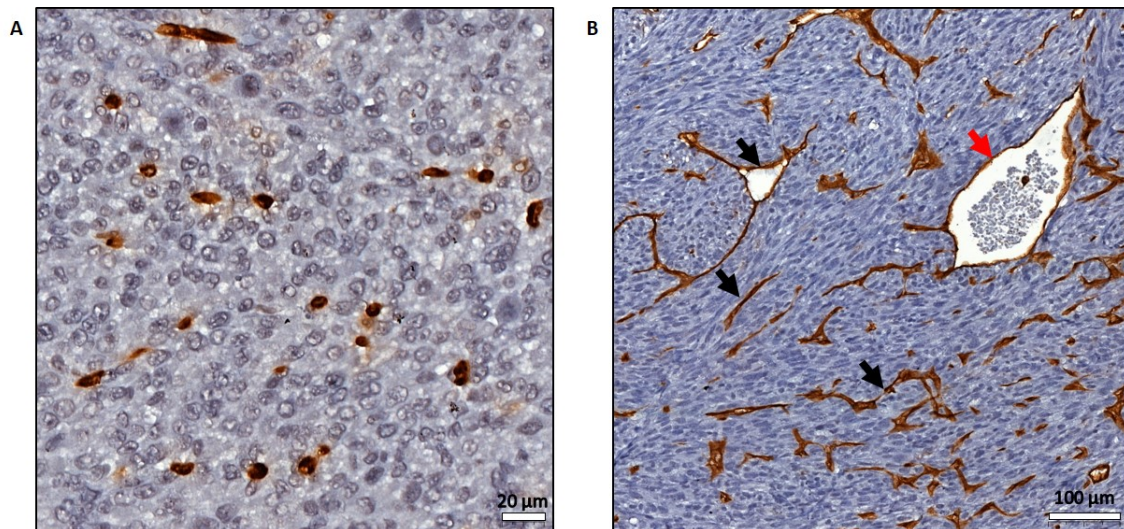


Figure 2.10 CD31 staining example

A) An example of a fs188 tumour stained for CD31 with a punctate pattern of staining at the periphery of the tumour (40x magnification). B) During the vessel counting to ascertain the mean vessel density, vessels were categorised as either 'intact' (black arrows) or 'large open' (red arrows) (10x magnification).

2.15 Masson's Trichrome staining

Masson's trichrome staining (Garvey, 1984) was used on FFPE tumour sections to detect intratumoural fibrillar collagen and tumour vessel associated collagen. Three dyes are employed, each of which selectively stains for collagen (light green), muscle fibres/ haemoglobin/ keratin (red) and cytoplasm/ adipose cells (light red/pink), thus enabling differentiation of structural components within the tumour. Nuclei are stained with iron haematoxylin, collagen with light green, and the cytoplasmic background with ponceau 2R/ acid fuchsin. Phosphomolybdic (ppm)/phosphotungstic (ppt) acid prevents staining of collagen with acid fuchsin thus allowing it to instead be stained with light green.

Sections were de-waxed in Xylene twice for 10 min, rehydrated in graded IMS (100%, 100%, 95%, 70%) for 3 min each and rinsed in H₂O before being fixed in Bouin's solution ON at RT. Slides were rinsed well in H₂O then immersed in Weigert's iron haematoxylin solution for 10 min RT, rinsed in Scott's tap water substitute (See Appendix 1 for preparation) and then H₂O for 30 sec each before being incubated in ponceau 2R: acid fuchsin (See Appendix 1 for preparation) for 10 min RT. Sections were rinsed in H₂O to remove excess dye before being placed in ppm/ppt (See Appendix 1 for preparation) for 2 min RT, slides were immersed in H₂O once then placed in 2% (w/v) light green SF yellowish in 2% acetic acid for 8 min RT. Following a 2-3 quick immersions in H₂O, sections were rapidly dehydrated through graded IMS (70%, 95%, 100%, 100%) (3-4 immersions in each solution), incubated in Xylene twice for 10 min before mounting with DPX mounting media and glass coverslips. Slides were scanned

using the Pannasonic 250 Digital Slide Scanner and examined/ imaged using the CaseViewer Version 2.1 (3DHitech) software.

2.16 Statistical analysis

Data were plotted and analysis carried out using GraphPad Prism 8.3.0. Pairwise analysis was carried out by unpaired t-test under the assumption that data was parametric. Grouped data were analysed by ANOVA, with either Tukey or Bonferroni correction, dependent on the number of pairwise comparisons being made within the group. The specific analyses used to analyse data for each experiment are detailed in the figure legends.

In all figures, n refers to the number of independent experiments and any replicates within a single experiment are noted separately.

Chapter 3

Consequences of transient NRP1 knockdown on fswt/fs188 behaviour *in vitro*

3.1 Introduction

NRP1 is a cell surface receptor that, either alone or as co-receptor, binds a diverse range of extracellular ligands, supports and enhances signalling of various RTKs and interacts with ECM components. NRP1 plays an essential role in both physiological and pathological processes which can be largely attributed to its capacity to integrate with mechanisms responsible for cellular motility and adhesion in immune, endothelial and tumour cells (Niland and Eble, 2019). Whether deregulated cancer cell NRP1 expression enhances or inhibits these known functions is context and cell type dependent, and to date, studies investigating its role in STS are severely lacking. Although studies in ECs and various cancers are indicative of NRP1 being required for optimal growth factor mediated cellular functions (Raimondi and Ruhrberg, 2013), the mechanisms and signalling events elicited by these interactions still remains largely unclear, especially so in tumour cells. Another question that remains unanswered is whether NRP1 influences cellular functions in the absence of growth factors or other ligands.

Our lab has previously developed fs cells expressing individual VEGF isoforms which exhibit distinct functions *in vivo* and *in vitro* (Tozer *et al.*, 2008a, Kanthou *et al.*, 2014, English *et al.*, 2017). NRP1 was among several proteins that were identified to be differentially expressed between the cell lines. Specifically, it was found that NRP1 expression levels were higher in the fswt and fs188s than the fs120 and fs164 cells (Kanthou *et al.*, 2014). *In vitro*, fs188 and fswt cells migrate at a faster rate than fs120 and fs164 cells across a 2D surface. However, *in vivo* fs120 cells metastasised to the lungs more readily than the fs188 cells. These seemingly contradictory data might be as a result of the fs120 cells being able to switch their cellular morphology from being ameboid/rounded to a mixture of more elongated and mesenchymal cells when in the ECM. *In vitro*, fs188 and fswt cells display phenotypical mesenchymal characteristics whereas fs120 and fs164 cells display a more rounded/amoeboid cellular morphology, mode of motility and close cell-cell contacts. These morphological differences can also be seen *in vivo*; fs188 cells retain their elongated shape whereas fs120 and fs164 cells appear more rounded in sub cutaneous tumour tissue (Tozer *et al.*, 2008a, Kanthou *et al.*, 2014, English *et al.*, 2017).

Furthermore, the fs120 cells exhibit the ability to switch from their innate rounded cellular morphology to a more mesenchymal state on fibrillar collagen (Tozer *et al.*, 2008a, Kanthou *et al.*, 2014, English *et al.*, 2017). The ability of tumour cells to switch between epithelial and mesenchymal phenotypes provides them with a distinct advantage in terms of invasive capacity. During the transition between phenotypes, the intermediate state confers the ability of cells to both migrate and adhere simultaneously thereby allowing them to move as a collective mass, which may be more resistant to apoptosis. The plasticity of these cells allows them to infiltrate distal tissues through assuming the cellular morphology that is most advantageous to their environment (Jolly *et al.*, 2015). The combined work of Kanthou *et al.* (2014) and English *et al.* (2017) has provided evidence that this may certainly be the case with the fs120 cells. This hypothesis is further strengthened by data showing stromal cells in the TME promote tumour cell motility through growth factor and protease secretion (Sahai, 2005). Additionally, *in vitro* invasion of fs188 cells through collagen-1 was significantly higher than fs120/fs164 cells whereas invasion of the fs188 cells through laminin was lower, again strengthening the argument that interaction of the fs tumour cells with the stromal cells and matrix *in vivo* are influenced by factors other than, or in conjunction with, VEGF isoform expression (English *et al.*, 2017). Finally, *in vitro* invasion of fs120 cells through laminin appeared to be VEGF dependent, whereas fs188 migration on laminin was unaffected in the presence of a VEGF blocking antibody (English *et al.*, 2017). Taken as a whole, these data suggest that fs cells expressing individual VEGF isoforms may respond to different signalling cues that are activated in an autocrine or paracrine manner *in vivo*.

Isoform dependent VEGF mediated interactions between NRP1 and VEGFR2 have been reported to influence migration. On this basis, given the well-established role of NRP1 in cellular functions and its association with a more aggressive phenotype in other cancers, together with the identification of differential NRP1 expression between fs188 and fs120 cells (Kanthou *et al.*, 2014), it seems plausible that NRP1 has a role to play in migration in these cells. This chapter set out to investigate the contribution of NRP1 to the phenotypic differences previously reported in these cells.

3.2 Aim

The aim of this chapter was to investigate whether NRP1 expression in fs cells expressing individual VEGF isoforms contributes to phenotypic differences *in vitro*. To achieve this, siRNA was used to KD NRP1 expression in fswt and fs188 cells previously shown to have higher expression levels. The effect of NRP1 KD on pathways and receptors known to be associated with this promiscuous receptor were

investigated by western blotting and functional biological assays of migration and adhesion were carried out.

3.3 Differential expression of NRP1 in fs cells expressing different VEGF isoforms

Previous work has shown that NRP1 expression is elevated in fswt and fs188 cells in comparison to fs120 and fs164 cells (Kanthou *et al.*, 2014). To confirm these data, all four cell lines were seeded at 1.5×10^5 cells/well in 6-well plates and incubated for 48 hours. Whole cell lysates were analysed for NRP1 expression by western blotting. In agreement with published data, fswt and fs188 cells expressed higher levels of NRP1 than fs120 and fs164 (Figure 3.1).

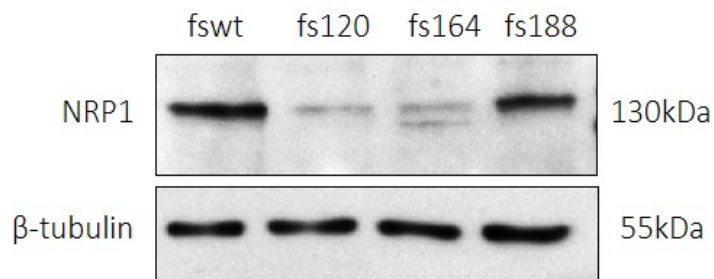


Figure 3.1 NRP1 expression in fibrosarcoma cells

Whole cell lysates from fswt, fs120, fs164 and fs188 cells were collected and quantified. Equal quantities of proteins (15 μ g) were analysed by western blotting for expression of NRP1. β -tubulin was used as an internal loading control. Results confirmed higher expression of NRP1 in fswt and fs188 cells in comparison to fs120 and fs164 cells. Representative blot of n=4.

3.4 Knockdown of NRP1 in fswt and fs188 cells

NRP1 expression was transiently knocked down in fswt and fs188 cells using siRNA. Cell lysates were analysed by western blotting to investigate any changes in expression of related proteins and the functional consequence of NRP1 depletion was studied.

3.4.1 NRP1 siRNA knockdown

Initially, ON-TARGETplus SMARTPool mouse NRP1 (Materials and Methods, Table 2.2) containing a mixture of 4 siRNAs was used to KD NRP1 expression in fs188 cells; however, this did not result in any significant decrease in NRP1 expression (data not shown). Protocols employing a single transfection and a double transfection (transfection repeated 24 hours following initial transfection) were investigated; neither of which resulted in KD of NRP1 (Materials and Methods, Section 2.2.3).

The individual siRNAs within the ON-TARGETplus SMARTPool mouse NRP1 siRNA (Materials and Methods, Table 2.2) were tested in the fs188 cells to establish whether individually they could KD NRP1 expression. Double transfection using siRNA1, with a target sequence in the MAM domain, resulted in significant NRP1 KD (Figure 3.2 A-D) in comparison to fs188 cells transfected with a non-silencing control siRNA (ns siRNA). Successful KD of NRP1 with siRNA1 was also achieved in the fswt cells (Figure 3.2 E & F). siGLO green, an RNA-induced silencing complex (RISC)-independent fluorescent indicator which localises to the nucleus, allowed visual evaluation of optimal transfection conditions. Although siGLO green was useful as a tool to identify successful transfection, it is not considered to be equivalent to a non-silencing negative control and therefore the data using proteins extracted from siGLO treated cells on the western blots may be disregarded.

A further set of NRP1 siRNAs (Materials and Methods, Table 2.2), targeting four different regions of the NRP1 transcript were analysed for their ability to KD NRP1 expression in the fswt and fs188 cells. In the first instance, successful NRP1 KD was achieved in the fs188 cells with siRNA 1_1 (Figure 3.3A) which targeted the start of the a2 domain (Materials and Methods, Table 2.2). However, in the same experiment, KD of NRP1 in the fswt cells was not achieved (Figure 3.3A). This was potentially due to lysis of the cells being delayed until 48 hours after the second transfection step as a result of poor confluency. When using siRNA1, NRP1 KD was sustained for 48 hours after the second transfection step; this suggests that although siRNA 1_1 resulted in successful NRP1 KD, it was less efficient and the gene silencing was not sustained. On repeat of siRNA transfection with the four new siRNAs, NRP1 KD was successful in both cell lines when cells were lysed 24 hours after the second transfection step (Figure 3.3B).

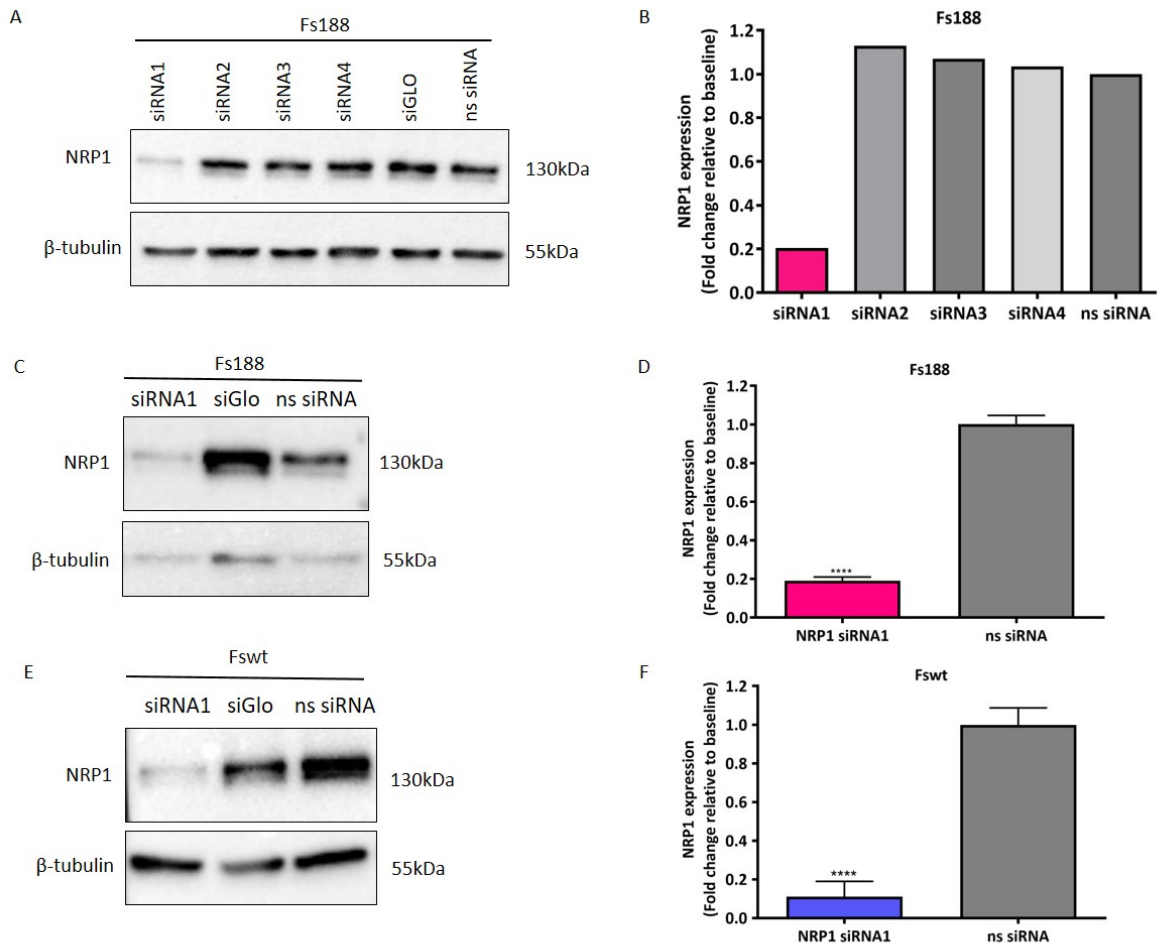


Figure 3.2 NRP1 siRNA KD in fswt and fs188 cells

A & B) Total cell lysates prepared from fs188 cells transfected with four individual siRNAs targeting NRP1 and a non-silencing (ns) siRNA were analysed by western blotting for expression of NRP1 (representative blot, n=2 independent experiments). C-F) Fs188 and fswt cells were transfected with NRP1 siRNA1 and ns siRNA, 24 hours following the second transfection total cell lysates were collected and quantified. Equal amounts of proteins (15 μ g) were analysed for NRP1 expression by western blotting in C & D) fs188 cells (representative blot, n=6 independent experiments), and E & F) fswt cells (representative blot, n=5 independent experiments). NRP1 band intensity was normalised to β -tubulin before the fold change in expression levels between NRP1 siRNA and ns siRNA treated cells were calculated. Data analysed by unpaired t-test (****p<0.0001, \pm SEM).

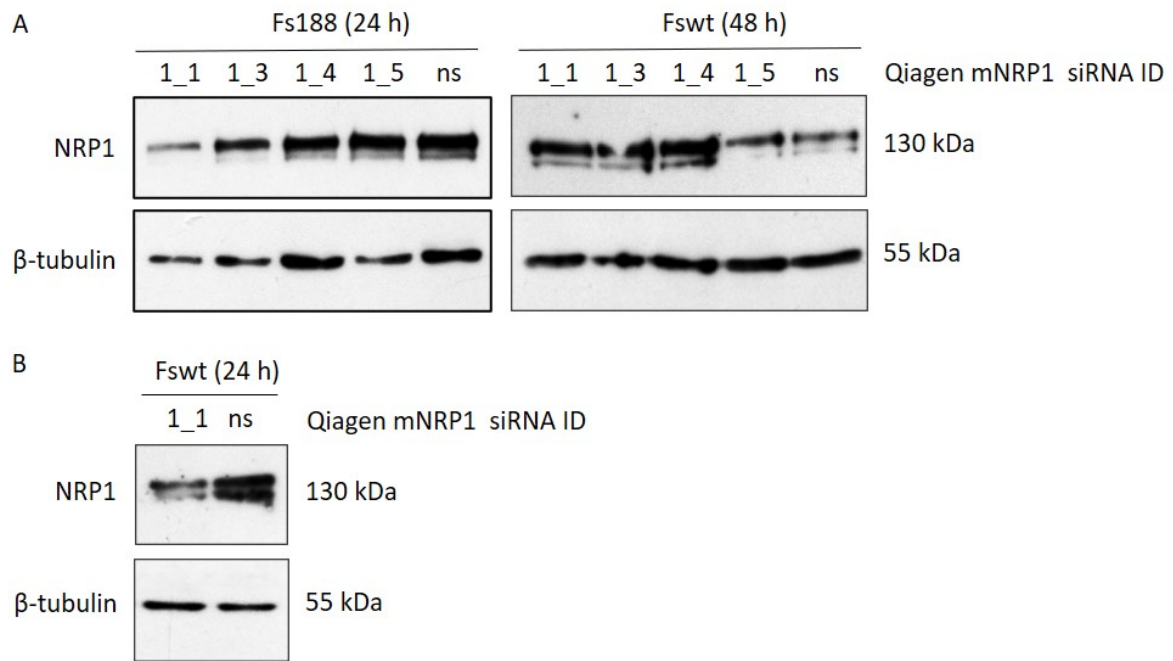


Figure 3.3 NRP1 KD in fs188 and fswt cells with alternative siRNA

Fs188 cells were transfected with four individual siRNAs targeting NRP1 and a non-silencing (ns) siRNA. A) Cell lysates were collected 24 h post second transfection from fs188 cells and 48 h post the second transfection from fswt cells and analysed by western blotting for expression of NRP1 (n=1 independent experiment). B) Fswt cells were transfected with NRP1 siRNA 1_1 and ns siRNA, 24 h post the second transfection total cell lysates were collected and were analysed for NRP1 expression by western blotting (representative blot, n=1 independent experiment).

3.5 Effects of NRP1 knockdown on NRP2 expression

NRP1 and NRP2 are structurally similar; overall their amino acid sequences are 44% homologous and in the MAM portion of the c domain, where siRNA1 binds, they share 37% amino acid identity (Chen *et al.*, 1997). Western blot analysis of fswt and fs188 cell lysates, previously validated for NRP1 KD, confirmed that NRP1 KD did not lead to any significant off target effects on NRP2 expression (Figure 3.4).

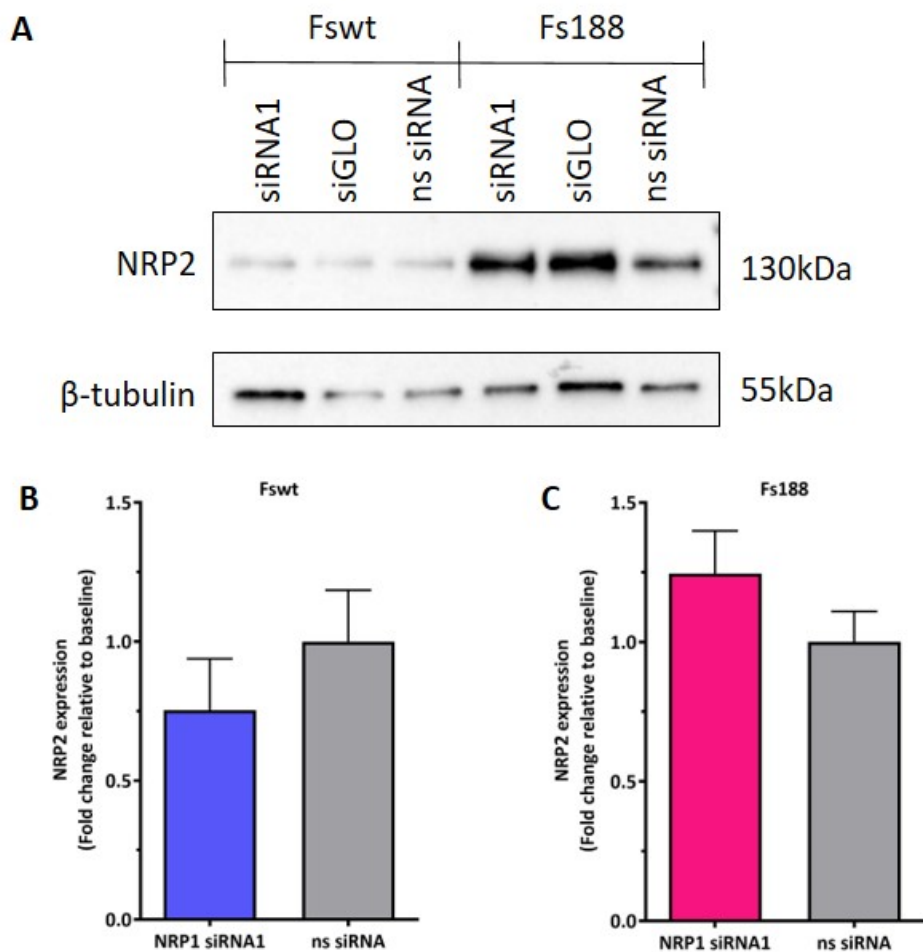


Figure 3.4 NRP2 expression in NRP1 KD cells

Cell lysates were prepared from fs188 and fswt cells transfected with either NRP1 siRNA1 or ns siRNA. Equal amounts of protein (15 μ g) were analysed by western blotting for A) NRP2 expression (representative blots, n=3-4 independent experiments). Analysis of western blots showed no significant change in NRP2 expression when NRP1 was depleted in B) fswt cells (n=3 independent experiments, \pm SEM) or C) fs188 (n=4 independent experiments, \pm SEM). NRP2 band intensity was normalised to β -tubulin before the fold change in expression levels between NRP1 siRNA1 and ns siRNA treated cells were calculated. Data analysed by unpaired t-test

3.6 Effect of NRP1 KD on VEGFR2, PDGFR β , β 1 integrin and fibronectin

NRP1 has been shown to influence cell surface expression of co-receptor VEGFR2 in ECs (Gelfand *et al.*, 2014) and modulate VEGFR2 signalling through promotion of receptor recycling (Ballmer-Hofer *et al.*, 2011). Several attempts were made to examine VEGFR2 expression in the fs188 NRP1 KD cells by western blotting. Although VEGFR2 has previously been detected in the fs188 cells (Kanthou *et al.*, 2014), it could not be detected in the fs188 cells in this study but it was present in HUVEC extracts thus excluding any antibody detection issues (Figure 3.5).

NRP1 co-localises with PDGFR β via PDGF ligand binding in hepatic stellate cells (HSCs) (Cao *et al.*, 2010) and fibroblasts (Muhl *et al.*, 2017) and influences PDGFR β homodimer signalling in mesenchymal stem cells (Ball *et al.*, 2010). NRP1 activates α 5 β 1 integrin to promote fibronectin fibril assembly in HSCs (LX2) (Yaqoob *et al.*, 2012) ECs (Valdembri *et al.*, 2009) and human glioma cells (U251) (Chen *et al.*, 2014). Additionally, in Panc-1 cells and MCF7 breast cancer cells (Zeng *et al.*, 2014) NRP1 complexes with β 1 integrin (Fukasawa *et al.*, 2007). Fswt and fs188 NRP1 KD cells were analysed for expression levels of PDGFR β , β 1 integrin and fibronectin by western blotting; NRP1 KD with siRNA1 did not result in any substantial changes in expression of these associated receptors or alter expression of fibronectin (Figure 3.5).

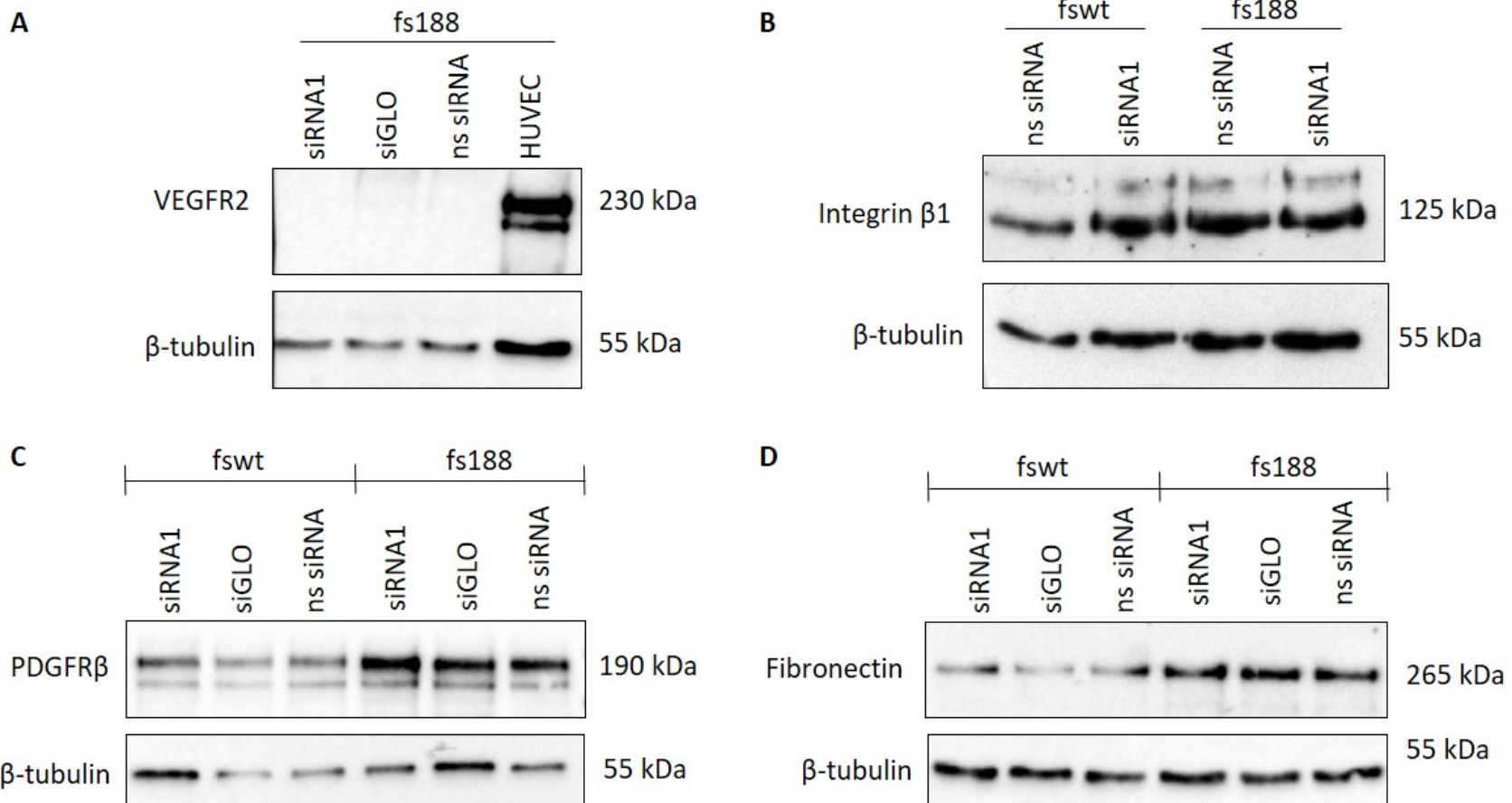


Figure 3.5 Expression of associated receptors and fibronectin following NRP1 siRNA1 KD in fswt and fs188 cells

Whole cell lysates were prepared from fs188 and fswt cells transfected with either NRP1 targeting siRNA1 or ns siRNA. Equal amounts of protein (20 µg) were analysed by western blotting for expression of A) VEGFR2 (representative blot shown, n=3 independent experiments), B) β1 integrin (n=1), C) PDGFRβ (representative blot shown, n=3 independent experiments) and D) fibronectin (n=1). No signal for VEGFR2 could be detected in fs188 cells, however it was detected in HUVECs, which were used as a positive control. No observable differences in expression levels of integrin β1, PDGFRβ or fibronectin between NRP1 siRNA1 and ns siRNA transfected cells were identified. β-tubulin was used as an internal loading control.

3.7 Effect of NRP1 KD on ERK1/2 phosphorylation

Investigation of the signalling mechanisms which could account for the different growth, survival and migration rates of the fibrosarcoma cells lines identified that cell regulatory proteins were differentially expressed and/or activated (Kanthou *et al.*, 2014). Fs188 and fswt cells were slower to proliferate but exhibited increased migration rates and pro-apoptotic tendencies in comparison to fs120 and fs164 cells. However, perhaps counter intuitively, the activation status (phosphorylation) of survival and proliferation proteins AKT, signal transducer and activator of transcription 3 (STAT3) and ERK1/2 was higher in the fs188 and fswt cells. Increased ERK1/2 phosphorylation in the fswt and fs188 cells could not be attributed to VEGF mediated VEGFR activation, suggesting activation via an unidentified compensatory pathway (Kanthou *et al.*, 2014). Evidence suggests that NRP1 plays an important, VEGFR2 independent role in VEGF mediated phosphatidylinositol 3-kinase (PI3K) pathway activation in metastatic breast cancer cells (Bachelder *et al.*, 2001). In addition, NRP1 has been shown to interact with members of the integrin family, therefore seemed plausible to postulate that NRP1 KD may lead to alterations in cell regulatory protein activation.

Western blot analysis of fswt and fs188 NRP1 KDs versus controls was carried out to investigate whether KD of NRP1 affected ERK1/2 phosphorylation. Unexpectedly, ERK1/2 phosphorylation increased in fswt cells, although this failed to reach significance. In the fs188 cells however, there was a significant increase in phosphorylated ERK1/2 (pERK1/2) when NRP1 expression was depleted (Figure 3.6). Western blot analysis of total ERK1/2 (tERK1/2) indicated that the increased activation was not as a result of an increase in overall protein expression (Figure 3.6).

Further analyses were carried out to investigate the effect of NRP1 KD on the activation of cell signalling and regulatory proteins p27 Kip1, pSTAT3, pAKT, pSrc (Tyr416) and pFAK (Tyr397). Expression levels remained unchanged between NRP1 siRNA1 and ns siRNA transfected cells (data not shown).

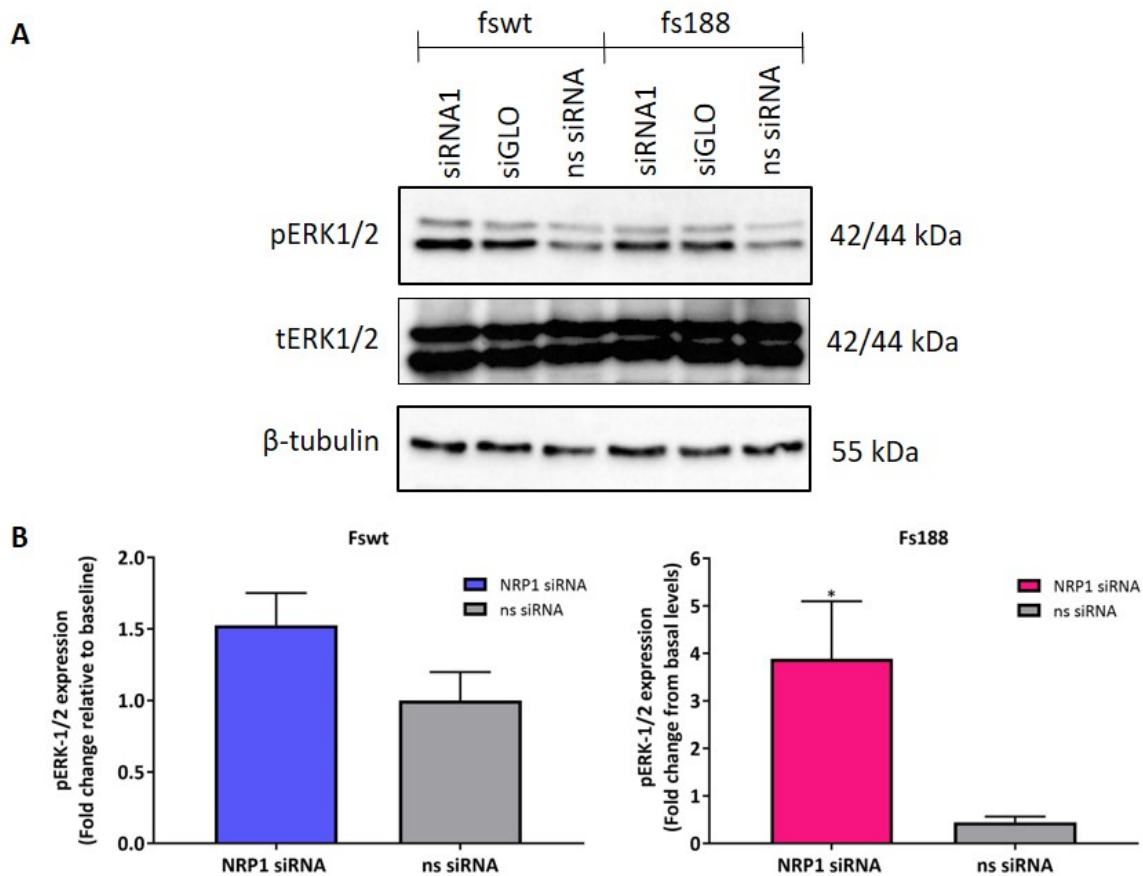


Figure 3.6 ERK1/2 phosphorylation in NRP1 KD cells

Cell lysates were prepared from fs188 and fswt cells transfected with either NRP1 siRNA1 or ns siRNA. Equal amounts of protein (10 µg) were analysed by western blotting for expression of A) pERK1/2 (representative blot of n=3-4 independent experiments) and total ERK1/2 (n=1). B) NRP1 KD with NRP1 siRNA1 in fs188 cells led to a significant increase in ERK-1/2 phosphorylation in comparison to cells transfected with ns siRNA (*p = <0.033, ±SEM). This trend was also observed in fswt cells but failed to reach statistical significance. Combined pERK1/2 band intensities were normalised to β-tubulin before the fold change in expression levels between NRP1 siRNA1 and ns siRNA treated cells were calculated. Data were analysed by unpaired t-test.

3.8 NRP1 KD in fibrosarcoma cells does not affect adhesion to various ECM proteins.

Previous work identified differences in adhesion of the fs cells lines to various matrix proteins (Kanthou *et al.*, 2014). Silencing of NRP1 in ECs has yielded contradictory results. Murga *et al.* (2005) found reduced NRP1 expression led to significant reductions in the adhesion of unstimulated HUVECs to laminin, gelatin and fibronectin after 7 hours, whereas in short-term adhesion assays of 15 min, loss of NRP1 led to a reduction in human umbilical arterial EC (HUAEC) adhesion to fibronectin (0.5 -2 $\mu\text{g/ml}$), yet had no effect on adhesion to other ECM proteins, collagen, vitronectin, or laminin 1 (Valdembri *et al.*, 2009). In human dermal microvascular ECs (HDMEC) and HUVECs Raimondi *et al.* (2014) found that loss of NRP1 did not affect EC ability to adhere to fibronectin over a period of 1 - 180 mins.

Adherence of NRP1 siRNA1 transfected fswt and fs188 cells to collagen-I, laminin, fibronectin and uncoated plastic was compared to their respective parental cell lines transfected with a ns siRNA. A single experiment was carried out to evaluate whether the concentration of fibronectin affected the adhesion kinetics of fs cells following NRP1 KD and may have led to the contradictory results previously noted in ECs (Murga *et al.*, 2005, Valdembri *et al.*, 2009). Although a decrease in fibronectin concentration led to a reduction in unmodified fs cell adhesion, which was more pronounced in the fswt cells, a parallel reduction in adhesion was also seen in the NRP1 KD fs cells (Supplementary data, Figure S1). In light of this, 5 $\mu\text{g/mL}$ fibronectin was used for all adhesion experiments. In contrast to findings of others in various other cell types, KD of NRP1 had no significant effect on the ability of fs188 or fswt cells to adhere to any of the ECM proteins tested or cell culture plastic after 45 min in comparison to their NRP1 expressing counterparts. Fswt and fs188 NRP1 depleted cells adhered significantly better to fibronectin than collagen-I, laminin and plastic (Figure 3.7). The avid adherence of fs188 and fswt cells treated with ns siRNA to fibronectin is in agreement with previously published data (Kanthou *et al.*, 2014).

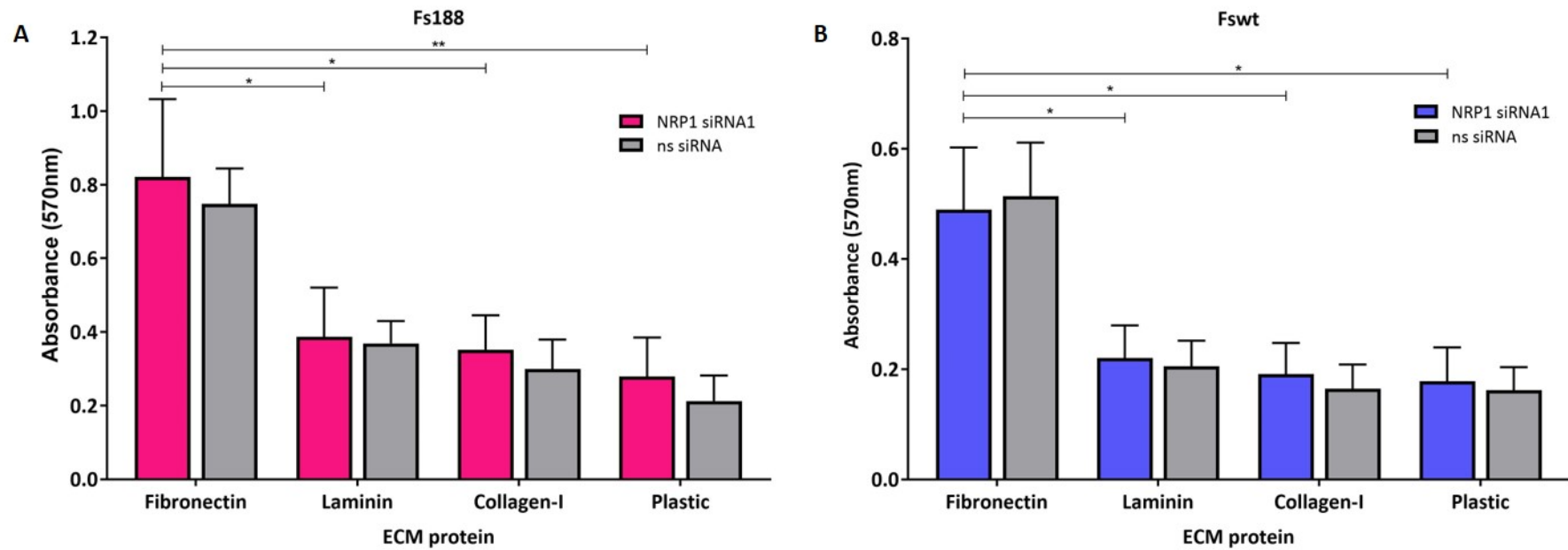


Figure 3.7 Effect of NRP1 KD on fswt and fs188 cell adhesion

Fs188 and fswt cells transfected with either NRP1 siRNA1 or ns siRNA were seeded in triplicate into wells of a 96-well plate coated with 5 $\mu\text{g}/\text{mL}$ fibronectin, 5 $\mu\text{g}/\text{mL}$ laminin, 5 $\mu\text{g}/\text{cm}^3$ collagen-1 or left uncoated. Cells were allowed to adhere for 45 min; media and non-adherent cells were aspirated and remaining adhered cells were fixed with formalin before being stained with crystal violet. Crystal violet was solubilised and the absorbance measured at 570 nm. NRP1 siRNA KD did not result in changes in adhesion between A) fs188 cells and B) fswt cells to laminin, fibronectin, collagen-I and plastic in comparison to cells treated with a ns siRNA. Both A) fs188 and B) fswt cells depleted of NRP1 adhered significantly better to fibronectin over collagen, laminin-1 and plastic ($n=8$ independent experiments carried out in triplicate). Data is analysed by 2-way ANOVA with Tukey post-test (* $p = 0.033$, ** $p = 0.002$, $\pm\text{SEM}$).

3.9 Effects of NRP1 KD on migration of fibrosarcoma cells

NRP1 plays a fundamental role in cellular motility during development, angiogenesis and in tumour metastases (Gerhardt *et al.*, 2004, Pan *et al.*, 2007a, Jia *et al.*, 2010, Li *et al.*, 2014, Yue *et al.*, 2014, Li *et al.*, 2016a, Matkar *et al.*, 2018). Relevant to these cells lines, Kanthou *et al.* (2014) previously showed that fswt and fs188 cells migrated faster across a 2D surface than fs120 and fs164 cells. To see whether NRP1 may, in part, play a role in these differences, the migration rates of the fswt and fs188 cells were measured against their NRP1 KD counterparts in a wound healing assay.

After 8 hours, wound closure in NRP1 expressing fs188 and fswt cells was significantly faster than that of the fs188 and fswt cells with decreased NRP1 expression. After 10 hours the wound area remaining in both the fs188 cells and the fswt cells expressing NRP1 was 22% less than the wound area remaining in the fs188 and fswt cells where NRP1 expression was depleted (Figure 3.8).

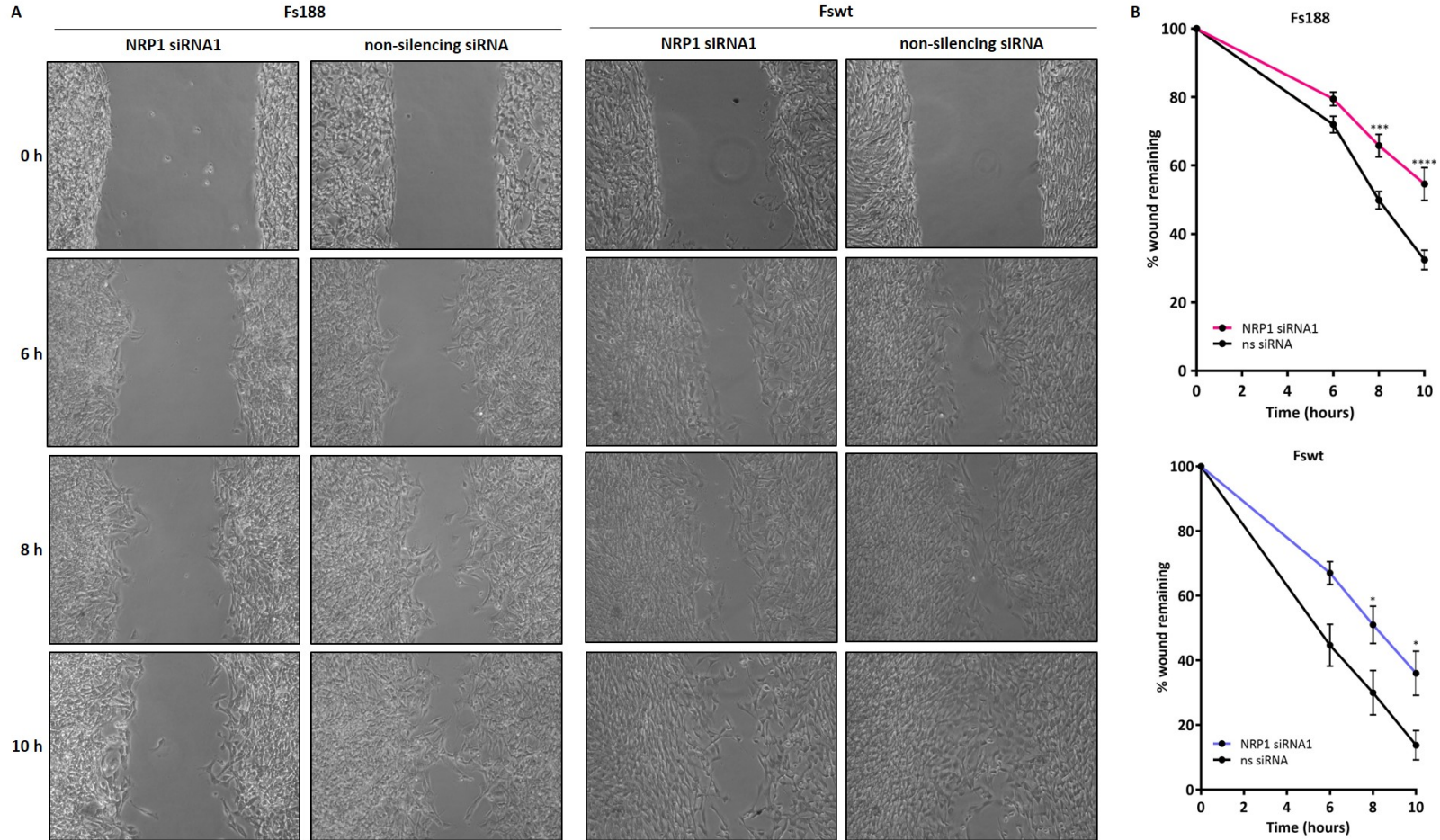


Figure 3.8 Migration of fs188 and fswt cells following NRP1 KD

Fs188 and fswt cells transfected with either NRP1 siRNA1 or ns siRNA were seeded in 2-well silicone cell culture inserts. Once confluent, inserts were removed to leave a 500 μm gap. A) Images were taken in the same area at each at 0 h, 6 h, 8 h and 10 h (representative images for each timepoint/ cell line shown). B) NRP1 KD led to a significant decrease in migration after 8 and 10 h in both fswt and fs188 cells. Cell free area was measured using Image J and the wound remaining was calculated as a percentage of the wound area at 0 h (n = 3-6 independent experiments carried out in duplicate). Data is analysed by 2-way ANOVA with Bonferonni post-test (* $p = 0.033$, *** $p = 0.0002$, **** $p = <0.0001$, \pm SEM).

3.10 Discussion

The pro-angiogenic and pleiotropic functions of NRP1 have been demonstrated in ECs and multiple tumour types. The aim of this chapter was to further elucidate the function of NRP1 in our panel of fs cells expressing individual VEGF isoforms. This was achieved through transient KD of NRP1 in fs188 and fswt cells and analysing any resulting differences in signalling, associated receptor expression, migration, proliferation and adhesion.

NRP2 expression was not effected by KD of NRP1 in either the fs188 or fswt cells thus confirming that there were no off target effects from the siRNA on this closely related receptor. Furthermore, the absence of increased NRP2 expression in response to NRP1 KD suggested that any compensatory mechanisms triggered were not through this receptor. This is in agreement with previous reports for the non-overlapping roles of NRP1 and NRP2 (Raimondi and Ruhrberg, 2013). Expression levels of PDGFR β , integrin β 1 and fibronectin also remained comparable between NRP1 KD cells and cells transfected with ns siRNA. Previously, VEGFR2 expression has been detected across the fs cell lines at similar levels (Kanthou *et al.*, 2014), however, during this study, VEGFR2 expression could not be detected in fs188 or fswt cells with either unaltered NRP1 or decreased NRP1 expression levels. The reason for this is unclear. The antibody used during western blotting experiments detected a high expression of VEGFR2 in HUVECs, therefore one possible explanation is that the quantity of total proteins used during these experiments from fs cells was not high enough to result in any detectable VEGFR2 signal. An increase in ERK-1/2 phosphorylation from baseline levels in the absence of any stimuli was detected in the NRP1 KD cells. Although this contradicts a previous study in glioma that found pERK-1/2 (and phosphorylated c-Jun N-terminal kinases) decreased following siRNA mediated NRP1 KD (Li *et al.*, 2011), it is in agreement with findings in pancreatic cancer (Gray *et al.*, 2005). In hindsight, the addition of exogenous ligands such as HGF, PDGF, PlGF or TGF β , followed by analysis of associated receptor phosphorylation would have been beneficial in identification of NRP1 binding partners in the fs cells.

Silencing of NRP1 in different tumour types and under varying conditions has yielded contradictory results in terms of adhesion to matrix proteins. In Panc-1 cells, adhesion to laminin, fibronectin and collagen IV significantly decreased in response to NRP1 KD after 6 hours (Fukasawa *et al.*, 2007). In contrast, although blocking NRP1 with the NRP1 antagonist EG3287 decreased adhesion of lung carcinoma and renal adenocarcinoma cells to fibronectin, it had no significant effect on adhesion to basement membrane protein complex (BMC), laminin 1 or collagen IV after 90 min (Jia *et al.*, 2010). Similarly, MCF7 breast cancer cells pre-treated with increasing concentrations of an anti-NRP1 mAb

showed a decrease in adhesion to fibronectin after 30 min in a dose-dependent manner (Zeng *et al.*, 2014). In prostate cancer cells both CRISPR/Cas9 knockout of NRP1 and NRP1 suppression with nordihydroguaiaretic acid led to decreased adhesion to fibronectin after 30 mins (Li *et al.*, 2016b). A common theme is that the reduced adhesion following NRP1 blocking/loss is due to the disruption of NRP1 interactions with β 1 integrins; indeed, NRP1 has been shown to engage with soluble fibronectin and mediate integrin activity (Yaqoob *et al.*, 2012). Given that fswt and fs188 cells express high levels of NRP1, coupled with higher integrin-linked kinase expression levels in these cell lines (Kanthou *et al.*, 2014), it was anticipated that KD of NRP1 may alter their capacity to bind to fibronectin, collagen-I and laminin. This, however was not the case; both fs188 and fswt NRP1 KD cells adhered to fibronectin more avidly than to laminin, collagen-1 and plastic after 45 min, which agreed with previous work (Kanthou *et al.*, 2014), yet there was no difference between the NRP1 modified and unmodified fs cell lines. Considering the varied timepoints used during the aforementioned published studies in other cancers (Fukasawa *et al.*, 2007, Zeng *et al.*, 2014, Li *et al.*, 2016b), that range from 30 min to 6 hours, the single timepoint of 45 min may not have been adequate to detect any knock-on effects of NRP1 depletion. The efficiency of cell adhesion is thought to correlate to surface levels of integrins. Previous characterisation of the fs cells has focussed on total levels of integrins therefore to what extent active integrins are expressed on the cells surface is currently unknown. In ECs, NRP1 does not directly mediate cell adhesion to fibronectin; interaction of the cytoplasmic SEA motif of NRP1 with the endocytic adaptor, GIPC1, and ABL stimulates endocytosis and trafficking of α 5 β 1 integrin (Valdembri *et al.*, 2009, Yaqoob *et al.*, 2012). Contrary to this, Fukasawa *et al.* (2007) had previously found that NRP1 interacted with β 1 integrin in the absence of an intracellular domain in Panc-1 cells. To add a further layer of complexity to the interactions of NRP1 and β 1 integrin, a recent study in CRC identified splice variants of NRP1 that are defective in N-linked glycosylation. One variant in particular, NRP1- Δ E4, was dominantly expressed in CRC and associated with tumour progression; furthermore, interaction of these two variants with cMET and β 1 integrin was found to be different to that of wt-NRP1 (Huang *et al.*, 2019). In the model presented by Huang *et al.* (2019), wt-NRP1 associated with cMET and β 1 integrin at the plasma membrane and, upon HGF stimulation, the cMET/HGF/NRP1/ β 1 integrin complex was internalised and degraded. The NRP1 splice variants however display enhanced binding capabilities with cMET and β 1 integrin upon HGF stimulation and, upon co-internalisation, the resulting complex was recycled to the plasma membrane or, under basal conditions, accumulated in late endosomes instead of being degraded. This constant recycling/endosomal accumulation resulted in persistent FAK/p130Cas pathway activation thus enhancing CRC migration and invasion. In tumour biology, the mechanisms by which NRP1 associates with integrins remains elusive. It may well be that NRP1 is present in macromolecular complexes that regulate and

facilitate integrin activation and trafficking and that NRP1 KD alone in the fs cells is not sufficient to disrupt these processes. One aspect that was not investigated here was whether or not the lack of significant changes in adhesion kinetics between NRP1 positive and NRP1 depleted fs cells was time dependent. The timepoint of 45 min and concentrations of ECM proteins were used so that data here could be related back to the findings by Kanthou *et al.* 2014, as it was originally postulated NRP1 KD may result in the fs188 and fswt cells mimicking a more fs120-like phenotype. Studies in ECs using timepoints ranging from 15 min to 7 hrs and differing concentrations of ECM proteins have been used by others, and in some cases have produced conflicting results (Murga *et al.*, 2005, Valdembri *et al.*, 2009, Raimondi *et al.*, 2014). Using lung carcinoma cells and a timepoint of 1.5 h, Jia *et al.* (2010) found that a NRP1 antagonist led to a decrease in cell adhesion to fibronectin. However, this mAb blocked NRP1 via disrupting VEGF binding therefore, given that VEGF does not appear to play a role in VEGFR2 activation in the fs cells (Kanthou *et al.*, 2014), these results are not directly comparable to the current study. Experiments using further timepoints and ECM protein concentrations would have given a more complete picture in determining whether NRP1 KD led to any differences in adhesion in fs188 and fswt cells.

High endogenous expression of NRP1 is repeatedly linked to a more migratory cancer cell phenotype (Miao *et al.*, 2000, Bachelder *et al.*, 2001). In agreement with this, depletion of NRP1 in both fswt and fs188 cells resulted in a significant decrease in migration across a 2D surface. In other tumour cells, this reduction in migration has been attributed to VEGF signalling and the role of NRP1 as a co-receptor with VEGFR2 (Bachelder *et al.*, 2001). However, in the fs cells this is unlikely to be the case given that there is no significant difference in the secretion of endogenous VEGF between the fs cell lines (Tozer *et al.*, 2008a) and recombinant VEGF does not appear to induce VEGFR2 phosphorylation and activation of downstream signalling such as pERK1/2 signalling *in vitro* (Kanthou *et al.*, 2014). Additionally, in ECs at least, the longer VEGF isoforms interact with NRP1 whereas, although VEGF_{120/1} binds NRP1, it does so in a way that fails to modulate VEGFR2 downstream signalling in the same way as the longer isoforms do (Soker *et al.*, 2002). Whether endogenous VEGF isoforms interact with NRP1 and do so in distinct isoform dependent ways to influence migration in these tumour cells is not known. In glioma, pancreatic and colorectal cancer cells, the role of NRP1 as a co-receptor for cMET has been suggested as an alternative HGF-mediated migratory pathway. What is interesting here is that HGF is overexpressed in pancreatic cancer (Matsushita *et al.*, 2007). Protein array data from our laboratory obtained by screening lysates from fs cells found that HGF is expressed at significantly higher levels in the fs188 cells than the other three fs cell lines (Kanthou *et al.*, unpublished data). Compared to fs188 cells, HGF expression was ~87% lower in the fswt cells, ~95% lower in the fs164

cells and barely detectable in the fs120 cells. It is possible that KD of NRP1 affects an autocrine signalling loop between NRP1, HGF and cMET in the fs188 cells, like pancreatic cancer and glioma cells, which subsequently leads to the reduction in migration. This does not however explain the slower migratory rates of the fswt cells upon NRP1 KD and suggests that a further ligand may also contribute to the migratory capabilities of the fs cells. In the same protein array data referred to above, PIGF2 was also identified as being differentially expressed in the fs cells. PIGF2 expression was higher in the fswt, fs164 and fs120 cells compared with the fs188 cells. In melanoma, NRP1 potentiates ECM invasion when acting as a co-receptor for PIGF2 with VEGFR1, furthermore, evidence suggests that PIGF2 may promote ECM invasion via NRP1 in the absence of VEGFR1 expression (Huang *et al.*, 2014). All the fs cells express VEGFR1 at comparable levels; moreover, fs120 cells, where NRP1 expression is inherently low, also exhibit slower migratory rates *in vitro* alongside higher PIGF2 expression. On this basis, it could be postulated that, much like HGF, endogenous PIGF2 expression is acting in an autocrine manner in the fs cells and the NRP1 is the master regulator. In the next chapter, the potential of HGF being one of the currently unidentified ligands that influences phenotypic changes in the fs cells via NRP1 will be investigated further using stably modified fs188 and fs120 cells in which NRP1 was knocked down and overexpressed respectively.

The transient KD of NRP1 identified a central role for NRP1 in fs cell migration and raised questions as to whether unidentified ligands were implicated in the reduced ability to migrate. Other than upregulation of pERK-1/2 following NRP1 KD, phosphorylation of other downstream proteins seemed to be unaffected. It is possible that although, on a protein level, transient NRP1 KD was achieved in the fs188 and fswt cells it was not sustainable or sufficient enough to detect any downstream signalling changes. In the subsequent chapter, fs188 cells with stable NRP1 KD were developed, not only for use *in vivo*, but also to investigate the role of NRP1 further and with the addition of exogenous ligands *in vitro*.

Chapter 4

Development of stable NRP1 overexpressing and knockdown fibrosarcoma cells

4.1 Introduction

NRP1 expression in the majority of cancers is associated with poorer prognosis, as a consequence studies have set out to elucidate the role it plays within the tumour and surrounding microenvironment. Much of this data however has focussed around NRP1s role on ECs and how NRP1 expression influences pathological angiogenesis. The majority of studies on tumour-associated NRP1 are in epithelial and neurological cancers with only a handful in sarcoma; moreover, whether tumour-associated NRP1 influences anti-VEGF therapy is relatively poorly studied. One effective method to study the role of tumour-derived NRP1 *in vivo*, specifically, its influence on tumour vascularisation and tumour sensitivity to anti-VEGF therapeutics, is to generate stable fs cell lines with manipulated NRP1 expression in comparison to their parental counterparts.

In Chapter 1, NRP1 was introduced as a co-receptor for multiple ligands and their cognate receptors. In Chapter 3, KD of NRP1 using siRNA resulted in a decrease in fs cell migratory capabilities without changing adhesion dynamics with ECM proteins. The possibility that changes in migration may have been as a result of NRP1s ability to associate with integrins or was perhaps regulating migration independently of ligand binding was introduced. Another proposed mechanism was that autocrine pathways under the control of ligands differentially expressed between fs188 and fs120 cells may be responsible for the decrease in migration. Two potential NRP1 ligands identified and discussed in the previous chapter were PlGF2 and HGF. In gastric cancer, depletion of NRP1 led to suppression of HGF/cMET pathways linked to proliferation (Li *et al.*, 2016a) and in pancreatic cancer HGF-mediated cell invasion was dependent on NRP1 expression (Matsushita *et al.*, 2007). Given that the fs120 cells had not been modified during Chapter 3 and that HGF had previously been found to expressed at higher levels in the fs188 cells (Kanthou *et al.* unpublished data), the HGF/cMET pathway was investigated in further depth during this chapter.

4.2 Aim

The aim of this chapter was to generate fswt, fs188 and fs120 cell lines, described in Chapter 3, with stable modification of NRP1 expression levels in order to establish its effect on tumour cell behaviour *in vitro*. This chapter first describes NRP1 KD in fs188 and fswt cells using a CRISPR/Cas9 mediated approach before going on to describe how NRP1 overexpression was achieved using a *piggyBac*-based gene transfer system. It addresses optimisation of the methodology used and subsequent verification of NRP1 expression levels. Modified cells were characterised using a range of biological assays to determine whether modified NRP1 expression affected the colony forming abilities, proliferation and migration of these cells. Finally, the effect of stable NRP1 modification on associated receptors and downstream signalling pathways was investigated. In addition to *in vitro* characterisation, stable modification of NRP1 in fs188 and fs120 cells was required for further *in vivo* studies which will be discussed in Chapter 5.

4.3 CRISPR/Cas9 gene-editing system

Nucleases that can be directed to cause site-specific DNA breaks are widely used to create gene-modified cell lines. An increasingly popular tool employed to facilitate precision editing of eukaryotic genomes is clustered regulatory interspaced short palindromic repeat/CRISPR-associated 9 (CRISPR/Cas9) genome editing technology (Garneau *et al.*, 2010, Jinek *et al.*, 2012). CRISPR/Cas9 is an acquired immune system found in a diverse range of bacteria and archaea that can rapidly adapt to target invading viral or plasmid DNA (Garneau *et al.*, 2010, Koonin *et al.*, 2017). CRISPRs are short repeats of ~28-48 nucleotides that are separated by unique sequences of a similar length, termed protospacers, derived from previously encountered foreign DNA (Hale *et al.*, 2009). CRISPR loci are transcribed to produce long precursor-RNAs (pre-crRNA) that, in a process which is mediated by *trans*-activating RNA (tracrRNA), are cleaved by RNase III in the presence of Cas9 to generate mature CRISPR-derived RNAs (crRNA) (Sternberg *et al.*, 2012). The resulting mature crRNA-tracrRNA duplex assembles with Cas9 to form a sequence-specific surveillance complex that seeks out, binds to and cleaves the foreign DNA at sites of complementarity to the guiding crRNA (Garneau *et al.*, 2010). The presence of a short 2-3 nucleotide repeat directly preceding the target DNA, referred to as a protospacer adjacent motif (PAM) site, is essential for Cas9 cleavage. The best characterised and most widely used CRISPR system is the *Streptococcus pyogenes* derived type II CRISPR/Cas9 system; in this system the required PAM is 5'-NGG (Jinek *et al.*, 2012). To exploit this system in the engineering of mammalian cells, the crRNA-tracrRNA are fused together to create a chimeric short guide RNA (sgRNA) which is introduced

to the cells along with human codon-optimised Cas9 (Cho *et al.*, 2013). Once the sgRNA-Cas9 complex binds to the RNA-guided sequence, the Cas9 nuclease induces a double-stranded break (DSB) which triggers one of two intrinsic cellular repair mechanisms; the error-prone non-homologous end-joining (NHEJ) or the precise homology directed repair (HDR) pathways (Figure 4.1) (Jinek *et al.*, 2012). The NHEJ repair pathway can be used to disrupt the coding region of a gene of interest (GOI) through the introduction of insertion or deletion mutations (indels). These indels result in frameshift mutations or premature stop codons which lead to either the transcription of a non-functional protein or abrogation of protein expression. Alternatively, the HDR pathway can be taken advantage of to mediate specific genomic alterations at the target locus through the inclusion of an exogenous repair template (Cong *et al.*, 2013, Mali *et al.*, 2013). Depending on their location and frequency, multiple mismatches between the sgRNA and target DNA sequence can be tolerated by Cas9, which could potentially lead to off-target effects (Hsu *et al.*, 2014). To improve Cas9 specificity and circumvent this issue Ran *et al.* (2013a) developed a method combining an HNH⁺/RuvC⁻ nickase mutant (D10A) Cas9 (Cas9n) (Figure 4.1B) with two offset sgRNA targeting opposite strands of the target site. Cas9n contains a mutation that deactivates the RuvC-like nuclease domain, the upshot of which is a Cas9 endonuclease only induces a single-strand DNA breaks, rather than the double-stranded break induced by the WT Cas9. By using a paired nickase strategy to induce the DSB, unwanted off-target events can be reduced by up to 1500-fold in comparison to WT Cas9.

Given the improved specificity of the double nicking strategy, this was the method used to create NRP1 knockout fs188 and fswt cell lines. Three pairs of sgRNAs were designed to direct Cas9n to discrete target loci of the NRP1 gene. In the absence of an exogenous repair construct, the endogenous NHEJ DNA repair pathway was exploited to introduce indels and interrupt NRP1 expression. Individual target-specific sgRNA sequences were cloned into the pSpCas9n(BB)-2A-GFP expression plasmid that contained the sgRNA scaffold backbone, Cas9n and a GFP tag for selection (Ran *et al.*, 2013b).

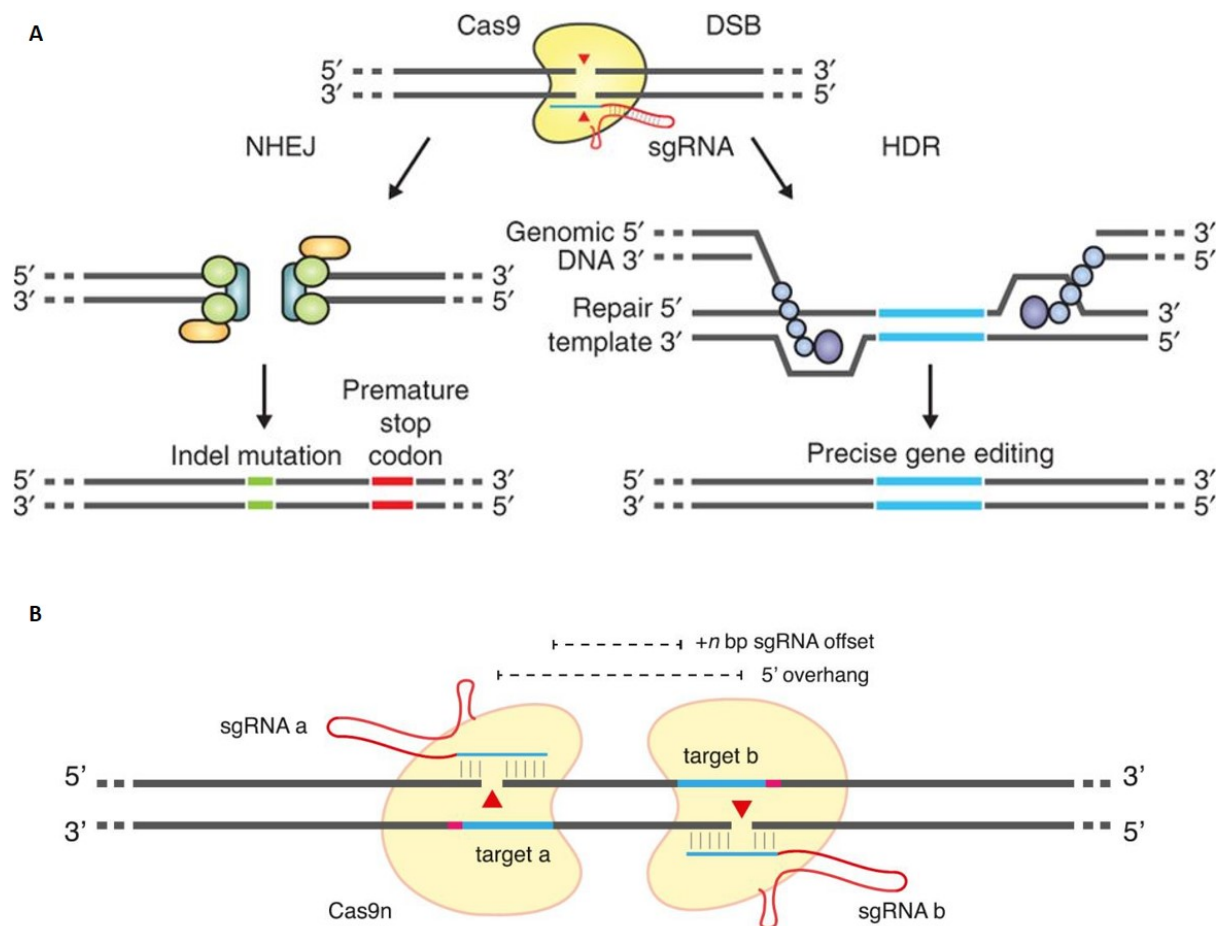


Figure 4.1 Schematic of Cas9 and Cas9n induced DSB

A) The Cas9 endonuclease is guided to the target DNA by a single sgRNA. Upon binding, strand-specific DNA cleavage is carried out by the HNH and RuvC nuclease domains of Cas9 to create a DSB. DNA repair via the NHEJ pathway can result in random indel mutations at the break site, leading to frameshift mutations and premature stop codons that knockout gene expression. Alternatively, the introduction of an exogenous repair template alongside the sgRNA and Cas9 allows for precision gene editing at the target loci. Figure reproduced with permission from (Ran et al., 2013b). B) A pair of sgRNAs, designed to flank the target gene loci on opposing DNA strands, directs Cas9n to the target site where it cleaves the strand complementary to the sgRNA. Simultaneous nicking of both strands can result in a DSB that is then repaired via the NHEJ or HDR pathways in the same way as if the break was induced by wild-type Cas9. Figure reproduced with permission from (Ran et al., 2013a).

4.4 TransIT-X2® delivers pSpCas9n(BB)-2A-GFP-sgRNA DNA to fs188 cells more effectively than Lipofectamine® and FuGene 6®

In order to maximise the probability of NRP1 KD using the CRISPR/Cas9n system, optimal transfection of fs cells with pSpCas9n(BB)-2A-GFP-sgRNA DNA was vital. Initial experiments with transfection reagents previously used with fs cell lines in our lab found the optimal ratio of transfection reagent to DNA for Lipofectamine® and FuGene 6® to be 3:1 (transfection reagent: DNA). Transfection efficiency of fs188 cells with pSpCas9n(BB)-2A-GFP-sgRNA1 using Lipofectamine® and FuGene 6® was analysed by flow cytometry (Chapter 2, Section 2.8) and, although successful, transfection was relatively poor and inconsistent, ranging from 1% - 16% and 10% -17% respectively (n=2). Transfection of fs188 cells with pcDNA-GFP, which is a smaller plasmid, using Lipofectamine® and FuGene 6® was more efficient at 30% and 50% respectively, suggesting the larger pSpCas9n(BB)-2A-GFP plasmid was a limiting factor in these experiments.

Using the same cell seeding density and 1 µg exogenous DNA, *TransIT-X2*® transfection reagent was trialled in the fs 188 cells at three different ratios of reagent: DNA (Materials and Methods, Section Optimised fs188 cell transfection with *TransIT-X2*® 2.7.5.7). GFP positivity of transfected fs188 cell populations was evaluated by flow cytometry. Results showed a nearly 3-fold increase in transfection efficiency using *TransIT-X2*® in comparison to Lipofectamine® and FuGene 6® regardless of the ratio of reagent: DNA that was used (Table 4.1). As there was a negligible difference in transfection efficiency between the 3:1 and 4:1 ratio, the 3:1 ratio of *TransIT-X2*®: DNA was selected as appropriate for future experiments.

Plasmid DNA	<i>TransIT-X2</i> [®] : DNA ratio	Transfection efficiency
pSpCas9n(BB)-2A-GFP	3:1	28%
	4:1	30%
	6:1	25%
pSpCas9n(BB)-2A-GFP-sgRNA1 sense & antisense (0.5 µg each)	3:1	37%
	4:1	39%
	6:1	32%
pcDNA-GFP	3:1	68%
	4:1	61%
	6:1	55%
	Transfection Reagent	
pSpCas9n(BB)-2A-GFP	Lipofectamine [®]	6%
	FuGene 6 [®]	2%
pSpCas9n(BB)-2A-GFP-sgRNA1 Sense & antisense (0.5 µg each)	Lipofectamine [®]	16%
	FuGene 6 [®]	17%

Table 4.1 Transfection efficiency using *TransIT-X2*[®], Lipofectamine[®] and FuGene 6[®] in fs188 cells

Three different ratios of *TransIT-X2*[®] to 1 µg exogenous DNA were tested in fs188 cells alongside Lipofectamine[®] and FuGene 6[®] at a previously optimised 3:1 ratio of reagent to DNA. Flow cytometry was used to identify GFP positive cells in the transfected cell populations and data was analysed using FlowJo V10 software. The *TransIT-X2*[®]: DNA ratio of 4:1 was marginally more efficient than 3:1 and nearly 3 times more efficacious than Lipofectamine[®] and FuGene 6[®]. These are the results of one independent experiment.

4.5 NRP1 protein expression is depleted in pooled CRISPR/Cas9n modified fs cells

As an initial assessment of whether NRP1 KD had been successful, western blot analysis of whole cell protein lysates from heterogenous pools of fs188 cells transfected with the 3 individual pairs of sgRNAs targeting the NRP1 gene was carried out. Results were indicative that sgRNA pairs from sgRNA pair 3, referred to hereon in as sgRNA3, had resulted in KD of NRP1 at the protein level (Figure 4.2).

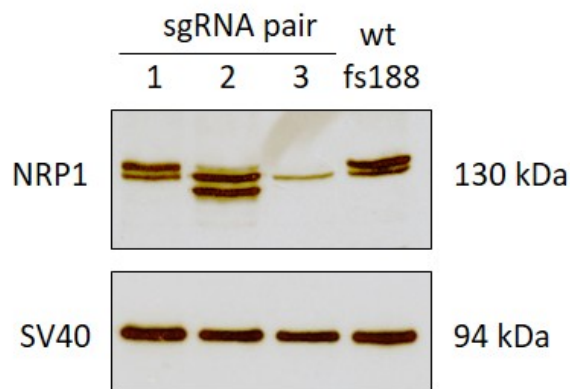


Figure 4.2 KD of NRP1 protein expression using CRISPR/Cas9n in pools of fs188 cells transfected with three sgRNA pairs targeting the NRP1 gene

1×10^6 fs188 cells transfected with pSpCas9n(BB)-2A-GFP-sgRNA1, -sgRNA2 or -sgRNA3 sense and antisense strand target pairs were harvested and whole cell protein lysates were prepared. Equal amounts of sample were analysed for NRP1 expression by western blotting. The membrane was re-probed for SV40 as an internal protein loading control. Results from a single experiment strongly suggested that KD of NRP1 protein had been successful with sgRNA3.

4.6 Successful KD of NRP1 protein expression in fs188 cells using CRISPR/Cas9n

Clonally isolated fs188 cells from each sgRNA pair were screened for NRP1 protein expression by western blotting (Figure 4.3). Thirteen clones were identified as having markedly depleted levels of NRP1 protein expression in comparison to the parental fs188wt cells. Ten of the thirteen clones identified were as a result of transfection of fs188 cells with CRISPR/Cas9n and sgRNA3. These results were in agreement with initial western blot results of the heterogenous CRISPR/Cas9n-sgRNA3 transfected fs188 cell populations (Figure 4.3).

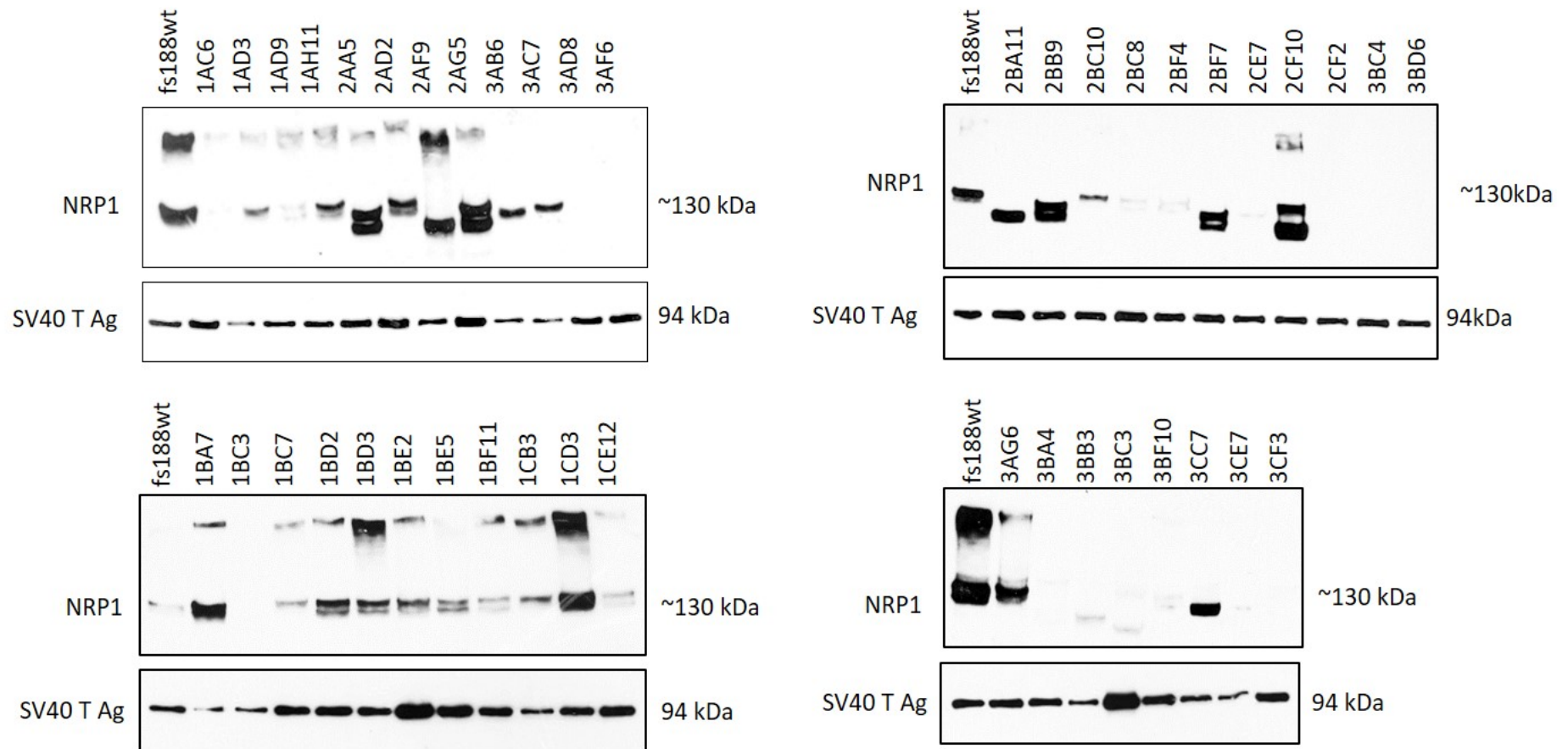


Figure 4.3 Evaluation of NRP1 protein expression in fs188 clones transfected with CRISPR/Cas9n and sgRNA1, sgRNA2 or sgRNA3

Whole cell protein lysates were extracted from clonally isolated fs188 cells transfected with CRISPR/Cas9n and sgRNA1, sgRNA2 or sgRNA3; equal sample volumes were analysed by western blotting for NRP1 protein expression. SV40 T Ag (large T antigen) was used to identify differences in protein content of the unquantified protein samples. Thirteen clones exhibited either a total lack of or highly depleted levels of NRP1 protein expression and were taken forward for further analysis. Results are from one independent experiment.

None of the CRISPR/Cas9n-sgRNA2 transfected clones were taken any further. A single CRISPR/Cas9n-sgRNA1 clone (1BC3) and nine CRISPR/Cas9n-sgRNA3 (3AD8, 3AF6, 3BF10, 3BD6, 3BA4, 3CF3, 3BC4, 3CE7 and 3BB3) clones were evaluated further for NRP1 and NRP2 expression by western blotting and flow cytometry. Growth of the ten clones in thick collagen was used to study any immediate differences in cell morphology and to examine their propensity for colony formation. The latter was used as an indication as to whether NRP1 KD might affect the ability of the cells to form solid tumours *in vivo*. PCR designed to amplify the VEGF region containing exons 6 & 7 (Harris *et al.*, 2012) (See Appendix 2 for primer sequences) confirmed expression of the single VEGF188 isoform in the five clones selected. On the basis of the level of NRP1 KD, effect on NRP2 expression and colony forming ability, five clones were taken forward for further biological experiments and for a pilot *in vivo* study (Figure 4.4). During routine subculturing it was observed that the clone referred to as 3BD6 (fs188^{3BD6}) presented a more rounded cell morphology compared to the parental cells.

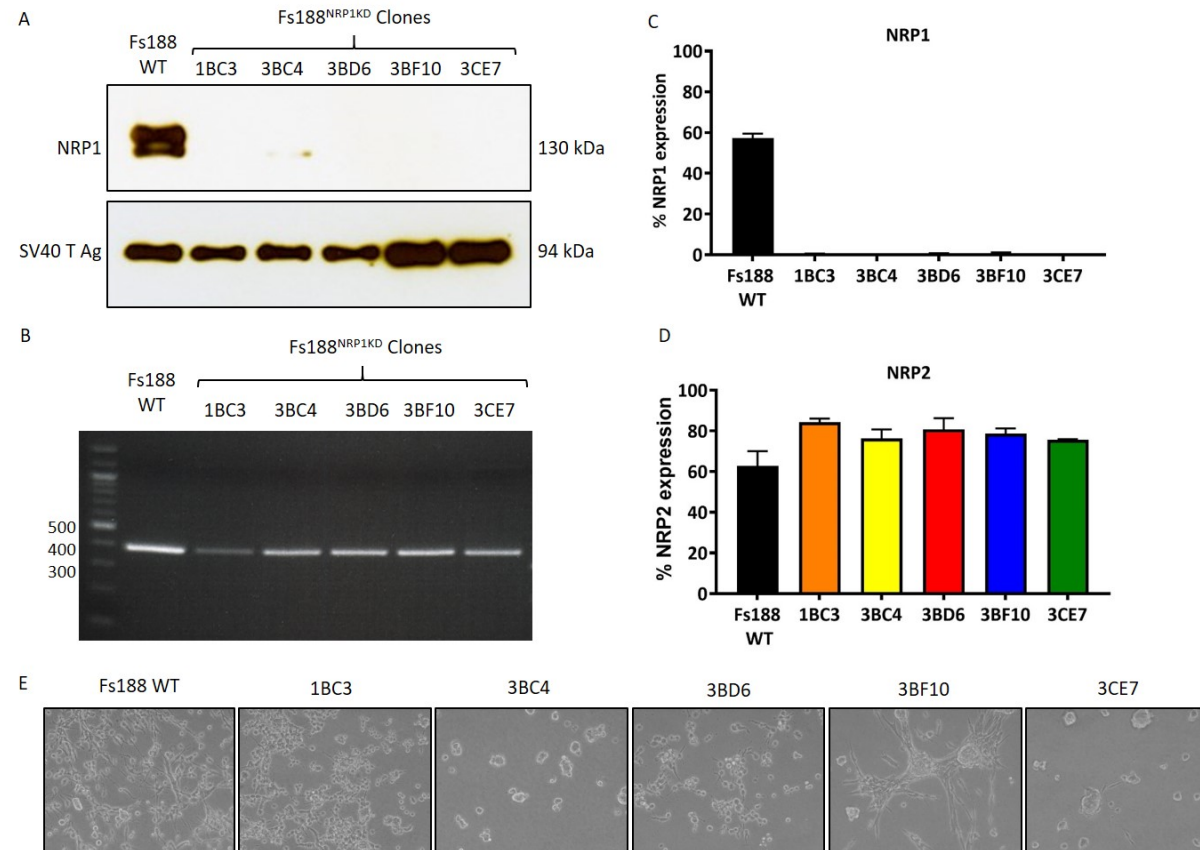


Figure 4.4 Fs188 NRP1 KD clones taken forward for *in vivo* studies

A) Western blot of whole cell lysates confirmed NRP1 KD in five selected fs188 clones modified with CRISPR/Cas9n and NRP1 targeting sgRNAs, SV40 T Ag was used as a loading control. B) PCR amplification of the VEGF gene region containing exons 6 & 7 confirmed expression of the single FS188 isoform with an expected product of 384 bp. Flow cytometric analysis of fs188wt and fs188^{NRP1KD} cells fluorescently labelled with C) NRP1 and D) NRP2 confirmed NRP1 KD without any significant off-target effects on NRP2 expression. The results are expressed as a % of fluorescently labelled cells detected within a cell population gated to exclude cell debris (G1), data collection was stopped upon reaching a count of 10,000 positive events within G1. E) Fs188wt and fs188^{NRP1KD} cells all exhibited the propensity to form colonies when cultured on thick collagen, indicating their suitability for use *in vivo*.

4.7 NRP1 overexpression in fs120 and fs164 cells

Overexpression (OE) of NRP1 was carried out using a *piggyBac*-based gene transfer system, which essentially 'cut and paste' NRP1 into the fs cell genome from a donor plasmid (pCLIIP-NRP1-GFP). The addition of a GFP tag to the NRP1 expression cassette facilitated identification of successfully transfected cells via FACS.

DNA transposons are self-mobilising DNA sequences that can move within a genome. They can be either autonomous or non-autonomous; autonomous DNA transposons encode the transposase protein and can therefore move on their own, whereas non-autonomous DNA transposons lack the gene for the transposase and therefore use transposases provided by other elements (Prey, 2008). The *piggyBac* transposon system is the latter (Figure 4.5). On both ends of a DNA transposon are inverted terminal repeats (ITR)s, it is these short sequences that are recognised by transposase. Additionally, the transposon is flanked by TTAA sequences, referred to as direct repeats (DR)s; these are not part of the transposon but play a role in insertion. Upon *piggyBac* transposase expression by plasmid pmPB, transposase bind to *piggyBac* ITRs in pCLIIP-NRP1-GFP, inducing DNA nicking, 3' hydrophilic attack of the TTAA ends and hairpin formation. This releases the transposable element containing the NRP1-GFP gene-expression cassette from the pCLIIP backbone. *piggyBac* transposase then locates TTAA sequences within the fs cells genomic DNA where it induces a transient ds break with TTAA overhangs. The NRP1-GFP transposable element is then inserted into the genomic DNA of the fs cells (Woodard and Wilson, 2015).

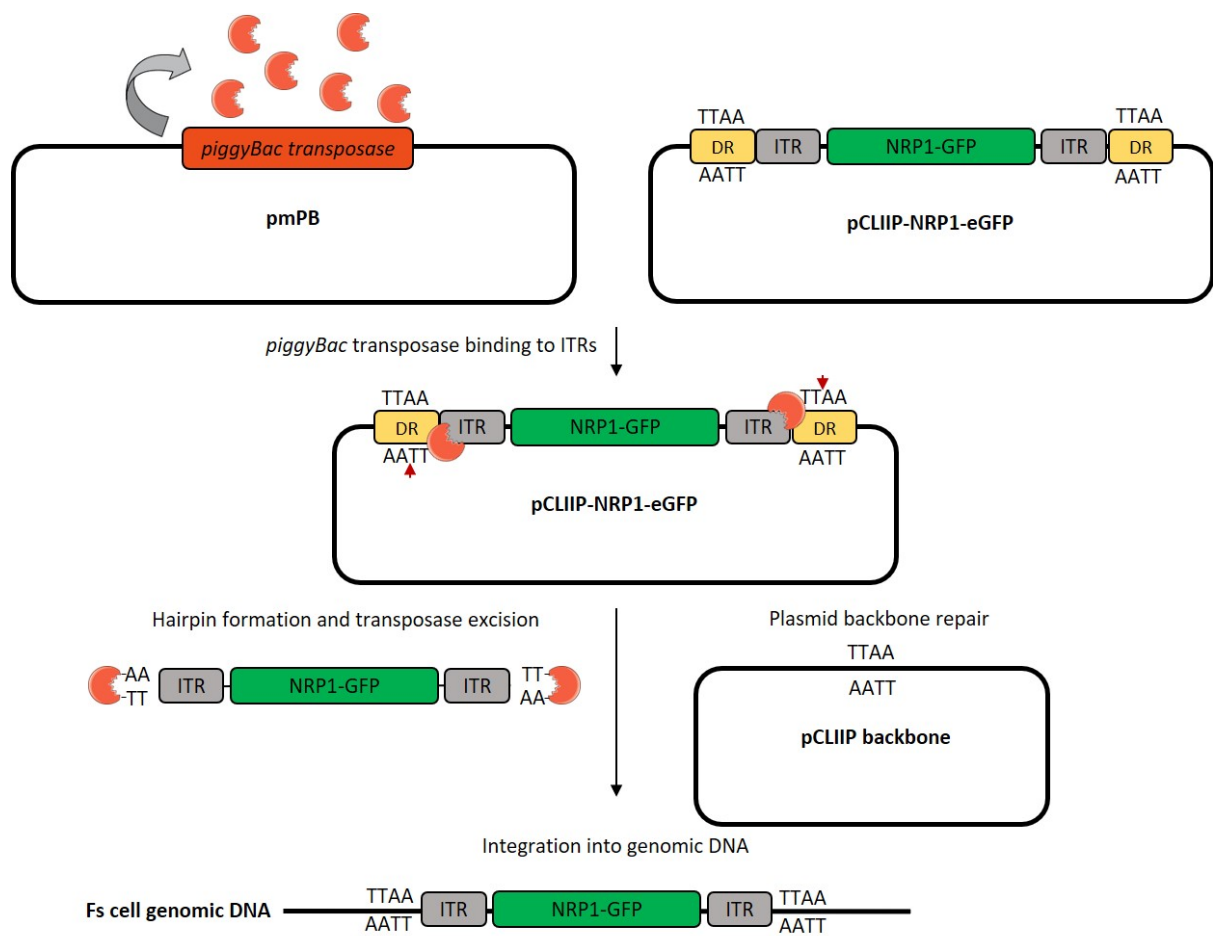


Figure 4.5 The *piggyBac* transposon overexpression system

Fs cells were co-transfected with the plasmids *pmPB* and *pCLIIP-NRP1-GFP* (Materials and Methods, Section 2.7.6.6). *piggyBac* transposase expressed by *pmPB* binds to *piggyBac* ITRs flanking the *NRP1-GFP* transposon in *pCLIIP-NRP1-GFP* to induce DNA nicking and 3' hydrophilic attack of the TTAA DR sequence (red arrows). The result is hairpin formation at both ends of the *NRP1-GFP* transposon and repair of the *pCLIIP* backbone via TTAA overhangs and endogenous cellular repair mechanisms. In parallel, the *piggyBac* transposase locates TTAA repeats within the *Fs* cell genome and creates a staggered 4 bp cut in the genomic DNA. The transposon is integrated into the genome at this transient ds break by hairpin resolution and hydrophilic attack. ITR, inverted terminal repeat; DR, direct repeats.

4.8 Successful overexpression of NRP1 in fs120 and fs164 cells

Clonally isolated fs120 and fs164 cells were initially screened for NRP1 expression by western blotting, five clones for each cell line were carried forward for further analysis. All the fs120^{NRP1+} clones expressed NRP1 at vastly elevated levels in comparison to the fs120^{wt} cells. Of the fs164^{NRP1+} clones, one clone (fs164^{A5}) expressed only moderately elevated NRP1 levels in comparison to fs164^{wt} cells; therefore, this clone was selected alongside four other clones with NRP1 expression (Figure 4.6). Flow cytometry was used to quantify levels of NRP1 overexpression in the fs164^{NRP1+} and fs120^{NRP1+} clones. NRP1 expression in the fs164^{NRP1+} clones ranged from 37% to 97% and in the fs120^{NRP1+} was consistent amongst all clones, at ~95%. PCR amplification of the VEGF region containing exons 6 & 7 (Harris *et al.*, 2012) (See Appendix 2 for primer sequences) confirmed that the clones expressed single VEGF isoforms as expected. A single product at the expected size of 194 bp in the fs120 cells and 324 bp in the fs164 cells was amplified (Figure 4.6).

All fs120^{NRP1+} clones overexpressed NRP1 to a similar degree and no differences in morphology or behaviour being observed during routine sub-culturing. In addition, the propensity of the NRP1 OE clones to form colonies in thick collagen was not different from the parental fs120 cell (Figure 4.6D), therefore clone G3 (fs120^{G3}) was taken forward for further characterisation and for use *in vivo*. Of the four fs164^{NRP1+} clones overexpressing similar levels of NRP1, C11 (fs164^{C11}) was selected alongside the modestly NRP1 expressing fs164^{A5} for *in vitro* analysis. As with the fs120 NRP1 OE expressing cells, the fs164^{NRP1+} clones were also comparable in both their morphology and colony forming ability (Figure 4.6D).

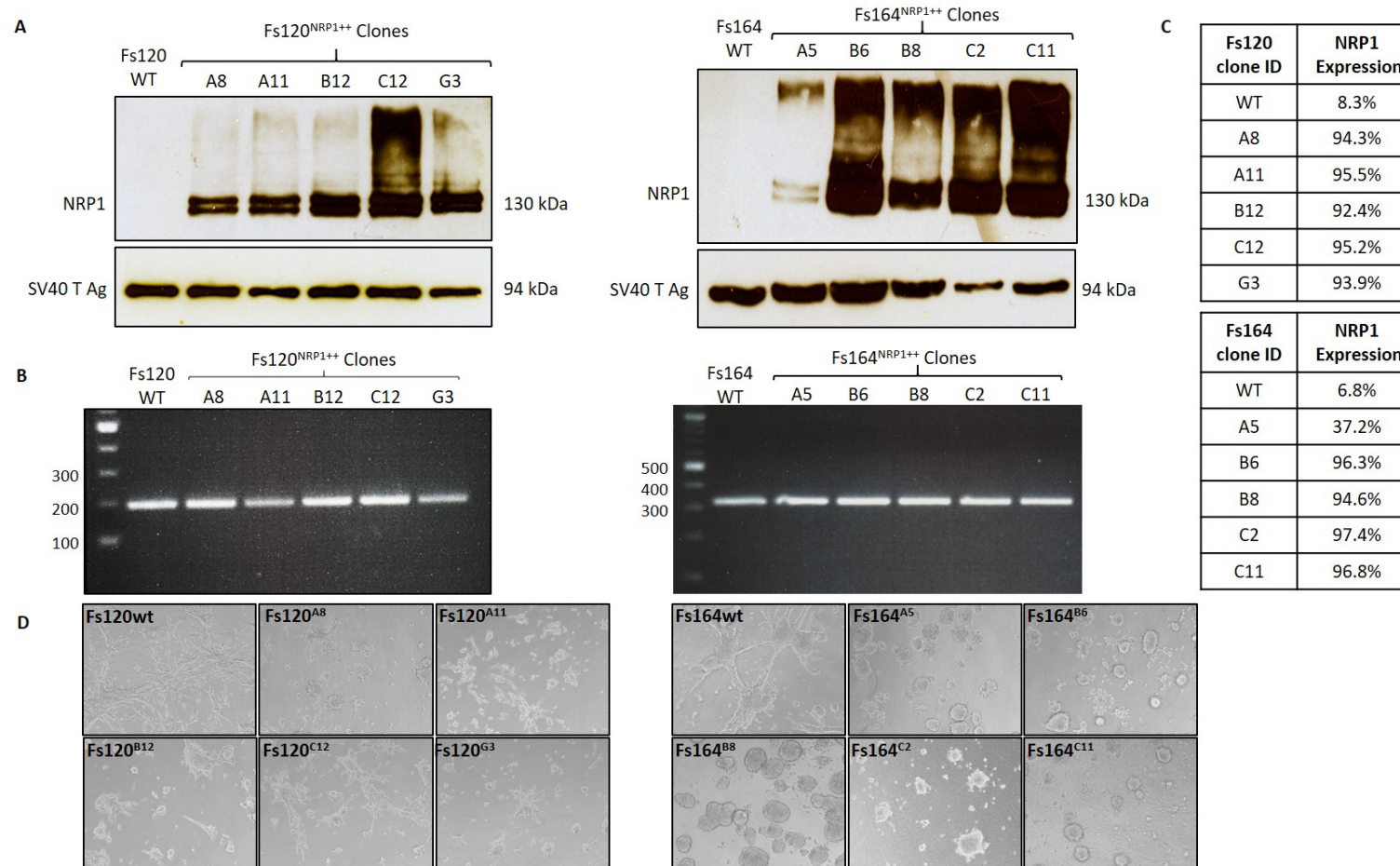


Figure 4.6 Fs120 and fs164 NRP1 overexpressing clones

A) Western blot of whole cell lysates confirmed NRP1 overexpression in five selected fs120 and fs164 clones modified with pCLIIP-NRP1-eGFP, SV40 T Ag was used as a loading control. B) PCR amplification of the VEGF gene region containing exons 6 & 7 confirmed expression of the single VEGF120 and VEGF164 isoforms with expected products of 194 bp and 324 bp respectively. C) Fs120wt, fs120^{NRP1++}, fs164wt and fs164^{NRP1++} cells were fluorescently labelled for NRP1 and analysed by flow cytometry. The results are from one independent experiment and expressed as the % of fluorescently labelled cells detected within a cell population gated to exclude cell debris (G1), data collection was stopped upon reaching 10,000 positive events within G1. D) Fs120wt, fs120^{NRP1++}, fs164wt and fs164^{NRP1++} cells all formed colonies in thick collagen-1.

4.9 Migration of fs cells expressing single VEGF isoforms is reliant on NRP1 expression levels

Previously, silencing NRP1 expression using siRNA in fs188wt cells resulted in a decrease in cell motility (Chapter 3, Section 3.9). Wound healing assays were used to determine whether stable KD of NRP1 had the same effect on migration as transient KD. In parallel, the effect of NRP1 overexpression on migration in fs120 and fs164 cells was investigated.

After 12 hours, wound closure in the fs188wt cells was significantly faster than fs188^{3BD6}. Migration of fs188^{3CE7} was noticeably slower than fs188wt cells at 12 hours, however the difference was not statistically significant. After 16 hours the wound remaining in the fs188^{3BD6} and fs188^{3CE7} cells was 49% and 30% greater respectively than that of the fs188wt cells. Furthermore, after 16 hours fs188^{3BD6} cells had also migrated to a lesser extent than the fs188^{3CE7} cells. Taken as a whole, NRP1 KD in the fs188 cells led to a decrease in motility across a 2D surface. There was also a difference in the migratory capabilities between the two clones in which NRP1 expression had been depleted after 16 h with fs188^{3CE} cells migrating faster than fs188^{3BD6} cells (Figure 4.7).

After 20 hours, gross overexpression of NRP1 in both fs120 and fs164 cells resulted in a reduction in their migratory capabilities in comparison to their wild-type counterparts. Fs164^{A5} cells, with only moderate overexpression of NRP1, migrated at a rate that was comparable to the fs164wt cells. Conversely, after 16 hours, the fs164^{C11} cells started to show differences in their migratory capabilities and after 20 hours the wound remaining was 25% larger than that of the fs164wt cells (Figure 4.8). This retardation in migration was also mirrored in the fs120^{G3} cells; after 20 hours the fs120wt cells had migrated 30% further than the fs120^{G3} cells (Figure 4.9).

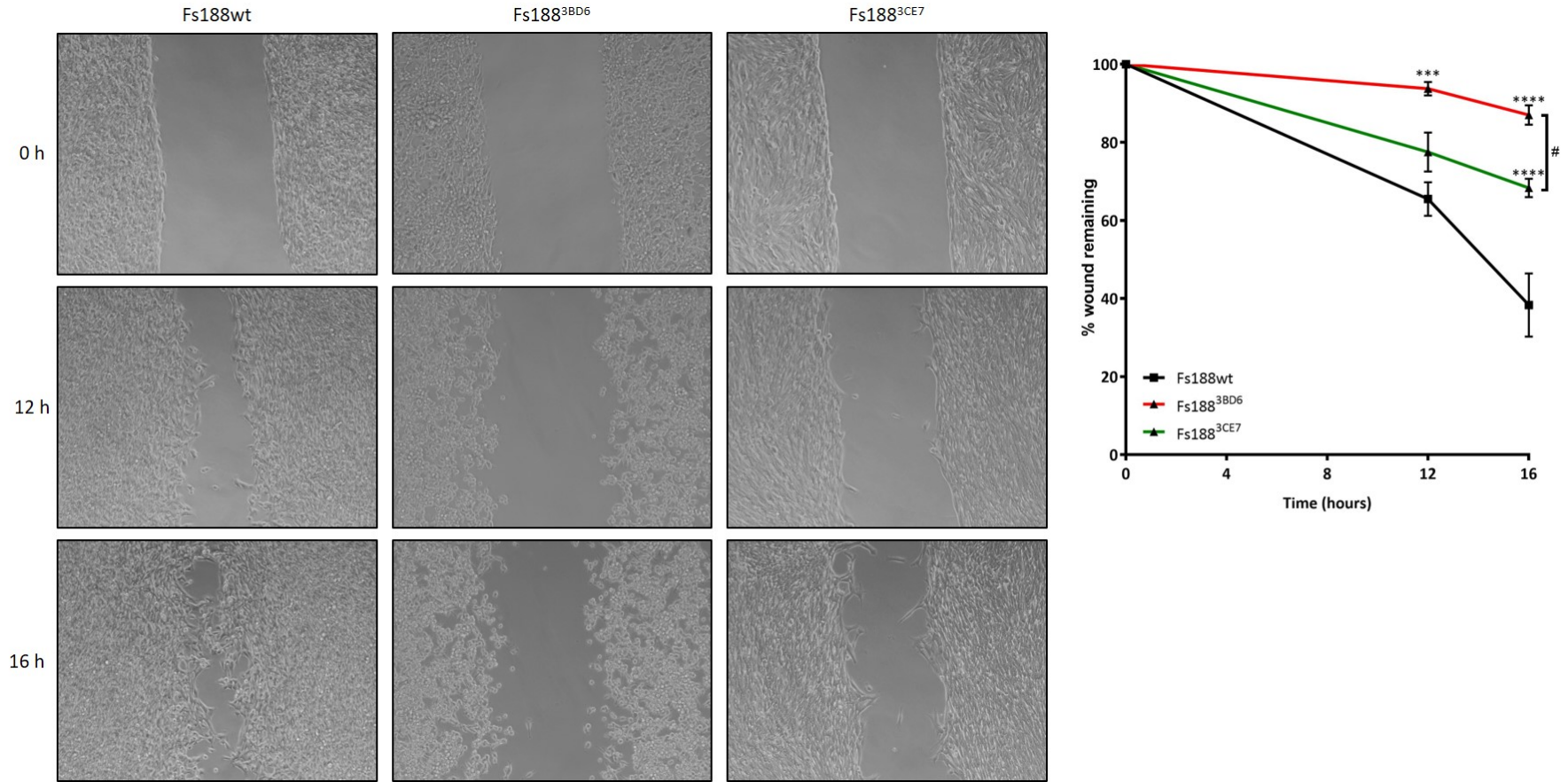


Figure 4.7 Migration of fs188 NRP1 KD cells

Fs188wt, fs188^{3BD6} and fs188^{3CE7} cells were seeded at 3.5×10^4 cells/mL in 2-well silicone inserts. Once confluent (typically after 36 hours), the insert was removed to leave a 500 μ m gap for cells to migrate into. Images were taken over 16 h in the same region and the wound area measured using Image J software. A) Representative image of cell culture of fs188wt cells and their NRP1 KD counterparts, fs188^{3BD6} and fs188^{3CE7}, at 0 h, 12 h and 16h. B) Wound closure was measured in the same area at each timepoint. Wound remaining is calculated as a percentage of the wound area at 0 h. Each point represents data obtained from 3-6 independent experiments carried out in duplicate, \pm SEM. Data is analysed by 2-way ANOVA with Bonferroni correction (** $p = 0.0002$, **** $p = <0.0001$. # $p = 0.0344$).

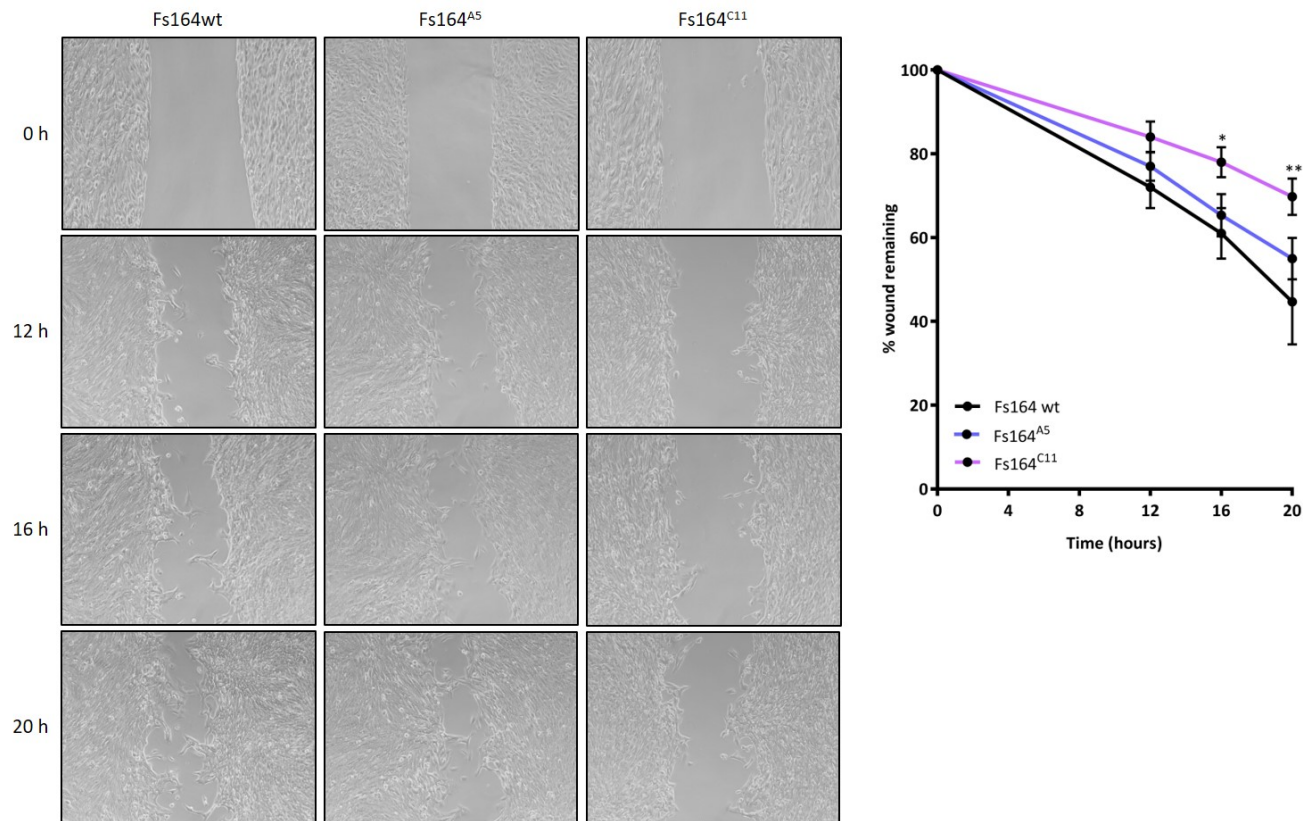


Figure 4.8 Migration of fs164 NRP1 overexpressing cells

Fs164wt, fs164^{A5} and fs164^{C11} cells were seeded at 4×10^4 cells/mL in 2-well silicone inserts. Once confluent (typically after 36 hours), the insert was removed to leave a 500 μm gap for cells to migrate into. Images were taken over 16 h in the same region and the wound area measured using Image J software. A) Representative image of cell culture of fs164wt cells and their NRP1 overexpressing counterparts, fs164^{A5} and fs164^{C11}, at 0 h, 12 h, 16h and 20 h. B) Wound closure was measured in the same area at each timepoint. Wound remaining is calculated as a percentage of the wound area at 0 h. Each timepoint represents data obtained from 4 independent experiments carried out in duplicate, \pm SEM. Data is analysed by 2-way ANOVA with Bonferroni correction (*p = 0.0332, **p = 0.0021).

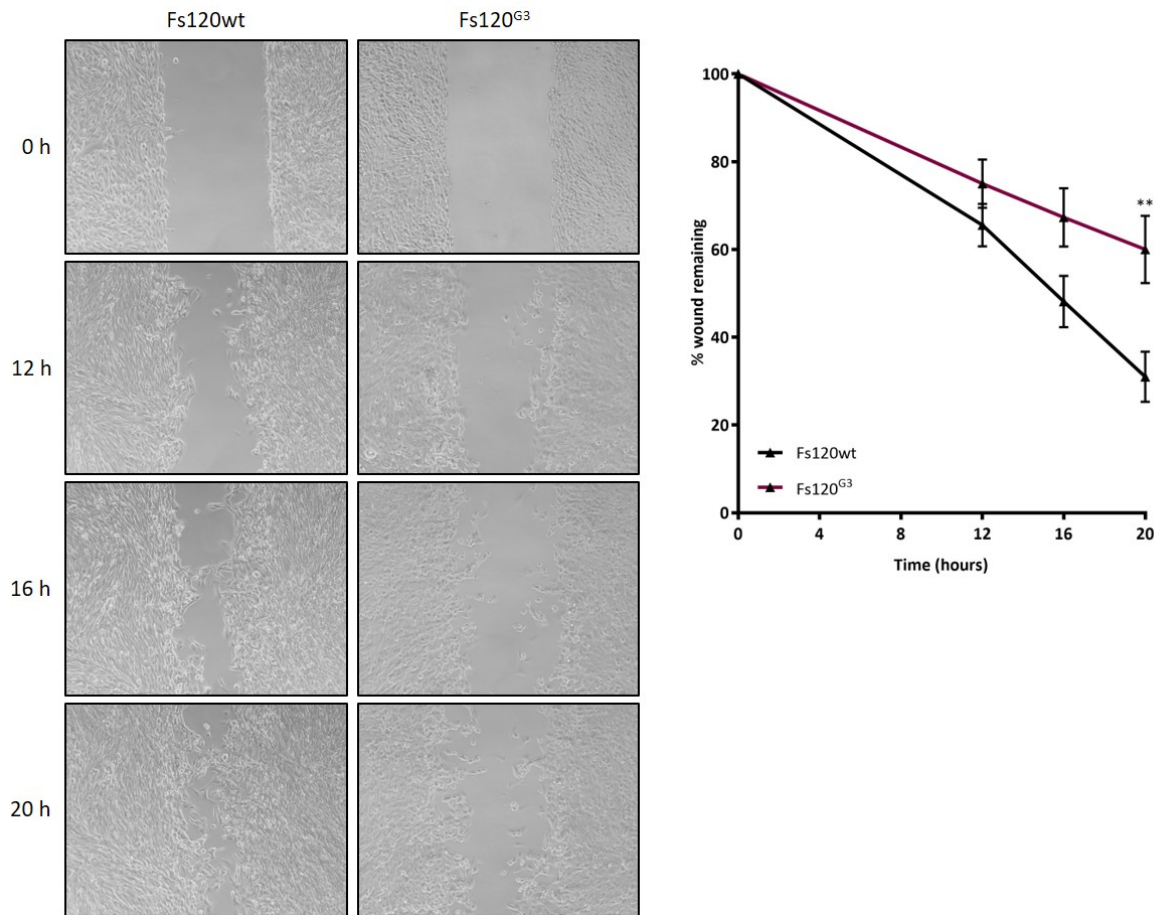


Figure 4.9 Migration of fs120 NRP1 overexpressing cells

Fs120wt and fs188^{G3} cells were seeded at 4×10^4 cells/mL in 2-well silicone inserts. Once confluent (typically after 36 hours), the insert was removed to leave a 500 μ m gap for cells to migrate into. Images were taken over 16 h in the same region and the wound area measured using Image J software. A): Representative image of cell culture of fs120wt cells and their NRP1 overexpressing counterparts, fs120^{G3}, at 0 h, 12 h, 16h and 20 h. B): Wound closure was measured in the same area at each timepoint. Wound remaining is calculated as a percentage of the wound area at 0 h. Each timepoint represents data obtained from 4 independent experiments carried out in duplicate, \pm SEM. Data is analysed by 2-way ANOVA with Bonferroni correction (**p = 0.0012).

4.10 NRP1 expression does not alter proliferation rates in fs cells expressing single VEGF isoforms

Previous experiments have shown that fs120 cells proliferate significantly faster than fs188 cells on uncoated cell culture plastic, collagen and fibronectin (Kanthou *et al.*, 2014). To investigate whether NRP1 was involved in these differences, fs188wt, fs188^{3BD6}, fs188^{3CE7}, fs120wt and fs120^{G3} cells were seeded on uncoated cell culture plastic and viable cells were counted every 24 h over 4 days. Fs188wt cell population doubling times of 18.99 h ± 0.40 were comparable to those previously reported (17.89 h ± 0.40) (Kanthou *et al.*, 2014). However, the population doubling times of fs120wt cells of 15.86 h ± 0.64 was significantly slower than the previous study had shown (13.67 h ± 0.26; Table 4.1) (Kanthou *et al.*, 2014). Minimal variance in population doubling times in the fs188^{3BD6} and fs188^{3CE7} cells (20.11 h ± 1.06 SEM and 17.08 ± 1.00 SEM respectively) was observed and was not found to be statistically significant. This was also found to be the case in between fs120 cells and fs120^{G3} cells, where population doubling times between the two cell lines were found to be comparable (Table 4.2). These results indicate that NRP1 expression levels do not significantly affect the proliferation rates of fs188 and fs120 cells on plastic. Furthermore, the lack of difference in proliferation rates between parental fs cells and their modified counterparts supports the role of NRP1 in migration; as it suggests that differences in migratory rates are motility associated rather than as a consequence of slower population doubling times.

Cell Line	Population doubling times (h)	
	Current Study	Kanthou <i>et al.</i> (2014)
Fs188wt	18.99 ± 0.40 (n=3)	17.89 h ± 0.40 (n=6)
Fs188 ^{3BD6}	20.11 ± 1.06 (n=3)	N/a
Fs188 ^{3CE7}	17.08 ± 1.00 (n=3)	N/a
Fs120wt	15.86 ± 0.64 (n=5)	13.67 h ± 0.26 (n=6)
Fs120 ^{G3}	14.43 ± 0.45 (n=4)	N/a

Table 4.2 Population doubling times of fs188wt, fs188 NRP1 KD cells, fs120wt and fs120 OE cells grown on plastic

Comparisons were made between cells of the same lineage i.e. population doubling times of fs188wt cells were compared to their NRP1 KD counterparts and fs120wt cells against their NRP1 OE counterparts. Values represent the mean population doubling times calculated from 3-5 independent experiments carried out in triplicate, ± SEM. Data is analysed by one-way ANOVA followed by Bonferroni post-test.

4.11 Downstream signalling consequences of modified NRP1 expression

Initial western blot analysis of whole cell lysates of NRP1 KD fs188 cells suggested a downregulation in basal levels of pERK-1/2 and pAKT (data not shown). Previously unpublished data from our group found that HGF was expressed at vastly higher levels in the fs188 cells than fs120 cells. As NRP1 is a co-receptor for HGF with cMET, it was hypothesised that the observed reduction in basal levels of pERK-1/2 may have been as a result of reduced activation in this pathway.

Total proteins extracted from fs188wt cells, fs120wt cells and their NRP1 modified counterparts were analysed for expression of cMET. Additionally, proteins associated with downstream signalling in the cMET/NRP1 axis, ERK-1/2, AKT and Src, were also investigated for any changes in expression levels. NRP1 KD in fs188 cells did not lead to any significant differences in basal expression levels of cMET, tERK-1/2, tAKT and tSrc (Figure 4.10A). In fs120 cells, NRP1 OE led to a small but significant decrease in cMET expression whilst expression levels of downstream proteins tERK-1/2, tAKT and tSrc remained comparable (Figure 4.10B).

To determine whether modification of NRP1 expression in fs cells had any influence on cMET activation and downstream signalling, cell lines were treated with 20 ng of recombinant murine HGF for 15 min before total proteins were extracted. Levels of phosphorylated proteins were taken as a ratio of total receptor expression before the fold change in expression from basal levels was calculated. Robust induction of phosphorylated cMET (p-cMET), ERK-1/2 and AKT above baseline levels were detected in fs188^{3CE7} following the addition of HGF. In the fswt and fs188^{3BD6} cells, expression levels of p-cMET or pERK-1/2 did not significantly change following the addition of HGF, however a small but significant induction of pAKT in the fs188wt cells was detected. Furthermore, in comparison to both fs188wt and fs188^{3BD6} cells, the increase in phosphorylation of cMET, ERK-1/2 and AKT above basal levels was significantly higher in fs188^{3CE7} cells. NRP1 KD did not lead to any significant changes in Src phosphorylation from baseline levels in any of the fs188 cell lines. However, as a result of a small decrease in fs188wt cells as opposed to a small increase in fs188^{3BD6} cells of pSrc, there was a small but significant difference between the levels of pSrc induction between these two cell lines (Figure 4.11).

In both fs120wt and fs120^{G3} cells, the addition of HGF led to significant increases in p-cMET and pERK-1/2 expression in comparison to baseline levels. Additionally, NRP1 OE resulted in a higher fold increase in levels of pERK-1/2 in comparison to fs120wt cells. NRP1 OE in the fs120 cells resulted in a minimal increase in AKT phosphorylation whereas, in wt fs120 cells, pAKT was highly upregulated

following the addition of HGF. As was seen in the fs188 cells, the addition of HGF had no significant effect on levels of pSrc in either f120wt or fs120^{G3} cells (Figure 4.12).

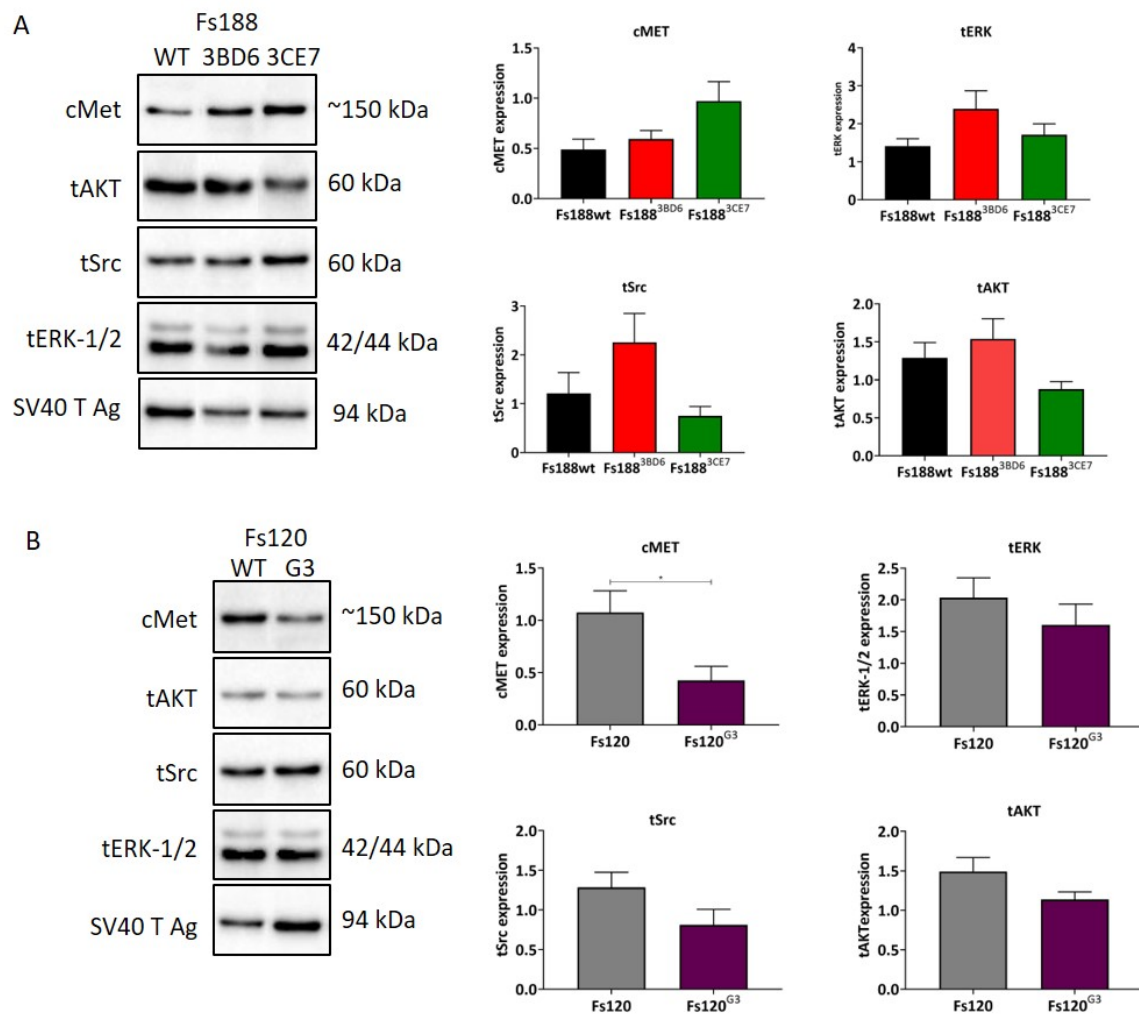


Figure 4.10 Expression levels of cMET and downstream signalling proteins in NRP1 modified fs188 and fs120 cells

Protein was extracted from fs188 NRP1 KD cells, fs120 NRP1 OE cells and their parental counterparts for analysis of cMET expression and downstream proteins associated with the NRP1/cMET signalling cascade. Samples were quantified and equal amounts of total proteins were analysed by western blotting to assess baseline expression levels. A) Expression levels of cMET, ERK-1/2, AKT and Src were not found to be significantly altered as a result of NRP1 KD. Data was analysed by one-way ANOVA followed by Tukey post-test, \pm SEM. B) cMET expression was lower in the fs120^{G3} cells in comparison to fs120wt cells. Expression of ERK-1/2, AKT and Src was not significantly altered by NRP1 OE. Data was analysed by unpaired t-test (* $p = 0.033$; \pm SEM). Blots are representative of $n = 3$ -5 independent experiments. Signals were normalised to SV40 T Ag to adjust for any variances in protein loading and blotting efficiency across the membrane.

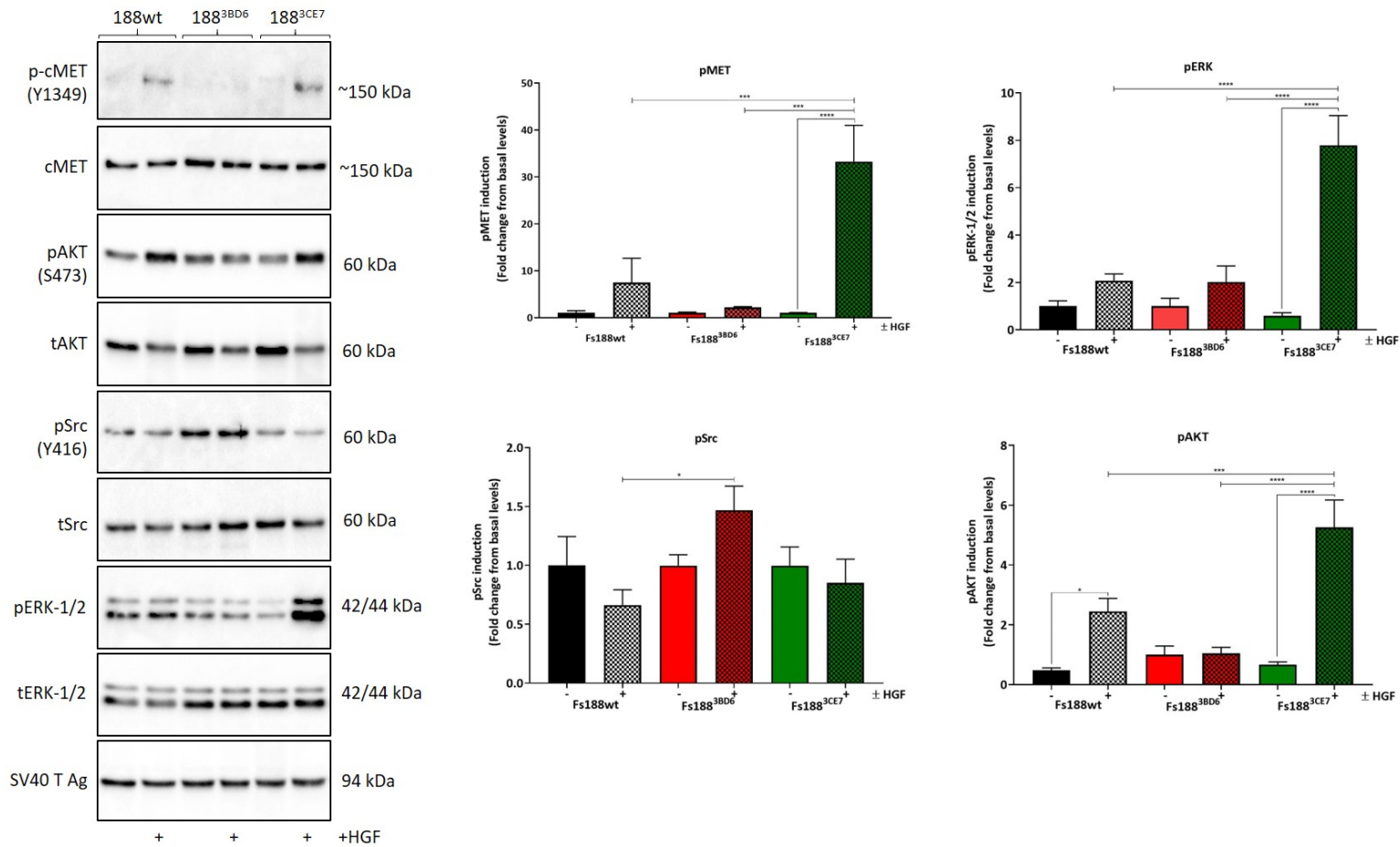


Figure 4.11 Effect of exogenous HGF on fs188 cells

Fs188, fs188^{3BD6} and fs188^{3CE7} were treated for 15 min with 20 ng of recombinant HGF before total proteins were extracted and quantified for analysis by western blotting. Addition of HGF led to phosphorylation of cMET, ERK-1/2 and AKT in fs188^{3CE7} cells, whereas fs188^{3BD6} failed to respond. Although phosphorylation of cMET above baseline levels failed to reach significance in the fs188wt cells, downstream AKT was activated in the presence of HGF. Blots are representative of n = 3-5 independent experiments. Data is analysed by one-way ANOVA with Bonferroni post-test (*p = 0.033, **p = 0.002, ***p = <0.001, ****p = <0.0001; ±SEM).

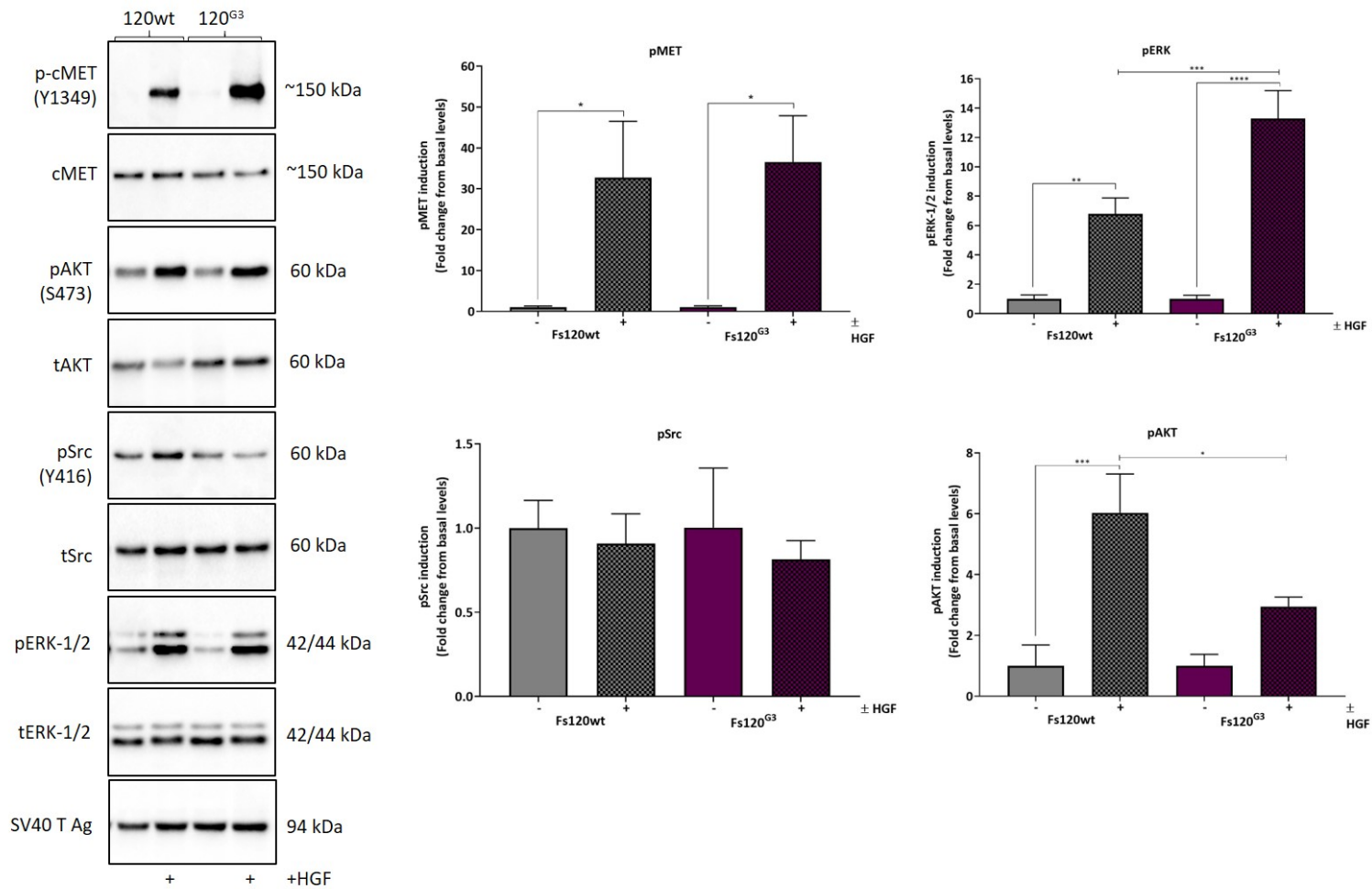


Figure 4.12 Effect of exogenous HGF on fs120 cells

Fs120 and fs120^{G3} were treated for 15 min with 20 ng of recombinant HGF before total proteins were extracted and quantified for analysis by western blotting. Addition of HGF led to phosphorylation of cMET, ERK-1/2 and AKT but not Src in fs120wt cells. In fs120^{G3} cells, HGF also led to phosphorylation of cMET and ERK-1/2, downstream AKT and Src levels of phosphorylation did not significantly exceed basal expression levels. Blots are representative of n = 3-5 independent experiments. Data is analysed by one-way ANOVA with Bonferroni post-test (*p = 0.033, **p = 0.002, ***p = <0.001, ****p = <0.0001; ±SEM).

4.12 Discussion

The main aim of this chapter was to permanently KD NRP1 expression in fs188 and fswt cells and OE NRP1 in fs120 and fs164 cells to enable investigation into the role of NRP1 in fs cell behaviour alongside individual VEGF isoforms. NRP1 KD was successfully achieved in fs188 cells using CRISPR/Cas9n gene editing techniques. Fswt cells were also successfully transfected using the same methodology and pooled cells from each sgRNA pair have been retained for future work. In parallel, NRP1 OE in fs120 and fs164 cells was achieved using *piggybac* transposon gene editing techniques. The modified fs120 and fs188 cells were then characterised for any alterations in their proliferation rates, ability to migrate and propensity to form colonies in a thick collagen-1 matrix.

The results show that stable NRP1 KD in fs188 cells and gross OE of NRP1 in fs120 and fs164 cells resulted in a reduction in migration across a 2D surface. The reduction in fs188 cell migration following NRP1 depletion is in alignment with what we found in the previous chapter when using siRNA. As discussed in detail in Chapter 3, the reduction in migration following NRP1 KD is the finding of many others in various different cancers. In contrast, NRP1 KD in Panc-1 cells has been shown to increase migration *in vitro* and exacerbate tumour growth *in vivo* (Gray *et al.*, 2005). This was also shown to be the case in neuroblastoma (NB); depletion of NRP1 in SK-N-AS cells (NRP1-high expressing human NB cells) resulted in increased Matrigel invasion and 2D migration in comparison to control siRNA transfected SK-N-AS cells (Ishizuka *et al.*, 2018). Although both fs188^{3BD6} and fs188^{3CE7} cells migrated at significantly slower rates than fs188wt cells, there was a difference in migratory rates between the two clones. Subsequent inconsistencies between the clones were discovered when signalling cascades in the fs188wt and fs188 KD clones were analysed which suggests that, somewhere during the genetic modification process, NRP1 KD led to the generation of clones with additional underlying differences. In light of NRP1s pivotal role in cellular migration, the decrease in migratory rate upon upregulation of NRP1 in fs120 and fs164 cells following massive OE of NRP1 was unexpected. However, there are reports in breast cancer cells that both siRNA KD of NRP1 and treatment with a NRP1 neutralising antibody increases chemotactic migration (Bachelder *et al.*, 2003). The interesting finding in the NRP1 OE model, was that modest OE of NRP1 in the fs164 cells did not result in any significant change in migratory capabilities of these cells, which infers that, in the fs cells lines at least, a finite level of NRP1 is required for optimal motility. During the migration experiments carried out here, there was no addition of exogenous ligands; as discussed in the previous chapter, expression of multiple ligands differs between the cell lines. Once again, the changes in migratory rates are likely to be influenced by NRP1s uncanny ability to act as a co-receptor with multiple cell surface receptors. Panc-1 cells do not express VEGFR1, 2 or 3 or plexin-A1 whereas many prostate and breast cancer cells do, as do our

fs cells which strengthens the hypothesis that NRP1 alone is not entirely responsible for phenotypic changes observed. It might be argued that, in the absence of serum starvation or addition of a cell cycle agonist such as mitomycin c, that the differences in migration could be attributed to differences in proliferation rates following NRP1 modification. Whilst this is certainly a limitation of the study, the inclusion of a step to block proliferation may have increased experimental reproducibility. However, as discussed below, there were no significant differences in proliferation rates between wt and modified fs cell lines. That said, *in vitro* cell survival of U87MG-NRP1 OE glioma cells was only found to increase in comparison U87MG cells in the absence of serum in the culture media. This led to the identification of an HGF mediated autocrine loop in that enhanced cell survival (Hu *et al.*, 2007). Proliferation/ cell survival experiments with the fs cells were not carried out in the absence of serum. In light of the signalling data that is discussed next, it would be interesting to see if the presence of serum during these experiments prevented the detection of changes to autocrine signalling in the NRP1 modified fs cells. To gain a better understanding of what other factors are at play in the *in vitro* NRP1 modified fs cell models, the addition of exogenous ligands in addition to HGF such as, EGF, FGF2, PIGF2 and PDGF would be of value. Furthermore, analysis of conditioned media from the fs cells by ELISA would give an indication on whether up or down regulation of NRP1 led to any differences in the expression of the various growth factors that have the ability to bridge complexes between NRP1 and their cognate receptors.

As with migration, the influence of NRP1 on cancer cell proliferation is unclear and appears to be cell type specific. In glioma cells, NRP1 downregulation significantly suppressed cell proliferation through induction of cell cycle arrest (Li *et al.*, 2011), significant decreases in doubling times were also reported in NRP1 antisense expressing Panc-1 cells (Fukasawa *et al.*, 2007) and in gastric cancer cells (Peng *et al.*, 2014). Again, this decrease was attributed to NRP1s contribution to apoptotic resistance. In contrast to this, Gray *et al.* (2005) found that neither KD nor OE of NRP1 significantly impacted on Panc-1 cell population doubling times. Also in RCC, although shRNA NRP1 KD led to a decrease in AKT phosphorylation, this did not lead to a reduction in proliferation or apoptosis. In this current study of the fs cells, modifications to NRP1 expression had no significant effect on the doubling times of either fs188 or fs120 cells. Furthermore, expression levels of cyclin-dependent kinase (CDK) p27 were not significantly different in the NRP1 modified cells in comparison to the parental cells (data not shown) suggesting that in the fs cells, NRP1 does participate in cell cycle regulation. Fukasawa *et al.* (2007) also found that diminished NRP1 expression in Panc-1 cells led to a decrease in colony formation in soft agar, whereas we found that NRP1 KD made no difference to the ability of fs cells to form colonies in a thick collagen-1 matrix. Recently, Borchardt *et al.* (2019) showed the anti-proliferative effects of

NRP1 KD in a range of pancreatic cancer cells may depend on the methodology used. Their results indicated that using anchorage-dependant proliferation assays rather than anchorage-independent growth in soft agar to measure proliferation rates underestimated the effect of NRP1 KD in three different pancreatic cancer cell lines (Colo357, PaTu9899t and AsPc1). These data must be interpreted with a certain amount of caution as Borchardt *et al.* (2019) go on to report that, although siRNA NRP1 inhibition in Panc-1 cells resulted in larger spheroids, it was a result of lower spheroid density rather than increased proliferation. Although NRP1 KD did not result in any observable differences in the ability to form colonies in a thick collagen matrix, or alter expression levels of the p27, the data presented by Borchardt *et al.* (2019) highlights a potential limitation within the current study, in that only one method was used to assess the proliferation rates of NRP1 modified cells

Previous work has identified major differences in the signalling interactions of the fs cells (Kanthou *et al.*, 2014), therefore to gain clearer insight into NRP1-associated changes in fs cell behaviour, fs188 and fs120 NRP1 modified cells were analysed separately. In Chapter 3, the potential consequences of NRP1 KD combined with the differential expression of HGF between the fs cell lines was introduced. Depending on which other TKIs participate, the HGF/cMET axis stimulates numerous signalling pathways inclusive of PI3K/AKT, Ras/MAPK and Src (Zhang *et al.*, 2018). Given that endogenous HGF secretion in fs188wt cells is relatively high in comparison to the other fs cell lines (Kanthou *et al.*, unpublished data) the assumption might be that cMET would be constitutively phosphorylated, yet this was not found to be the case. Basal levels of p-cMET were not significantly different between both NRP1 high and NRP1 low fs188 cells or between fs120wt and fs120^{G3} cells. The fact that fs188^{3BD6} cells failed to respond to stimulation with recombinant HGF whilst robust cMET phosphorylation and downstream signalling was evident in the fs188^{3CE7} cells is a peculiarity that requires further investigation. There are a number of potential reasons why this might have occurred; the first being that an underlying spontaneous mutation was already present in one of two NRP1 modified fs188 clones. An early passage of the fs188wt cells was used in these experiments to reduce the likelihood of selecting clones that carried any mutations, however it is feasible that this is the case. One way to circumvent this would have been to first isolate clonal populations of fs188wt cells and then use CRISPR to knock NRP1 down. Another possibility for the observed variability in the NRP1 KD clones is the introduction of an off-target mutation as a result of CRISPR/Cas9n gene editing. The paired sgRNAs were screened for specificity not only through the sgRNA design websites used but also through The Basic Local Alignment Search Tool (BLAST) (Altschul *et al.*, 1990); this said, the algorithms used to determine potential off-target effects work on the assumption that off-target sequences might share a high degree of similarity to the target sequence, which may therefore fail to identify off-target sites

with less similarity (Zhang *et al.*, 2015). Although protein expression of NRP1 was below detectable levels in WBs, during flow cytometry experiments, NRP1 was detected at negligible levels (< 1% of the population tested) in the fs188^{3BD6} and fs188^{3CE7} cells, it would seem unlikely that these imperceptible levels of NRP1 would lead to such significant differences between the clones. Although the diverse nature of the results between the NRP1 KD clones have given rise to somewhat contradictory and inconclusive data, it is a vital lesson in the importance of including more than one clone when investigating the effects of KD or OE of proteins in cell lines. Given more time, it would have been extremely interesting to look at the other fs188 NRP1 KD clones in the same depth to see whether they shared similarities with fs188^{3BD6} and fs188^{3CE7} cells. In gastric cancer, NRP1 supports activation of the PI3K/AKT signalling pathway by acting as a co-receptor for HGF with cMET (Li *et al.*, 2016a), in complete contrast, NRP1 KD in the fs188^{3CE7} cells led to an increase in both pAKT and pERK-1/2 following stimulation with HGF. This increase in pAKT was also seen in the fs188wt cells, which suggests that NRP1 KD effects other as yet unidentified binding partners or receptors. Li *et al.* (2016) also found downstream p27 expression levels were affected by NRP1, this was not the case in any of the fs cells, thus suggesting that alternative signalling pathways were influenced by NRP1 KD in the fs cells. In CRC cells, upon HGF binding with cMET, NRP1 and β 1 integrin are recruited to form a complex that is rapidly internalised and degraded to prevent sustained receptor stimulation. However, as discussed in Chapter 3, the internalisation dynamics of NRP1 splice variants (NRP1- Δ 4 and NRP1- Δ 5) in NRP1/HGF/cMET/ β 1 integrin complexes are very different; receptor complexes that contain NRP1 variants are recycled to the cell surface, resulting in persistent signalling through the FAK/p130 Cas pathway (Huang *et al.*, 2019). NRP1 also plays a central role in receptor recycling of activated VEGFR2 (Ballmer-Hofer *et al.*, 2011) and EGFR (Rizzolio *et al.*, 2012) which results in dysregulated pERK-1/2 and pAKT respectively. One hypothesis may be that, in the fs188^{3CE7} cells, NRP1 depletion either abrogates HGF/cMET internalisation all together or that, without NRP1, the HGF/cMET complex is not degraded upon internalisation and is recycled to the cell surface. In both cases, in the absence of HGF/cMET degradation, signalling through the MEK/ERK and/or PI3K/AKT pathways may then be sustained. A robust induction of p-cMET with HGF in both the fs120wt and fs120^{G3} was evident, however downstream pAKT differed between the two cell lines. This suggests that, in the fs120 cells, NRP1 expression has a regulatory role over PI3K/Akt signalling. The greater induction of pERK-1/2 in the fs120^{G3} cells following HGF stimulation also is indicative of NRP1 having an influence over Ras/MAPK signalling. In order to investigate the functional consequences of these pathway alterations fully, migration, adhesion and proliferation experiments with the addition of HGF need to be carried out.

Genome-wide analysis of NRP1-depleted A549 lung cancer cells found over 200 deregulated transcripts; network analysis of these dysregulated genes identified a role of NRP1 in modulating numerous cellular and molecular functions inclusive of cell migration and drug metabolism (Jimenez-Hernandez *et al.*, 2018). In view of this, without single-cell genome analysis of the clones selected during this study, it is impossible to know what the precise knock-on effects of NRP1 KD and OE in these cells were. In cMET-addicted lung and gastric carcinoma cells, NRP1 overexpression led to an increase in EGFR expression (Rizzolio *et al.*, 2018), which highlights the likelihood that NRP1 manipulation in the fs cells may well have disrupted further signalling pathways that are as yet to be discovered. Furthermore, identifying the differences between the activation of signalling cascades in the fs cells is made all the more complex due to differential ligand expression which was discussed in Chapter 3.

It is apparent from these data that NRP1 does play a role in the migratory characteristics of the fs cells, however, the downstream pathways that it affects in order to achieve this requires further investigation. Successful development of the stable cell lines with modified NRP1 expression will allow for this at a later date, however, the main focus here was to determine whether NRP1 influenced the sensitivity of fs cells to anti-VEGF therapy. Chapter 5 utilises the cells developed during this chapter to test this *in vivo*.

Chapter 5

***In vivo* effects of NRP1 modification in fibrosarcoma cells expressing VEGF188 or VEGF120 on anti-VEGF therapy**

5.1 Introduction

To investigate the role of NRP1 on tumour response to anti-VEGF treatment, *in vivo* models are necessary. In the previous chapter, stable fs188 and fs120 cells lines were successfully developed with abrogated and augmented NRP1 expression levels respectively. In the current chapter, the behaviour of these cell lines *in vivo* was investigated. In a previous study with human fibrosarcoma cells (HT1080), NRP1 KD abrogated the cells' tumour forming capabilities (Misra *et al.*, 2012), therefore an initial pilot experiment with fs188wt and five fs188 NRP1 KD clones was undertaken to assess whether the solid tumours would arise from our modified fs cells in severe combined immunodeficient (SCID) mice. Following on from this, two fs188 NRP1 KD clones and one fs120 NRP1 OE clone, along with their parental cell lines, were selected and used to establish tumours in SCID mice that were then treated with either the VEGF blocking antibody (B20-4.1.1), directed towards amino acids 8 – 109 of VEGFA, or a corresponding IgG control antibody. The resulting tumours were routinely measured to track their growth with or without anti-VEGF treatment. Once experimental (or humane) end-points had been met, tumours were excised and preserved for subsequent analysis of tumour vascularity and other parameters. Data in this chapter from experiments that included anti-VEGF treatment are shown at the experimental end-point of 48 hours after the fourth treatment with B20-4.1.1 or control IgG (or at a maximum tumour volume of 1200 mm³, if this occurred sooner).

5.2 Aim

The aim of this chapter was to successfully create a fibrosarcoma mouse model in which the influence NRP1 expression over anti-VEGF treatment could be investigated.

5.3 NRP1 KD in fs188 cells does not attenuate solid tumour formation

In Chapter 4 it was established that NRP1 depletion in fs188 cells did not impede colony formation in a thick collagen-1 matrix. Conflicting reports in the literature raised the possibility that NRP1 KD might prevent the establishment of tumours *in vivo* (Misra *et al.*, 2012, Koch *et al.*, 2014). To determine

whether this was the case with the fs188 cells, a pilot study was carried out with five fs188 NRP1 KD clones and the fs188wt cells. The results of this initial study also provided information that influenced decision about which two fs188 NRP1 KD clones to take forward for further *in vivo* work. Fs188wt and fs188 NRP1 KD cells were injected subcutaneously into the rear dorsum of SCID mice (Materials and Methods, Section 2.11.2). All the fs188 NRP1 KD cell lines established tumours *in vivo* (Figure 5.1). Mice were monitored daily and once tumours reached a maximum volume of 520 mm³, they were excised. However, the lag time from implantation to tumour establishment with the fs188^{3BD6}, fs188^{3CE7} and fs188^{3BC4} cells was longer than that of the fs188wt, fs188^{1BC3} and fs188^{3BF10} cells. All tumours in the fs188^{1BC3} group reached the maximal experimental end-point size by day 20; this was closely followed by the fs188wt and fs188^{3BF10} tumours at 22 and 23 days respectively. Tumours in the fs188^{3CE7} group became ulcerated, therefore animals were culled at 23 days before the tumours reached the end-point size of 520 mm³. As a result of the delay in initial tumour establishment, fs188wt, fs188^{1BC3} and fs188^{3BF10} tumours were all significantly larger than fs188^{3BD6}, fs188^{3CE7} and fs188^{3BC4} tumours at day 20. CD31 staining showed that all tumours were well vascularised (Figure 5.2A). Subsequent quantification of CD31 positive vessels (Figure 5.2B) indicated that, except for clone fs188^{3BC4} that exhibited a small reduction in vascular area in comparison to fs188wt tumours, all other clones had similar levels of vascularisation to fs188wt tumours in terms of vascular area. Furthermore, the vascular morphology was similar in the fs188 NRP1 KD tumours in comparison to the fs188wt tumours. As a consequence of the differing tumour establishment kinetics between the clones, it was surmised that the clones exhibiting delayed tumour onset may be of more interest to study further *in vivo*. Of the three clones that displayed a delay in tumour establishment, western blotting analysis of the fs188 NRP1 KD clones identified a small amount of residual NRP1 protein expression in fs188^{3BC4} (Chapter 4, Figure 4.4A), seeing as this was not evident in any of the other four clones, this clone was discounted. As noted in the previous chapter fs188^{3BD6} was morphologically distinct to the other clones, this interesting characteristic associated with NRP1 KD made it of interest to study further *in vivo*. Therefore, the two fs188 NRP1 KD clones taken forward for study with anti-VEGF therapy *in vivo* were fs188^{3BD6} and fs188^{3CE7}.

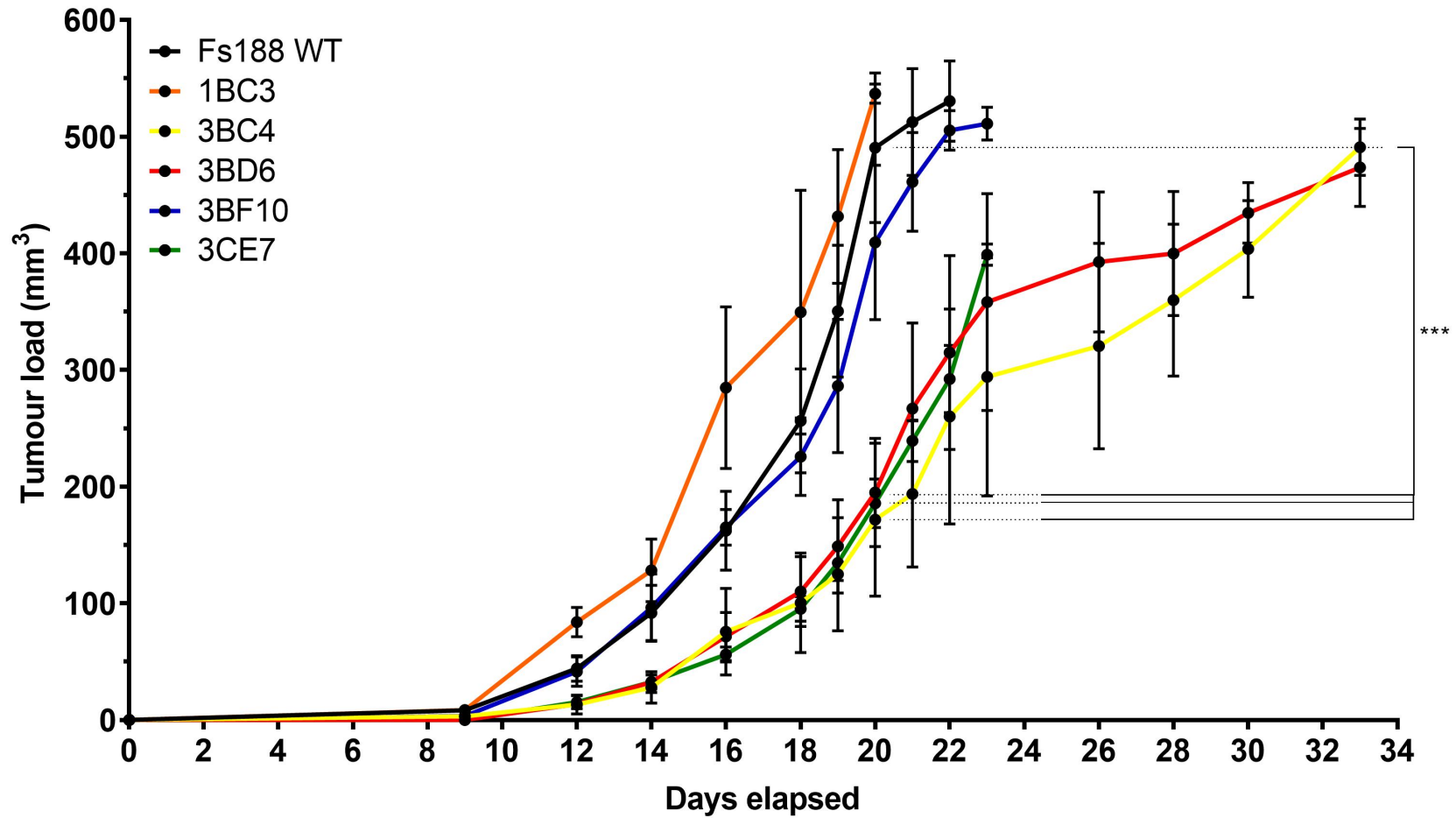


Figure 5.1 Fs188wt and fs188 NRP1 KD tumour growth curves

1 x 10⁶ fs188wt or fs188 NRP1 KD cells were injected subcutaneously on day 0. Calliper measurements were taken every 1-2 days and tumours grown to a maximum volume of 520 mm³ or until the humane end-point was reached. A lag time in the establishment fs188^{3BD6}, fs188^{3CE7} and fs188^{3BC4} in comparison to the fs188wt tumours resulted in a significant difference in tumour volume at day 20. Data analysed at day 20 by two-way ANOVA with Tukey correction (**p = <0.001, ±SEM; n=4 animals per group).

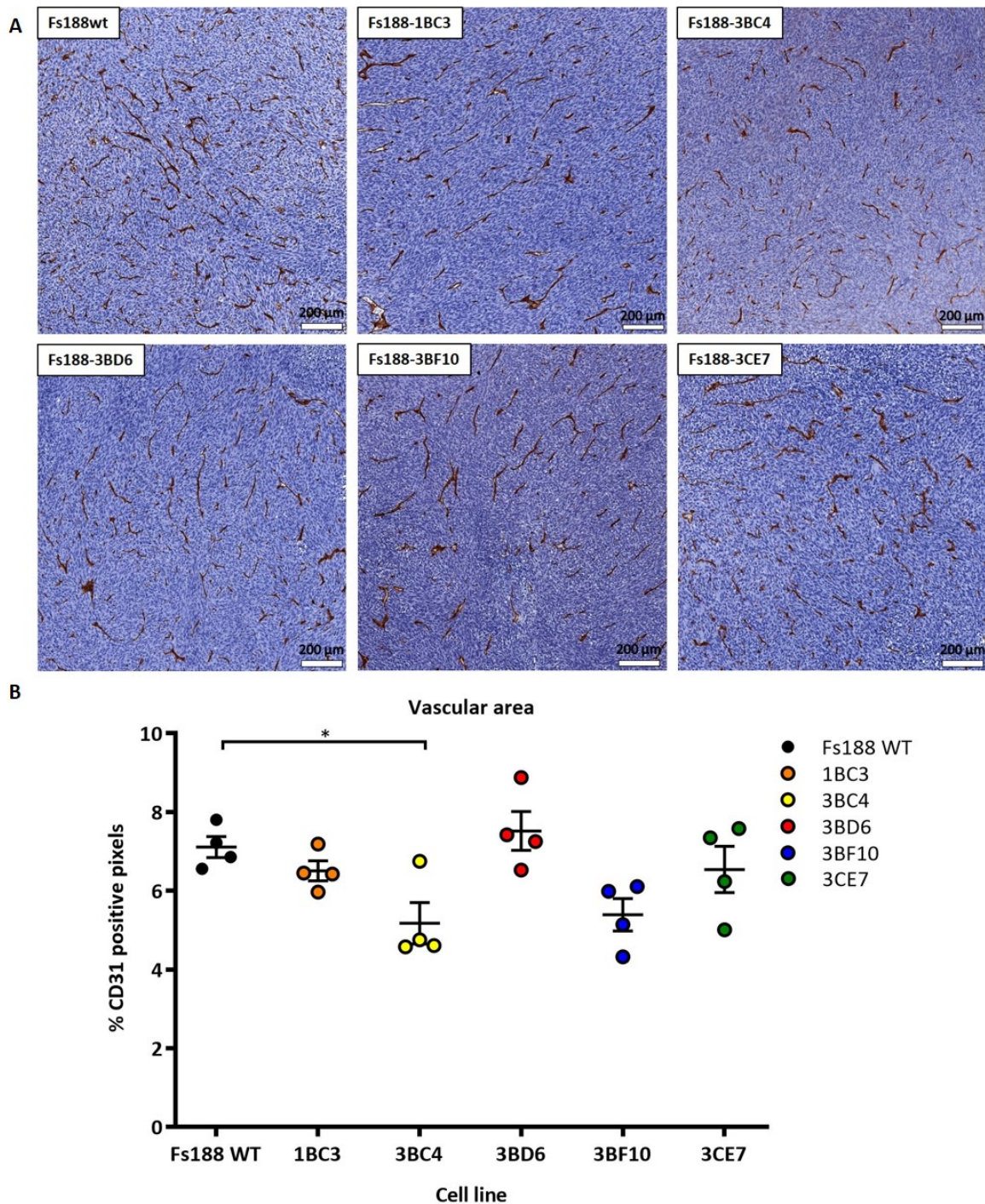


Figure 5.2 Fs188wt and fs188 NRP1 KD pilot experiment tumour vascularity

Mice were injected subcutaneously with 1×10^6 fs188wt or fs188 NRP1 KD cells and tumours grown to a maximum volume of 520 mm^3 or until the humane end-point was reached. Using IHC, FFPE tumour sections for CD31 and counterstained with haematoxylin. A) Representative images from viable tumour regions at 10x magnification from whole slide scanning. B) Vascular area was quantified by calculating the mean percentage of DAB positive staining in 10 random 750×750 micron squares (from whole slide scanning) in areas of viable tumour tissue using QuPath. Data analysed by one-way ANOVA with Bonferroni post-test. (* $p = 0.03$, \pm SEM; $n = 4$ animals per group).

5.4 Effect of NRP1 on fs188 and fs120 tumour growth and response to anti-VEGF treatment

In order to study whether NRP1 influenced the effect of anti-VEGF therapy in a VEGF isoform-selective manner, fs188^{3BD6}, fs188^{3CE7} and fs120^{G3} cells were injected subcutaneously into the rear dorsum of SCID mice alongside their wt counterpart cells (Materials and Methods, Section 2.11.2). Once tumours reached a volume of 100 mm³, 5 mg/kg B20-4.1.1 or control IgG was administered by IP injection every two days for the first three treatments. From the fourth day following the initial dose of control IgG or B20-4.1.1 (annotated as day four), treatment was administered every three days. Tumour measurements were taken daily until they reached either a maximum end-point volume of 1200 mm³ or 48 hours following the fourth treatment, dependent on which occurred sooner. Tumours were excised, weighed and preserved for further analysis, which will be discussed in detail during the subsequent sections.

Between tumour volumes of 100 mm³ and approximately 300 mm³ the untreated fs188 clones grew at approximately the same rate as the fs188wt tumours (Figure 5.3A), consistent with the pilot data shown in Figure 5.2. However, at the experimental end-point, fs188^{3BD6} and fs188^{3CE7} tumours not receiving anti-VEGF treatment were significantly smaller than their corresponding fs188wt tumours (Figure 5.3A), indicating an influence of NRP1 in the later stages of tumour growth. OE of NRP1 in the fs120^{G3} tumours also resulted in a reduction in tumour size at day 9 in comparison to fs120wt tumours (Figure 5.3C); however, the difference was not as pronounced as between the fs188 NRP1 KD and fs188wt tumours. Tumours were stained with Ki67 to assess *in vivo* tumour cell proliferation; no significant differences were found between VEGF188 and VEGF120-expressing tumours regardless of NRP1 expression (Supplementary data, Figure S2).

In contrast to fs188wt tumours, three treatments of B20-4.1.1 started to retard the growth of both fs188^{3BD6} and fs188^{3CE7} tumours (Figure 5.4A). However, after four B20-4.1.1 treatments, fs188wt tumours started to exhibit a slowdown in growth and tumours were ~30% smaller than those treated with control IgG (Figure 5.4B). The effect of four B20-4.1.1 treatments was greater in the fs188^{3BD6} and fs188^{3CE7} tumours than in the fs188wt tumours; tumours were on average 49% and 38% smaller respectively (Figure 5.4B). Conversely, fs120wt tumours failed to respond to treatment with B20-4.1.1 (Figure 5.3D, Figure 5.4A & B) whilst the fs120^{G3} tumours expressing high NRP1 showed a significant decrease tumour volume following both three and four treatments with B20-4.1.1 (Figure 5.3D, Figure 5.4A & B). These results show that increased NRP1 expression in the fs120 cells led to an improvement in the efficacy of B20-4.1.1 whereas in the fs188 cells, although tumour growth was retarded by B20-

4.1.1 following NRP1 KD, there was no sustained difference in efficacy of B20-4.1.1 over and above what was obtained in the fs188wt tumours.

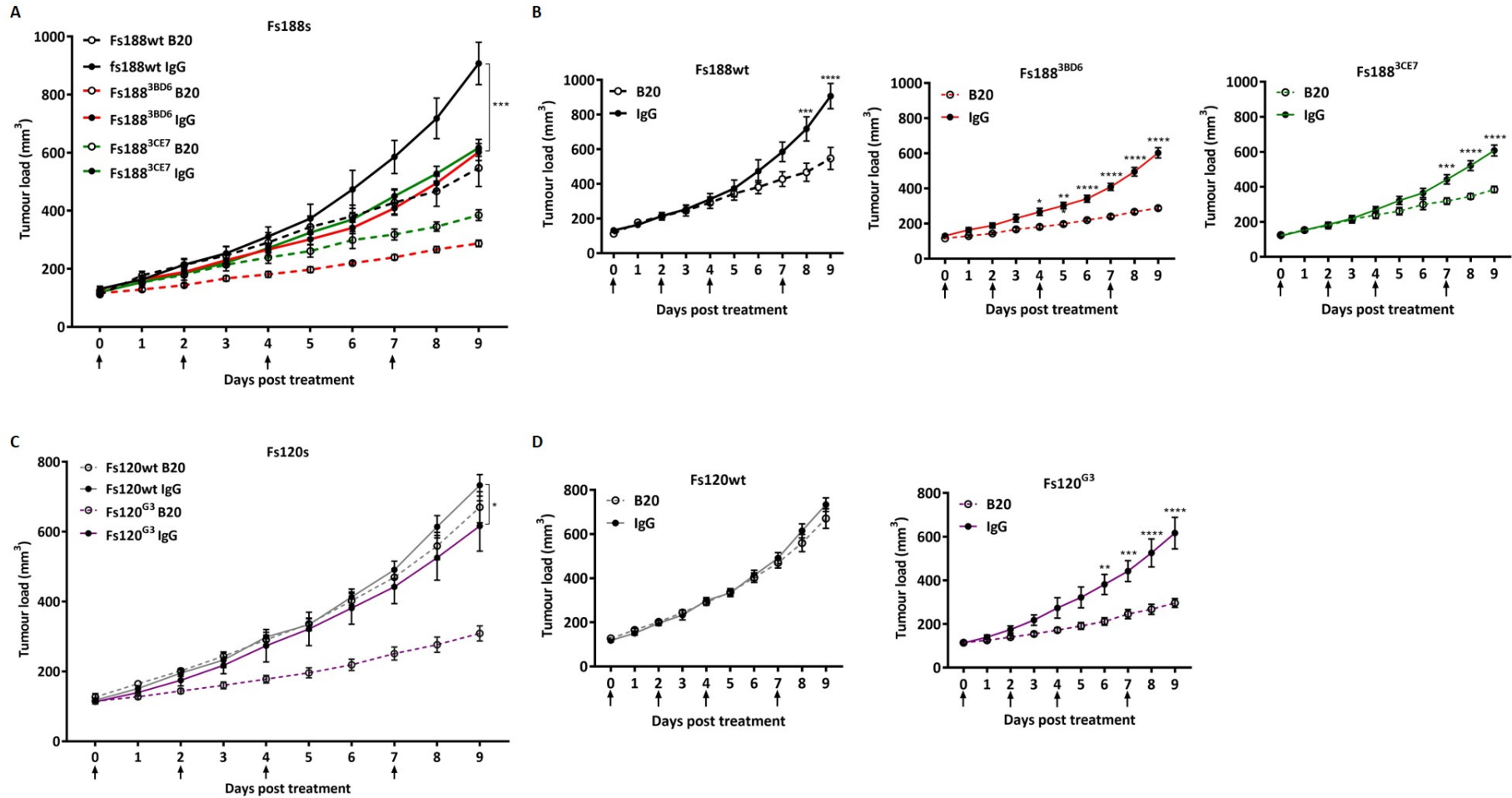


Figure 5.3 Growth of fs188 and fs120 tumours with modified NRP1 expression receiving anti-VEGF treatment

Mice were injected subcutaneously with 1×10^6 A & B) fs188, fs188^{3BD6} or fs188^{3CE7} cells and C & D) fs120wt or fs120^{G3} cells and tumours grown to 100 mm³ before treatment with 5 mg/kg B20-4.1.1 or control IgG at the timepoints indicated with black arrows. Tumour volume was measured with callipers until end-point (48 h post fourth treatment). Two separate cohorts of 50 animals, divided between the 10 groups, were used. The results presented are the combined data from both studies. Data analysed by two-way ANOVA with Bonferroni correction (* $p < 0.05$, ** $p < 0.01$, *** $p < 0.001$, **** $p < 0.0001$, \pm SEM; $n = 6-9$ animals per group).

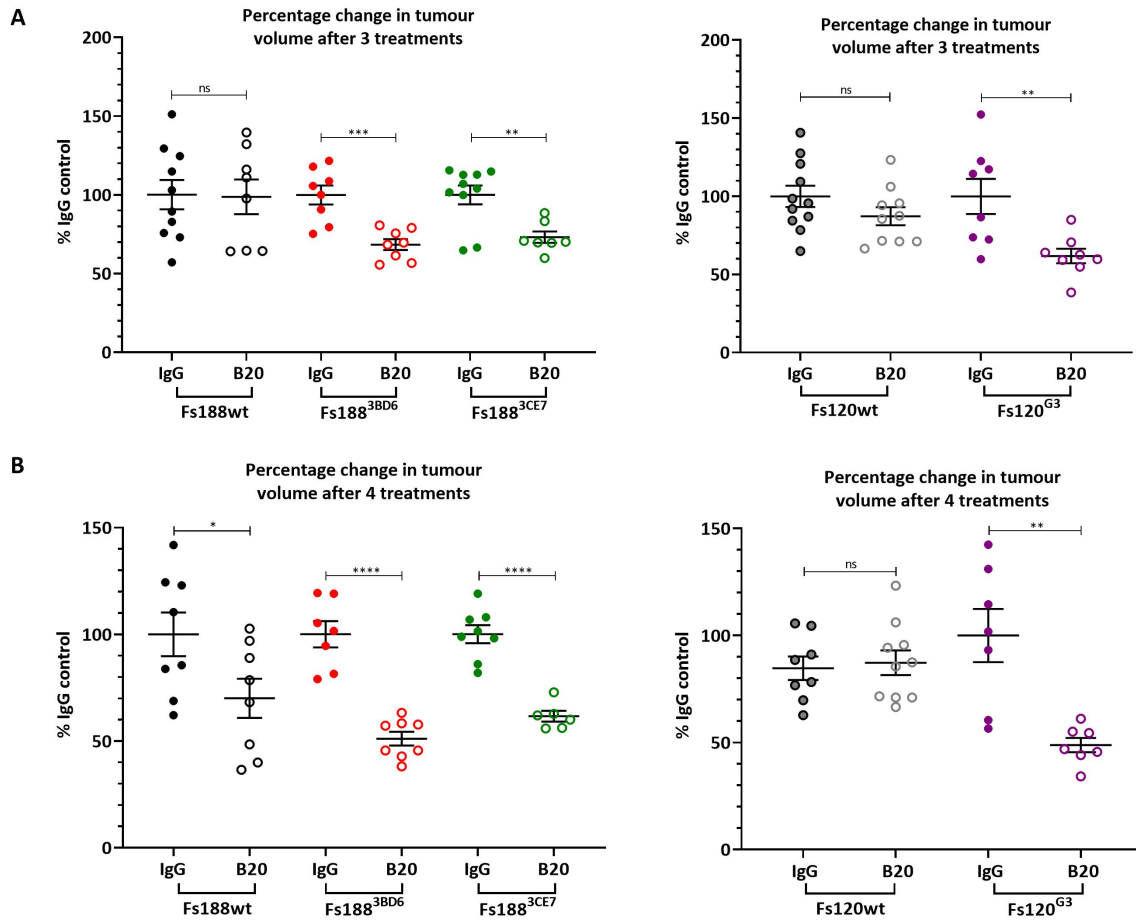


Figure 5.4 Response of fs188 and fs120 tumours with modified NRP1 expression to anti-VEGF treatment

Mice were injected subcutaneously with 1×10^6 fs188wt, fs188^{3BD6}, fs188^{3CE7}, fs120wt or fs120^{G3} cells and tumours grown to 100 mm³ before treatment with 5 mg/kg B20-4.1.1 or control IgG. Tumour volume was measured with callipers until end-point (48 h post fourth treatment). Tumour volume is expressed as a percent of control IgG mean tumour volume 48 h after A) three (n = 7-10 animals per group) and B) four (n = 6-8 animals per group) treatments with B20-4.1.1 or control IgG. Data analysed by unpaired t-test (ns = not significant, *p = < 0.05, **p = < 0.01, ***p = < 0.001, ****p = < 0.0001, \pm SEM.)

5.5 Fs188 tumours were more necrotic than fs120 tumours

To examine gross tumour tissue morphology and to analyse necrosis, s/c tumours described in Section 5.4 were H & E stained (Materials and Methods, Section 2.12). Across the board there was a high amount of intragroup variability in the level of necrosis within all the sections analysed (Figure 5.5). In the fs188wt, fs188^{3BD6} and fs120^{G3} tumours treated with B20-4.1.1 this variance appeared to be more pronounced with the level of necrosis ranging from 16 – 68%, 23 – 82% and 1 – 37% respectively. Modification of NRP1 expression in the fs188 and fs120 cells did not appear to impact on the level of necrosis in the tumours, however, on the whole, VEGF188 expressing tumours were significantly more necrotic than VEGF120-expressing tumours (Figure 5.5). Treatment with B20-4.1.1 did not lead to any significant changes in the level of necrosis regardless of NRP1 expression status in either the fs188 or fs120 tumours (Figure 5.5). These results suggest that the retardation in growth following treatment with B20-4.1.1 identified in Section 5.4 above was not due to an increase in necrotic fraction.

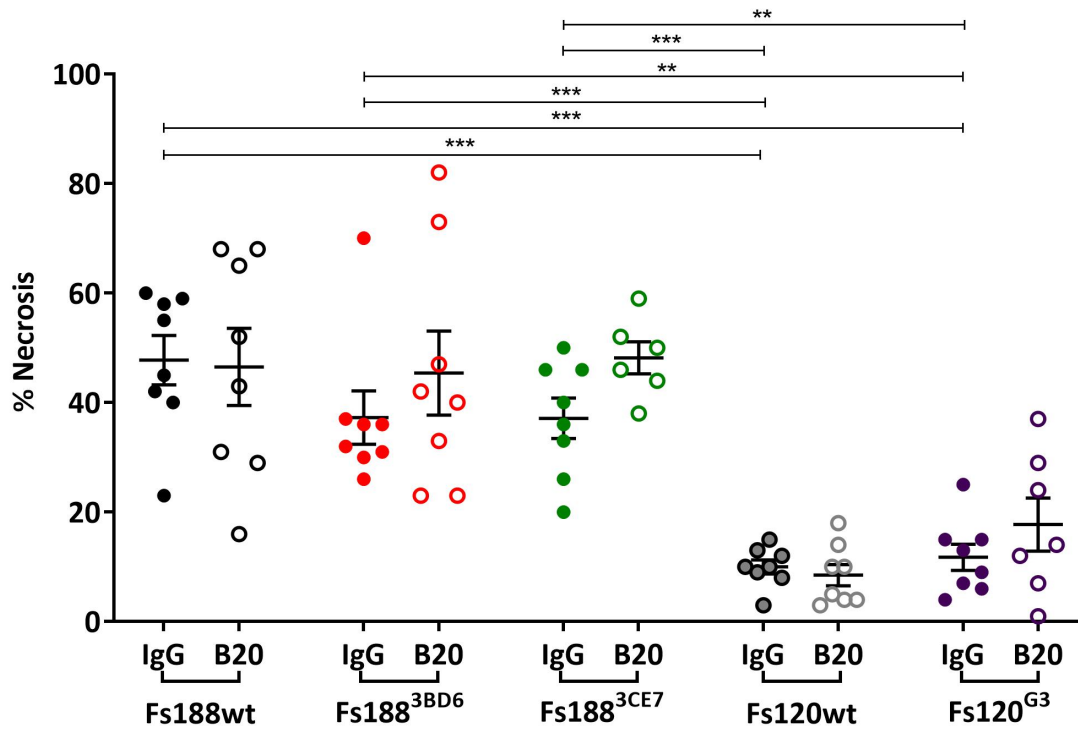


Figure 5.5 Tumours expressing VEGF188 are more necrotic than those expressing VEGF120

Mice were injected subcutaneously with 1×10^6 fs188wt, fs188^{3BD6}, fs188^{3CE7}, fs120wt or fs120^{G3} cells and tumours grown to 100 mm³ before receiving 5 mg/kg B20-4.1.1 or control IgG every 2 days for the first 3 treatments then every 3 days thereafter. FFPE tumour sections were haematoxylin and eosin stained and the percentage of necrosis calculated as a ratio of the whole section area using Qupath (Materials and Methods, Section 2.12). Data analysed by two-way ANOVA with Tukey correction (**p = <0.01 ***p = <0.001, \pm SEM; n = 7-8 animals per group).

5.6 Tumour vascular effects of NRP1 modification and anti-VEGF treatment

To examine the vascularity of the tumours, IHC was used to stain for CD31 (Materials and Methods, Section 2.14). Quantification of CD31 staining showed that vascular area as a percentage tumour area (% CD31 positive pixels), in all the VEGF188 expressing tumours was higher than in fs120wt tumours (Figure 5.6A). Vascular density as determined by the mean number of vessels/ 10 fields of view, was also higher in the fs188wt and fs188^{3BD6} tumours than both the fs120wt and fs120^{G3} tumours (Figure 5.6D). There was no significant difference in the vascular area between fs188 tumours with abrogated NRP1 expression in comparison to fs188wt tumours. However, there was a significant reduction in vascular area between all the VEGF188 expressing tumours, regardless of NRP1 expression levels, receiving B20-4.1.1 in comparison to their control IgG counterparts (Figure 5.6B). Fs120^{G3} tumours had a higher vascular area than fs120wt tumours (Figure 5.6C) however there was no difference in the vascular density between the two tumour groups (Figure 5.6F). Neither fs120wt nor fs120^{G3} tumours showed any significant difference in vascular area or density following treatment with B20-4.1.1, although there was a trend in this direction (Figure 5.6C & F).

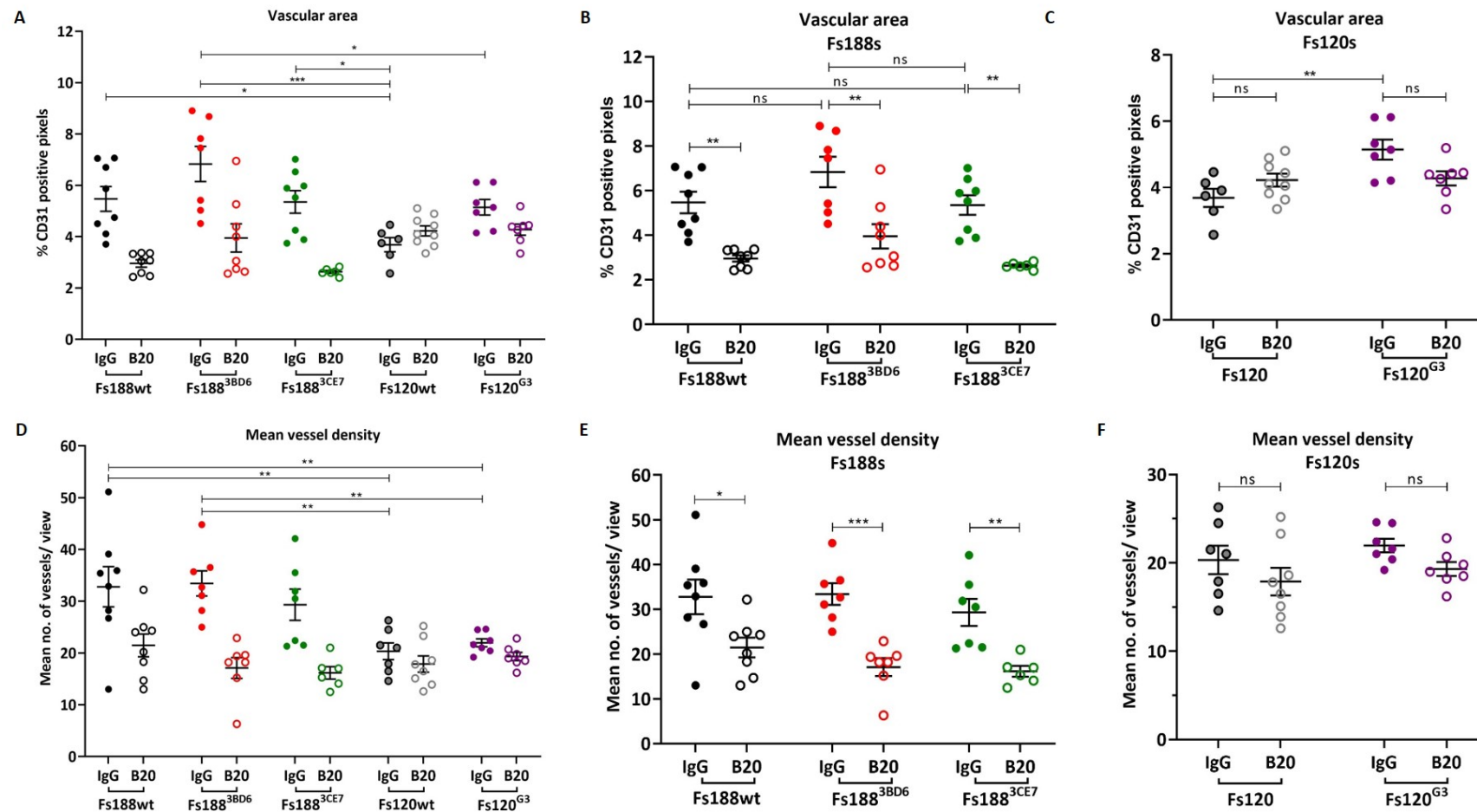


Figure 5.6 Anti-VEGF treatment reduces vascular density in tumours expressing VEGF188 but not VEGF120

Mice were injected subcutaneously with 1×10^6 fs188wt, fs188^{3BD6}, fs188^{3CE7}, fs120wt or fs120^{G3} cells and tumours grown to 100 mm³ before IP injection of 5 mg/kg B20-4.1.1 or control IgG every 2 days for the first 3 treatments then every 3 days thereafter. Using IHC, FFPE tumour sections for CD31 (Materials and Methods, Section 2.13). A-C) Vascular area was quantified by calculating the mean percentage of DAB positive staining in 10 random 750 x 750 micron squares (from whole slide scanning) in areas of viable tumour tissue using QuPath. In the same 10 squares the no. of vessels were counted to give D-E) mean vascular density. **p = <0.01 ***p = <0.001, \pm SEM; n = 7-8 animals per group).

5.7 Effect of NRP1 modification and anti-VEGF therapy on vascular morphology

Vascular morphology differed between the VEGF188 and VEGF120 tumours; in agreement with previous studies using these cell lines, VEGF120 tumours had a higher number of large open vessels in comparison to VEGF188 tumours (Tozer *et al.*, 2008a, Akerman *et al.*, 2013). Furthermore, fs120wt tumours tended to have a higher number of these large open vessel in comparison to fs120^{G3} tumours (Figure 5.7A). This result does not explain why vascular area, but not vascular density, was significantly lower in the fs120wt compared with the fs120^{G3} tumours (Figure 5.6C & F). Presumably the average area of blood vessels was lower in fs120wt than in fs120^{G3} tumours to account for this result. Regardless of treatment or NRP1 expression status, the presence of large open vessels was variable within all the groups, therefore no significant difference was found between tumours treated with B20-4.1.1 and their respective controls. That said, treatment with B20-4.1.1 in the fs188^{3BD6} tumours did appear to show a trend towards the appearance of more of the large open vessels (Figure 5.7B). To a lesser extent, an increase in the number of open vessels was also evident in the fs120wt tumours (Figure 5.7C), however there was a high level of intragroup variability.

In general, NRP1 KD in the fs188 tumours did not lead to any obvious differences in vascular morphology between the tumours. On the whole, treatment with B20-4.1.1 in both fs188 NRP1 KD and fs188wt tumours resulted in seemingly shorter, less branching vessels (Figure 5.8A). As discussed in the previous paragraph, there were subtle changes in the fs188^{3BD6} tumours following treatment with B20-4.1.1 in terms of the number of large open vessels, however, the number of these vessels was relatively low and the majority of vessels were the smaller vessels shown in Figure 5.8A.

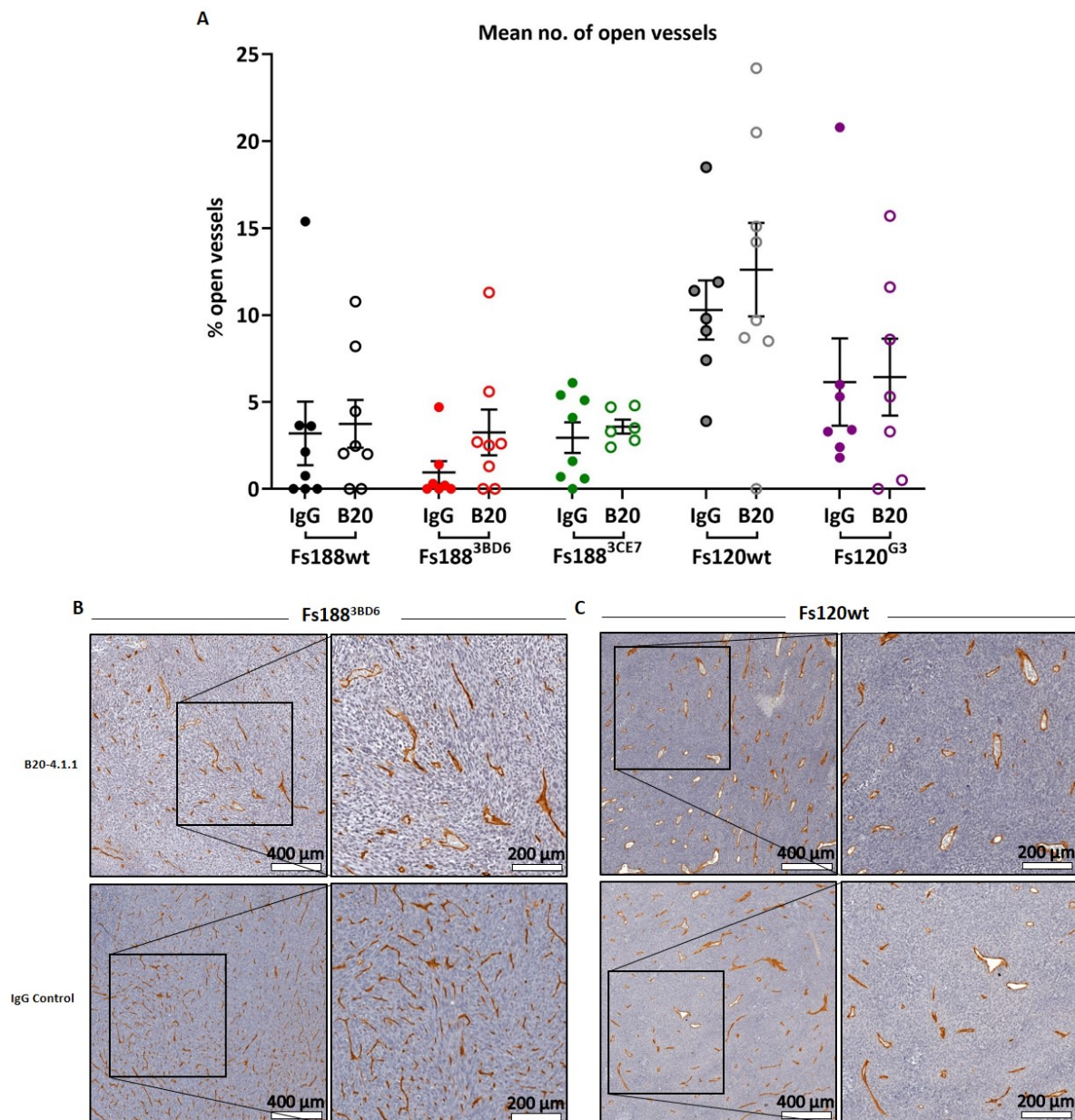


Figure 5.7 Vessel morphology in NRP1 modified fs188 and fs120 tumours following B20-4.1.1 treatment

Mice were injected subcutaneously with 1×10^6 fs188, fs188^{3BD6}, fs188^{3CE7}, fs120wt or fs120^{G3} cells and tumours grown to 100 mm³ before IP injection of 5 mg/kg B20-4.1.1 or control IgG every 2 days for the first 3 treatments then every 3 days thereafter. Using IHC, FFPE tumour sections were stained for CD31 and counterstained with haematoxylin (Materials and Methods, Section 2.13). A) the mean number of vessels in 10 random 750 x 750 micron squares of viable tumour tissue (from whole slide scanning) were counted using QuPath. Vessels were categorised as either 'intact' or 'large open', the mean number of large open vessels was taken as a percentage of mean total vessel number per tumour. Representative images of B) fs188^{3BD6} and C) fs120wt vessels (Images captured at 5x and 10x magnification from whole slide scanning).

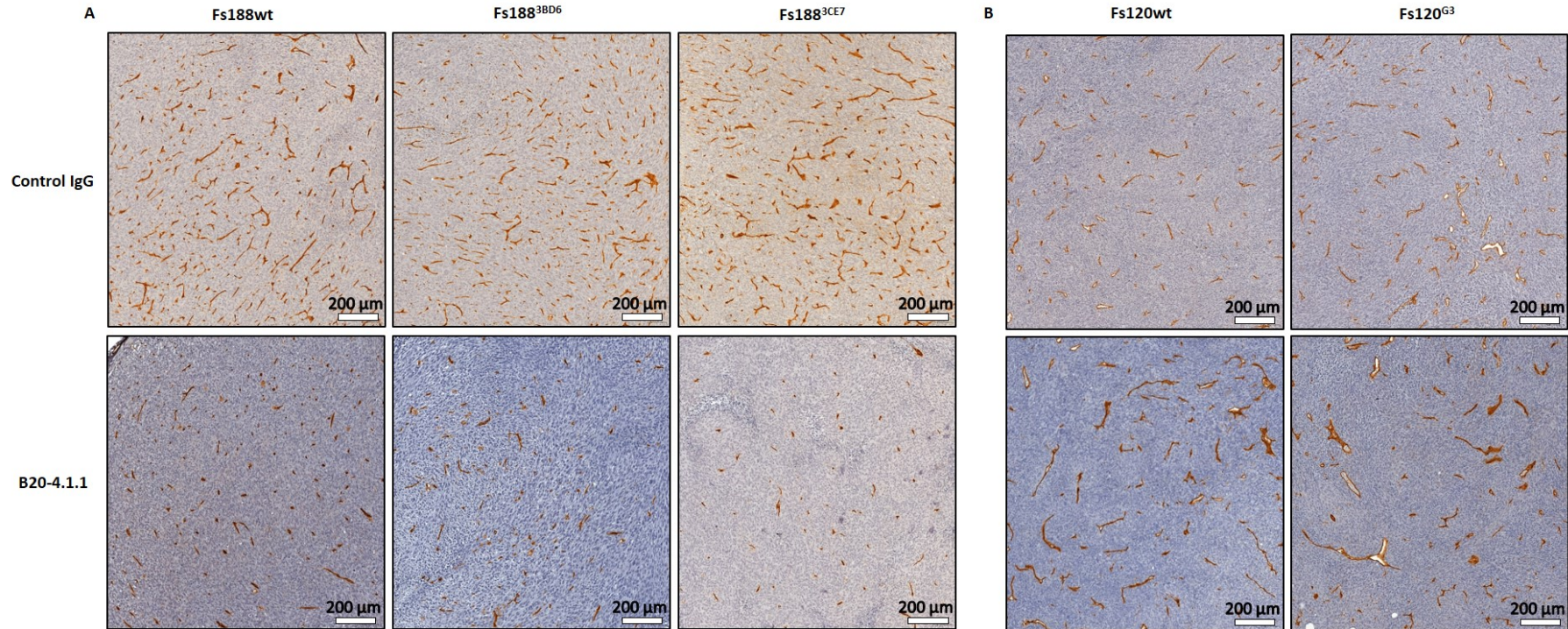


Figure 5.8 Fs188 and fs120 NRP1 modified tumour vascularity following treatment with B20-4.1.1 or control IgG

Mice were injected subcutaneously with 1×10^6 fs188wt, fs188^{3BD6}, fs188^{3CE7}, fs120wt or fs120^{G3} cells and tumours grown to 100 mm³ before treatment with 5 mg/kg B20-4.1.1 or control IgG. FFPE tumour sections were stained for CD31 and counterstained with haematoxylin. Representative images from viable tumour regions taken at 10x magnification from whole slide scanning of A) fs188, fs188^{3BD6} and fs188^{3CE7} and B) fs120wt and fs120^{G3} tumours treated with either B20-4.1.1 or control IgG.

5.8 Vascular wall maturity in fs188 and fs120 NRP1 modified tumours

Previously, the assessment of vascular pericyte coverage has been used to gauge the vascular maturity of VEGF188 and VEGF120-expressing tumours. The higher abundance of α SMA positive pericytes that colocalised with CD31 in VEGF188-expressing tumours was indicative of a more mature vasculature than VEGF120-expressing tumours (Tozer *et al.*, 2008a, Akerman *et al.*, 2013, English *et al.*, 2017). To examine whether NRP1 expression or B20-4.1.1 treatment impacted on the maturity of the tumour vascular walls in VEGF188 and VEGF120 expressing tumours, α SMA staining was carried out on FFPE tumours sections. Initially, the intention was to carry out dual immunofluorescence (IF) with α SMA and CD31 on frozen tumour sections. However, the high level of necrosis in a number of the tumours resulted in poor cryosection adhesion to slides and subsequently suboptimal material on which to carry out the dual IF. Following this, α SMA/ CD31 IF staining of FFPE sections was attempted; although various methods were employed to try and circumvent the issue of autofluorescence, none of the techniques tested reduced the autofluorescence enough to allow for reasonable assessment of staining. Finally, a selection of near adjacent sections to CD31-stained sections were stained for α SMA using IHC and the presence of vascular associated α SMA positive pericytes were assessed. Regardless of NRP1 expression in the VEGF188-expressing tumours, the majority of vessels had good pericyte coverage which was unaffected by treatment with B20-4.1.1 (Table 5.1). Only three sections per treatment group for the fs120wt tumours were successfully stained and the pericyte coverage was variable; in the abundant dilated vessel though it was clear that pericyte coverage was much poorer than the narrower vessels. In the small number of fs120^{G3} tumours it appeared that not only was vascular associated α SMA stronger, but also that treatment with B20-4.1.1 had a tendency to decrease the appearance of vascular pericytes (Table 5.1). It was noted that there was significant extravascular α SMA staining was present in all the tumours, consistent with published data (Tozer *et al.*, 2008a).

Tumour	Treatment/ α SMA Score	1	2	3	4
Fs188wt	Control IgG	0	0	2	2
	B20-4.1.1	0	0	2	2
Fs188 ^{3BD6}	Control IgG	0	1	1	3
	B20-4.1.1	1	0	2	0
Fs188 ^{3CE7}	Control IgG	0	0	1	3
	B20-4.1.1	0	0	0	4
Fs120wt	Control IgG	1	1	1	0
	B20-4.1.1	1	0	2	0
Fs120 ^{G3}	Control IgG	0	1	3	0
	B20-4.1.1	3	0	1	0

Table 5.1 Vascular associated α SMA staining scoring

Using IHC, near-adjacent tumour sections were stained for α SMA and CD31 and counterstained with haematoxylin. The presence of vascular associated α SMA positive pericytes was assessed using a 1-4 scoring criteria; see Figure 5.9 for examples of scoring and full explanation of scoring criteria. Each box shows the number of tumours scoring 1,2, 3 or 4 for the corresponding treatment group. Sections were scored on a blinded basis.

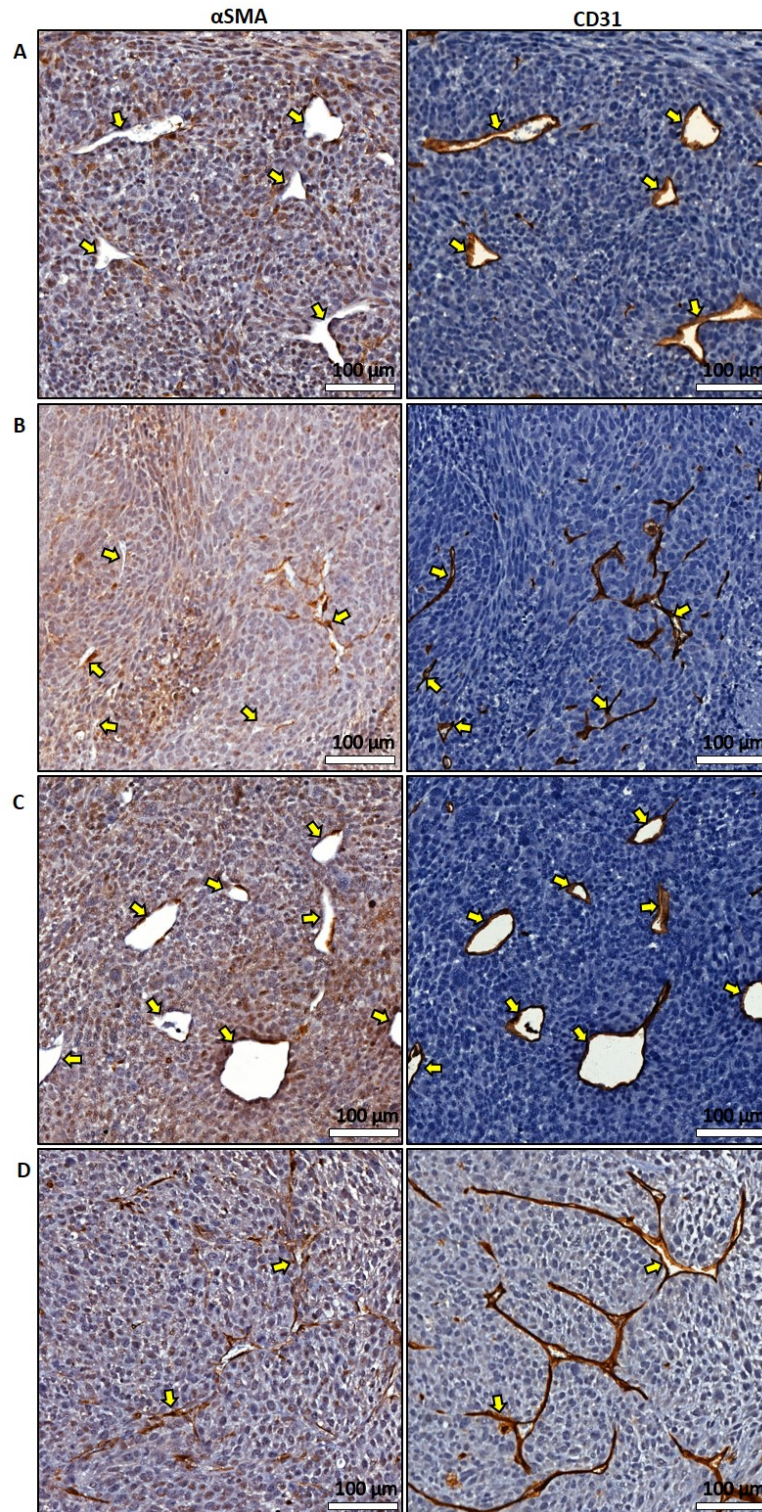


Figure 5.9 Vascular wall maturity in fs188 and fs120 NRP1 modified tumours

Using IHC, near-adjacent tumour sections were stained for α SMA and CD31 and counterstained with haematoxylin. The presence of vascular associated α SMA +ve pericytes was assessed using a 1-4 scale. A) 1 - vast majority of vessels were negative for α SMA, B) 2 – presence of some α SMA positive vessels but the majority were α SMA negative C) 3 – majority, but not all of vessels were α SMA positive with some only weakly positive vessels or D) 4 – vast majority of vessels showed strong α SMA staining. Arrows indicate the same blood vessels in paired images. Sections were scored on a blind basis. Figures are presented as the total number of tumours in each group that scored the corresponding scores. All images at captured at 20x magnification from whole slide scanning.

5.9 Collagen expression in fs188 NRP1 KD and fs120 NRP1 OE tumours

Fs188 and fs120 tumours display different tumour stromal features. Tumours derived from fs188 cells exhibit intense stromal activation characterised by increased myofibroblast recruitment in comparison to fs120 tumours. In a co-implantation tumour model of mouse embryonic fibroblasts (MEF) and lung carcinoma cells, NRP1 expression was found to increase fibronectin fibril assembly via promoting integrin activation resulting in a more desmoplastic and aggressive phenotype (Yaqoob *et al.*, 2012). Previously, fs tumours expressing only VEGF120 were found to have significantly lower levels of collagen than those expressing only VEGF188, furthermore the fs120 cells themselves expressed lower levels of collagen-1 *in vitro* (English *et al.*, 2017). Interestingly, NRP1 overexpression in hepatic stem cells has also been shown to directly promote collagen secretion (Cao *et al.*, 2010). To investigate whether tumour associated-NRP1 expression levels effected the stromal composition of VEGF188 and VEGF120-expressing tumours, in particular with regard to collagen, Masson's trichrome staining was carried out. Qualitative assessment using a scoring system of 1 - 4 with 1 being low levels of ECM collagen and 4 being high, showed that contrary to previous findings, collagen was detectable in both fs120 and fs188 tumours, regardless of NRP1 expression levels (Table 5.2 & Figure 5.10A). Furthermore, visual assessment suggested the fs120wt tumours had slightly higher ECM collagen than the fs188 tumours, with 7/8 fs120wt tumours scoring 3 and above in comparison to only 3/8 of the fs188wt tumours achieving the same score (Table 5.2). Additionally, in NRP1 low fs188 tumours there was tendency toward an increase in ECM collagen, more so in the fs188^{3CE7} tumours than fs188^{3BD6} tumours (Table 5.2). The expression pattern of collagen in the fs120wt tumours seemed to be diffuse throughout the tumours, and in agreement with English *et al.* 2017, there appeared to be less collagen associated with the vasculature. Dilated vessels in the fs188wt and fs188^{3CE7}, of which there were relatively low numbers in comparison to the VEGF120-expressing tumours, tended to have more vessel-associated collagen than VEGF120-expressing tumours (Figure 5.10B). Conversely, in fs188^{3BD6} tumours, collagen associated with the dilated vessels appeared to be less pronounced and more similar to that of the fs120wt and fs120^{G3} tumours (Figure 5.10B). In the VEGF120-expressing tumours, the association of collagen with the dilated vessels was generally poor, yet collagen staining throughout the ECM of fs120^{G3} was consistently high and slightly higher than that of fs120wt tumours (Table 5.2). The caveat these observations are that currently they are purely subjective and require further corroboration; with that said, assessment of the level of collagen staining was carried out on a blind basis.

Tumour/ collagen deposition score	1	2	3	4
Fs188wt	1	4	2	1
Fs188 ^{3BD6}	0	1	4	2
Fs188 ^{3CE7}	1	0	2	5
Fs120wt	0	1	5	2
Fs120 ^{G3}	0	0	0	7

Table 5.2 Collagen scoring in untreated fs tumours

FFPE tumour sections of fs188wt, fs188^{3BD6}, fs188^{3CE7}, fs120wt and fs120^{G3} tumours treated with control IgG stained with Masson's trichrome (Materials and methods section 2.15) were qualitatively assessed on the level of ECM associated collagen and given a score from 1 to 4; 1 being relatively low levels of collagen up to 4 which is indicative of high levels of collagen. Assessment was carried out independently and on a blind basis. Figures are presented as the total number of tumours in each group that scored the corresponding scores.

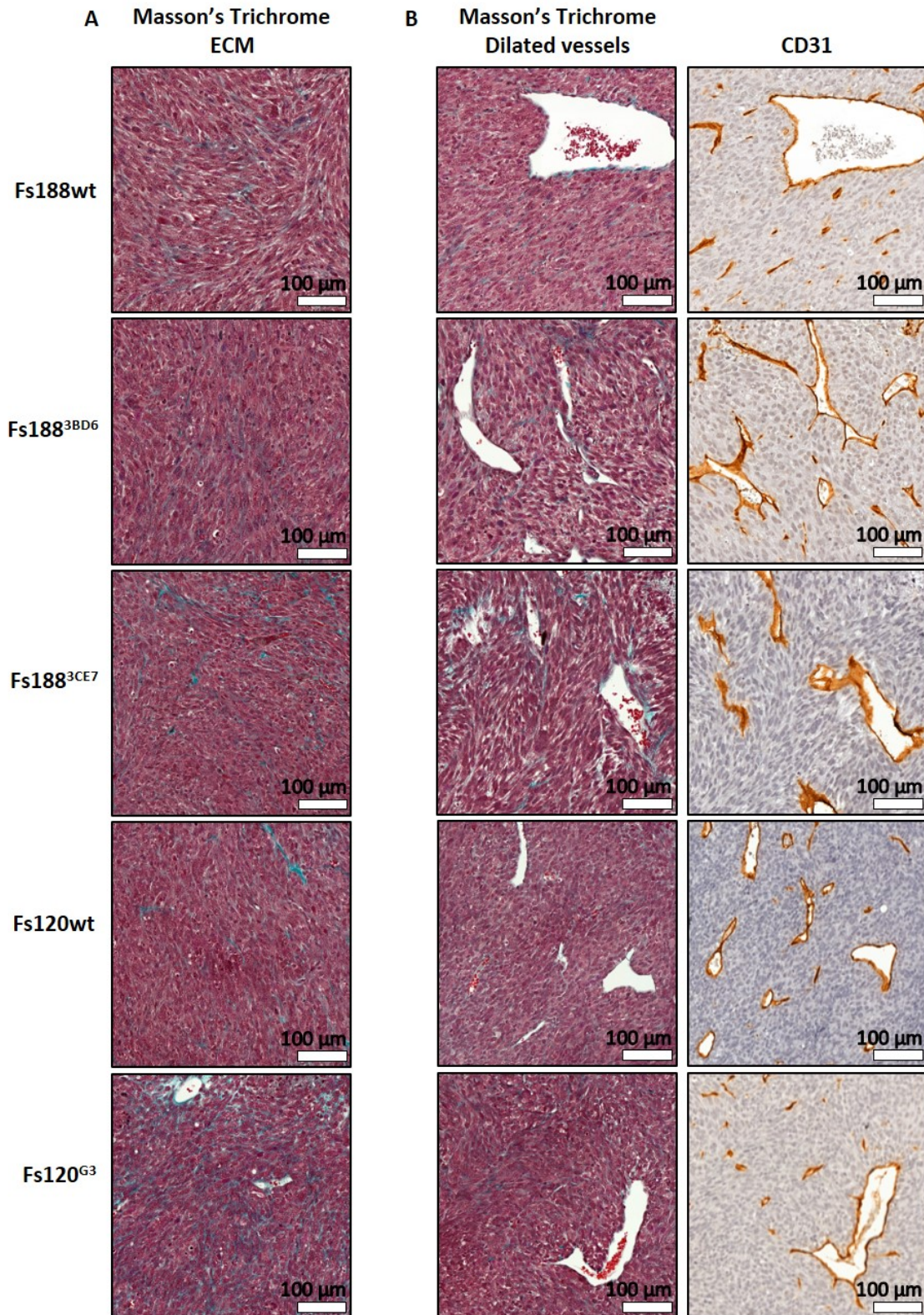


Figure 5.10 Collagen expression in fs188 and fs120 NRP1 modified tumours

FFPE tumour sections of fs188wt, fs188^{3BD6}, fs188^{3CE7}, fs120wt and fs120^{G3} tumours treated with control IgG and stained with Masson's trichrome (Materials and methods section 2.15). Representative images of A) ECM collagen expression and B) tumour areas containing dilated vessels matched to corresponding CD31 stained sections to visualise vessel-associated collagen. Collagen (light green), muscle fibres/ haemoglobin/ keratin (red) and cytoplasm/ adipose cells (light red/pink). All images at captured at 20x magnification from whole slide scanning.

5.10 Discussion

The primary aim of this chapter was development of an *in vivo* tumour model utilising the NRP1 modified fs188 and fs120 cells developed during Chapter 4. This model was then used to study whether NRP1 expression might play a role in previous *in vivo* differences identified in these cell lines (Tozer *et al.*, 2008a, Akerman *et al.*, 2013, English *et al.*, 2017) or whether it influenced the response of tumours to the anti-VEGF agent B20-4.1.1. Tumour growth, vascularity, tumour ECM composition and fs cell proliferation *in vivo* were analysed to assess any differences.

Previous animal models in which tumour-associated NRP1 was depleted have produced variable results in terms of the impact this had on initial tumorigenesis (Misra *et al.*, 2012, Koch *et al.*, 2014, Li *et al.*, 2016a). Li *et al.* (2016a) reported only half of the mice injected with NRP1 depleted gastric tumour cells formed s/c tumours, whereas parental cells formed s/c tumours in 9/10 of the mice. Furthermore, melanoma cells expressing only VEGF₁₈₉ and no NRP1 (Yu *et al.*, 2002) and NRP1 KD in human fs cells (HT1080) and has been shown to result in a complete abrogation of tumour growth (Misra *et al.*, 2012). Similarly to Misra *et al.* (2012), NRP1 KD in the fs188 cells did not lead to any significant reduction in proliferation rates *in vitro*. Furthermore, NRP1 KD did not impact on the anchorage-independent growth of fs188 cells, whereas in HT1080 cells, NRP1 KD significantly reduced their ability to form colonies *in vitro* (Misra *et al.*, 2012). HT1080 and fs188 cells are both Ras mutated (N-Ras and H-Ras respectively) which ordinarily confers tumourigenic properties and ability to grow in an anchorage-independent manner (Pylayeva-Gupta *et al.*, 2011). How NRP1 depletion interfered with anchorage independent growth in the HT1080 cells without affecting their proliferation was not clear, however, given that both fs188 and HT1080 cells harbour Ras mutations it is unlikely to be through this pathway. *In vitro* studies in PDAC have found that inhibitory effects of NRP1 KD on anchorage-independent growth were not only cell line dependent but also assay dependent (Borchardt *et al.*, 2019). Colony forming assays carried out by Misra *et al.* (2012) were performed in soft agar and in this current study a thick collagen matrix was used; this might suggest that anchorage-independent growth following NRP1 KD is reliant on surrounding matrix as fs188 cells themselves express high levels of collagen (English *et al.*, 2017). Unlike the fs188 cells, the HT1080 cells used during the Misra *et al.* (2012) study express VEGFR2 that is phosphorylated upon the addition of exogenous VEGF, this might suggest that HT1080 tumours require VEGFR2/ VEGF/ NRP1 interactions to support autocrine signalling and proliferation as well as vascularisation. In breast cancer, experimental data suggests that VEGF₁₆₅, but not VEGF₁₂₁, can act in an autocrine manner via NRP1 to enhance cell survival (Bachelder *et al.*, 2001). However, using the same breast cancer cell line (MDA-MB-231) engineered to express VEGF₁₈₉ or VEGF₁₆₅ individually, NRP1 depletion exacerbated

apoptosis in VEGF₁₈₉ expressing cells whilst having no effect in VEGF₁₆₅ expressing cells and slightly increasing cell viability in the control cells (Vintonenko *et al.*, 2011). The absence of any change in proliferation following NRP1 modification in the fs cells are more in keeping with Cao *et al.* (2008), who found that in RCC, even though NRP1 resulted in a decrease in AKT phosphorylation, it did not translate to any significant differences in proliferation or apoptosis. In ovarian surface epithelial cells, although higher NRP1 expression at G2/S phase than G0/G1 phase suggested a correlation with proliferative activity, at the point where proliferation was most pronounced, NRP1 expression was in fact reduced (Baba *et al.*, 2007). The inconsistencies surrounding NRP1s influence on proliferation and apoptosis have still not been fully resolved and are deeply complex; it is most likely that they result from the involvement of different cell-specific signalling pathways. In a fibrosarcoma model, high tumour-associated NRP1 has been shown to suppress tumour initiation, growth and vascularisation by increasing the VEGFR2/VEGF/NRP1 juxtacrine (*trans*) interactions between tumour and ECs thus leading to an arrest in VEGFR2 internalisation and signalling (Koch *et al.*, 2014). However, in the same study, Koch *et al.* (2014) found that tumour NRP1 expression levels had no effect on tumour initiation in a melanoma model provided NRP1 was also expressed by the ECs. These data suggest that interactions between NRP1 and VEGFR2 guiding tumour initiation and vascularisation are likely to be dependent on multiple factors. In the current model, the reduction of VEGFR2/ VEGF/ NRP1 complexes following NRP1 KD, may not be as detrimental to tumour initiation and suggests that NRP1s role in the fs188 cells with other receptors may be more dominant for this particular function.

In the fs188 tumour model, NRP1 KD did not inhibit tumour initiation which, given the *in vitro* data, was not entirely unexpected. NRP1 KD in the fs188 cells did however significantly retard tumour growth and, on average, fs188 NRP1 KD tumours were 32% smaller than fs188wt tumours at the experimental end-point. These data are consistent with studies in other cancers that have also reported slowing of tumour growth following NRP1 KD (Misra *et al.*, 2012, Li *et al.*, 2016a, Vivekanandhan *et al.*, 2017, Zhang *et al.*, 2017a, Shi *et al.*, 2018). In contrast to other *in vivo* models in which NRP1 has been depleted (Li *et al.*, 2016a, Vivekanandhan *et al.*, 2017), this deceleration in fs tumour growth could not be attributed to a reduction in the proliferative capabilities of the tumour cells. Consistent with *in vitro* results, quantification of IHC for Ki67 in fs tumour tissue showed no significant difference in proliferation between wt and NRP1 modified fs cells. Taken together with the *in vitro* data, this suggests that NRP1 does not play a determining role in tumour cell proliferation as such. This lack of correlation between proliferation rates *in vitro* and tumour growth *in vivo* following NRP1 KD has also been reported in GBM. However, although shRNA mediated NRP1 KD in GBM cells did not affect *in vitro* proliferation, unlike NRP1 KD in the fs188 cells, it led to larger *in vivo* tumours

(Kwiatkowski *et al.*, 2017). Whilst these data showing that NRP1 has growth suppressive functions in GBM contradict the majority of published studies that associate high NRP1 expression with the promotion of tumour growth, they are in agreement with the NRP1 OE fs120 model which also showed NRP1 low fs120wt cells forming larger tumours than NRP1 high fs120^{G3} cells. In pancreatic cells, that reportedly lack NRP1 co-receptors, NRP1 OE has also been shown to suppress anchorage-independent growth and migration through VEGF/Sema3a-independent mechanisms *in vitro* and lowered tumour volume *in vivo* (Gray *et al.*, 2005). Although these results are seemingly contradictory to the fs188 data, they are consistent with the notion of NRP1 having opposing roles in tumorigenesis that is context dependent (Vivekanandhan *et al.*, 2017). Vivekanandhan *et al.* (2017) have presented data showing that NRP1 KD in KRAS mutated PDAC cells promoted tumour formation, whilst in wt KRAS NSCLC cells NRP1 KD suppressed tumour incidence. Additionally, upon examination of published literature they found that in tumours with wt KRAS, NRP1 acted as a tumour promoter, whereas in tumours with oncogenic KRAS, NRP1 acted as a tumour suppressor (Vivekanandhan and Mukhopadhyay, 2019). Fs188 and fs120 cells are both H-Ras mutated, so this doesn't explain the why both NRP1 KD in the fs188 cells and NRP1 OE in the fs120 cells both resulted in smaller tumours. However, it opens up the possibility that mutations in other oncogenes that have not yet been identified could influence the consequences of NRP1 expression levels. The inconsistent data surrounding the function of NRP1 in tumour cells highlights its complex nature as a co-receptor that is involved in numerous signalling pathways. HGF (Panigrahy *et al.*, 2014), Sema3a and VEGF₁₆₅ (Miao *et al.*, 1999, Palodetto *et al.*, 2017) have been identified as competitive ligands that can influence both paracrine and autocrine signalling through NRP1 (Bachelder *et al.*, 2003, Hu *et al.*, 2007), therefore the differential availability of ligands and associated receptors both endogenously and in the tumour cells themselves are highly likely to be influential factors.

The effect of tumour associated NRP1 on angiogenesis is not clear cut and appears to be dependent on multiple factors. In glioma for example, U87MG-NRP1 OE cells resulted in larger tumours and increased angiogenesis, which was attributed to the potentiation of autocrine HGF/NRP1/c-MET signalling pathways alongside juxtacrine NRP1/VEGF interactions between EC and tumour cells (Hu *et al.*, 2007). In GBM however, NRP1 KD enhanced tumour vascularisation which was driven by competitively modulation of TGF β and VEGF signalling (Kwiatkowski *et al.*, 2017). Quantification of CD31 staining found no significant difference in vascular area or density between untreated fs188wt and fs188 NRP1 KD tumours. In the fs120 tumours, vascular area but not density increased following NRP1 OE. This increase brought the vascular area of fs120^{G3} tumours to a level comparable with that of fs188wt and fs188^{3BD6} tumours but not fs188^{3CE7} tumours. The original hypothesis was that NRP1

had a role to play in the morphological differences between the vessels in fs188wt and fs120wt tumours; given that depletion of NRP1 in fs188 tumours did not lead to any obvious changes in vascular morphology or reduce vascularity to levels comparable with fs120wt tumours, it seems unlikely that this is the case. The results of CD31 quantification in untreated tumours differ from early studies, in that the fs188wt tumours were significantly more vascular than the fs120wt tumours, in terms of both vascular area and vessel density. They do however agree with lung tumour xenograft models that found overexpression of VEGF₁₈₉ resulted in higher vessel density than that of VEGF₁₂₁ tumours (Yuan *et al.*, 2011) and in VEGF189 overexpressing breast cancer cells that resulted in hypervascularised tumours (Hervé *et al.*, 2008). Original *in vivo* findings with these cell lines showed the opposite results for vascular area (Tozer *et al.*, 2008a), whereas results in a subsequent study (Akerman *et al.*, 2013) were consistent with the current results. In the original study the Chalkley method (Chalkley, 1943), a random point scoring method using a microscope eyepiece graticule, was used which included CD31-negative vascular lumens in vascular area measurements, as opposed to the positive pixel counting technique used in the current study and by Akerman *et al.* (2013). The decision to use a computerised image analysis system to determine vascular density was in part influenced by the lack of a second observer being available to verify the results. The “hot-spot” (Weidner *et al.*, 1991) and the use of a Chalkley grid (Chalkley, 1943) to assess microvascular density are open to differences in interpretation, therefore this variability can be partially mitigated by using a software package that, after initial parameter setting, is able to quantify the level of CD31 staining in a uniform manner in each section. The three studies are consistent in that large open vessels tended to be more prevalent in fs120wt than fs188wt tumours, which could account for the relatively large vascular area measurements made for fs120wt tumours in the original study. Although it failed to reach significance, the fs120^{G3} tumours tended to have fewer large open vessels than the fs120wt tumours. These observations are suggestive of tumour-associated NRP1 having an influential role over vascular branching in this particular model. Contrary to early studies (Gitay-Goren *et al.*, 1996, Soker *et al.*, 1996, Soker *et al.*, 1998), it is now thought that VEGF_{120/121} can bind directly to NRP1, albeit at a lower affinity than that of VEGF_{164/165} and with the caveat that, in PAE cells, it cannot bind VEGF₁₂₁ in the absence of VEGFR2 (Pan *et al.*, 2007b, Parker *et al.*, 2012a, Parker *et al.*, 2012b, Delcombel *et al.*, 2013). Furthermore, co-expression of NRP1 and VEGFR2 on PAE cells increases the binding affinity of VEGF₁₂₁ to VEGFR2 and enhances VEGFR2 signalling. Notably, the same study suggests that NRP1 can enhance VEGF₁₂₁ mediated VEGFR2 signalling via mechanisms that differ from VEGF₁₆₅ in the absence of bridging the two receptors (Sarabipour and Mac Gabhann, 2018). There is currently a lack of data exploring these interactions *in vivo* therefore, whether these interactions occur and their effects are unknown. In the absence of any *in vitro* data, it is not possible to comment on whether NRP1 OE in

fs120 cells has impacted on VEGFR2 phosphorylation in the current model. There is also the possibility that NRP1 OE in the fs120 cells upregulates other angiogenic factors that could influence vessel branching.

Selecting the most appropriate EC marker for quantification of tumour angiogenesis is a complex issue that requires careful consideration. Whilst the most commonly used EC markers include CD31, CD34, von Willebrand Factor (vWF, factor VIII-related antigen) (Müller *et al.*, 2002), VE-cadherin and CD105 (endoglin) (Yao *et al.*, 2005, Seaman *et al.*, 2007), this is not an exhaustive list and there are many other markers that have been found to be expressed by endothelial cells in various tissues. The body of literature surrounding selection of the most appropriate marker reflects the heterogeneity of EC phenotypes and as a result there is no one single marker that is considered as being reliable across all tumours and tissues. During this study, the widely used pan-endothelial marker CD31 was used to assess tumour vascularity as it is generally accepted to be expressed on most EC phenotypes (Scholz and Schaper, 1997). Although this provided a clear representation of the overall vascular structure within the tumours, CD31 doesn't provide any further information with regard to the maturation status or origin of the vessels and, as noted in the Materials and Methods (Section 2.14). CD31 is also expressed by a selection of mononuclear cells such as macrophages and lymphocytes (Pusztaszeri *et al.*, 2006). As depicted in Figure 2.10, populations of CD31 positive cells within the fs tumours that were not thought to be ECs were evident, and it was assumed that these were macrophages. Although these were discounted from tumour vascularity analyses, it cannot be said with any degree of certainty that these were macrophages and not ECs. CD34 is also regarded as a sensitive, yet less specific, EC marker (Fina *et al.*, 1990) that is upregulated during angiogenesis, but as with CD31, its expression is not limited to ECs and CD34 is reported to be expressed on hematopoietic cells from all lineages (Krause *et al.*, 1996, Sauter *et al.*, 1998, Ordóñez, 2012). An *In vitro* HUVEC model characterised CD34 positive cells to be representative of the tip cell phenotype, furthermore, in human tumours strong CD34 staining of EC filapodial extensions was detected at active angiogenic sites *in vivo* (Siemerink *et al.*, 2012).

In relation to the status of the fs tumour vessels, i.e. whether they were actively proliferating, quiescent or mature vessels, although CD31 is regarded as more sensitive than CD34 and vWF (Ordóñez, 2012), the use of further EC markers might have provided more information. *In vivo*, CD105 is more frequently associated with activated ECs that are proliferating and participating in angiogenesis whereas the expression of CD34 or vWF is associated with differentiated ECs and mature vessels (Wang *et al.*, 1994, Tanaka *et al.*, 2001). Studies in BC and NSCLC have shown that, contrary to

the large amounts of CD105 detected on ECs within tissues undergoing angiogenesis, weak to no expression of CD105 was detected in normal tissues (Kumar *et al.*, 1999, Tanaka *et al.*, 2001). In terms of alternative ways that tumours can vascularise, the use of CD105 in conjunction with other pan-endothelial markers such as CD31 or CD34 could be a useful marker in differentiating between vessels that have been co-opted and vessels resulting from sprouting angiogenesis. A limited number of published studies in sarcoma have identified Friend leukaemia integration-1 (Flt-1), a member of the erythroblast transformation specific (ETS) family, as a reliable pan-endothelial marker but, as with CD31 and CD34, there is some overlap between expression patterns between ECs and hematopoietic cells so interpretation of the data it provides has to be carefully considered (Folpe *et al.*, 2001, Puztaszeri *et al.*, 2006). A related member of the ETS family, ETS related gene (ERG), is emerging as a sensitive marker for EC differentiation that is involved in angiogenesis and EC migration. This potentially more specific vascular marker is reported to be exclusively expressed on ECs, although it is not known whether it is specific for certain phenotypes of ECs (Ordóñez, 2012, Naeem *et al.*, 2018). The use of a single EC marker during the current study somewhat limits the conclusions that can be drawn in terms of vascular structure of the tumours. Further analysis with other EC markers would have been beneficial in providing further insight into how NRP1 expression together with VEGF isoforms effects the tumour vasculature both with and without anti-VEGF therapy.

Differences in vascular patterning have been identified in tumours expressing single VEGF isoforms using a similar fs model as ours (Grunstein *et al.*, 2000) and in experimental models of metastatic melanoma (Küsters *et al.*, 2003) and glioma (Cheng *et al.*, 1997). In the single VEGF-isoform expressing fs model, VEGF188 expression is associated with high pericyte recruitment and improved vessel function in comparison to VEGF120 tumours which display a more fragile vasculature with poor pericyte coverage (Tozer *et al.*, 2008a, Akerman *et al.*, 2013). NRP1 is associated with increased activation of fibroblasts that are prominent features in desmoplastic tumours. NRP1 directly engages with FN to promote FN fibril assembly and integrin activation and promotes collagen deposition (Cao *et al.*, 2010, Yaqoob *et al.*, 2012, Matkar *et al.*, 2016). It was therefore hypothesised that high versus low NRP1 expression in the fs188 and fs120 cells respectively may contribute to these vascular differences and furthermore may result in a more desmoplastic phenotype. In concordance with the original data (Tozer *et al.*, 2008a) and , IHC for α SMA identified higher vascular associated staining patterns in VEGF188 tumours than VEGF120 tumours that were assumed to be pericytes, regardless of NRP1 modification. The correlation of NRP1 OE with more α SMA positive pericytes in the fs120⁶³ tumours might suggest that, in a scenario where short VEGF isoforms predominate, NRP1 participates

in vessel stabilisation and maturity. Extravascular α SMA positive cells were also identified across all the tumours, however whether or not these were activated fibroblasts is unclear, as unpublished data from Dr Will English indicated that the fs cells themselves express α SMA (W English, personal communication). In human PDAC xenografts, Matkar *et al.* (2016) found a positive correlation between NRP1 expression and collagen content along with increased expression of EndMT and pro-fibrotic (α SMA and CTGF) makers. Using an orthoptic model of PDAC in athymic rats, modest but significant KD of NRP1 was achieved with shNRP1. The result was a reduction in tumour fibrosis, tumour load, microvascular blood volume and blood flow (Matkar *et al.*, 2016). Masson's trichrome staining did not identify any observable difference in collagen deposition between fs188wt and fs120wt tumours, which contradicted English *et al.* (2017), however in agreement with original findings, there was clearly less vessel-associated collagen in the fs120wt tumours than in the fs188wt tumours. These differences may have arisen as a result of the techniques used to detect collagen; English *et al.* (2017) used immunofluorescence staining on frozen tissue, whereas Masson's trichrome was carried out in FFPE tissue. Additional differences such as the length of time tumours were allowed to grow and the fact that fs188 and fs120 cells had been modified to express luciferase may have contributed to some of the differences between the current study and work by English *et al.* (2017). NRP1 OE in fs120 tumours led to noticeably more collagen levels within the tumour stroma, but unexpectedly, so did NRP1 KD in the fs188 tumours. Interactions between NRP1 and integrins have still to be fully elucidated. In ECs, functioning as a co-receptor for VEGF₁₆₅ and independently of ligand binding, NRP1 can modulate activation and internalisation of integrin α 5 β 1 thus influencing the deposition of ECM proteins (Valdembri *et al.*, 2009). Whether or not other VEGF isoforms modulate endocytosis and α 5 β 1 recycling in quite the same manner is unknown.

Although the prognostic value of NRP1 has been well documented, its predictive potential is less clear. Likewise, there is a shortage of studies that have explored the possibility that long VEGF isoforms might hold predictive potential with regard to anti-VEGF therapy. Some clinical biomarker studies have suggested that low baseline levels of NRP1 may be useful in stratifying patients that would gain the greatest benefit from treatment with bevacizumab (Jubb *et al.*, 2011, Van Cutsem *et al.*, 2012, Lambrechts *et al.*, 2013, Benson *et al.*, 2016), whereas others could find no association between NRP1 expression and treatment efficacy (Miles *et al.*, 2013, Baumgarten *et al.*, 2015). A recently published study has suggested that the presence of cancer-derived small extracellular vesicles (sEVs) enriched with dimeric VEGF₁₈₉ (sEV-VEGF) hold the potential to be predictive of resistance to bevacizumab (Ko *et al.*, 2019). Previously it was thought that bevacizumab neutralises all VEGF isoforms (Ferrara *et al.*, 2004), yet Ko *et al.* (2019) have challenged this view, suggesting that conformational differences

between membrane bound VEGF and soluble VEGF may influence the ability of bevacizumab to neutralise VEGF189 when associated with high molecular weight heparin. Furthermore, analysis of 17 patient plasma samples from a phase II trial in Stage IV mRCC found levels of sEV-VEGF were nearly five times higher in patients with progressive disease after bevacizumab treatment than those with stable or regressing disease (Ko *et al.*, 2019). In the fs model used during the current study, anti-VEGF treatment with B20-4.1.1 slowed tumour growth in VEGF188 expressing tumours regardless of their NRP1 expression levels. However, low NRP1 expression in the fs188 NRP1 KD tumours appeared to confer an improvement in initial response of tumours to anti-VEGF treatment in comparison to fs188wt tumours. In contrast, NRP1 OE in VEGF120 tumours led to a significant reduction in tumour growth following treatment with B20-4.1.1 in comparison to endogenously low NRP1 expressing VEGF120. Although the latter results are contradictory to clinical data, this study illustrates that NRP1 expression levels that are divergent from initial baseline levels appear to influence tumour growth rate following anti-VEGF treatment. Additionally, they strongly suggest that any predictive value that NRP1 may have is context dependent. Contrary to both clinical and preclinical data (English *et al.*, 2017, Martini *et al.*, 2018), B20-4.1.1 retarded tumour growth in the fs188wt tumours, however it failed to have the same effect in the fs120wt tumours. One possible explanation for this discordance with previous studies using the fs cells, is the more aggressive treatment regimen used in comparison to English *et al.* (2017). Preclinical studies have suggested that anti-VEGF therapy can have opposing effects on tumour growth depending on the dosing schedule and that a more aggressive treatment strategy might actually accelerate tumour progression (Ebos *et al.*, 2009, Pàez-Ribes *et al.*, 2009). In the current study anti-VEGF treatment commenced once tumours reached 100 mm³ whereas in the original study by English *et al.* (2017), treatment did not start until tumours reached 200mm³. Additionally, in the current study a slightly more aggressive dosing regimen was employed for the first three B20-4.1.1 doses, as they were administered every other day as opposed to every two days.

B20-4.1.1 treatment had a significant anti-vascular effect on all VEGF188 tumours, regardless of the level of NRP1 expression. In 120wt tumours no appreciable differences in vascularity were found between treatment groups, which although differs from the previous study with these tumours (English *et al.*, 2017), it likely accounts for the similar growth kinetics between both treated and untreated groups. That said, although there was a tendency towards decreased vascularity in B20-4.1.1 treated fs120^{G3} tumours that failed to reach significance. In a preclinical model of ovarian granulosa cell tumour (GCT) results suggested that anti-VEGF therapy acted directly on the tumour cells themselves, however, it was unclear as to which signalling pathway this was as a result of (Tsoi *et al.*, 2013). Taken in the context of the current model, this might suggest that interruption of

autocrine VEGF signalling by B20-4.1.1 was in part responsible for retarded tumour growth of fs120^{G3} tumours. Future *in vitro* studies such as comparing fs120^{G3} proliferation in the presence or absence of B20-4.1.1 may be able to provide a clearer picture of whether or not this is the case. Having said that, whilst *in vitro* studies are undoubtedly useful in determining whether B20-4.1.1 directly effects fs120^{G3} cells it doesn't account for the diffusion of VEGF₁₂₁ to other tissues and the effect this has on potentially diluting the anti-tumour effects of bevacizumab *in vivo*. Using a melanoma xenograft model, it has been demonstrated that VEGF isoform expression dictates tumour specific uptake of bevacizumab. In melanoma xenografts exclusively expressing VEGF₁₆₅ and VEGF₁₈₉, tumour specific bevacizumab uptake was significantly higher than in tumours expressing VEGF₁₂₁ (Stollman *et al.*, 2009). Considering the diffusible nature of VEGF₁₂₁, this is not particularly surprising, but if indeed bevacizumab does act directly on tumour cells and not just tumour vasculature, then it follows that VEGF isoforms have some potential for predicting primary tumour response to anti-VEGF treatment.

Vessel maturation and integrity have been implicated in the response of tumours to vascular-targeted therapies. Anti-VEGF therapy can transiently redress the balance of pro- and antiangiogenic signalling to induce vascular normalisation, which is characterised by the pruning of immature vessels, an increase in vessel stability and greater investment of pericytes (Jain, 2001, Jain, 2003). Fs tumours expressing only VEGF₁₂₀ have been suggested to be more susceptible to VEGF pathway inhibitor-induced vascular normalisation than VEGF₁₈₈ expressing tumours (Akerman *et al.*, 2013) and a tendency for an increase in pericyte positive vessels was previously seen in fs120 tumours following B20-4.1.1 treatment (English *et al.* 2017). Results here were in partial agreement with English *et al.* (2017), in so far that treatment with B20-4.1.1 had no obvious effect on the vascular integrity of fs188wt tumours, yet in the small number of fs120wt tumours stained for α SMA there were no obvious changes in vessel associated pericytes. NRP1 OE in the fs120^{G3} tumours did appear to correlate to a reduction in vascular pericytes following anti-VEGF treatment suggesting that high tumour associated NRP1 expression in this system suppressed vascular normalisation. Given that NRP1 is a co-receptor for numerous ligands that are regarded as proangiogenic, and has been shown to modulate TGF β signalling (Kwiatkowski *et al.*, 2017), it stands to reason that blockade of VEGF alone in an environment where NRP1 is grossly overexpressed is not enough to equilibrate the imbalance of angiogenic factors.

Taken as a whole, whether or not NRP1 has the potential to be a robust biomarker in the response of fs tumours to anti-VEGF treatment remains to be determined. It obviously has a role to play, however it is likely that this is entirely context dependent. As a result of the fs120 and fs188 cells expressing

different levels of ligands and receptors that are associated with NRP1 and its role as a co-receptor, it is most likely that NRP1 expression levels alone are insufficient in predicting how a tumour will respond to VEGF treatment. Whether NRP1 holds predictive potential for the efficacy of other VEGF specific therapy, such as aflibercept, or the less specific TKIs was outside the scope of this study and warrants further investigation.

Chapter 6

General Discussion and Future work

6.1 Why look at VEGF isoforms and NRP1 in cancer?

Since Judah Folkman first hypothesised the potential of targeting tumour angiogenesis as a cancer treatment (Folkman, 1971), studies into what drives the process and how it could be inhibited have been extensive. Once it was established that VEGF was the master regulator of angiogenesis and was expressed almost ubiquitously at high levels across the majority of malignant tumours (Goel and Mercurio, 2013), development of therapeutic agents that could interrupt the VEGF signalling cascade commenced. VEGF exists as multiple isoforms that arise from alternative splicing of the VEGFA gene or through proteolytic cleavage. The major human isoforms, VEGF₁₂₁, VEGF₁₆₅ and VEGF₁₈₉ (VEGF₁₂₀, VEGF₁₆₄ and VEGF₁₈₈ in mice) differ in their affinity to the ECM and differentially bind to VEGFRs and the co-receptor NRP1 (Vempati *et al.*, 2014, Fearnley *et al.*, 2016). FDA-approval of bevacizumab in 2004, a VEGF blocking antibody that binds all isoforms, led to the development of VEGF pathway targeted therapies that are now used routinely in the clinic which work by directly sequestering VEGF, blocking VEGF binding sites on VEGFRs or through receptor TK inhibition (Ferrara and Adamis, 2016).

STS are a rare group of tumours that have seen limited progress in the expansion of treatment options over the last decade (Casali *et al.*, 2018). In this diverse range of tumours, high VEGF expression correlates with poorer patient prognosis (Chao *et al.*, 2001), therefore targeting VEGF may prove a promising approach for improving patient survival. Indeed, FDA-approval of pazopanib, a multi-TKI, in 2012 has been the most notable progression in treatment for STS in recent years (Van Der Graaf *et al.*, 2012). VEGF pathway inhibitors have undoubtedly improved treatment options in numerous cancers in terms of both OS and PFS. However, the promising preclinical data that accelerated these drugs into the clinic was followed by disappointing clinical results and wildly variable patient responses indicating a 'one size fits all' approach to be suboptimal for this class of drugs (Ferrara and Adamis, 2016, Hegde *et al.*, 2018). Investigation into molecules that might serve as indicators of whether or not a patient is likely to respond to treatment with anti-VEGF therapy have, as yet, failed to identify one single factor that might serve as a robust biomarker. Retrospective analysis of clinical trials led to speculation that the VEGF co-receptor NRP1 and individual VEGF isoforms are potential candidates as predictive biomarkers. Specifically, high circulating levels of the short VEGF₁₂₀ isoform and low NRP1 have been suggested to have predictive potential in terms of identifying patients who will gain the

greatest benefit from the addition of anti-VEGF to their treatment regimen (Van Cutsem *et al.*, 2012, Lambrechts *et al.*, 2013, Miles *et al.*, 2013). The interaction of VEGF isoforms with NRP1 and downstream signalling consequences in tumour cells are still largely unclear and how direct inhibition of VEGF might disrupt this signalling even more so.

The single VEGF isoform expressing mouse fibrosarcomas used in the current study develop distinct vascular characteristics and have shown differing responses to anti-VEGF therapy (Tozer *et al.*, 2008a, Akerman *et al.*, 2013, English *et al.*, 2017). *In vitro* the fs cells are phenotypically distinct, with different morphologies and traits that are associated with their invasive potential (Kanthou *et al.*, 2014, English *et al.*, 2017). During investigations to elucidate the pathways involved in the different fs cell characteristics, NRP1 was identified to be differentially expressed by the fs cells (Kanthou *et al.*, 2014). NRP1 is not only a co-receptor for VEGF, it also binds multiple ligands inclusive of Sema3A, PlGF, HGF, PDGF, bFGF TGF β and EGF, to form complexes with their cognate receptors (Sulpice *et al.*, 2008, Niland and Eble, 2019). Furthermore, NRP1 is found within adhesomes where, through collaboration with specific integrins, it supports tumour stroma activation and ECM stiffening (Yaqoob *et al.*, 2012). NRP1 expression was found to be higher in fs188 and fswt cells than fs120 and fs164 cells (Kanthou *et al.*, 2014). These findings led to the hypothesis that, through its role as a prolific co-receptor, NRP1 might be a key instigator in the distinct fs cell characteristics both *in vitro* and *in vivo*. Moreover, it provided a model system where, through loss and gain of function experiments performed in this thesis, the influence of NRP1 expression levels together with VEGF isoforms could be evaluated as possible predictive biomarkers for anti-VEGF therapy.

6.2 Influence of NRP1 expression with single VEGF isoforms *in vitro*

As a prolific co-receptor for multiple ligands, it is of no surprise that there are still many unanswered questions as to the role NRP1 plays when expressed on different cell types. Numerous studies have been undertaken to elucidate its role in ECs, yet information on the function of NRP1 expression in different cancer cells remains incomplete. Through modifying NRP1 expression on single VEGF isoform expressing fs cells, *in vitro* studies were carried out to unravel whether NRP1 was responsible for some of the phenotypical differences between these cell lines, thus providing information on how modified cells might behave *in vivo*.

Originally, one of the principal aims of this study was to explore mechanistic links between VEGF isoforms and NRP1 in the fs cells *in vitro*. In light of protein array and quantitative proteomics data using an isobaric labelling method that identified differential expression of 160 proteins between the

fs120 and fs188 cells, it became clear that establishing the exact mechanisms using the model developed during the current study was likely to be more complex. Furthermore, next generation sequencing revealed ~1000 genes that differed between fs120 and fs188 tumours (English *et al.*, unpublished data). The discovery that fs cells and tumours were different not only in terms of isoform expression and NRP1, but also differ widely in terms of their protein and gene expression profiles made it more difficult to establish the exact mechanisms through which NRP1 and VEGF isoforms interact to influence cell behaviour and tumour growth. It also meant that direct comparisons could not be drawn between fs120 NRP1 OE cells and fs188wt (NRP1 high) cells or fs 188 NRP1 KD and fs120wt (NRP1 low) cells as originally planned.

6.2.1 *In vitro* Migration

NRP1 knockdown led to a significant reduction in the fs188 cells' ability to migrate *in vitro*, with the effects being more pronounced in the fs188 cells where stable NRP1 KD had been achieved in comparison to transient siRNA NRP1 KD. This reliance on NRP1 for migration in the fs188 cells is in agreement with the vast majority of literature across several different cancers that have associated high NRP1 expression with superior invasion/migration *in vitro* and a more metastatic phenotype *in vivo* (Baba *et al.*, 2007, Cao *et al.*, 2008, Li *et al.*, 2016a, Huang *et al.*, 2018b, Naik *et al.*, 2018). Chapter 4 showed that multiple clones were isolated during the fs188 NRP1 KD cell development. Through WB, ICC and flow cytometry analysis, it was confirmed that at least five of these clones had no or below detectable levels of NRP1, whilst still expressing comparable levels of NRP2. Migration experiments found the two clones taken forward for further study *in vivo*, fs188^{3BD6} and fs188^{3CE7}, not only migrated more slowly than fs188wt cells, but fs188^{3BD6} cells also migrated at a slower rate than fs188^{3CE7} cells. One possible explanation for this is that the methods used to measure NRP1 expression in the clones were not sensitive enough to detect any negligible residual NRP1. Using qRT-PCR to quantify relative NRP1 mRNA expression, a recent study using three different NRP1 expressing nasopharyngeal carcinoma (NPC) cell lines showed a positive correlation between NRP1 expression levels and their ability to migrate and invade (Huang *et al.*, 2018b). Moreover, CRISPRi depletion of NRP1 expression levels in the NPC cell lines resulted in reduced migration and invasion. NRP1 protein expression levels were not published, however, qRT-PCR still detected residual NRP1 expression, albeit at extremely low quantities, in the three different NPC NRP1 KD cells (Huang *et al.*, 2018b). In view of this, carrying out qRT-PCR to analyse NRP1 mRNA expression would have been advantageous in clarifying whether these differences occurred as a result of differing low level residual NRP1 expression.

Conversely, it was found that OE of NRP1 in the fs120 cells, and to a certain extent in the fs164 cells, resulted in a reduction in migration. This was unexpected in so much as it might have been assumed that, given the cell lines are essentially from the same lineage, opposing expression levels of the same protein would lead to contrasting results. The majority of published studies looking at the role of NRP1 in cancer have based their findings on loss of function experiments or through comparison of multiple cell lines with endogenously low versus high NRP1 expression. Studies utilising ectopic overexpression of NRP1 are less frequent, however in the limited number of studies that have used this method, the results are not consistent. In Panc-1 cells NRP1 OE decreased migration relative to the parental cells (Gray *et al.*, 2005), yet in NPC and breast cancer cells NRP1 OE resulted in an increase in migratory rates in relation to unmodified cells (Huang *et al.*, 2018b, Naik *et al.*, 2018).

It could be argued that high overexpression NRP1 in the fs120 cells contributed to the unexpected results shown in Chapter 4, and that if a clone could have been successfully isolated with lower NRP1 expression levels, more in line with endogenous levels in the fs188 cells then this would have been a more relevant model. This is a valid argument, given that more modest overexpression of NRP1 in the fs164 cells did not affect migration to the same degree as the fs164 clone with high NRP1. However, in light of the lack of difference in basal levels of downstream AKT, Src and ERK1/2 and given that proliferation was unaffected, it seems improbable that the high levels of NRP1 were detrimental to the fs120 cells. To ensure that OE of NRP1 did not lead to un-physiological results it would have been beneficial to include an experimental condition of fs120^{G3} plus NRP1 siRNA to determine whether this returned migratory rates to levels comparable with fs120wt cells.

One particular aspect that was not explored further was the specific mode of migration used by the fs cells. The fact that the fs cells are of mesenchymal origin suggests that their preferred method of migration would be 'mesenchymal'. Unlike high NRP1 expressing fs188wt cells, fs120wt and fs164wt cells have the ability to switch between both a rounded amoeboid and mesenchymal mode of migration which, for the fs120 cells at least, may provide them with a metastatic advantage *in vivo* (Kanthou *et al.*, 2014, English *et al.*, 2017). The wound healing assay used during the current study measures the migration rate of cells that favour the more mesenchymal mode of migration, either collectively or in large sheets rather than as single cells. In order to successfully metastasise, tumour cells must invade the ECM, intravasate successfully, survive in the circulation and arrest and extravasate at the distant site. To achieve this, they generally undergo EMT to adopt a more migratory phenotype, but also it is important that they display plasticity and ability to switch from a mesenchymal to an amoeboid phenotype and survive in the circulation. NRP1 has been identified as

playing a regulatory role in the ability of cells to undergo EMT (Chu *et al.*, 2014, Luo *et al.*, 2016, Matkar *et al.*, 2016). Transwell migration and matrix invasion assays would have provided a more comprehensive analysis of the role of NRP1 during migration *in vitro* and their likely metastatic potential *in vivo*.

6.2.2 *In vitro* Signalling

In seeking to identify the mechanisms underpinning the reduced migration kinetics of fs cells following NRP1 modification, the basal expression levels of a small number of protein kinases associated with cellular migration were analysed. During transient KD of NRP1 basal levels of pERK-1/2 increased, which was not recapitulated following stable NRP1 KD. Furthermore, no significant differences were found in basal levels of pAKT or pSrc between fs188wt cells and either of the fs188 NRP1 KD clones. Results from the fs cell model developed during the current study are concordant with an early study in panc-1 cells that showed both NRP1 OE and NRP1 expression but without the VEGF/SEMA3a domain, resulted in a reduction in migratory rate (Gray *et al.*, 2005). Yet, Gray *et al.* (2005) also reported an inverse correlation of basal levels of total AKT, pERK-1/2 and pAKT in response to NRP1 expression, which was only evident in the fs188s when NRP1 expression was depleted through siRNA but not evident in the stably modified fs cells. Given that proliferation and survival are associated with the MAPK and PI3K pathways, and ERK and AKT phosphorylation can be measured, perhaps the lack of significant changes are not wholly unexpected, as proliferation rates of the modified fs cells remained comparable to their parental counterparts.

In gastric cancer (MGC-803 cells), NRP1 depletion has been shown to inhibit VEGF₁₆₅, EGF and HGF activated pathways. In the case of the VEGF₁₆₅ activated pathway, siRNA inhibition of VEGFR2 in parallel to NRP1 depletion resulted in a reduction in pFAK, which is a key factor in migration (Li *et al.*, 2016a). This was not an avenue that was explored during the current study, in part due to previous work with the fs cells that has shown a lack of VEGFR2 activation, and subsequent downstream signalling in the presence of VEGF (Kanthou *et al.*, 2014). Using RNA-seq, Naik *et al.* (2018) identified differentially expressed genes following NRP1 OE in BT-474 breast cancer cells, one of which was TNC. TNC encodes the glycoprotein tenascin c, which signals via integrins. Subsequent experiments showed the NRP1 OE in BT-474 cells triggered global changes, one of which was activating the integrin $\beta 3$ pathway via FAK which was dependant on TNC expression. Given the absence of any change to basal levels of the proteins analysed in the current study, the FAK pathway and integrin activation pathways warrant further investigation.

Studies in human glioma and pancreatic cancer cells showed that NRP1 expression potentiated cMET signalling in response to HGF (Hu *et al.*, 2007, Matsushita *et al.*, 2007), therefore the effects of HGF stimulation were analysed on the NRP1 modified fs cells. This further emphasised clonal variations between fs188^{3BD6} and fs188^{3CE7}. In fs188^{3CE7} cells, since incubation with exogenous HGF resulted in cMET activation and induced downstream phosphorylation of ERK-1/2 and AKT in fs188^{3CE7} cells whilst in fs188^{3BD6}, cMET activation was not detected and Src was phosphorylated. In fs120 cells the overexpression of NRP1 had no significant effect on HGF induced cMET activation in comparison to fs120wt cells, yet downstream kinase phosphorylation was subtly different between the two cell lines. In NRP1 high fs120^{G3} cells HGF induced ERK-1/2 phosphorylation was stronger, yet in fs120wt cells it was pAKT that was more highly upregulated.

Since migration experiments were carried out in the absence of any exogenous ligand addition and basal expression level of receptors and protein kinases tested were not significantly different, it is hard to draw any conclusions as to why both up and down regulation of NRP1 led to a reduction in migration. This is made especially difficult not least because NRP1 being such a prolific co-receptor, but also in light of the data showing differential expression of such a large number of genes between the fs188 and fs120 cells. To gain a greater understanding of how NRP1 influences migration in the fs cells, future studies need to examine the role of growth factors other than VEGF, such as HGF, PlGF2, bFGF, EGF and PDGF-B, that interact with NRP1 in its capacity as a co-receptor migratory regulator (Matsushita *et al.*, 2007, Cao *et al.*, 2010, Evans *et al.*, 2011, Huang *et al.*, 2014). It would also be useful to study other signalling pathways that are associated with cell migration including the RhoGTPases which are known regulators of the actin cytoskeleton and cell migration. VEGF and other growth factors activate RhoA and other Rho proteins and NRP1 has been shown to be involved in these processes (Shimizu *et al.*, 2018). Fs120 cells have previously shown a dependency on VEGF for migration on laminin but not collagen-1, whereas the migration of fs188 cells on the same matrices was insensitive to B20-4.1.1 (English *et al.*, 2017). English *et al.*, (2017) suggested that these differences might have arisen from NRP1s regulatory role during migration being isoform dependent in some cell types; this hypothesis can now be investigated further with the cells developed during the current study.

6.3 NRP1 modification in fs cells results in smaller tumours *in vivo*

In vivo, both fs188 NRP1 KD clones resulted in smaller tumours than fs188wt cells, furthermore the endpoint tumour volumes of fs188^{3BD6} and fs188^{3CE7} were strikingly similar. In keeping with the seemingly discordant results *in vitro*, NRP1 OE in fs120 cells also resulted in smaller tumours, yet the

difference between fs120wt and fs120^{G3} tumours was not as profound as between fs188wt and fs188^{3BD6}/fs188^{3CE7} tumours. *In vitro*, neither up nor downregulation of NRP1 in the fs120 and fs188 cells respectively, effected population doubling times and expression levels of p27 were comparable between modified and wt cell lines. *In vivo*, Ki67 staining of untreated tumour sections supported the *in vitro* data, showing no significant change in the proportion of proliferating tumour cells following NRP1 KD or OE. The smaller tumours resulting from NRP1 KD could also not be attributed to poor vascularisation, as both vascular density and area were comparable between both fs188wt and fs188 NRP1 KD tumours. NRP1 OE in the fs120 tumours did result in an increase in vascular area, yet no had no effect on vessel density. There are distinct signalling consequences following VEGF-mediated NRP1 and VEGFR2 complex formation on ECs that are dependent on whether receptors are on the same cell (*cis*) or on opposing cells (*trans*) (Koch *et al.*, 2014). In an experimental fs model and in PDAC, VEGF-associated juxtacrine interactions (*trans* complexes between two differing cell types) between tumour-associated NRP1 and EC VEGFR2 can lead to an arrest in VEGFR2 signalling that reduces tumour angiogenesis (Koch *et al.*, 2014, Morin *et al.*, 2018). The frequency of these juxtacrine interactions are influenced by relative expression levels of endothelial NRP1 and the proximity of NRP1-expressing tumour cells to the vasculature (Morin *et al.*, 2018). Given the lack of difference in vascularity between wt and NRP1 modified fs tumours, the assumption was made that VEGF-mediated NRP1/ VEGFR2 signalling was largely dispensable for initial tumour vascularisation in the current model. Assessment of NRP1 expression in the fs tumour vasculature would provide a clearer picture of total NRP1 expression levels and distribution within the tumours. The caveat to this is that the pan-endothelial marker CD31 was the only marker used to identify tumour vessels. As discussed in Chapter 5, although CD31 is a reliable EC marker it does not distinguish between mature and immature vessels and also does not provide any information as to the origin of the vessels.

It had been hoped that an *in vitro* model, co-culturing EC and fs cells, could be developed to study juxtacrine interactions and that the extent of EC VEGFR2 phosphorylation would serve as an indicator of EC activation. Initially pilot experiments were carried out either seeding ECs on top of fs cells or seeding a mixture of EC and fs cells and measuring VEGFR2 phosphorylation \pm recombinant VEGF₁₆₅. However, reproducibility was an issue and it was unclear as to whether the different cell types were oriented in culture in a way that would facilitate the juxtacrine interactions. Whether or not other ligands such as HGF can bridge similar complexes between NRP1 and cMET in fibrosarcoma and endothelial cells is not known and warrants further investigation. In the absence of any changes in tumour vascularisation it might be assumed that the reduction in tumour growth following NRP1 modification in the fs cells resulted from altered autocrine signalling although this is not supported by

the proliferation data. Once again, since NRP1 has the capacity to bind multiple ligands and receptors, further studies are required to elucidate which ligands are involved in NRP1 mediated autocrine signalling pathways in the fs120 and fs188 tumours. VEGF mediated VEGFR2/ NRP1 signalling has been shown to promote GBM growth (Hamerlik *et al.*, 2012), however, VEGFR2 is not activatable *in vitro* in the fibrosarcoma cells (Kanthou *et al.*, 2014) which makes it more likely that a different autocrine or paracrine signalling loop may be responsible for the reduction in tumour growth following NRP1 KD in fs188 cells. This may indeed depend on cytokines and other factors produced by the fibrosarcoma cells *in vivo*, but also by other cells within the TME that could act in a paracrine manner. In breast cancer cells, autocrine Sema3a through NRP1 increases $\alpha 2\beta 1$ integrin expression which in turn enhances adhesion to collagen-1. This increase in $\alpha 2\beta 1$ integrin expression was found to inhibit breast tumour migration and growth (Pan *et al.*, 2008). Given that qualitative independent assessment of Masson's Trichrome staining suggested that NRP1 OE in fs120 tumours increased ECM collagen deposition, further *in vitro* studies of the fs120 cells with the addition of Sema3A are required to investigate this further. In glioma, NRP1 has been found to potentiate autocrine HGF/cMET signalling and promote tumour progression (Hu *et al.*, 2007), therefore, with the aforementioned upregulated HGF expression in the fs188 cells, the KD of NRP1 may have disrupted this signalling pathway, thus leading to a reduction in VEGF188-expressing NRP1 KD tumour growth.

6.4 Fibrosarcoma sensitivity to B20-4.1.1 following NRP1 modification

Overall, NRP1 expression level had no significant effect on end-point tumour volume or vascularisation in VEGF188-expressing tumours treated with B20-4.1.1, however fs188wt tumours were slower to respond to treatment than fs188 NRP1 KD tumours. Conversely, whilst B20-4.1.1 treatment failed to have any effect on fs120wt tumour growth, high NRP1 expression in fs120^{G3} tumours resulted in significantly smaller end-point tumours. B20-4.1.1 treatment did not result in any NRP1-specific changes in vascular area or density in VEGF120 expressing tumours, however α SMA staining suggested that B20-4.1.1 treatment compromised vascular integrity in the fs120^{G3} tumours. Dual immunofluorescence for CD31 and α SMA would provide a clearer picture of how the vessels were affected by B20-4.1.1 treatment in the fs120^{G3} tumours. Of note, NRP1 OE in fs120 cells resulted in fewer of the dilated vessels that are characteristic of tumours expressing the VEGF120 isoform (Tozer *et al.*, 2008a). This may be indicative of a shift towards a more 'normal' vasculature, as is seen in the fs188wt tumours. If this were to be the case, then it could be speculated that improved vessel perfusion and lower interstitial fluid pressure (IFP) might result in improved drug delivery to the tumours. Along similar lines, the level of hypoxia within both VEGF188 and VEGF120 expressing tumours may have played a key role in their susceptibility to treatment with B20-4.1.1. Tozer et al.

(2008) found VEGF levels between VEGF120 and VEGF188 tumours were comparable, whilst English et al (2017) found plasma VEGF to be higher in fs120-LS tumours than fs188-LS tumours. Tumour cells are not the only source of VEGF in the tumour microenvironment, host VEGF expression as well as hypoxia caused by structural abnormality of tumour vessels are likely to result in different levels of total VEGF within the tumours. There is a danger that too high dose of bevacizumab may over-prune vessels, and induce hypoxia leading to increased VEGF secretion and loss of anti-tumour activity (Falk *et al.*, 2015). On the other hand, severe hypoxia can be beneficial in achieving tumour cell death. The mechanisms of action of bevacizumab are still not fully understood and whether they are influenced by tumour origin is even less clear. In high grade glioblastoma for instance, where VEGF expression is high, subclinical doses of bevacizumab can achieve vascular normalisation, whilst higher doses are required to decrease/delay tumour growth (Von Baumgarten *et al.*, 2011). In the current study, tumour hypoxia was not measured so firm conclusions cannot be made, however, determination of VEGF expression levels within the tumour would be pertinent to assess in the future.

There is also the possibility that B20-4.1.1 was acting directly on the fs120^{G3} tumour cells themselves. It would be of interest to determine whether increasing NRP1 expression in the fs120 cells has altered their characteristics such as sensitivity to apoptosis, secretion of growth factors and adhesion to ECM proteins in the presence and absence of B20-4.1.1 *in vitro*. It may also be that suppression of tumour growth by B20-4.1.1 is achieved via different mechanisms in the VEGF188 and VEGF120-expressing tumours, which are most likely to arise from the aforementioned differences in protein and gene expression profiles. The lack of effect of B20-4.1.1 in the fs120wt tumours both in terms of growth and vascularity differs from previous work by English *et al.* (2017). Aside from the difference in treatment regimen outlined in Chapter 5, the fs cells that were used in the study by English *et al.* were further modified by transfection with a luciferase-2 (LS) expression cassette and were clonally isolated and it is possible that the fs120-LS clone selected harboured a mutation(s) absent in the original fs120wt population. No differences in tumour growth or *in vitro* characteristics were originally observed between the parental and LS-derivative fs cells (English *et al.*, 2017), however there is the possibility that LS expression has in some way altered how the cells respond to B20-4.1.1. It would be useful to investigate characteristics such as population doubling times and migration rates between LS and parental cell lines following the addition of B20-4.1.1 *in vitro* to determine whether this has contributed to the discrepancies between the current study and the findings of English et al (2017). Finally, innate differences between endogenous expression of growth factors, including VEGF, may exist between the C57Bl6/SCID mice used by English *et al.* (2017) and the CB17-SCID mice used during the current study. Again, in order to draw any direct comparisons between the studies, use of the

same mouse strain with the LS and parental cells and using the same treatment regimen may provide further clarification. .

Metastatic fs120-LS tumours were sensitive to treatment with B20-4.1.1, which was reliant on the presence of the VEGF120 expressing primary tumour, indicative that B20-4.1.1 was acting at the primary tumour rather than on the metastatic site. The cell lines used during the current study did not include the LS expression cassette, therefore *in vivo* cell tracking or *ex vivo* assessment of bioluminescence in lung tissue was not possible. However, to circumvent the lack of LS expression, lungs were harvested and retained for subsequent RNA extraction and RT-qPCR to see whether the expression of SV40 could be detected. In principle, only the immortalised fs cells should express SV40, therefore the detection of this in the lung tissue could be used to estimate the level of lung metastases in B20-4.1.1 and control IgG mice. Optimisation of RNA extraction from the preserved lung tissue was more challenging than originally anticipated, however a single pilot RT-qPCR experiment was carried out that detected SV40 in some of the lung samples tested (data not shown in the thesis). It is anticipated that with some further optimisation, RT-qPCR could be carried out on the lungs excised during this study and that an estimate of tumour metastases can be made. In the study by English *et al.*, (2017), primary tumour growth was inhibited in both fs188-LS and fs120-LS tumours but metastasis was only significantly inhibited in the fs120-LS tumours. These data correlated with the clinical data that showed that benefit from anti-VEGF therapy was associated with short isoform VEGF expression. It will therefore be important to study the influence of B20-4.1.1 on metastasis in the NRP1 knockdown and overexpressing fibrosarcomas to gain a better understanding of the role of NRP1 in tumour response to anti-VEGF therapy.

6.5 Conclusions

Fibrosarcoma cells expressing the single VEGF120 and VEGF188 isoforms with up and downregulated NRP1 expression respectively, were successfully developed to examine whether NRP1 was influenced by differences in the cells' behaviour identified previously both *in vitro* and *in vivo* (Tozer *et al.*, 2008a, Akerman *et al.*, 2013, Kanthou *et al.*, 2014, English *et al.*, 2017). Furthermore, the modified cells were used *in vivo* to examine whether NRP1 expression, in conjunction with single VEGF isoform expression, influenced tumours growth, vascularisation and fibrosis with and without anti-VEGF treatment.

Results of this study (summarised in Table 6.1 and Table 6.2) have further highlighted the complexity and diversity of tumour associated NRP1. This is largely due to its widespread role as a co-receptor for multiple ligands and hence it is involved in numerous signalling cascades other than VEGF signalling.

Since commencing this study, results from genomic profiling of the single VEGF isoform expressing fibrosarcoma cells have identified a plethora of differences. Whether these differences are consequential of adaptive response to long-term single VEGF isoform expression or whether they arose when the cells were originally created is not clear. It was envisaged that mechanisms of single VEGF isoforms with NRP1 interaction with could be characterised through direct comparisons between upregulated NRP1 expression in fs120 cells and downregulated NRP1 expression in fs188 cells. However, it is now clear that ligands and receptors associated with NRP1 could have influenced some of the differences identified following NRP1 manipulation. NRP1 clearly plays a pivotal role in migration in the fs cells, but whether this is VEGF isoform dependent was not clear. *In vivo*, NRP1 KD in the fs188 cells did not confer any significant benefit to anti-VEGF treatment whereas high NRP1 expression in fs120 cells did result in improved anti-VEGF efficacy. These data are somewhat contradictory of the clinical data suggesting low NRP1 and/ or high VEGF120 might be predictive of patient benefit from anti-VEGF therapy. What has become increasingly clear, not only from the data presented here, but also from the published literature is that predictive biomarkers are likely to be context dependent and proteins or factors in isolation are unlikely to predict responsiveness to anti-VEGF therapy. This is not to say that no predictive biomarkers exist, it just means that more work is needed in the clinic in order to collect samples that can be examined for potential biomarkers and further pre-clinical research to follow up the promising candidates.

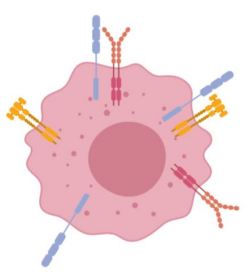
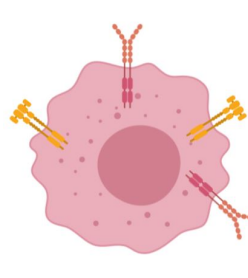
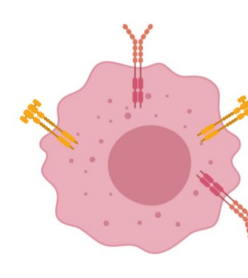
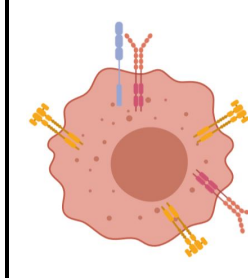
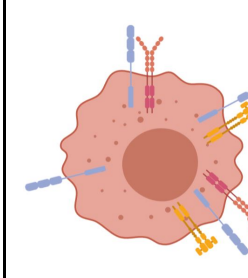
	Fs188wt <i>High endogenous NRP1</i>	Fs188^{3BD6} <i>Low/undetectable NRP1</i>	Fs188^{3CE7} <i>Low/undetectable NRP1</i>	Fs120wt <i>Low endogenous NRP1</i>	Fs120^{G3} <i>NRP1 Overexpression</i>
 NRP1 VEGFR2 c-MET					
Migration <i>Relative to wt</i>	N/a	↓↓↓↓	↓↓↓	N/a	↓↓
Proliferation <i>Relative to wt</i>	N/a	NS	NS	N/a	NS
	Phosphorylation status + HGF <i>Relative to total receptor/protein expression</i>				
c-MET	NS	NS	↑↑↑↑	↑	↑
ERK-1/2	NS	NS	↑↑↑	↑↑	↑↑↑↑
Src	NS	NS	NS	NS	NS
AKT	↑	NS	↑↑↑↑	↑↑↑	NS

Table 6.1 Summary of *in vitro* results

Summary of key findings from *in vitro* work detailed in Chapter 4.

Arrows represent the extent of any changes with respect to statistical significance. NS, not significant; HGF, hepatocyte growth factor

	Fs188wt	Fs188 ^{3BD6}	Fs188 ^{3CE7}	Fs120wt	Fs120 ^{G3}
 NRP1 VEGFR2 c-MET					
Untreated tumours					
Tumour volume <i>Relative to wt</i>	N/a	↓↓↓	↓↓↓	N/a	↓
Vascular area <i>Relative to wt</i>	N/a	NS	NS	N/a	↑↑
Vascular density <i>Relative to wt</i>	N/a	NS	NS	N/a	NS
Necrosis (Mean %)	48%	37%	37%	10%	12%
αSMA (Avg score)	3.5	3.4	3.8	2	2.8
Collagen (Avg score)	2.4	3.1	3.4	3.1	4
Proliferating cells (Mean Ki67 %)	44%	36%	45%	40%	41%
Effect of treatment with anti-VEGF therapy B20-4.1.1 <i>Relative to IgG control</i>					
Tumour volume:					
3 treatments	NS	↓↓↓	↓↓	NS	↓↓
4 treatments	↓	↓↓↓↓	↓↓↓↓	NS	↓↓
Vascular area	↓↓	↓↓	↓↓	NS	NS
Vascular density	↓	↓↓↓	↓↓	NS	NS
Necrosis	NS	NS	NS	NS	NS
αSMA	NS	NS	NS	NS	↓

Table 6.2 Summary of *in vivo* results

Summary of key findings from *in vivo* work detailed in Chapter 5.

Arrows represent the extent of any changes with respect to statistical significance. NS, not significant.

6.6 Lessons learned and future work

The data presented within this thesis has resulted in a number of additional questions, not only in relation to the fs cells themselves, but also in the broader context with regard to experimental design and choosing an appropriate model system. The difference in behaviour of the fs188 NRP1 KD clones used during the study clearly shows how disparate results, both *in vitro* and *in vivo*, can occur from what was assumed to be the same genetic modification. Future experiments to determine whether these differences are solely due to NRP1 KD might include NRP1 knock-in studies in fs188^{3BD6} and fs188^{3CE7} cells, to determine whether reintroduction of NRP1 expression restores more fs188wt-like behaviour. Further *in vitro* studies comparing all fs188 NRP1 KD clones isolated in Chapter 4 may also provide more conclusive results in terms of NRP1s functional role within the fs188 cells. In an ideal world, with no financial constraints, single cell RNA-seq would provide a wealth of information, however this is costly exercise that requires analysis by an experienced bioinformatician if the data is to be interpreted in a meaningful way. . A more accessible method would be to carry out RT-qPCR arrays; for example, Qiagen provides kits that can profile gene sets associated with VEGF signalling (RT² Profiler™ PCR Array Mouse VEGF Signaling) that include ‘AKT & PI3K signalling’, ‘Growth factors & Receptors’, ‘MAPK kinase signaling’ gene expression arrays (Qiagen, 2020). A promising and more cost effective approach that is very much still in its infancy is bulk RNA barcoding and sequencing (BRB-Seq). This technique “combines the high-through-put capacity of single-cell transcriptomics and the high performance of standard RNA-seq” and promises to make full transcriptome analysis more accessible in the future (Alpern *et al.*, 2019).

CRISPR/Cas9 was selected for NRP1 KD on the premise that it was (and still remains) an increasingly robust method of genetic modification. At the time it was used in this study, it was still a relatively novel technique and the all-in-one plasmid delivery of CRISPR/Cas9n and sgRNA approach was considered highly efficient and specific in editing genes of interest. Since then, the CRISPR/Cas9 gene editing process has evolved and become more refined. The algorithms for predicting off-target effects have been improved, moreover the delivery of custom sgRNAs alongside recombinant Cas9 to cells (Cas9-gRNA ribonucleoproteins [RNP]) is considered superior, due to the relatively short half-life of the Cas9 protein. This RNP method circumvents the issue of plasmid DNA being incorporated into the cells genome and limits prolonged expression of Cas9 which can lead to off-target events. If I were to repeat this work, the RNP method would be my method of choice for CRISPR/Cas9 gene editing.

In terms of the fs120 cells, it was unfortunate that NRP1 OE clones with more moderate, and potentially more physiologically relevant, levels of NRP1 expression were not successfully maintained.

Although the fact that NRP1 is so highly overexpressed in the fs120^{G3} cells is not a major limitation of this study, it does somewhat limit the scope for comparison and translation to other cell lines with endogenously high NRP1 expression levels. Rather than repeating the whole OE process and selecting clones with a range of NRP1 expression, perhaps the use of NRP1 siRNA with fs120^{G3} cells could be studied. Several different NRP1 siRNAs were trialled during this study (Chapter 3), two of which were identified as being highly efficient in depleting NRP1 expression; there is potentially some scope for using one of these siRNAs and a further, less efficient siRNA, to determine the levels of NRP1 depletion required to return the fs120^{G3} cells to a more fs120-like phenotype.

An original aim of the study was to develop a co-culture model of fs cells and ECs to examine the juxtacrine interactions of tumour-NRP1 and EC VEGFR2. Numerous attempts were made and a 2D model system was created that mixed fs cells and ECs, however it was never fully optimised and a method for accurately assessing VEGFR2 activation in the ECs was not successfully developed. Such an approach remains valid and should be explored further.

The *in vivo* study has provided a substantial amount of tissue (normal and tumour) for further investigation. Once fully optimised, RT-qPCR data examining SV40 expression in the lungs from mice bearing subcutaneous tumours will provide more information on whether *in vitro* migration results translate to differences in metastases and whether B20-4.1.1 can influence metastasis in a NRP1 dependent manner. As discussed in Chapter 5, the use of other vascular markers to examine fs tumour vascular structure is also likely to provide more information on vessel maturity and possibly provenance. Another avenue that has yet to be explored in the fs tumours is immune cell infiltration. Do VEGF isoform or NRP1 expression influence the tumour immune response? In light of the number of ongoing clinical trials combining anti-angiogenic therapy with immunotherapeutics, this is a relevant question and a valid line of enquiry.

In summary, the results from this study strongly suggest that NRP1 and VEGF isoforms are not suitable biomarkers of response to anti-VEGF therapy in this particular model. However, it has provided a foundation for other areas of study with regard to the role of NRP1 within cancer progression.

Chapter 7

Bibliography

Adams, R. H. & Alitalo, K. (2007). Molecular regulation of angiogenesis and lymphangiogenesis. *Nature Reviews Molecular Cell Biology*, **8**(6), 464.

Aerts, H. J. W. L., Velazquez, E. R., *et al.* (2014). Decoding tumour phenotype by noninvasive imaging using a quantitative radiomics approach. *Nature Communications*, **5**(1), 4006.

Agulnik, M., Yarber, J. L., *et al.* (2012). An open-label, multicenter, phase II study of bevacizumab for the treatment of angiosarcoma and epithelioid hemangioendotheliomas[†]. *Annals of Oncology*, **24**(1), 257-263.

Akerman, S., Fisher, M., *et al.* (2013). Influence of soluble or matrix-bound isoforms of vascular endothelial growth factor-A on tumor response to vascular-targeted strategies. *International Journal of Cancer*, **133**(11), 2563-2576.

Alpern, D., Gardeux, V., *et al.* (2019). BRB-seq: ultra-affordable high-throughput transcriptomics enabled by bulk RNA barcoding and sequencing. *Genome Biology*, **20**(1), 71.

Altschul, S. F., Gish, W., *et al.* (1990). Basic local alignment search tool. *J Mol Biol*, **215**(3), 403-10.

Appleton, B. A., Wu, P., *et al.* (2007). Structural studies of neuropilin/antibody complexes provide insights into semaphorin and VEGF binding. *The EMBO Journal*, **26**(23), 4902-4912.

Artym, V. V. & Matsumoto, K. (2010). Imaging cells in three-dimensional collagen matrix. *Current protocols in cell biology*, **Chapter 10**Unit-10.18.20.

Asahara, T., Murohara, T., *et al.* (1997). Isolation of Putative Progenitor Endothelial Cells for Angiogenesis. *Science*, **275**(5302), 964-966.

Attia, S., Sankhala, K. K., *et al.* (2016). A phase 1B/ phase 2A study of TRC105 (Endoglin Antibody) in combination with pazopanib (P) in patients (pts) with advanced soft tissue sarcoma (STS). *Journal of Clinical Oncology*, **34**(15_suppl), 11016-11016.

Atum. (2019). *CRISPR gRNA Design tool* [Online]. Online: ATUM. Available: <https://www.atum.bio> [Accessed 26 February 2019 2019].

Baba, T., Kariya, M., *et al.* (2007). Neuropilin-1 promotes unlimited growth of ovarian cancer by evading contact inhibition. *Gynecol Oncol*, **105**(3), 703-11.

Bachelder, R. E., Crago, A., *et al.* (2001). Vascular endothelial growth factor is an autocrine survival factor for neuropilin- expressing breast carcinoma cells. *Cancer Research*, **61**(15), 5736-5740.

Bachelder, R. E., Lipscomb, E. A., *et al.* (2003). Competing autocrine pathways involving alternative neuropilin-1 ligands regulate chemotaxis of carcinoma cells. *Cancer Res*, **63**(17), 5230-3.

- Ball, Stephen g., Bayley, C., *et al.* (2010). Neuropilin-1 regulates platelet-derived growth factor receptor signalling in mesenchymal stem cells. *Biochemical Journal*, **427**(1), 29-40.
- Ballmer-Hofer, K., Andersson, A. E., *et al.* (2011). Neuropilin-1 promotes VEGFR-2 trafficking through Rab11 vesicles thereby specifying signal output. *Blood*, **118**(3), 816-826.
- Bankhead, P., Loughrey, M. B., *et al.* (2017). QuPath: Open source software for digital pathology image analysis. *Scientific Reports*, **7**(1), 16878.
- Bates, D. O., Cui, T.-G., *et al.* (2002). VEGF165b, an inhibitory splice variant of vascular endothelial growth factor, is down-regulated in renal cell carcinoma. *Cancer Research*, **62**(14), 4123-4131.
- Baumgarten, P., Blank, A.-E., *et al.* (2015). Differential expression of vascular endothelial growth factor A, its receptors VEGFR-1, -2, and -3 and co-receptors neuropilin-1 and -2 does not predict bevacizumab response in human astrocytomas. *Neuro-Oncology*, **18**(2), 10.
- Benedito, R., Roca, C., *et al.* (2009). The Notch Ligands Dll4 and Jagged1 Have Opposing Effects on Angiogenesis. *Cell*, **137**(6), 1124-1135.
- Benson, A. B., 3rd, Kiss, I., *et al.* (2016). BATON-CRC: A Phase II Randomized Trial Comparing Tivozanib Plus mFOLFOX6 with Bevacizumab Plus mFOLFOX6 in Stage IV Metastatic Colorectal Cancer. *Clinical Cancer Research*, **22**(20), 9.
- Bergers, G. & Benjamin, L. E. (2003). Tumorigenesis and the angiogenic switch. *Nature Reviews Cancer*, **3**(6), 401-410.
- Berry, V., Basson, L., *et al.* (2017). REGOSARC: Regorafenib versus placebo in doxorubicin-refractory soft-tissue sarcoma—A quality-adjusted time without symptoms of progression or toxicity analysis. *Cancer*, **123**(12), 2294-2302.
- Bertolini, F., Marighetti, P., *et al.* (2011). Anti-VEGF and beyond: shaping a new generation of anti-angiogenic therapies for cancer. *Drug Discovery Today*, **16**(23), 1052-1060.
- Bielenberg, D. R., Pettaway, C. A., *et al.* (2006). Neuropilins in neoplasms: Expression, regulation, and function. *Experimental Cell Research*, **312**(5), 584–593.
- Bio-Rad. (2016). *Protein Blotting Methods* [Online]. Online. Available: <http://www.bio-rad.com/> [Accessed 15 July 2016].
- Biselli-Chicote, P. M., Oliveira, A. R., *et al.* (2012). VEGF gene alternative splicing: pro- and anti-angiogenic isoforms in cancer. *Journal of Cancer Research and Clinical Oncology*, **138**(3), 363-70.
- Bleloch, J. S., Ballim, R. D., *et al.* (2017). Managing sarcoma: where have we come from and where are we going? *Therapeutic advances in medical oncology*, **9**(10), 637-659.
- Bobinski, M., Okla, K., *et al.* (2018). Neuropilin 1 in uterine leiomyosarcoma. Clinical and pathological analysis. *Ginekol Pol*, **89**(1), 7-12.
- Borchardt, H., Schulz, A., *et al.* (2019). Silencing of Neuropilins and GIPC1 in pancreatic ductal adenocarcinoma exerts multiple cellular and molecular antitumor effects. *Scientific Reports*, **9**(1), 15471.

Bridgett, S., Dellett, M., *et al.* (2017). RNA-Sequencing data supports the existence of novel VEGFA splicing events but not of VEGFAxxx isoforms. *Sci Rep*, **7**(1), 58.

Bui, N., Kamat, N., *et al.* (2018). A multicenter phase II study of Q3 week or weekly paclitaxel in combination with bevacizumab for the treatment of metastatic or unresectable angiosarcoma. *Rare Tumors [Online]*, **10**.

Burri, P. H., Hlushchuk, R., *et al.* (2004). Intussusceptive angiogenesis: Its emergence, its characteristics, and its significance. *Developmental Dynamics*, **231**(3), 474-488.

Burri, P. H. & Tarek, M. R. (1990). A novel mechanism of capillary growth in the rat pulmonary microcirculation. *The Anatomical Record*, **228**(1), 35-45.

Cackowski, F. C., Xu, L., *et al.* (2004). Identification of two novel alternatively spliced Neuropilin-1 isoforms. *Genomics*, **84**(1), 82-94.

Cai, H. & Reed, R. R. (1999). Cloning and characterization of neuropilin-1-interacting protein: a PSD-95/Dlg/ZO-1 domain-containing protein that interacts with the cytoplasmic domain of neuropilin-1. *J Neurosci*, **19**(15), 6519-6527.

Calzi, S. L., Neu, M. B., *et al.* (2010). EPCs and pathological angiogenesis: When good cells go bad. *Microvascular Research*, **79**(3), 207-216.

Cao, S., Yaqoob, U., *et al.* (2010). Neuropilin-1 promotes cirrhosis of the rodent and human liver by enhancing PDGF/TGF- β signaling in hepatic stellate cells. *The Journal of Clinical Investigation*, **120**(7), 2379-2394.

Cao, Y., Wang, L., *et al.* (2008). Neuropilin-1 upholds dedifferentiation and propagation phenotypes of renal cell carcinoma cells by activating Akt and sonic hedgehog axes. *Cancer Res*, **68**(21), 8667-72.

Carbonell, W. S., Ansgore, O., *et al.* (2009). The Vascular Basement Membrane as "Soil" in Brain Metastasis. *PLOS ONE*, **4**(6), e5857.

Carmeliet, P. & Jain, R. K. (2011). Molecular mechanisms and clinical applications of angiogenesis. *Nature*, **473**(7347), 298-307.

Carmeliet, P., Ng, Y.-S., *et al.* (1999). Impaired myocardial angiogenesis and ischemic cardiomyopathy in mice lacking the vascular endothelial growth factor isoforms VEGF164 and VEGF188. *Nat Med*, **5**(5), 495-502.

Casali, P. G., Abecassis, N., *et al.* (2018). Soft tissue and visceral sarcomas: ESMO–EURACAN Clinical Practice Guidelines for diagnosis, treatment and follow-up†. *Annals of Oncology*, **29**(Supplement_4), iv51-iv67.

Chalkley, H. W. (1943). Method for the Quantitative Morphologic Analysis of Tissues. *JNCI: Journal of the National Cancer Institute*, **4**(1), 47-53.

Chao, C., Al-Saleem, T., *et al.* (2001). Vascular Endothelial Growth Factor and Soft Tissue Sarcomas: Tumor Expression Correlates With Grade. *Annals of Surgical Oncology*, **8**(3), 260-267.

Chappell, J. C., Mouillisseaux, K. P., *et al.* (2013). Flt-1 (vascular endothelial growth factor receptor-1) is essential for the vascular endothelial growth factor–notch feedback loop during angiogenesis. *Arteriosclerosis, Thrombosis, and Vascular Biology*, **33**(8), 1952-1959.

Chen, H., Chédotal, A., *et al.* (1997). Neuropilin-2, a Novel Member of the Neuropilin Family, Is a High Affinity Receptor for the Semaphorins Sema E and Sema IV but Not Sema III. *Neuron*, **19**(3), 547-559.

Chen, L., Miao, W., *et al.* (2014). The Inhibitory Effects of a Monoclonal Antibody Targeting Neuropilin-1 on Adhesion of Glioma Cells to Fibronectin. *Journal of Biomedical Nanotechnology*, **10**(11), 3373-3380.

Chen, T. T., Luque, A., *et al.* (2010). Anchorage of VEGF to the extracellular matrix conveys differential signaling responses to endothelial cells. *The Journal of Cell Biology*, **188**(4), 595-609.

Cheng, S. Y., Nagane, M., *et al.* (1997). Intracerebral tumor-associated hemorrhage caused by overexpression of the vascular endothelial growth factor isoforms VEGF121 and VEGF165 but not VEGF189. *Proceedings of the National Academy of Sciences of the United States of America*, **94**(22), 12081-12087.

Chiche, J., Brahimi-Horn, M. C., *et al.* (2010). Tumour hypoxia induces a metabolic shift causing acidosis: a common feature in cancer. *Journal of Cellular and Molecular Medicine*, **14**(4), 771-794.

Chisholm, J. C., Merks, J. H. M., *et al.* (2017). Open-label, multicentre, randomised, phase II study of the EpSSG and the ITCC evaluating the addition of bevacizumab to chemotherapy in childhood and adolescent patients with metastatic soft tissue sarcoma (the BERNIE study). *European Journal of Cancer*, **83**177-184.

Cho, S. W., Kim, S., *et al.* (2013). Targeted genome engineering in human cells with the Cas9 RNA-guided endonuclease. *Nature Biotechnology*, **31**(3), 230.

Choe, J. & Riedel, R. (2018). Making progress in a rare disease: emerging therapeutics in soft tissue sarcomas [version 1; referees: 2 approved]. *F1000Res*, **7**(1737).

Chu, W., Song, X., *et al.* (2014). Neuropilin-1 Promotes Epithelial-to-Mesenchymal Transition by Stimulating Nuclear Factor-Kappa B and Is Associated with Poor Prognosis in Human Oral Squamous Cell Carcinoma. *PLOS ONE*, **9**(7), e101931.

Chung, A. S. & Ferrara, N. (2011). Developmental and pathological angiogenesis. *Annual Reviews Cell and Developmental Biology*, **27**(1), 563-584.

Ciciola, P., Cascetta, P., *et al.* (2020). Combining Immune Checkpoint Inhibitors with Anti-Angiogenic Agents. *Journal of Clinical Medicine*, **9**(3), 675.

Claes, A., Idema, A. J., *et al.* (2007). Diffuse glioma growth: a guerilla war. *Acta neuropathologica*, **114**(5), 443-458.

Clémenson, C., Chargari, C., *et al.* (2013). Combination of vascular disrupting agents and ionizing radiation. *Critical Reviews in Oncology/Hematology*, **86**(2), 143-160.

Clinicaltrials.Gov. (2019). *ClinicalTrials.gov* [Online]. NIH. [Accessed 25 October 2019 2019].

- Comunanza, V. & Bussolino, F. (2017). Therapy for Cancer: Strategy of Combining Anti-Angiogenic and Target Therapies. *Frontiers in Cell and Developmental Biology*, **5**(101).
- Cong, L., Ran, F. A., *et al.* (2013). Multiplex Genome Engineering Using CRISPR/Cas Systems. *Science*, **339**(6121), 819-823.
- Connolly, D. T., Heuvelman, D. M., *et al.* (1989). Tumor vascular permeability factor stimulates endothelial cell growth and angiogenesis. *The Journal of Clinical Investigation*, **84**(5), 1470-1478.
- D'alessandris, Q. G., Martini, M., *et al.* (2015). VEGF isoforms as outcome biomarker for anti-angiogenic therapy in recurrent glioblastoma. *Neurology*, **84**(18), 1906-8.
- De Haas, S., Delmar, P., *et al.* (2014). Genetic variability of VEGF pathway genes in six randomized phase III trials assessing the addition of bevacizumab to standard therapy. *Angiogenesis*, **17**(4), 909-920.
- Debiec-Rychter, M., Sciot, R., *et al.* (2006). KIT mutations and dose selection for imatinib in patients with advanced gastrointestinal stromal tumours. *European Journal of Cancer*, **42**(8), 1093-103.
- Delcombel, R., Janssen, L., *et al.* (2013). New prospects in the roles of the C-terminal domains of VEGF-A and their cooperation for ligand binding, cellular signaling and vessels formation. *Angiogenesis*, **16**(2), 353-371.
- Di Benedetto, M., Toullec, A., *et al.* (2015). MDA-MB-231 breast cancer cells overexpressing single VEGF isoforms display distinct colonisation characteristics. *British Journal of Cancer*, **113**(5), 773-785.
- Dickson, M. A., #X, *et al.* (2015). Phase II Trial of Gemcitabine and Docetaxel with Bevacizumab in Soft Tissue Sarcoma %J Sarcoma. *Sarcoma*, **2015**7.
- Ding, M., Liu, L., *et al.* (2014). Expression of VEGFR2 and NRP-1 in non-small cell lung cancer and their clinical significance. *Chinese Journal of Cancer Research*, **26**(6), 669-677.
- Dings, R. P. M., Loren, M., *et al.* (2007). Scheduling of radiation with angiogenesis inhibitors anginex and Avastin improves therapeutic outcome via vessel normalization. *Clinical cancer research : an official journal of the American Association for Cancer Research*, **13**(11), 3395-3402.
- Djonov, V., Schmid, M., *et al.* (2000). Intussusceptive Angiogenesis. *Circulation Research*, **86**(3), 286-292.
- Djonov, V. G., Kurz, H., *et al.* (2002). Optimality in the developing vascular system: Branching remodeling by means of intussusception as an efficient adaptation mechanism. *Developmental Dynamics*, **224**(4), 391-402.
- Donnem, T., Reynolds, A. R., *et al.* (2018). Non-angiogenic tumours and their influence on cancer biology. *Nat Rev Cancer*, **18**(5), 323-336.
- Dos Santos, L. V., Cruz, M. R., *et al.* (2015). VEGF-A levels in bevacizumab-treated breast cancer patients: a systematic review and meta-analysis. *Breast Cancer Research and Treatment*, **151**(3), 481-489.

- Dowlati, A., Gray, R., *et al.* (2008). Cell Adhesion Molecules, Vascular Endothelial Growth Factor, and Basic Fibroblast Growth Factor in Patients with Non-Small Cell Lung Cancer Treated with Chemotherapy with or without Bevacizumab—an Eastern Cooperative Oncology Group Study. *Clinical Cancer Research*, **14**(5), 1407-1412.
- Dumontet, C. & Jordan, M. A. (2010). Microtubule-binding agents: a dynamic field of cancer therapeutics. *Nature reviews. Drug discovery*, **9**(10), 790-803.
- Dvorak, H. F., Orenstein, N. S., *et al.* (1979). Induction of a Fibrin-Gel Investment: An Early Event in Line 10 Hepatocarcinoma Growth Mediated by Tumor-Secreted Products. *The Journal of Immunology*, **122**(1), 166-174.
- Eberst, L., Cropet, C., *et al.* (2014). The off-label use of targeted therapies in sarcomas: the OUTC'S program. *BioMed Central Cancer*, **14**870.
- Ebos, J. M. L., Lee, C. R., *et al.* (2009). Accelerated Metastasis after Short-Term Treatment with a Potent Inhibitor of Tumor Angiogenesis. *Cancer Cell*, **15**(3), 232-239.
- Eisenhauer, E. A., Therasse, P., *et al.* (2009). New response evaluation criteria in solid tumours: Revised RECIST guideline (version 1.1). *European Journal of Cancer*, **45**(2), 228-247.
- El-Emir, E., Boxer, G. M., *et al.* (2005). Tumour parameters affected by combretastatin A-4 phosphate therapy in a human colorectal xenograft model in nude mice. *Eur J Cancer*, **41**(5), 799-806.
- English, W. R., Lunt, S. J., *et al.* (2017). Differential Expression of VEGFA Isoforms Regulates Metastasis and Response to Anti-VEGFA Therapy in Sarcoma. *Cancer Research*, **77**(10), 2633-2646.
- Escudier, B., Szczylik, C., *et al.* (2012). Treatment selection in metastatic renal cell carcinoma: expert consensus. *Nature Reviews Clinical Oncology*, **9**(6), 327-337.
- Evans, I. M., Yamaji, M., *et al.* (2011). Neuropilin-1 Signaling through p130^{Cas} Tyrosine Phosphorylation Is Essential for Growth Factor-Dependent Migration of Glioma and Endothelial Cells. *Molecular and Cellular Biology*, **31**(6), 1174-1185.
- Fagiani, E. & Christofori, G. (2013). Angiopoietins in angiogenesis. *Cancer Letters*, **328**(1), 18-26.
- Falk, A. T., Barrière, J., *et al.* (2015). Bevacizumab: A dose review. *Critical Reviews in Oncology/Hematology*, **94**(3), 311-322.
- Fantin, A., Herzog, B., *et al.* (2014). Neuropilin 1 (NRP1) hypomorphism combined with defective VEGF-A binding reveals novel roles for NRP1 in developmental and pathological angiogenesis. *Development*, **141**(3), 556-562.
- Fantin, A., Vieira, J. M., *et al.* (2013). NRP1 acts cell autonomously in endothelium to promote tip cell function during sprouting angiogenesis. *American Society of Hematology*, **121**(12), 2352-2362.
- Fearnley, G. W., Smith, G. A., *et al.* (2016). VEGF-A isoforms program differential VEGFR2 signal transduction, trafficking and proteolysis. *Biology Open*, **5**(5), 571-583.

- Feng, Y. H., Tung, C. L., *et al.* (2019). Proteomic Profile of Sorafenib Resistance in Hepatocellular Carcinoma; GRP78 Expression Is Associated With Inferior Response to Sorafenib. *Cancer Genomics Proteomics*, **16**(6), 569-576.
- Ferrara, N. & Adamis, A. P. (2016). Ten years of anti-vascular endothelial growth factor therapy. *Nature Reviews Drug Discovery*, **15**(6), 385.
- Ferrara, N., Gerber, H. P., *et al.* (2003). The biology of VEGF and its receptors. *Nature Medicine*, **9**(6), 669-76.
- Ferrara, N., Hillan, K. J., *et al.* (2004). Discovery and development of bevacizumab, an anti-VEGF antibody for treating cancer. *Nat Rev Drug Discov*, **3**(5), 391-400.
- Fina, L., Molgaard, H. V., *et al.* (1990). Expression of the CD34 gene in vascular endothelial cells. *Blood*, **75**(12), 2417-26.
- Folberg, R., Hendrix, M. J. C., *et al.* (2000). Vasculogenic Mimicry and Tumor Angiogenesis. *The American Journal of Pathology*, **156**(2), 361-381.
- Folkman, J. (1971). Tumor angiogenesis: therapeutic implications. *New England Journal of Medicine*, **285**(21), 1182-1186.
- Folkman, J., Long Jr., D. M., *et al.* (1963). Growth and metastasis of tumor in organ culture. *Cancer*, **16**(4), 453-467.
- Folpe, A. L., Chand, E. M., *et al.* (2001). Expression of Fli-1, a nuclear transcription factor, distinguishes vascular neoplasms from potential mimics. *Am J Surg Pathol*, **25**(8), 1061-6.
- Fong, G.-H., Rossant, J., *et al.* (1995). Role of the Flt-1 receptor tyrosine kinase in regulating the assembly of vascular endothelium. *Nature*, **376**(6535), 66-70.
- Frezza, A. M., Stacchiotti, S., *et al.* (2017). Systemic treatment in advanced soft tissue sarcoma: what is standard, what is new. *BMC Medicine*, **15**(1), 109.
- Fridlender, Z. G., Sun, J., *et al.* (2009). Polarization of Tumor-Associated Neutrophil Phenotype by TGF- β : "N1" versus "N2" TAN. *Cancer Cell*, **16**(3), 183-194.
- Friedman, H. S., Prados, M. D., *et al.* (2009). Bevacizumab alone and in combination with irinotecan in recurrent glioblastoma. *J Clin Oncol*, **27**(28), 4733-40.
- Fuh, G., Garcia, K. C., *et al.* (2000). The interaction of Neuropilin-1 with Vascular Endothelial Growth Factor and its receptor Flt-1. *Journal of Biological Chemistry*, **275**(35), 26690-5.
- Fukasawa, M., Matsushita, A., *et al.* (2007). Neuropilin-1 interacts with integrin β 1 and modulates pancreatic cancer cell growth, survival and invasion. *Cancer Biology & Therapy*, **6**(8), 1184-1191.
- Fukumura, D., Kloepper, J., *et al.* (2018). Enhancing cancer immunotherapy using antiangiogenics: opportunities and challenges. *Nature Reviews Clinical Oncology*, **15**(5), 325-340.

- Gabhann, M. F. & Popel, A. S. (2005). Differential binding of VEGF isoforms to VEGF receptor 2 in the presence of neuropilin-1: a computational model. *Heart and Circulatory Physiology*, **288**(6), 2851-2860.
- Gacche, R. N. (2015). Compensatory angiogenesis and tumor refractoriness. *Oncogenesis*, **4**(6), e153-e153.
- Gagnon, M. L., Bielenberg, D. R., *et al.* (2000). Identification of a natural soluble neuropilin-1 that binds vascular endothelial growth factor: In vivo expression and antitumor activity. *Proc Natl Acad Sci U S A*, **97**(6), 2573-8.
- Galdiero, M. R., Bonavita, E., *et al.* (2013). Tumor associated macrophages and neutrophils in cancer. *Immunobiology*, **218**(11), 1402-1410.
- Garlanda, C., Parravicini, C., *et al.* (1994). Progressive growth in immunodeficient mice and host cell recruitment by mouse endothelial cells transformed by polyoma middle-sized T antigen: implications for the pathogenesis of opportunistic vascular tumors. *Proc Natl Acad Sci U S A*, **91**(15), 7291-7295.
- Garneau, J. E., Dupuis, M. E., *et al.* (2010). The CRISPR/Cas bacterial immune system cleaves bacteriophage and plasmid DNA. *Nature*, **468**(7320), 67-71.
- Garvey, W. (1984). Modified Elastic Tissue-Masson Trichrome Stain. *Stain Technology*, **59**(4), 213-216.
- Gelfand, M. V., Hagan, N., *et al.* (2014). Neuropilin-1 functions as a VEGFR2 co-receptor to guide developmental angiogenesis independent of ligand binding. *Elife*, **3**e03720.
- Gerhardt, H., Golding, M., *et al.* (2003). VEGF guides angiogenic sprouting utilizing endothelial tip cell filopodia. *Journal of Cell Biology*, **161**(6), 1163-77.
- Gerhardt, H., Ruhrberg, C., *et al.* (2004). Neuropilin-1 is required for endothelial tip cell guidance in the developing central nervous system. *Developmental Dynamics*, **231**(3), 503-9.
- Gill, J. H., Rockley, K. L., *et al.* (2019). Vascular Disrupting Agents in cancer treatment: Cardiovascular toxicity and implications for co-administration with other cancer chemotherapeutics. *Pharmacology & Therapeutics*, **202**18-31.
- Gitay-Goren, H., Cohen, T., *et al.* (1996). Selective Binding of VEGF to One of the Three Vascular Endothelial Growth Factor Receptors of Vascular Endothelial Cells. *Journal of Biological Chemistry*, **271**(10), 5519-5523.
- Goel, H. L. & Mercurio, A. M. (2013). VEGF targets the tumour cell. *Nature reviews. Cancer*, **13**(12), 871-882.
- Goel, S., Duda, D. G., *et al.* (2011). Normalization of the Vasculature for Treatment of Cancer and Other Diseases. *Physiological Reviews*, **91**(3), 1071-1121.
- Goldblum, J. R., Folpe, A. L., *et al.* (2014). *Enzinger and Weiss's soft tissue tumors*, Philadelphia, PA, Elsevier Saunders.

- Gordon, M. S., Robert, F., *et al.* (2014). An Open-Label Phase Ib Dose-Escalation Study of TRC105 (Anti-Endoglin Antibody) with Bevacizumab in Patients with Advanced Cancer. *Clin Cancer Res*, **20**(23), 5918-5926.
- Gorski, D. H., Beckett, M. A., *et al.* (1999). Blockage of the vascular endothelial growth factor stress response increases the antitumor effects of ionizing radiation. *Cancer Res*, **59**(14), 3374-8.
- Gounder, M. M., Lefkowitz, R. A., *et al.* (2011). Activity of Sorafenib against Desmoid Tumor/Deep Fibromatosis. *Clinical Cancer Research*, **17**(12), 4082-4090.
- Gounder, M. M., Mahoney, M. R., *et al.* (2018). Sorafenib for Advanced and Refractory Desmoid Tumors. *New England Journal of Medicine*, **379**(25), 2417-2428.
- Graeven, U., Andre, N., *et al.* (1999). Serum levels of vascular endothelial growth factor and basic fibroblast growth factor in patients with soft-tissue sarcoma. *Journal of Cancer Research and Clinical Oncology*, **125**(10), 577-581.
- Gray, M. J., Wey, J. S., *et al.* (2005). Neuropilin-1 Suppresses Tumorigenic Properties in a Human Pancreatic Adenocarcinoma Cell Line Lacking Neuropilin-1 Coreceptors. *Cancer Research*, **65**(9), 3664-3670.
- Grunstein, J., Masbad, J. J., *et al.* (2000). Isoforms of vascular endothelial growth factor act in a coordinate fashion to recruit and expand tumor vasculature. *Molecular and Cellular Biology*, **20**(19), 7282-91.
- Gu, C. & Giraudo, E. (2013). The role of semaphorins and their receptors in vascular development and cancer. *Experimental Cell Research*, **319**(9), 1306-1316.
- Gu, C., Limberg, B. J., *et al.* (2002). Characterization of neuropilin-1 structural features that confer binding to semaphorin 3A and vascular endothelial growth factor 165. *The Journal of Biological Chemistry*, **277**(20), 18069-76.
- Gu, C., Rodriguez, E. R., *et al.* (2003). Neuropilin-1 conveys semaphorin and VEGF signaling during neural and cardiovascular development. *Developmental Cell*, **5**(1), 45-57.
- Guo, H. F. & Vander Kooi, C. W. (2015). Neuropilin Functions as an Essential Cell Surface Receptor. *The Journal of Biological Chemistry*, **290**(49), 29120-6.
- Guo, J., Glass, J. O., *et al.* (2015). Assessing vascular effects of adding bevacizumab to neoadjuvant chemotherapy in osteosarcoma using DCE-MRI. *British journal of cancer*, **113**(9), 1282-1288.
- Guyot, M. & Pagès, G. (2015). VEGF Splicing and the Role of VEGF Splice Variants: From Physiological-Pathological Conditions to Specific Pre-mRNA Splicing. In: FIEDLER, L. (ed.) *VEGF Signaling: Methods and Protocols*. New York, NY: Springer New York.
- Hale, C. R., Zhao, P., *et al.* (2009). RNA-Guided RNA Cleavage by a CRISPR RNA-Cas Protein Complex. *Cell*, **139**(5), 945-956.
- Hamerlik, P., Lathia, J. D., *et al.* (2012). Autocrine VEGF-VEGFR2-Neuropilin-1 signalling promotes glioma stem-like cell viability and tumor growth. *J Exp Med*, **209**(3), 507-20.

- Hamming, L. C., Slotman, B. J., *et al.* (2017). The clinical application of angiostatic therapy in combination with radiotherapy: past, present, future. *Angiogenesis*, **20**(2), 217-232.
- Hanahan, D. & Weinberg, R. A. (2000). The Hallmarks of Cancer. *Cell*, **100**(1), 57-70.
- Hanahan, D. & Weinberg, R. A. (2011). Hallmarks of Cancer: The Next Generation. *Cell*, **144**(5), 646-674.
- Harper, S. J. & Bates, D. O. (2008). VEGF-A splicing: the key to anti-angiogenic therapeutics? *Nature Reviews Cancer*, **8**(11), 880-887.
- Harris, S., Craze, M., *et al.* (2012). Do anti-angiogenic VEGF (VEGF_{xxx}b) isoforms exist? A cautionary tale. *PLoS ONE*, **7**(5), e35231.
- He, Z. & Tessier-Lavigne, M. (1997). Neuropilin Is a Receptor for the Axonal Chemorepellent Semaphorin III. *Cell*, **90**(4), 739-751.
- Hegde, P. S., Jubb, A. M., *et al.* (2013). Predictive Impact of Circulating Vascular Endothelial Growth Factor in Four Phase III Trials Evaluating Bevacizumab. *Clinical Cancer Research*, **19**(4), 929-937.
- Hegde, P. S., Wallin, J. J., *et al.* (2018). Predictive markers of anti-VEGF and emerging role of angiogenesis inhibitors as immunotherapeutics. *Seminars in Cancer Biology*, **52**(Pt 2), 117-124.
- Heigwer, F., Kerr, G., *et al.* (2014). E-CRISP: fast CRISPR target site identification. *Nature Methods*, **11**(2), 122.
- Hendricks, C., Dubail, J., *et al.* (2016). A Novel Physiological Glycosaminoglycan-Deficient Splice Variant of Neuropilin-1 Is Anti-Tumorigenic In Vitro and In Vivo. *PLOS ONE*, **11**(10), e0165153.
- Hervé, M.-A., Buteau-Lozano, H., *et al.* (2008). Overexpression of vascular endothelial growth factor 189 in breast cancer cells leads to delayed tumor uptake with dilated intratumoral vessels. *The American Journal of Pathology*, **172**(1), 167-178.
- Herzog, B., Pellet-Many, C., *et al.* (2011). VEGF binding to NRP1 is essential for VEGF stimulation of endothelial cell migration, complex formation between NRP1 and VEGFR2, and signaling via FAK Tyr407 phosphorylation. *Molecular Biology of the Cell*, **22**(15), 2766-2776.
- Horsman, M. R., Wittenborn, T. R., *et al.* (2020). Tumors Resistant to Checkpoint Inhibitors Can Become Sensitive after Treatment with Vascular Disrupting Agents. *International Journal of Molecular Sciences*, **21**(13), 4778.
- Hse (2014). The Genetically Modified Organisms (Contained Use) Regulations 2014 *In: EXECUTIVE*, H. S. (ed.) L29 (Fifth edition) ed.: Crown.
- Hsu, Patrick d., Lander, Eric s., *et al.* (2014). Development and Applications of CRISPR-Cas9 for Genome Engineering. *Cell*, **157**(6), 1262-1278.
- Hu, B., Guo, P., *et al.* (2007). Neuropilin-1 promotes human glioma progression through potentiating the activity of the HGF/SF autocrine pathway. *Oncogene*, **26**(38), 5577-5586.

- Huang, H., Song, J., *et al.* (2018a). Autophagy activation promotes bevacizumab resistance in glioblastoma by suppressing Akt/mTOR signaling pathway. *Oncol Lett*, **15**(2), 1487-1494.
- Huang, W., Zhu, S., *et al.* (2014). Placenta growth factor promotes migration through regulating epithelial-mesenchymal transition-related protein expression in cervical cancer. *Int J Clin Exp Pathol*, **7**(12), 8506-19.
- Huang, X., Ye, Q., *et al.* (2019). N-glycosylation-defective splice variants of neuropilin-1 promote metastasis by activating endosomal signals. *Nature communications*, **10**(1), 3708-3708.
- Huang, Z., Cheng, C., *et al.* (2018b). NRP1 promotes cell migration and invasion and serves as a therapeutic target in nasopharyngeal carcinoma. *International journal of clinical and experimental pathology*, **11**(5), 2460-2469.
- Hurwitz, H., Fehrenbacher, L., *et al.* (2004). Bevacizumab plus Irinotecan, Fluorouracil, and Leucovorin for Metastatic Colorectal Cancer. *N Engl J Med*, **350**(23), 2335-2342.
- Ishizuka, Y., Koshinaga, T., *et al.* (2018). NRP1 knockdown promotes the migration and invasion of human neuroblastoma-derived SKNAS cells via the activation of beta1 integrin expression. *Int J Oncol*, **53**(1), 159-166.
- Jablonska, J., Leschner, S., *et al.* (2010). Neutrophils responsive to endogenous IFN-beta regulate tumor angiogenesis and growth in a mouse tumor model. *The Journal of clinical investigation*, **120**(4), 1151-1164.
- Jahangiri, A. & Aghi, M. K. (2012). Biomarkers predicting tumor response and evasion to anti-angiogenic therapy. *Biochimica et Biophysica Acta (BBA) - Reviews on Cancer*, **1825**(1), 86-100.
- Jain, R. K. (2001). Normalizing tumor vasculature with anti-angiogenic therapy: A new paradigm for combination therapy. *Nature Medicine*, **7**(9), 987-989.
- Jain, R. K. (2003). Molecular regulation of vessel maturation. *Nature Medicine*, **9**(6), 685-693.
- Jain, R. K. (2005). Normalization of tumor vasculature: An emerging concept in antiangiogenic therapy. *Science*, **307**(5706), 58-62.
- Jain, R. K., Duda, D. G., *et al.* (2006). Lessons from phase III clinical trials on anti-VEGF therapy for cancer. *Nature Clinical Practice Oncology*, **3**(1), 24-40.
- Jain, R. K., Duda, D. G., *et al.* (2009). Biomarkers of response and resistance to antiangiogenic therapy. *Nature reviews. Clinical oncology*, **6**(6), 327-338.
- Jászai, J. & Schmidt, M. H. H. (2019). Trends and Challenges in Tumor Anti-Angiogenic Therapies. *Cells*, **8**(9), 1102.
- Jayson, G. C., Kerbel, R., *et al.* (2016). Antiangiogenic therapy in oncology: current status and future directions. *The Lancet*, **388**(10043), 518-529.
- Jia, H., Aqil, R., *et al.* (2014). N-terminal modification of VEGF-A C terminus-derived peptides delineates structural features involved in neuropilin-1 binding and functional activity. *ChemBiochem*, **15**(8), 1161-70.

- Jia, H., Bagherzadeh, A., *et al.* (2006). Characterization of a bicyclic peptide neuropilin-1 (NP-1) antagonist (EG3287) reveals importance of vascular endothelial growth factor exon 8 for NP-1 binding and role of NP-1 in KDR signaling. *The Journal of Biological Chemistry*, **281**(19), 13493-502.
- Jia, H., Cheng, L., *et al.* (2010). Neuropilin-1 antagonism in human carcinoma cells inhibits migration and enhances chemosensitivity. *British Journal of Cancer*, **102**(3), 541-552.
- Jimenez-Hernandez, L. E., Vazquez-Santillan, K., *et al.* (2018). NRP1-positive lung cancer cells possess tumor-initiating properties. *Oncol Rep*, **39**(1), 349-357.
- Jiménez-Valerio, G. & Casanovas, O. (2017). Angiogenesis and Metabolism: Entwined for Therapy Resistance. *Trends in Cancer*, **3**(1), 10-18.
- Jinek, M., Chylinski, K., *et al.* (2012). A programmable dual-RNA-guided DNA endonuclease in adaptive bacterial immunity. *Science*, **337**(6096), 816-21.
- Jo, V. Y. & Fletcher, C. D. M. (2014). WHO classification of soft tissue tumours: an update based on the 2013 (4th) edition. *Pathology*, **46**(2), 95-104.
- Jolly, M. K., Boareto, M., *et al.* (2015). Implications of the Hybrid Epithelial/Mesenchymal Phenotype in Metastasis. *Frontiers in Oncology*, **5**(155), 155.
- Jubb, A. M., Hurwitz, H. I., *et al.* (2006). Impact of Vascular Endothelial Growth Factor-A Expression, Thrombospondin-2 Expression, and Microvessel Density on the Treatment Effect of Bevacizumab in Metastatic Colorectal Cancer. *Journal of Clinical Oncology*, **24**(2), 217-227.
- Jubb, A. M., Miller, K. D., *et al.* (2011). Impact of Exploratory Biomarkers on the Treatment Effect of Bevacizumab in Metastatic Breast Cancer. *Clinical Cancer Research*, **17**(2), 372-381.
- Jubb, A. M., Strickland, L. A., *et al.* (2012). Neuropilin-1 expression in cancer and development. *The Journal of Pathology*, **226**(1), 50-60.
- Kamiya, T., Kawakami, T., *et al.* (2006). The preserved expression of neuropilin (NRP) 1 contributes to a better prognosis in colon cancer. *Oncol Rep*, **15**(2), 369-73.
- Kanthou, C., Dachs, G. U., *et al.* (2014). Tumour cells expressing single VEGF isoforms display distinct growth, survival and migration characteristics. *PLoS ONE*, **9**(8), e104015.
- Kanthou, C. & Tozer, G. (2019). Targeting the vasculature of tumours: combining VEGF pathway inhibitors with radiotherapy. *Br J Radiol*, **92**(1093), 20180405.
- Kappas, N. C., Zeng, G., *et al.* (2008). The VEGF receptor Flt-1 spatially modulates Flk-1 signaling and blood vessel branching. *The Journal of Cell Biology*, **181**(5), 847-858.
- Kawamura, H., Li, X., *et al.* (2008). Neuropilin-1 in regulation of VEGF-induced activation of p38MAPK and endothelial cell organization. *Blood*, **112**(9), 3638-3649.
- Khan, K. A. & Bicknell, R. (2016). Anti-angiogenic alternatives to VEGF blockade. *Clinical & experimental metastasis*, **33**(2), 197-210.

- Kilvaer, T. K., Smeland, E., *et al.* (2014). The VEGF- and PDGF-family of angiogenic markers have prognostic impact in soft tissue sarcomas arising in the extremities and trunk. *BMC Clinical Pathology*, **14**(1), 5.
- Kim, K. J., Li, B., *et al.* (1993). Inhibition of vascular endothelial growth factor-induced angiogenesis suppresses tumour growth in vivo. *Nature*, **362**(6423), 841-844.
- Kiso, M., Tanaka, S., *et al.* (2018). Long isoform of VEGF stimulates cell migration of breast cancer by filopodia formation via NRP1/ARHGAP17/Cdc42 regulatory network. *Int J Cancer*, **143**(11), 2905-2918.
- Klagsbrun, M. & D'Amore, P. A. (1991). Regulators of Angiogenesis. *Annual Review of Physiology*, **53**(1), 217-239.
- Ko, S. Y., Lee, W., *et al.* (2019). Cancer-derived small extracellular vesicles promote angiogenesis by heparin-bound, bevacizumab-insensitive VEGF, independent of vesicle uptake. *Communications Biology*, **2**(1), 386.
- Koch, S., Tugues, S., *et al.* (2011). Signal transduction by vascular endothelial growth factor receptors. *Biochemical Journal*, **437**(2), 169-83.
- Koch, S., Van meeteren, Laurens a., *et al.* (2014). NRP1 presented in trans to the endothelium arrests VEGFR2 endocytosis, preventing angiogenic signaling and tumor initiation. *Developmental Cell*, **28**(6), 633-646.
- Kontos, C. D., Cha, E. H., *et al.* (2002). The Endothelial Receptor Tyrosine Kinase Tie1 Activates Phosphatidylinositol 3-Kinase and Akt To Inhibit Apoptosis. *Molecular and Cellular Biology*, **22**(6), 1704-1713.
- Koonin, E. V., Makarova, K. S., *et al.* (2017). Diversity, classification and evolution of CRISPR-Cas systems. *Current Opinion in Microbiology*, **37**67-78.
- Kopp, H.-G., Ramos, C. A., *et al.* (2006). Contribution of endothelial progenitors and proangiogenic hematopoietic cells to vascularization of tumor and ischemic tissue. *Current opinion in hematology*, **13**(3), 175-181.
- Krause, D., Fackler, M., *et al.* (1996). CD34: structure, biology, and clinical utility *Blood*, **87**(1), 1-13.
- Kuczynski, E. A., Vermeulen, P. B., *et al.* (2019). Vessel co-option in cancer. *Nature Reviews Clinical Oncology*, **16**(8), 469-493.
- Kumar, S., Ghellal, A., *et al.* (1999). Breast carcinoma: vascular density determined using CD105 antibody correlates with tumor prognosis. *Cancer Res*, **59**(4), 856-61.
- Küstern, B., De Waal, R. M., *et al.* (2003). Differential effects of vascular endothelial growth factor A isoforms in a mouse brain metastasis model of human melanoma. *Cancer Res*, **63**(17), 5408-13.
- Kwiatkowski, S. C., Guerrero, P. A., *et al.* (2017). Neuropilin-1 modulates TGF β signaling to drive glioblastoma growth and recurrence after anti-angiogenic therapy. *PLOS ONE*, **12**(9), e0185065.
- Lai, X. & Friedman, A. (2019). How to schedule VEGF and PD-1 inhibitors in combination cancer therapy? *BMC Systems Biology*, **13**(1), 30.

- Lambin, P., Rios-Velazquez, E., *et al.* (2012). Radiomics: Extracting more information from medical images using advanced feature analysis. *European Journal of Cancer*, **48**(4), 441-446.
- Lambrechts, D., Claes, B., *et al.* (2012). VEGF pathway genetic variants as biomarkers of treatment outcome with bevacizumab: an analysis of data from the AViTA and AVOREN randomised trials. *The Lancet Oncology*, **13**(7), 724-733.
- Lambrechts, D., Lenz, H.-J., *et al.* (2013). Markers of response for the antiangiogenic agent bevacizumab. *Journal of Clinical Oncology*, **31**(9), 1219-1230.
- Lee, D. Y., Staddon, A. P., *et al.* (2019). Phase I and phase II clinical trials in sarcoma: Implications for drug discovery and development. *Cancer Medicine*, **8**(2), 585-592.
- Lee, S., Chen, T. T., *et al.* (2007). Autocrine VEGF Signaling Is Required for Vascular Homeostasis. *Cell*, **130**(4), 691-703.
- Lehnhardt, M., Muehlberger, T., *et al.* (2005). Feasibility of chemosensitivity testing in soft tissue sarcomas. *World J Surg Oncol*, **3**(1), 20.
- Leung, D., Cachianes, G., *et al.* (1989). Vascular endothelial growth factor is a secreted angiogenic mitogen. *Science*, **246**(4935), 1306-1309.
- Levental, K. R., Yu, H., *et al.* (2009). Matrix crosslinking forces tumor progression by enhancing integrin signaling. *Cell*, **139**(5), 891-906.
- Li, L., Jiang, X., *et al.* (2016a). Neuropilin-1 is associated with clinicopathology of gastric cancer and contributes to cell proliferation and migration as multifunctional co-receptors. *Journal of Experimental & Clinical Cancer Research*, **35**(1), 16.
- Li, W., Quan, Y.-Y., *et al.* (2018). Monitoring of tumor vascular normalization: the key points from basic research to clinical application. *Cancer management and research*, **104**163-4172.
- Li, X., Fan, S., *et al.* (2016b). Nordihydroguaiaretic acid impairs prostate cancer cell migration and tumor metastasis by suppressing neuropilin 1. *Oncotarget*, **7**(52), 86225-86238.
- Li, X., Parker, M. W., *et al.* (2014). Control of cellular motility by neuropilin-mediated physical interactions. *Biomol Concepts*, **5**(2), 157-66.
- Li, X., Tang, T., *et al.* (2011). RNA interference targeting NRP-1 inhibits human glioma cell proliferation and enhances cell apoptosis. *Mol Med Rep*, **4**(6), 1261-6.
- Liang, W., Ni, Y., *et al.* (2016). Tumor resistance to vascular disrupting agents: mechanisms, imaging, and solutions. *Oncotarget*, **7**(13).
- Lin, Y., Weisdorf, D. J., *et al.* (2000). Origins of circulating endothelial cells and endothelial outgrowth from blood. *The Journal of clinical investigation*, **105**(1), 71-77.
- Linch, M., Miah, A. B., *et al.* (2014). Systemic treatment of soft-tissue sarcoma—gold standard and novel therapies. *Nature Reviews Clinical Oncology*, **11**(4), 187.

- Lippert, J. W. (2007). Vascular disrupting agents. *Bioorganic & Medicinal Chemistry*, **15**(2), 605-615.
- Liu, W.-Q., Borriello, L., *et al.* (2015). New peptides structurally related to VEGF-A165 exon-7 and -8 encoded domains antagonize its binding to NRP-1 and VEGF-R1. *International Journal of Peptide Research and Therapeutics*, **21**(1), 117-124.
- Lomet, D., Piegu, B., *et al.* (2018). Anti-angiogenic VEGFAxxx transcripts are not expressed in the medio-basal hypothalamus of the seasonal sheep. *PLoS One*, **13**(5), e0197123.
- Luo, M., Hou, L., *et al.* (2016). VEGF/NRP-1 axis promotes progression of breast cancer via enhancement of epithelial-mesenchymal transition and activation of NF- κ B and β -catenin. *Cancer Letters*, **373**(1), 1-11.
- Lyden, D., Hattori, K., *et al.* (2001). Impaired recruitment of bone-marrow-derived endothelial and hematopoietic precursor cells blocks tumor angiogenesis and growth. *Nature Medicine*, **7**(11), 1194-1201.
- Maharaj, A. S. R., Saint-Geniez, M., *et al.* (2006). Vascular Endothelial Growth Factor Localization in the Adult. *The American Journal of Pathology*, **168**(2), 639-648.
- Mahmood, T. & Yang, P.-C. (2012). Western blot: technique, theory, and troubleshooting. *North American Journal of Medical Sciences*, **4**(9), 429-434.
- Makanya, A. N., Hlushchuk, R., *et al.* (2009). Intussusceptive angiogenesis and its role in vascular morphogenesis, patterning, and remodeling. *Angiogenesis*, **12**(2), 113.
- Mali, P., Yang, L., *et al.* (2013). RNA-Guided Human Genome Engineering via Cas9. *Science*, **339**(6121), 823-826.
- Mamluk, R., Gechtman, Z. E., *et al.* (2002). Neuropilin-1 Binds Vascular Endothelial Growth Factor 165, Placenta Growth Factor-2, and Heparin via Its b1b2 Domain. *Journal of Biological Chemistry*, **277**(27), 24818-24825.
- Manetti, M., Guiducci, S., *et al.* (2011). Overexpression of VEGF165b, an inhibitory splice variant of vascular endothelial growth factor, leads to insufficient angiogenesis in patients with systemic sclerosis. *Circ Res*, **109**(3), e14-26.
- Maniotis, A. J., Folberg, R., *et al.* (1999). Vascular Channel Formation by Human Melanoma Cells in Vivo and in Vitro: Vasculogenic Mimicry. *The American Journal of Pathology*, **155**(3), 739-752.
- Martinelli, M., Bonezzi, K., *et al.* (2007). Sequence dependent antitumour efficacy of the vascular disrupting agent ZD6126 in combination with paclitaxel. *British Journal of Cancer*, **97**(7), 888-894.
- Martini, M., De Pascalis, I., *et al.* (2018). VEGF-121 plasma level as biomarker for response to anti-angiogenetic therapy in recurrent glioblastoma. *BMC cancer*, **18**(1), 553-553.
- Matkar, P. N., Jong, E. D., *et al.* (2018). Jack of many trades: Multifaceted role of neuropilins in pancreatic cancer. *Cancer Medicine*, **7**(10), 5036-5046.

- Matkar, P. N., Singh, K. K., *et al.* (2016). Novel regulatory role of neuropilin-1 in endothelial-to-mesenchymal transition and fibrosis in pancreatic ductal adenocarcinoma. *Oncotarget*, **7**(43), 69489-69506.
- Matsushita, A., Götze, T., *et al.* (2007). Hepatocyte Growth Factor–Mediated Cell Invasion in Pancreatic Cancer Cells Is Dependent on Neuropilin-1. *Cancer Research*, **67**(21), 10309-10316.
- Mckenney, J. K., Weiss, S. W., *et al.* (2001). CD31 Expression in Intratumoral Macrophages: A Potential Diagnostic Pitfall. *The American Journal of Surgical Pathology*, **25**(9), 1167-1173.
- Mehta, C. R., Liu, L., *et al.* (2019). An adaptive population enrichment phase III trial of TRC105 and pazopanib versus pazopanib alone in patients with advanced angiosarcoma (TAPPAS trial). *Ann Oncol*, **30**(1), 103-108.
- Miao, H.-Q., Percy, L., *et al.* (2000). Neuropilin-1 expression by tumor cells promotes tumor angiogenesis and progression. *FASEB Journal*, **14**(15), 2532-2539.
- Miao, H.-Q., Soker, S., *et al.* (1999). Neuropilin-1 Mediates Collapsin-1/Semaphorin III Inhibition of Endothelial Cell Motility: Functional Competition of Collapsin-1 and Vascular Endothelial Growth Factor-165. *The Journal of Cell Biology*, **146**(1), 233-242.
- Migdal, M., Huppertz, B., *et al.* (1998). Neuropilin-1 Is a Placenta Growth Factor-2 Receptor. *J Biol Chem*, **273**(35), 22272-22278.
- Miles, D., Cameron, D., *et al.* (2017). Bevacizumab plus paclitaxel versus placebo plus paclitaxel as first-line therapy for HER2-negative metastatic breast cancer (MERiDiAN): A double-blind placebo-controlled randomised phase III trial with prospective biomarker evaluation. *European Journal of Cancer*, **70**146-155.
- Miles, D. W., Chan, A., *et al.* (2010). Phase III study of bevacizumab plus docetaxel compared with placebo plus docetaxel for the first-line treatment of human epidermal growth factor receptor 2–negative metastatic breast cancer. *Journal of Clinical Oncology*, **28**(20), 3239-3247.
- Miles, D. W., De Haas, S. L., *et al.* (2013). Biomarker results from the AVADO phase 3 trial of first-line bevacizumab plus docetaxel for HER2-negative metastatic breast cancer. *British Journal of Cancer*, **108**(5), 1052-60.
- Miller, K., Wang, M., *et al.* (2007). Paclitaxel plus bevacizumab versus paclitaxel alone for metastatic breast cancer. *New England Journal of Medicine*, **357**(26), 2666-2676.
- Mineur, P., Colige, A. C., *et al.* (2007). Newly identified biologically active and proteolysis-resistant VEGF-A isoform VEGF111 is induced by genotoxic agents. *The Journal of Cell Biology*, **179**(6), 1261-1273.
- Misra, R. M., Bajaj, M. S., *et al.* (2012). Vasculogenic mimicry of HT1080 tumour cells in vivo: critical role of HIF-1alpha-neuropilin-1 axis. *PLoS One*, **7**(11), e50153.
- Morgan, R. D., Jayson, G. C., *et al.* (2018). A phase Ib and randomised phase II trial of pazopanib with or without fosbretabulin in advanced recurrent ovarian cancer. *Annals of Oncology*, **29**viii342.

- Morin, E., Sjöberg, E., *et al.* (2018). VEGF receptor-2/neuropilin 1 trans-complex formation between endothelial and tumor cells is an independent predictor of pancreatic cancer survival. *J Pathol*, **246**(3), 311-322.
- Mueller, S. B. & Kontos, C. D. (2016). Tie1: an orphan receptor provides context for angiopoietin-2/Tie2 signaling. *The Journal of clinical investigation*, **126**(9), 3188-3191.
- Muhl, L., Folestad, E. B., *et al.* (2017). Neuropilin 1 binds PDGF-D and is a co-receptor in PDGF-D–PDGFR β signaling. *Journal of Cell Science*, **130**(8), 1365-1378.
- Müller, A. M., Hermanns, M. I., *et al.* (2002). Expression of the Endothelial Markers PECAM-1, vWf, and CD34 in Vivo and in Vitro. *Experimental and Molecular Pathology*, **72**(3), 221-229.
- Murga, M., Fernandez-Capetillo, O., *et al.* (2005). Neuropilin-1 regulates attachment in human endothelial cells independently of vascular endothelial growth factor receptor-2. *Blood*, **105**(5), 1992-1999.
- Naeem, N., Mushtaq, S., *et al.* (2018). Effectiveness of Vascular Markers (Immunohistochemical Stains) in Soft Tissue Sarcomas. *J Coll Physicians Surg Pak*, **28**(5), 352-356.
- Naik, A., Al-Yahyaee, A., *et al.* (2018). Neuropilin-1 promotes the oncogenic Tenascin-C/integrin $\beta 3$ pathway and modulates chemoresistance in breast cancer cells. *BMC Cancer*, **18**(1), 533.
- Nakamura, N., Naruse, K., *et al.* (2009). Adiponectin promotes migration activities of endothelial progenitor cells via Cdc42/Rac1. *FEBS Letters*, **583**(15), 2457-2463.
- Nam, D. K., Lee, S., *et al.* (2002). Oligo(dT) primer generates a high frequency of truncated cDNAs through internal poly(A) priming during reverse transcription. *Proceedings of the National Academy of Sciences of the United States of America*, **99**(9), 6152-6156.
- Naoyo, N., Hirohisa, Y., *et al.* (2006). Angiogenesis in cancer. *Vascular health and risk management*, **2**(3), 213-219.
- Neufeld, G., Cohen, T., *et al.* (1996). Similarities and differences between the vascular endothelial growth factor (VEGF) splice variants. *Cancer and Metastasis Reviews*, **15**(2), 153-158.
- Ng, Y.-S., Rohan, R., *et al.* (2001). Differential expression of VEGF isoforms in mouse during development and in the adult. *Developmental Dynamics*, **220**(2), 112-121.
- Nguyen, L., Fifis, T., *et al.* (2016). Vascular disruptive agent OXi4503 and anti-angiogenic agent Sunitinib combination treatment prolong survival of mice with CRC liver metastasis. *BMC Cancer*, **16**533.
- Niland, S., Ditkowski, B., *et al.* (2013). Rhodocetin- $\alpha\beta$ –induced Neuropilin-1–cMet Association Triggers Restructuring of Matrix Contacts in Endothelial Cells. *Arteriosclerosis, Thrombosis, and Vascular Biology*, **33**(3), 544-554.
- Niland, S. & Eble, J. A. (2019). Neuropilins in the Context of Tumor Vasculature. *International Journal of Molecular Sciences*, **20**(3), 639.

- Niland, S., Komljenovic, D., *et al.* (2018). Rhodocetin- $\alpha\beta$ selectively breaks the endothelial barrier of the tumor vasculature in HT1080 fibrosarcoma and A431 epidermoid carcinoma tumor models. *Oncotarget*, **9**(32), 22406-22422.
- Nowak, D. G., Amin, E. M., *et al.* (2010). Regulation of vascular endothelial growth factor (VEGF) splicing from pro-angiogenic to anti-angiogenic isoforms: a novel therapeutic strategy for angiogenesis. *The Journal of Biological Chemistry*, **285**(8), 5532-40.
- Olsson, A.-K., Dimberg, A., *et al.* (2006). VEGF receptor signalling ? in control of vascular function. *Nature Reviews Molecular Cell Biology*, **7**(5), 359-371.
- Ordóñez, N. G. (2012). Immunohistochemical Endothelial Markers: A Review. *Advances in Anatomic Pathology*, **19**(5), 281-295.
- Pàez-Ribes, M., Allen, E., *et al.* (2009). Antiangiogenic Therapy Elicits Malignant Progression of Tumors to Increased Local Invasion and Distant Metastasis. *Cancer Cell*, **15**(3), 220-231.
- Palodetto, B., Da Silva Santos Duarte, A., *et al.* (2017). SEMA3A partially reverses VEGF effects through binding to neuropilin-1. *Stem Cell Research*, **22**(0), 70-78.
- Pan, H., Wanami, L. S., *et al.* (2008). Autocrine semaphorin3A stimulates alpha2 beta1 integrin expression/function in breast tumor cells. *Breast Cancer Research and Treatment*, **118**(1), 197.
- Pan, Q., Chanthery, Y., *et al.* (2007a). Blocking neuropilin-1 function has an additive effect with anti-VEGF to inhibit tumor growth. *Cancer cell*, **11**(1), 53-67.
- Pan, Q., Chathery, Y., *et al.* (2007b). Neuropilin-1 binds to VEGF121 and regulates endothelial cell migration and sprouting. *J Biol Chem*, **282**(33), 24049-56.
- Panigrahy, D., Adini, I., *et al.* (2014). Regulation of soluble neuropilin 1, an endogenous angiogenesis inhibitor, in liver development and regeneration. *Pathology*, **46**(5), 416-423.
- Papetti, M. & Herman, I. M. (2002). Mechanisms of normal and tumor-derived angiogenesis. *American Journal of Physiology - Cell Physiology*, **282**(5), C947-C970.
- Parikh, A. A., Fan, F., *et al.* (2004). Neuropilin-1 in human colon cancer: expression, regulation, and role in induction of angiogenesis. *The American journal of pathology*, **164**(6), 2139-2151.
- Parker, M. W., Xu, P., *et al.* (2012a). Mechanism of Selective VEGF-A Binding by Neuropilin-1 Reveals a Basis for Specific Ligand Inhibition. *PLOS ONE*, **7**(11), e49177.
- Parker, M. W., Xu, P., *et al.* (2012b). Structural basis for selective vascular endothelial growth factor-A (VEGF-A) binding to Neuropilin-1. *American Society for Biochemistry and Molecular Biology*, **287**(14), 11082-11089.
- Pasquali, S., Bonvalot, S., *et al.* (2019). Treatment challenges in and outside a network setting: Soft tissue sarcomas. *European Journal of Surgical Oncology*, **45**(1), 31-39.
- Pasquali, S. & Gronchi, A. (2017). Neoadjuvant chemotherapy in soft tissue sarcomas: latest evidence and clinical implications. *Therapeutic advances in medical oncology*, **9**(6), 415-429.

- Passalidou, E., Trivella, M., *et al.* (2002). Vascular phenotype in angiogenic and non-angiogenic lung non-small cell carcinomas. *British journal of cancer*, **86**(2), 244-249.
- Paszek, M. J., Zahir, N., *et al.* (2005). Tensional homeostasis and the malignant phenotype. *Cancer Cell*, **8**(3), 241-254.
- Paule, B., Bastien, L., *et al.* (2010). Soluble Isoforms of Vascular Endothelial Growth Factor Are Predictors of Response to Sunitinib in Metastatic Renal Cell Carcinomas. *PLOS ONE*, **5**(5), e10715.
- Peach, C. J., Mignone, V. W., *et al.* (2018). Molecular Pharmacology of VEGF-A Isoforms: Binding and Signalling at VEGFR2. *International Journal of Molecular Sciences*, **19**(4), 1264.
- Peng, Y., Liu, Y.-M., *et al.* (2014). MicroRNA-338 Inhibits Growth, Invasion and Metastasis of Gastric Cancer by Targeting NRP1 Expression. *PLOS ONE*, **9**(4), e94422.
- Pezzella, F., Pastorino, U., *et al.* (1997). Non-small-cell lung carcinoma tumor growth without morphological evidence of neo-angiogenesis. *The American journal of pathology*, **151**(5), 1417-1423.
- Plouët, J., Moro, F., *et al.* (1997). Extracellular Cleavage of the Vascular Endothelial Growth Factor 189-Amino Acid Form by Urokinase Is Required for Its Mitogenic Effect. *Journal of Biological Chemistry*, **272**(20), 13390-13396.
- Potente, M., Gerhardt, H., *et al.* (2011). Basic and Therapeutic Aspects of Angiogenesis. *Cell*, **146**(6), 873-887.
- Prey, L. A. (2008). Transposons: The Jumping Genes. *Nature Education* **11**.
- Pusztaszeri, M. P., Seelentag, W., *et al.* (2006). Immunohistochemical Expression of Endothelial Markers CD31, CD34, von Willebrand Factor, and Fli-1 in Normal Human Tissues. *Journal of Histochemistry & Cytochemistry*, **54**(4), 385-395.
- Pylayeva-Gupta, Y., Grabocka, E., *et al.* (2011). RAS oncogenes: weaving a tumorigenic web. *Nature Reviews Cancer*, **11**(11), 761-774.
- Qiagen. (2020). *GeneGlobe, RT2 Profiler™ PCR Arrays* [Online]. Available: <https://geneglobe.qiagen.com/product-groups/rt2-profiler-pcr-arrays> [Accessed July 2020 2020].
- Qiu, Y., Hoareau-Aveilla, C., *et al.* (2009). The anti-angiogenic isoforms of VEGF in health and disease. *Biochem Soc Trans*, **37**(Pt 6), 1207-13.
- Raimondi, C., Fantin, A., *et al.* (2014). Imatinib inhibits VEGF-independent angiogenesis by targeting neuropilin 1-dependent ABL1 activation in endothelial cells. *The Journal of Experimental Medicine*, **211**(6), 1167-1183.
- Raimondi, C. & Ruhrberg, C. (2013). Neuropilin signalling in vessels, neurons and tumours. *Seminars in Cell & Developmental Biology*, **24**(3), 172-178.
- Ran, F. A., Hsu, P. D., *et al.* (2013a). Double nicking by RNA-guided CRISPR Cas9 for enhanced genome editing specificity. *Cell*, **154**(6), 1380-9.

- Ran, F. A., Hsu, P. D., *et al.* (2013b). Genome engineering using the CRISPR-Cas9 system. *Nat Protoc*, **8**(11), 2281-2308.
- Raut, C. P., Boucher, Y., *et al.* (2012). Effects of sorafenib on intra-tumoral interstitial fluid pressure and circulating biomarkers in patients with refractory sarcomas (NCI Protocol 6948). *PLoS ONE*, **7**(2), e26331.
- Ray-Coquard, I. L., Domont, J., *et al.* (2015). Paclitaxel Given Once Per Week With or Without Bevacizumab in Patients With Advanced Angiosarcoma: A Randomized Phase II Trial. *Journal of Clinical Oncology*, **33**(25), 2797-2802.
- Real, C., Caiado, F., *et al.* (2008). Endothelial Progenitors in Vascular Repair and Angiogenesis: How Many are Needed and What to do? *Cardiovascular & Hematological Disorders-Drug Targets*, **8**(3), 185-192.
- Ribatti, D. (2004). The involvement of endothelial progenitor cells in tumor angiogenesis. *Journal of Cellular and Molecular Medicine*, **8**(3), 294-300.
- Ribatti, D. (2016). Tumor refractoriness to anti-VEGF therapy. *Oncotarget*, **7**(29), 46668-46677.
- Ribatti, D. & Crivellato, E. (2012). "Sprouting angiogenesis", a reappraisal. *Dev Biol*, **372**(2), 157-65.
- Risau, W. (1997). Mechanisms of angiogenesis. *Nature*, **386**(6626), 671-674.
- Rizzolio, S., Rabinowicz, N., *et al.* (2012). Neuropilin-1-dependent regulation of EGF-receptor signaling. *Cancer Res*, **72**(22), 5801-11.
- Robert, N. J., Diéras, V., *et al.* (2011). RIBBON-1: Randomized, double-blind, placebo-controlled, phase III trial of chemotherapy with or without bevacizumab for first-line treatment of human epidermal growth factor receptor 2–negative, locally recurrent or metastatic breast cancer. *Journal of Clinical Oncology*, **29**(10), 1252-1260.
- Roberts, Z. J., Goutagny, N., *et al.* (2007). The chemotherapeutic agent DMXAA potently and specifically activates the TBK1-IRF-3 signaling axis. *The Journal of experimental medicine*, **204**(7), 1559-1569.
- Robinson, C. J. & Stringer, S. E. (2001). The splice variants of vascular endothelial growth factor (VEGF) and their receptors. *Journal of Cell Science*, **114**(5), 853-865.
- Rossignol, M., Beggs, A. H., *et al.* (1999). Human Neuropilin-1 and Neuropilin-2 Map to 10p12 and 2q34, Respectively. *Genomics*, **57**(3), 459-460.
- Rovida, A., Castiglioni, V., *et al.* (2013). Chemotherapy Counteracts Metastatic Dissemination Induced by Antiangiogenic Treatment in Mice. *Molecular Cancer Therapeutics*, **12**(10), 2237-2247.
- Roy, S., Bag, A. K., *et al.* (2017). Multifaceted Role of Neuropilins in the Immune System: Potential Targets for Immunotherapy. *Front Immunol*, **8**(1228), 1228.
- Ruffini, F., D'atri, S., *et al.* (2013). Neuropilin-1 expression promotes invasiveness of melanoma cells through vascular endothelial growth factor receptor-2-dependent and-independent mechanisms. *International journal of oncology*, **43**(1), 297-306.

- Sahai, E. (2005). Mechanisms of cancer cell invasion. *Current Opinion in Genetics & Development*, **15**(1), 87-96.
- Salikhova, A., Wang, L., *et al.* (2008). Vascular Endothelial Growth Factor and Semaphorin Induce Neuropilin-1 Endocytosis via Separate Pathways. *Circulation Research*, **103**(6), e71-e79.
- Saponara, M., Stacchiotti, S., *et al.* (2017). (Neo)adjuvant treatment in localised soft tissue sarcoma: The unsolved affair. *European Journal of Cancer*, **70**1-11.
- Sarabipour, S., Ballmer-Hofer, K., *et al.* (2016). VEGFR-2 conformational switch in response to ligand binding. *Elife*, **5**e13876.
- Sarabipour, S. & Mac Gabhann, F. (2018). VEGF-A121a binding to Neuropilins – A concept revisited. *Cell Adhesion & Migration*, **12**(3), 204-214.
- Sauter, B., Foedinger, D., *et al.* (1998). Immunoelectron microscopic characterization of human dermal lymphatic microvascular endothelial cells. Differential expression of CD31, CD34, and type IV collagen with lymphatic endothelial cells vs blood capillary endothelial cells in normal human skin, lymphangioma, and hemangioma in situ. *J Histochem Cytochem*, **46**(2), 165-76.
- Savant, S., La porta, S., *et al.* (2015). The Orphan Receptor Tie1 Controls Angiogenesis and Vascular Remodeling by Differentially Regulating Tie2 in Tip and Stalk Cells. *Cell Reports*, **12**(11), 1761-1773.
- Schedin, P. & Keely, P. J. (2011). Mammary gland ECM remodeling, stiffness, and mechanosignaling in normal development and tumor progression. *Cold Spring Harbor Perspectives in Biology*, **3**(1), a003228.
- Scholz, D. & Schaper, J. (1997). Platelet/endothelial cell adhesion molecule-1 (PECAM-1) is localized over the entire plasma membrane of endothelial cells. *Cell Tissue Res*, **290**(3), 623-31.
- Seaman, S., Stevens, J., *et al.* (2007). Genes that distinguish physiological and pathological angiogenesis. *Cancer cell*, **11**(6), 539-554.
- Senger, D. R. (2010). Vascular Endothelial Growth Factor: Much More than an Angiogenesis Factor. *Molecular Biology of the Cell*, **21**(3), 377-379.
- Shalaby, F., Rossant, J., *et al.* (1995). Failure of blood-island formation and vasculogenesis in Flk-1-deficient mice. *Nature*, **376**(6535), 62-66.
- Sharma, S., Takyar, S., *et al.* (2013). Efficacy and safety of pharmacological interventions in second- or later-line treatment of patients with advanced soft tissue sarcoma: a systematic review. *BMC Cancer*, **13**(1), 385.
- Sheng, Y., Hua, J., *et al.* (2004). Combretastatin family member OXI4503 induces tumor vascular collapse through the induction of endothelial apoptosis. *Int J Cancer*, **111**(4), 604-10.
- Shi, F., Shang, L., *et al.* (2018). Neuropilin-1 contributes to esophageal squamous cancer progression via promoting P65-dependent cell proliferation. *Oncogene*, **37**(7), 935-943.

- Shimizu, A., Zankov, D. P., *et al.* (2018). Vascular Endothelial Growth Factor-A Exerts Diverse Cellular Effects via Small G Proteins, Rho and Rap. *International Journal of Molecular Sciences*, **19**(4), 1203.
- Shintani, Y., Takashima, S., *et al.* (2006). Glycosaminoglycan modification of neuropilin-1 modulates VEGFR2 signaling. *The EMBO Journal*, **25**(13), 3045-3055.
- Siegel, R. L., Miller, K. D., *et al.* (2019). Cancer statistics, 2019. *American Cancer Society*, **69**(1), 7-34.
- Siemann, D. W. (2011). The unique characteristics of tumor vasculature and preclinical evidence for its selective disruption by Tumor-Vascular Disrupting Agents. *Cancer Treatment Reviews*, **37**(1), 63-74.
- Siemann, D. W., Bibby, M. C., *et al.* (2005). Differentiation and definition of vascular-targeted therapies. *Clin Cancer Res*, **11**(2 Pt 1), 416-20.
- Siemann, D. W., Chaplin, D. J., *et al.* (2017). Realizing the Potential of Vascular Targeted Therapy: The Rationale for Combining Vascular Disrupting Agents and Anti-Angiogenic Agents to Treat Cancer. *Cancer Investigation*, **35**(8), 519-534.
- Siemann, D. W., Mercer, E., *et al.* (2002). Vascular targeting agents enhance chemotherapeutic agent activities in solid tumor therapy. *Int J Cancer*, **99**(1), 1-6.
- Siemann, D. W. & Rojiani, A. M. (2002). Enhancement of radiation therapy by the novel vascular targeting agent ZD6126. *Int J Radiat Oncol Biol Phys*, **53**(1), 164-71.
- Siemerink, M. J., Klaassen, I., *et al.* (2013). Endothelial tip cells in ocular angiogenesis: potential target for anti-angiogenesis therapy. *The journal of histochemistry and cytochemistry : official journal of the Histochemistry Society*, **61**(2), 101-115.
- Siemerink, M. J., Klaassen, I., *et al.* (2012). CD34 marks angiogenic tip cells in human vascular endothelial cell cultures. *Angiogenesis*, **15**(1), 151-63.
- Simons, M., Gordon, E., *et al.* (2016). Mechanisms and regulation of endothelial VEGF receptor signalling. *Nature Reviews Molecular Cell Biology*, **17**(10), 611.
- Singh, M., Couto, S. S., *et al.* (2012). Anti-VEGF antibody therapy does not promote metastasis in genetically engineered mouse tumour models. *The Journal of Pathology*, **227**(4), 417-430.
- Skapek, S. X., Ferrari, A., *et al.* (2019). Rhabdomyosarcoma. *Nature Reviews Disease Primers*, **5**(1), 1.
- Sleijfer, S., Van Der Graaf, W. T., *et al.* (2008). Angiogenesis inhibition in non-GIST soft tissue sarcomas. *Oncologist*, **13**(11), 1193-200.
- Smith, Gina a., Fearnley, Gareth w., *et al.* (2015). The cellular response to vascular endothelial growth factors requires co-ordinated signal transduction, trafficking and proteolysis. *Bioscience Reports*, **35**(5), e00253.
- Soker, S., Fidler, H., *et al.* (1996). Characterization of Novel Vascular Endothelial Growth Factor (VEGF) Receptors on Tumor Cells That Bind VEGF via Its Exon 7-encoded Domain. *Journal of Biological Chemistry*, **271**(10), 5761-5767.

- Soker, S., Miao, H. Q., *et al.* (2002). VEGF165 mediates formation of complexes containing VEGFR-2 and neuropilin-1 that enhance VEGF165-receptor binding. *Journal of Cellular Biochemistry*, **85**(2), 357-68.
- Soker, S., Takashima, S., *et al.* (1998). Neuropilin-1 is expressed by endothelial and tumor cells as an isoform-specific receptor for vascular endothelial growth factor. *Cell*, **92**(6), 735-745.
- Spring, H., Schüler, T., *et al.* (2005). Chemokines direct endothelial progenitors into tumor neovessels. *Proceedings of the National Academy of Sciences of the United States of America*, **102**(50), 18111-18116.
- Staton, C. A., Koay, I., *et al.* (2013). Neuropilin-1 and neuropilin-2 expression in the adenoma-carcinoma sequence of colorectal cancer. *Histopathology*, **62**(6), 908-15.
- Sternberg, S. H., Haurwitz, R. E., *et al.* (2012). Mechanism of substrate selection by a highly specific CRISPR endoribonuclease. *RNA*, **18**(4), 661-672.
- Stessels, F., Van Den Eynden, G., *et al.* (2004). Breast adenocarcinoma liver metastases, in contrast to colorectal cancer liver metastases, display a non-angiogenic growth pattern that preserves the stroma and lacks hypoxia. *Br J Cancer*, **90**(7), 1429-36.
- Stiller, C. A., Trama, A., *et al.* (2013). Descriptive epidemiology of sarcomas in Europe: Report from the RARECARE project. *European Journal of Cancer*, **49**(3), 684-695.
- Stollman, T. H., Scheer, M. G. W., *et al.* (2009). Tumor Accumulation of Radiolabeled Bevacizumab due to Targeting of Cell- and Matrix-Associated VEGF-A Isoforms. *Cancer Biotherapy and Radiopharmaceuticals*, **24**(2), 195-200.
- Sulpice, E., Plouët, J., *et al.* (2008). Neuropilin-1 and neuropilin-2 act as coreceptors, potentiating proangiogenic activity. *Blood*, **111**(4), 2036-2045.
- Takagi, S., Hirata, T., *et al.* (1991). The A5 antigen, a candidate for the neuronal recognition molecule, has homologies to complement components and coagulation factors. *Neuron*, **7**(2), 295-307.
- Tanaka, F., Otake, Y., *et al.* (2001). Evaluation of Angiogenesis in Non-small Cell Lung Cancer. *Comparison between Anti-CD34 Antibody and Anti-CD105 Antibody*, **7**(11), 3410-3415.
- Teesalu, T., Sugahara, K. N., *et al.* (2009). C-end rule peptides mediate neuropilin-1-dependent cell, vascular, and tissue penetration. *Proceedings of the National Academy of Sciences*, **106**(38), 16157-16162.
- Thomas, M. & Augustin, H. G. (2009). The role of the Angiopoietins in vascular morphogenesis. *Angiogenesis*, **12**(2), 125.
- Thomlinson, R. H. & Gray, L. H. (1955). The histological structure of some human lung cancers and the possible implications for radiotherapy. *British journal of cancer*, **9**(4), 539-549.
- Tillo, M., Erskine, L., *et al.* (2015). VEGF189 binds NRP1 and is sufficient for VEGF/NRP1-dependent neuronal patterning in the developing brain. *Development*, **142**(2), 314-319.

- Tozer, G. M., Akerman, S., *et al.* (2008a). Blood vessel maturation and response to vascular-disrupting therapy in single vascular endothelial growth factor-A isoform-producing tumors. *Cancer Research*, **68**(7), 2301-2311.
- Tozer, G. M., Kanthou, C., *et al.* (2005). Disrupting tumour blood vessels. *Nature Reviews Cancer*, **5**(6), 423-435.
- Tozer, G. M., Kanthou, C., *et al.* (2008b). Tumour vascular disrupting agents: combating treatment resistance. *Br J Radiol*, **81 Spec No 1S12-20**.
- Tsoi, M., Laguë, M.-N., *et al.* (2013). Anti-VEGFA Therapy Reduces Tumor Growth and Extends Survival in a Murine Model of Ovarian Granulosa Cell Tumor. *Translational oncology*, **6**(3), 226-233.
- Valdembri, D., Caswell, P. T., *et al.* (2009). Neuropilin-1/GIPC1 signaling regulates $\alpha 5\beta 1$ integrin traffic and function in endothelial cells. *PLoS Biology*, **7**(1), e1000025.
- Van Beijnum, J. R., Nowak-Sliwinska, P., *et al.* (2015). The Great Escape; the Hallmarks of Resistance to Antiangiogenic Therapy. *Pharmacological Reviews*, **67**(2), 441-461.
- Van Cutsem, E., De Haas, S., *et al.* (2012). Bevacizumab in combination with chemotherapy as first-line therapy in advanced gastric cancer: A biomarker evaluation from the AVAGAST randomized phase III trial. *Journal of Clinical Oncology*, **30**(17), 2119-2127.
- Van Der Graaf, W. T., Blay, J. Y., *et al.* (2012). Pazopanib for metastatic soft-tissue sarcoma (PALETTE): a randomised, double-blind, placebo-controlled phase 3 trial. *Lancet*, **379**(9829), 1879-86.
- Van der veldt, Astrid a. M., Lubberink, M., *et al.* (2012). Rapid Decrease in Delivery of Chemotherapy to Tumors after Anti-VEGF Therapy: Implications for Scheduling of Anti-Angiogenic Drugs. *Cancer Cell*, **21**(1), 82-91.
- Vander Kooi, C. W., Jusino, M. A., *et al.* (2007). Structural basis for ligand and heparin binding to neuropilin B domains. *PNAS*, **104**(15), 6152-6157.
- Vasudev, N. S. & Reynolds, A. R. (2014). Anti-angiogenic therapy for cancer: current progress, unresolved questions and future directions. *Angiogenesis*, **17**(3), 471-494.
- Vempati, P., Popel, A. S., *et al.* (2014). Extracellular regulation of VEGF: Isoforms, proteolysis, and vascular patterning. *Cytokine & Growth Factor Reviews*, **25**(1), 1-19.
- Vieira, J. M., Schwarz, Q., *et al.* (2007). Selective requirements for NRP1 ligands during neurovascular patterning. *Development*, **134**(10), 1833-1843.
- Vintonenko, N., Pelaez-Garavito, I., *et al.* (2011). Overexpression of VEGF189 in breast cancer cells induces apoptosis via NRP1 under stress conditions. *Cell Adhesion and Migration*, **5**(4), 332-43.
- Vivekanandhan, S. & Mukhopadhyay, D. (2019). Genetic status of KRAS influences Transforming Growth Factor-beta (TGF- β) signaling: An insight into Neuropilin-1 (NRP1) mediated tumorigenesis. *Seminars in Cancer Biology*, **54**72-79.
- Vivekanandhan, S., Yang, L., *et al.* (2017). Genetic status of KRAS modulates the role of Neuropilin-1 in tumorigenesis. *Scientific Reports*, **7**(1), 12877.

- Vo, K. T., Matthay, K. K., *et al.* (2016). Targeted antiangiogenic agents in combination with cytotoxic chemotherapy in preclinical and clinical studies in sarcoma. *Clinical Sarcoma Research*, **6**(1), 9.
- Von Baumgarten, L., Brucker, D., *et al.* (2011). Bevacizumab Has Differential and Dose-Dependent Effects on Glioma Blood Vessels and Tumor Cells. *Clinical Cancer Research*, **17**(19), 6192-6205.
- Von Mehren, M., Randall, R., *et al.* (2018). Soft tissue sarcoma version 2.2018, clinical practice guidelines in oncology (NCCN guidelines). . *Journal of the National Comprehensive Cancer Network*, **16**(5), 28.
- Wang, J. M., Kumar, S., *et al.* (1994). Breast Carcinoma: Comparative Study of Tumor Vasculature Using Two Endothelial Cell Markers. *JNCI: Journal of the National Cancer Institute*, **86**(5), 386-389.
- Warren, R. S., Yuan, H., *et al.* (1995). Regulation by vascular endothelial growth factor of human colon cancer tumorigenesis in a mouse model of experimental liver metastasis. *The Journal of Clinical Investigation*, **95**(4), 1789-1797.
- Weidner, N., Semple, J. P., *et al.* (1991). Tumor Angiogenesis and Metastasis — Correlation in Invasive Breast Carcinoma. *New England Journal of Medicine*, **324**(1), 1-8.
- Werno, C., Menrad, H., *et al.* (2010). Knockout of HIF-1 α in tumor-associated macrophages enhances M2 polarization and attenuates their pro-angiogenic responses. *Carcinogenesis*, **31**(10), 1863-72.
- West, D. C., Rees, C. G., *et al.* (2005). Interactions of Multiple Heparin Binding Growth Factors with Neuropilin-1 and Potentiation of the Activity of Fibroblast Growth Factor-2. *Journal of Biological Chemistry*, **280**(14), 13457-13464.
- Wey, J. S., Gray, M. J., *et al.* (2005). Overexpression of neuropilin-1 promotes constitutive MAPK signalling and chemoresistance in pancreatic cancer cells. *British Journal of Cancer*, **93**(2), 8.
- Whitaker, G. B., Limberg, B. J., *et al.* (2001). Vascular endothelial growth factor receptor-2 and neuropilin-1 form a receptor complex that is responsible for the differential signaling potency of VEGF(165) and VEGF(121). *The Journal of Biological Chemistry*, **276**(27), 25520-31.
- Williams, K. J., Telfer, B. A., *et al.* (2007). Combining radiotherapy with AZD2171, a potent inhibitor of vascular endothelial growth factor signaling: pathophysiologic effects and therapeutic benefit. *Molecular Cancer Therapeutics*, **6**(2), 599-606.
- Winkler, F., Kozin, S. V., *et al.* (2004). Kinetics of vascular normalization by VEGFR2 blockade governs brain tumor response to radiation: Role of oxygenation, angiopoietin-1, and matrix metalloproteinases. *Cancer Cell*, **6**(6), 553-563.
- Woodard, L. E. & Wilson, M. H. (2015). piggyBac-ing models and new therapeutic strategies. *Trends in Biotechnology*, **33**(9), 525-533.
- Workman, P., Aboagye, E. O., *et al.* (2010). Guidelines for the welfare and use of animals in cancer research. *British Journal of Cancer*, **102**(11), 1555-1577.
- Xu, J. & Xia, J. (2013). NRP-1 silencing suppresses hepatocellular carcinoma cell growth in vitro and in vivo. *Experimental and therapeutic medicine*, **5**(1), 150-154.

- Yacoub, M., Coulon, A., *et al.* (2009). Differential expression of the semaphorin 3A pathway in prostatic cancer. *Histopathology*, **55**(4), 392-398.
- Yamamoto, H., Rundqvist, H., *et al.* (2016). Autocrine VEGF Isoforms Differentially Regulate Endothelial Cell Behavior. *Frontiers in Cell and Developmental Biology*, **4**(99), eCollection.
- Yancopoulos, G. D., Davis, S., *et al.* (2000). Vascular-specific growth factors and blood vessel formation. *Nature*, **407**(6801), 242-248.
- Yao, Y., Kubota, T., *et al.* (2005). Prognostic significance of microvessel density determined by an anti-CD105/endoglin monoclonal antibody in astrocytic tumors: Comparison with an anti-CD31 monoclonal antibody. *Neuropathology*, **25**(3), 201-206.
- Yaqoob, U., Cao, S., *et al.* (2012). Neuropilin-1 stimulates tumor growth by increasing fibronectin fibril assembly in the tumor microenvironment. *Cancer research*, **72**(16), 4047-4059.
- Yin, Q., Hung, S.-C., *et al.* (2017). Associations between Tumor Vascularity, Vascular Endothelial Growth Factor Expression and PET/MRI Radiomic Signatures in Primary Clear-Cell–Renal-Cell-Carcinoma: Proof-of-Concept Study. *Scientific Reports*, **7**(1), 43356.
- Yoon, S. S., Segal, N. H., *et al.* (2006). Angiogenic profile of soft tissue sarcomas based on analysis of circulating factors and microarray gene expression. *J Surg Res*, **135**(2), 282-90.
- Young, R. J. & Woll, P. J. (2017). Anti-angiogenic therapies for the treatment of angiosarcoma: a clinical update. *Memo*, **10**(4), 190-193.
- Yu, J. L., Rak, J. W., *et al.* (2002). Vascular Endothelial Growth Factor Isoform Expression as a Determinant of Blood Vessel Patterning in Human Melanoma Xenografts. *Cancer Research*, **62**(6), 1838-1846.
- Yuan, A., Lin, C.-Y., *et al.* (2011). Functional and structural characteristics of tumor angiogenesis in lung cancers overexpressing different VEGF isoforms assessed by DCE- and SSCE-MRI. *PLoS one*, **6**(1), e16062-e16062.
- Yudoh, K., Kanamori, M., *et al.* (2001). Concentration of vascular endothelial growth factor in the tumour tissue as a prognostic factor of soft tissue sarcomas. *British Journal of Cancer*, **84**(12), 1610-1615.
- Yue, B., Ma, J. F., *et al.* (2014). Knockdown of neuropilin-1 suppresses invasion, angiogenesis, and increases the chemosensitivity to doxorubicin in osteosarcoma cells - an in vitro study. *Eur Rev Med Pharmacol Sci*, **18**(12), 1735-41.
- Zanuy, D., Kotla, R., *et al.* (2013). Sequence dependence of C-end rule peptides in binding and activation of neuropilin-1 receptor. *Journal of Structural Biology*, **182**(2), 78-86.
- Zecchin, A., Kalucka, J., *et al.* (2017). How Endothelial Cells Adapt Their Metabolism to Form Vessels in Tumors. *Frontiers in Immunology*, **8**(1750), 1750.

Zeng, F., Luo, F., *et al.* (2014). A monoclonal antibody targeting neuropilin-1 inhibits adhesion of MCF7 breast cancer cells to fibronectin by suppressing the FAK/p130cas signaling pathway. *Anticancer Drugs*, **25**(6), 663-672.

Zhang, L., Wang, H., *et al.* (2017a). VEGF-A/Neuropilin 1 Pathway Confers Cancer Stemness via Activating Wnt/ β -Catenin Axis in Breast Cancer Cells. *Cellular Physiology and Biochemistry*, **44**(3), 1251-1262.

Zhang, W., Azuma, M., *et al.* (2010). Molecular predictors of combination targeted therapies (cetuximab, bevacizumab) in irinotecan-refractory colorectal cancer (BOND-2 study). *Anticancer Res*, **30**(10), 4209-17.

Zhang, W., Shen, Z., *et al.* (2017b). The Benefits and Side Effects of Bevacizumab for the Treatment of Recurrent Ovarian Cancer. *Curr Drug Targets*, **18**(10), 1125-1131.

Zhang, X.-H., Tee, L. Y., *et al.* (2015). Off-target Effects in CRISPR/Cas9-mediated Genome Engineering. *Molecular Therapy - Nucleic Acids*, **4**e264.

Zhang, Y., Xia, M., *et al.* (2018). Function of the c-Met receptor tyrosine kinase in carcinogenesis and associated therapeutic opportunities. *Molecular Cancer*, **17**(1), 45.

Zhao, L., Zhang, D., *et al.* (2016). High VEGF-A level at baseline predicts poor treatment effect of bevacizumab-based chemotherapy in metastatic colorectal cancer: a meta-analysis. *Panminerva Med*, **58**(1), 48-58.

Zhu, H., Cai, H., *et al.* (2014). Neuropilin-1 is overexpressed in osteosarcoma and contributes to tumor progression and poor prognosis. *Clinical Translational Oncology*, **16**(8), 732-8.

Supplementary Data

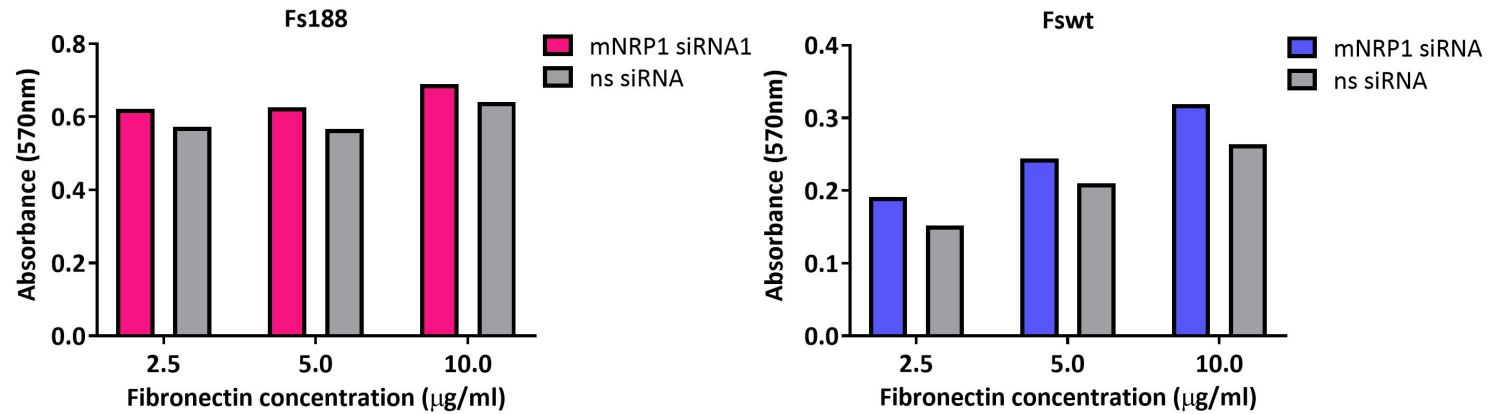


Figure S1. Effect of fibronectin concentration on adhesion of fs188 and fswt cells with and without NRP1 KD

Fs188 and fswt cells transfected with either NRP1 siRNA1 or ns siRNA were seeded in triplicate into wells of a 96-well plate coated with 2.5 µg/mL, 5 µg/mL or 10 µg/mL fibronectin. Cells were allowed to adhere for 45 min; media and non-adherent cells were aspirated and remaining adhered cells were fixed with formalin before being stained with crystal violet. Crystal violet was solubilised and the absorbance measured at 570 nm (n=1 experiment performed in triplicate).

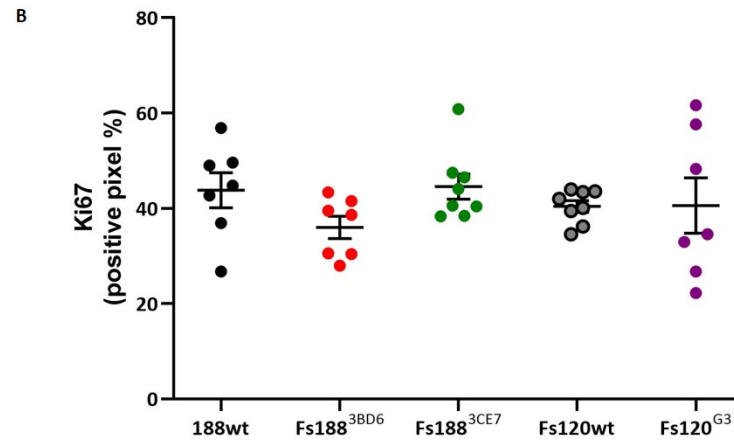
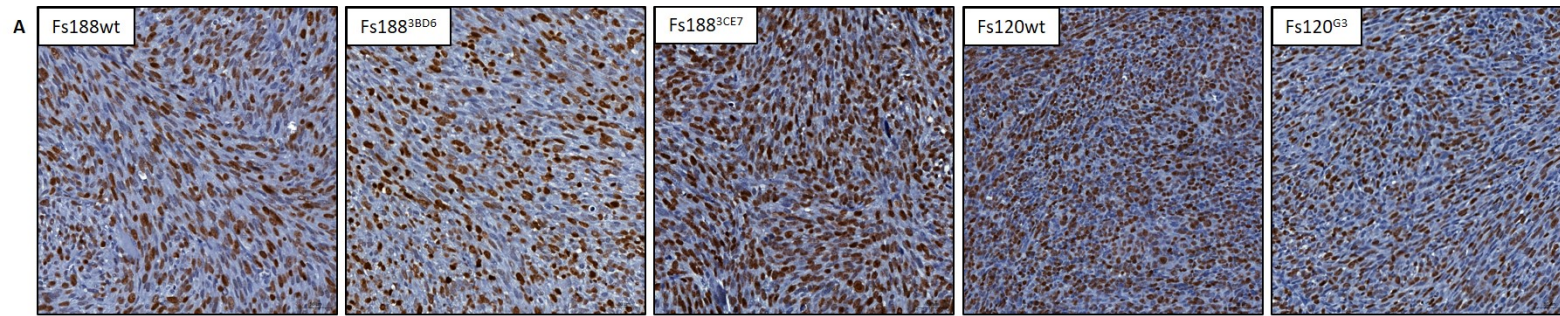


Figure S2. Ki67 staining of untreated VEGF188 and VEGF120 expressing tumours

IHC was used to stain FFPE tumour sections from control IgG treated mice for Ki67 (Materials and Methods, Section 2.13). Ki67 positivity was quantified using QuPath (Version 10.1.2) by calculating the mean percentage of DAB positive staining in 10 random 750 x 750 micron squares (from whole section scanning) in viable tumour tissue.

Appendix 1

Reagent	Supplier
0.2 µm nitrocellulose membrane	Bio-Rad
0.2 µm polyvinylidene fluoride membrane (PVDF)	Bio-Rad
1 Kb DNA ladder	NE Biolabs, N3232
100 bp DNA ladder	NE Biolabs, N3231
10X DMEM-low glucose	Sigma, D2429
3,3'-diaminobenzidine (DAB) peroxidase reagent	Vectorlabs, SK-4100
37% formaldehyde	Sigma, 252549
5X Colourless/green GoTaq® reaction buffer	Promega, M792
Acetic acid	VWR
Acid fuschin	Sigma, F8129
Ampicillin	Sigma, A0166
B20-4.1.1	Genentech
Bouin's solution	Sigma, HT101128
Bovine plasma fibronectin	Sigma, F1141
Bovine serum albumin (BSA)	Sigma, A2058
Cell extraction buffer	Invitrogen, FNN0011
Chloroform	Sigma, C2432
Clarity™ Western ECL reagent	Bio-Rad, 1705060
cOmplete™ mini protease inhibitor cocktail	Roche, 11836153001
Crystal violet	Sigma, C0775
Custom single strand oligonucleotides for sgRNAs	ThermoFisher Scientific
DH5α competent cells	Kindly provided by the Akhtar Lab, UoS
Dithiothreitol (DTT)	ThermoFisher Scientific, R0861
DMEM Ultraglutamine	Lonza, BE12-604F
Donkey anti-goat Alexa fluor-488	Thermo Fisher, A11055
DPX mounting media	Sigma, 06522
Dulbecco's phosphate buffered saline (DPBS)	Lonza
EBM	PromoCell, C-22210
EHS-laminin	Sigma, L2020
Eosin	Sigma, E4009
Ethanol	Fisher Scientific
EZ-ECL chemiluminescence detection kit for HRP	Biological Industries
FBS	Invitrogen, 10270
Formalin, 10% neutral buffered	Sigma
FuGene® 6	Promega, E2691
Gel loading dye, purple (6X)	NE Biolabs, B7024S
Gelatin	Sigma, G1393
GeneAmp® dNTP blend	ThermoFisher Scientific N8080260
GeneJet Gel extraction and DNA cleanup micro kit	ThermoFisher Scientific, K0831
Geneticin G418 sulphate	Gibco, 11811

Reagent	Supplier
Gill's haematoxylin	Sigma, GHS116
GoTaq® G2 DNA polymerase	Promega, M791
Growth Supplement Mix	PromoCell, C-39215
Halt™ phosphatase inhibitor cocktail	ThermoFisher Scientific, 78420
Halt™ protease inhibitor cocktail	ThermoFisher Scientific, 78429
HBSS containing Ca ²⁺ and Mg ²⁺	ThermoFisher Scientific
HBSS without Ca ²⁺ Mg ²⁺	ThermoFisher Scientific
Heat inactivated FBS	Invitrogen
HEPES	Gibco, 15630
HindIII-HF, EcoRV-HF, XbaI, BbsI-HF, FseI	NE Biolabs
Hi-res standard molecular biology grade agarose	Geneflow, A4-0700
Histo-Clear II	National Diagnostics
Horseradish peroxidase-conjugated avidin-biotin complex (ABC-HRP) reagent	Vectorlabs, PK-6100
Hydrogen peroxide (30%)	Sigma
IgG2a control antibody (GP120:9674)	Genentech
Industrial methylated spirit (IMS)	Fisher Scientific
In-Fusion® HD Cloning kit	Takara Bio, 639648
Isoflurane	Abbvie
Kanamycin	Sigma, K1377
Kodak GBX Developer	Sigma
Kodak GBX Fixer and Replenisher	Sigma
LB agar power	Invitrogen, 22700-25
LB broth powder	Invitrogen, 12780-052
L-Glutamine	Lonza, BE17-605E
Light green SF yellowish	Sigma, L1886
Lipofectamine®	Thermo Fisher, 18324-010
Methanol (MeOH)	Fisher Scientific
Micro BCA™ Protein Assay Kit	ThermoFisher Scientific, 23225
Midori green direct DNA stain	Geneflow
Monarch® plasmid mini-prep kit	NE Biolabs, T1010
Monarch® RNA mini-prep kit	NE Biolabs, T2010
Non-enzymatic cell dissociation buffer	Sigma, C5914
Normal donkey serum	Sigma
NuPAGE LDS sample buffer	Novex, NP0008
Opti-MEM™	ThermoFisher Scientific
Penicillin and streptomycin	Life Technologies, 15140
Phenylmethylsulfonyl fluoride (PMSF)	Calbiochem, 52332
Phosphomolybdic acid solution 20% wt in EtOH	Sigma, 319279
Phosphotungstic acid solution 10 % (w/v)	Sigma, HT152
Ponceau xylidine (Ponceau 2R)	Sigma, P2395
Prestained protein ladder	N E Biolabs, P7712

Reagent	Supplier
PromoFectin-siRNA Transfection Reagent	PromoKine, PK-CT-2000-RNA
ProtoScript [®] II First Strand cDNA Synthesis Kit	NEBiolabs, E6560
Puromycin	Calbiochem, 540411
Q5 [®] High-Fidelity DNA polymerase	NE Biolabs, M0491
QIAfilter plasmid Maxi kit	Qiagen, 12262
Rat tail collagen I	Corning, 354236
NaCl 0.9% w/v (Saline solution)	B. Braun
SDS solution (20%)	National Diagnostics, EC-874
siRNA diluent	PromoKine, PK-CT-2000-RNA
SOC media	ThermoFisher Scientific
Sodium bicarbonate	Sigma, S-8875
T4 DNA ligase buffer	NE Biolabs, B0202
T4 polynucleotide kinase (PNK)	ThermoFisher Scientific, EK0031
T7 Ligase with 2X T7 Ligase reaction buffer	NE Biolabs, M0318
TAE Buffer 50X	National Diagnostics, EC-872
Target Retrieval Solution	DAKO, S1699
Transfer stacks/ filter paper	Bio-Rad
<i>TransIT-X2[®]</i> transfection reagent	Mirus, MIR6000
Tris-EDTA (TE) buffer pH 8.0	Qiagen
Tris-glycine electroblotting buffer	National Diagnostics, EC-880
Tris-glycine SDS PAGE buffer	National Diagnostics, EC-870
Tris-HCl	Sigma
TRIzol [™] Reagent	Invitrogen
Trypsin EDTA	Lonza
Weigert's iron hematoxylin solution	Sigma, HT1079
X-ray film	Scientific Laboratory Supplies
Xylene	ThermoFisher Scientific

List of reagents and suppliers detailed in the Materials and Methods (Chapter 2)

Consumables	Supplier
Microlance needles	BD Bioscience
25 cm ² /75 cm ² filter-cap flasks	ThermoFisher Scientific
6, 12, 24 & 96 well cell culture plates	ThermoFisher Scientific
Two-well silicone cell culture inserts	Ibidi, 81176
0.2 µm syringe filter	ThermoFisher Scientific
5 mL round-bottomed polystyrene tubes	ThermoFisher Scientific
Macrosette processing/embedding cassettes	Simport Scientific

Consumables detailed in the Materials and Methods (Chapter 2)

Equipment	Supplier
Applied Biosystems 3730 DNA Analyser	Applied Biosystems
BD FACSAria IIu	BD Biosciences
Beckman Coulter Avanti J-26 XP	Beckman Coulter
BioDoc-it Imaging System	AnalytikJena
ChemiDoc™ MP System	Bio-Rad
FACSCaliber™	BD Biosciences
FLUORStar Galaxy	BMF
HIER pressure cooker	Aptum
Hypercassette™ Autoradiography Cassette	Amersham Biosciences
Nanodrop ND-1000 Spectrophotometer	ThermoFisher Scientific
Nikon Eclipse TS100 phase contrast microscope	Nikon
Novex™ Semi-Dry Blotter	ThermoFisher Scientific
Pannasonic 250 Digital Slide Scanner	3DHistech
SensoQuest Gradient labcyler	Geneflow
TC20 Automated Cell Counter	Bio-Rad
Trans-Blot® Turbo™ Blotting system	Bio-Rad

Appendix table 1 Equipment detailed in Materials and Methods (Chapter 2)

Specific reagent preparation

Lennox L (LB) broth and agar plate preparation

16g of LB agar powder was dissolved in 500 mL dH₂O and autoclaved for 15 min at 121°C; this was allowed to cool to 55°C before the addition of 1 mg/mL ampicillin or kanamycin to give a final concentration of 100 µg/mL or 50 µg/mL respectively. 10-15 mL agar was poured into sterile 10 cm petri dishes and allowed to cool completely at RT before storage at 4°C. 10g LB broth powder was dissolved in 500 mL dH₂O and autoclaved for 15min at 121°C; this was allowed to cool to 55°C before the addition of 1 mg/mL ampicillin or kanamycin to give a final concentration of 100 µg/mL or 50 µg/mL respectively.

2:1 Ponceau 2R/acid fuschin solution

Mix two parts 0.5% (w/v) ponceau 2R in 1% acetic acid with one part 0.5% (w/v) acid fuschin in 1% acetic acid.

2.5% phosphotungstic (ppt) acid: 2.5% phosphotungstic (ppm) acid solution in 2% acetic acid

Dilute ppt and ppm acids with an equal volume of 4% acetic acid to give 5% solutions then mix equal quantities of 5% ppt and 5% ppm to give a 2.5% ppt:2.5% ppm solution in 2% acetic acid.

Appendix 2

	Species /clonality	Dilution	Blocking solution	Supplier
Primary antibodies				
Actin (clone AC-40)	Ms mAb	1:2000	2% BSA/TBST	Sigma (A4700)
Akt	Rb pAb	1:1000	2% BSA/TBST	Cell Signaling (9272)
CD31	Rb pAb	1:500	5% NFDm/TBST	Abcam (ab28364)
c-MET	Rb mAb	1:1000	5% NFDm/TBST	Abcam (ab51067)
c-MET (phospho Y1349)	Rb mAb	1:1000	5% NFDm/TBST	Abcam (ab68141)
Fibronectin	Rb pAb	1:5000	2% BSA/TBST	Abcam (ab2413)
MAP Kinase (ERK-1, ERK-2)	Ms pAb	1:10,000	2% BSA/TBST	Sigma (M5670)
MAP Kinase, activated (diphosphorylated ERK-1 & 2)	Ms mAb	1:10,000	2% BSA/TBST	Sigma (M8159)
NRP1	Rb mAb	1:1000	5% NFDm/TBST	Abcam (ab81321)
NRP2 (D39A5)	Rb mAb	1:1000	2% BSA/TBST	Cell Signaling (3366)
p27 Kip1 (D37H1)	Rb mAb	1:1000	2% BSA/TBST	Cell Signaling (3688)
PDGFR β (28E1)	Rb mAb	1:1000	2% BSA/TBST	Cell signaling (3169)
Phospho-Akt (ser473)	Rb pAb	1:1000	2% BSA/TBST	Cell Signaling (9271)
Phospho-FAK (Tyr397) (D20B1)	Rb mAb	1:1000	2% BSA/TBST	Cell Signaling (8556)
Phospho-Src (Y416)		1:1000	2% BSA/TBST	Cell Signaling
Phospho-Stat3 (Tyr705)	Rb pAb	1:1000	2% BSA/TBST	Cell Signaling (9131)
Phospho-VEGFR2 (Tyr1175) (19A10)	Rb mAb	1:1000	2% BSA/TBST	Cell Signaling (2478)
Src (36D10)	Rb mAb	1:1000	2% BSA/TBST	Cell Signaling (2109)
SV40 T Ag (v-300)	Rb pAb	1:750	2% BSA/TBST	Santa Cruz (sc-20800)
VEGFR2 (55B11)	Rb mAb	1:1000	2% BSA/TBST	Cell Signaling (2479)
β -tubulin	Ms mAb	1:3000	2% BSA/TBST	Sigma (T4026)
Secondary antibodies				
Rb IgG/HRP	Goat pAb	1:2000	2% BSA/TBST or 5% NFDm/TBST	DAKO (P0448)
Ms IgG/HRP	Goat pAb	1:2000	2% BSA/TBST or 5% NFDm/TBST	DAKO (P0447)
Peroxidase AffiniPure Anti-Rb IgG (H+L)	Goat pAb	1:10,000	2% BSA/TBST or 5% NFDm/TBST	Jackson ImmunoResearch Europe Ltd (111-035-144)
Peroxidase AffiniPure Anti-Ms IgG (H+L)	Goat pAb	1:10,000	2% BSA/TBST or 5% NFDm/TBST	Jackson ImmunoResearch Europe Ltd (111-035-003)

Appendix table 2 Antibodies used for western blotting

Primary antibody dilution ranges were selected using the manufacturers recommendations as guidance or from previous work carried out in the Kanthou Lab.

Appendix 3

Primary antibody	Supplier	Antibody concentrations	Blocking serum	Biotinylated secondary antibody
Goat anti-NRP1	R & D Systems AF566	1:20, 1:40, 1:80	10% normal horse serum (Vectorlabs, S-2000)	Horse anti-goat (Vectorlabs, BA-9500)
Rabbit anti-NRP1	Abcam ab81321	1:100, 1:200, 1:300, 1:400	10% normal goat serum (Vectorlabs, S-1000)	Goat anti-rabbit (Vectorlabs, BA-1000)
Rat anti-CD31	Dianova DIA-310	1:200	10% normal rabbit serum (Vectorlabs, S-5000)	Rabbit anti-rat (Vectorlabs, BA-4001)
Rabbit anti-Ki67	Abcam Ab16667	1:400	10% normal goat serum (Vectorlabs, S-1000)	Goat anti-rabbit (Vectorlabs, BA-1000)
Mouse anti- α SMA	Sigma A5228	1:10,000	M.O.M kit (Vectorlabs BMK-2202)	M.O.M kit (Vectorlabs BMK-2202)

Appendix table 3 Antibodies used for IHC

Primary antibody dilution ranges were selected using the manufacturers recommendations as guidance or from previous work carried out in the Kanthou Lab. Blocking solutions, primary and secondary antibodies were prepared in 1%BSA/PBS.